ANALYSIS OF THE ROLE OF TDP-43 AND ITS BINDING PARTNERS IN NEURODEGENERATIVE DISEASES

Kattuah, Wejdan Fawzi

Awarding institution:
King's College London

ANALYSIS OF THE ROLE OF TDP-43 AND ITS BINDING PARTNERS IN NEURODEGENERATIVE DISEASES

Wejdan Fawzi Kattuah

Institute of Psychiatry, Psychology and Neuroscience, King's College London

Thesis submitted for the degree of Doctor of Philosophy

Abstract

Frontotemporal dementia (FTD) is a clinically, genetically and pathologically heterogeneous disorder characterised by a change in language, behaviour and personality, which can also be accompanied by the signs of motor neuron disease (MND). Further, it is considered to be the second most common form of presenile dementia. Pathologically, it is characterised by atrophy of the frontal and anterior temporal lobes. In 2006, TDP-43 was identified as the major component of the ubiquitinated neuronal inclusions found in both frontotemporal lobar degeneration (FTLD) and MND. However, the role of TDP-43 in the neurodegenerative process of FTLD and MND is not yet fully understood. Identifying the TDP-43 protein network could assist in understanding TDP-43's pathological mechanism in neurodegeneration.

In this study, I screened for candidate TDP-43-binding proteins in the brain and spinal cord tissue of FTLD and MND cases using immunohistochemistry. Striking inclusions were detected with hnRNP-E2 in the brain of 16 out of 30 FTLD-TDP cases which do not carry the *C9orf72* mutation. The hnRNP-E2 pathology is significantly related to the TDP-43 pathological subtypes A and C. Furthermore, hnRNP-E2 inclusions colocalised with 84.5% of TDP-43 inclusions and with 67% of ubiquitin inclusions that were also seen in the brain tissue of the FTLD-TDP cases found to exhibit hnRNP-E2 pathology. hnRNP-E2 inclusions were not detected in any of the other neurodegenerative diseases examined in this study, which suggests the close relation of hnRNP-E2 to the pathology of TDP-43.

In order to explore the mechanistic connection between TDP-43 and hnRNP-E2 as well as the possible role of this interaction in TDP-43 pathogenesis, cell biology techniques were utilised to manipulate the levels of TDP-43 and hnRNP-E2 expression in the HEK293T cell line. The knockdown of hnRNP-E2 caused a significant reduction in the TDP-43 levels; however, the interaction was not confirmed. Yet, the hnRNP-E2 interacted with the TDP-43 in the stress granules of HeLa cells under combined osmotic and oxidative stress. At this point, it remains unclear how and why hnRNP-E2 interacted with TDP-43 in a subset of FTLD-TDP cases. However, the results presented here demonstrate that the role of hnRNP-E2 in TDP-43 proteinopathy warrants further investigation.

Table of Contents

List of Figures

List of Tables

Acknowledgements

First and foremost, I would like to thank my supervisors, Professor Christopher Shaw, Dr Claire Troakes and Dr Tibor Hortobagyi, for giving me the opportunity to participate in such a challenging and innovative project. I would also like to thank them for all the support they provided to me during times of difficulty in both science and my personal life. Thank you millions. Completing this project would not have been possible without the help and constant support of a number of brilliant scientists. My thanks go to Dr Emma Scotter, who initiated and followed the cell biology aspect of this study and who trained me in all the cell biology experiments. Further, a big thank you to Dr Caroline Vance, an IP expert, for all the help and advice she provided on the cell biology aspect of this study. A big thank you also to Dr Boris Rogelj for all his support and advice regarding the hnRNP-E2 findings.

I would also like to express my deep appreciation for all the support and advice I received from all the members of our research group, especially Dr Agnes Nishimura, who has been a great help with editing the cell biology chapter, Dr Han-Jou Chen, who provided the TDP-43 plasmids and supervised some parts of this study, Dr Jackie Mitchell, for providing significant help with the Western blot aspect of the study, and Dr Bradley Smith and Dr Younbok Lee for all their advice and help throughout my PhD.

I would also like to say thank you to the other PhD students in our lab, who all helped to make the experiments seem easier and more fun, namely Martina de Majo, Chun Hao Wong, Jorge Gomez Deza, Jenny Craig, Ricky Patel, Shakir Salam and our newest student, Nada Alahmadi. I also extend my thanks to graduated students Athina Gazki, Carole Shum, Valentina Sardon and Simona Darovic. Thank you all for all the happiness and laughter you always brought to the lab.

I dedicate this work to my family, especially my dad and my mum, who trusted me, supported me, prayed for me and allowed me to take the biggest opportunity of my life and never held me back. To my older sisters Suzan and Jehan, and to our big brother, Sido Medo, thank you for everything you do for me; no words can describe my love and appreciation. Thanks also to my nieces and nephews, who always tell me to just finish it and come back! To my little sister, Rana, and my brother, Reda, thank you for all the love and respect you provided me and my crazy children. I love you all.

The biggest thank you and my deepest appreciation goes to my husband, Abdullah, and my mother-in-law, Ami Salma, for all their love and understanding as well as the massive help of looking after the kids. There are no words to describe how lucky I am and how thankful to have you all by my side. To my daughter, Laian, and my son, Elias, who fill my life with joy and somehow push me to reach my targets, thank you for teaching me that patience and time are the most important things we have to give.

Finally, I also wish to express my appreciation to my friends, who always listen to me, believe in me and pray for me. Thank you Alaa Bothainah, Hind, Noura, Rahma, Amani, Mai, Reem, Fatmah, and Alaa; you guys are soul mates, not just friends. Thanks also to Amani, Nouf, Hanan, Nadiah, Mai, Amaal, Ahlam, and Dalia for the coffees we shared and the joy you spread. Love to you all.

Abbreviations

Abbreviation	Meaning
AD	Alzheimer's Disease
aFTLD-U	Atypical FTLD-U
AGD	Argyrophilic grain disease
ALS	Amyotrophic Lateral Sclerosis
BSA	Bovine Serum Albumin
bvFTD	behavioural variant frontotemporal dementia
C9orf72	Chromosome 9 open reading frame 72
CBD	Corticobasal Degeneration
cDNA	Complementary Deoxyribonucleic Acid
CHMP2B	Charged Multivesicular Body Protein 2B
CNT	Control
Co-IP	Co transfection Immunoprecipitation
DAB	3,3'-Diaminobenzidine tetrahydrochloride
DAPI	4', 6-diamidino-2-phenylindole
dIF	double labelling immunofluorescence
DLB	Dementia with Lewy Bodies
DN	Dystrophic Neurites
DNA	Deoxyribonucleic Acid
DPBS	Dulbecco's Phosphate-Buffered Saline
DPR	Dipeptide repeat proteins
DTT	DL-dithiothreitol
EDTA	Ethylenediaminetetraacetic acid
fALS	Familial Amyotrophic Lateral Sclerosis
FET	FUS, EWS and TAF15
FFPE	Formalin fixed paraffin embedded
FTD	Frontotemporal Dementia
FTLD	Frontotemporal Lobar Degeneration
FTLD-17	Chromosome 17 associated FTLD
FUS	Fused-in-sarcoma
GA	Glycine-Alanine
GAPDH	Glyceraldehyde 3-phosphate dehydrogenase
GCI	Glial Cytoplasmic Inclusions
GGT	Globular glial tauopathy
GP	Glycine-Proline
GR	Glycine-Arginine
GRN	Granulin gene
hnRNA	heterogenous nuclear RNA
hnRNP	heterogeneous nuclear ribonucleoprotein
IHC	Immunohistochemistry
IP	Immunoprecipitation
kDa	Kilo Dalton
MAPT	microtubule-associated protein tau
miRNA	micro-RNA
MND	Motor Neuron Disease
MRI	Magnetic resonance imaging
nfvPPA	Non-fluent Primary Progressive Aphasia
NGS	normal goat serum
NIFID	neuronal intermediate filament inclusion disease

NII	Neuronal Intranuclear Inclusions
NLS	Nuclear Localising Signal
NRS	normal rabbit serum
NSS	normal swine serum
PA	Proline-Alanine
PABP1	Polyadenylate-Binding Protein
PBS	phosphate buffer saline
PIs	Protease inhibitors
PPA	Primary Progressive Aphasia
PR	Proline-Arginine
PSP	progressive supranuclear palsy
RAM	rabbit anti-mouse biotinylated immunoglobulin
RANBP1	Ran binding protein 1 regulates the RanGTPase system
RIPA	Radio-Immunoprecipitation Assay
RNA	Ribonucleic Acid
RNAi	Ribonucleic Acid Interference
RRM	RNA Recognition Motif
sALS	Sporadic ALS
SARK	Sarkosyl
SCA	Spinocerebellar Ataxia
SDS	Sodium Deoxycholate
SG	Stress Granule
SILAC	Stable isotope labelling with amino acids in cell culture
siRNA	Small Interfering RNA
svPPA	Semantic variant Primary Progressive Aphasia
TAF15	TATA-binding protein-associated factor 15
TARDBP	Transactive response DNA-binding protein
TBS	Tris Buffered Solution
TDP-43	Trans-Activation response DNA-Binding protein-43
TIA-1	T Cell Intercellular Antigen 1
VCP	Valosin-containing protein
WB	Western Blot

Chapter 1 Introduction

1.1 Frontotemporal Dementia and Motor Neuron Disease

1.1.1 Overview

Frontotemporal dementia (FTD) is the third most common type of dementia in all age groups as well as the leading type of dementia in presenile cases after Alzheimer's disease (AD) and dementia with Lewy bodies (DLB). The most prominent characteristic of frontotemporal lobar degeneration (FTLD) is atrophy of the frontal and temporal lobes, which renders it an umbrella term for a group of neurodegenerative diseases characterised by behavioural changes or language deficits (Miyoshi, 2009, Bang et al., 2015). Arnold Pick (1892) was the first to describe FTLD in a patient with presenile dementia, aphasia and lobar atrophy. Two decades later, Alois Alzheimer (1911) recognised the characteristic pathological association of Pick bodies and hence named the clinicopathological entity Pick's Disease. From that point, Pick's disease was used as a synonym for FTLD until 1982, when Mesulam described a language subtype of the disorder that is now defined as primary progressive aphasia (Bang et al., 2015). According to the predominant clinical presentation, FTD can be classified into three major clinical subtypes, namely the behavioural variant (bvFTD) and two forms of primary progressive aphasia (PPA), that is, the non-fluent variant (nfvPPA) and the semantic variant (svPPA) (Mackenzie and Neumann, 2016). The clinical diagnosis of FTD is challenging due to the similarities of the associated behavioural changes to those seen in psychiatric disorders.

Abnormal protein aggregation in the neuronal cytoplasm is a key feature of most neurodegenerative diseases and a number of disease-specific pathological proteins were identified decades ago, for example, tau protein, which composes the neurofibrillary tangles of Alzheimer's disease. However, the protein composition of the ubiquitinated inclusions found in motor neuron disease (MND) and FTLD-U (the most common form of frontotemporal dementia) was not identified until 2006, when the trans-activation response DNA-binding protein-43 (TDP-43) was identified as the major component of these inclusions (Neumann et al., 2006b, Arai et al., 2006, Kwiatkowski et al., 2009, Vance et al., 2009), which led to the novel molecular classification of FTLD. In this chapter, I will discuss the clinical features and clinical classification of FTLD as well as the FTLD pathological and molecular classification according to recent findings. Thereafter, I will discuss the role of TDP-43 in the pathology of FTLD and the most promising

areas for therapeutic development. Finally, a brief overview of the heterogeneous nuclear ribonucleoproteins (hnRNPs) will be presented.

1.1.2 Clinical features of FTD

Clinically, FTD is classified into three types, namely the behavioural variant frontotemporal dementia (bvFTD), the semantic variant primary progressive aphasia (svPPA) and the non-fluent variant primary progressive aphasia (nfvPPA). FTLD is further classified into frontal lobar degeneration, Pick FTLD and FTLD with motor neuron disease (FTLD-MND). MND refers to a group of diseases wherein the upper and/or lower motor neurons are affected. FTLD is often associated with MND, specifically with the narrower spectrum of MND known as amyotrophic lateral sclerosis (ALS). The prevalence of FTLD ranges from 3% to 26% in most studies (Lambert et al., 2014, Hodges et al., 2003, Kansal et al., 2016). It has been estimated by the World Health Organization (WHO) (2017) that dementia rates will double every year, reaching 135.5 million cases in 2050. The epidemiology of FTD is summarised in Table 1. The chance of survival in FTD varies among the different FTLD phenotypes, with FTLD with MND having the shortest average survival period of 2.5 years while the survival period ranges from 8–12 years among the rest of the FTLD phenotypes (Kansal et al., 2016). The survival rate is not affected by either age or gender, and the effect of education was found to be equivocal. Further, the survival heterogeneity is not completely explained by the heterogeneity of the FTLD phenotypes (Kansal et al., 2016).

Table 1: Epidemiology of frontotemporal dementia (Bang et al., 2015)

	Age	Prevalence
Patients with early dementia	<65	3–26%
US general population	45–64	12–22 per 100,000
UK general population	45–64	3–26 per 100,000
Japan, UK and Netherlands	30–64	1–16 per 100,000

The diagnostic criteria for FTD outline the clinical symptoms, imaging features and genetically confirmed diagnosis. Applying these diagnostic criteria increases the possibility of identifying related neuropathology. As frontotemporal dementia progresses, global cognitive impairment develops and the symptoms of the three clinical variants can converge. Over time, patients develop motor deficits, including parkinsonism and MND. At the end stage of the disease, patients experience difficulty moving, feeding and swallowing, and death is typically caused by pneumonia or other secondary infections (Bang et al., 2015). The emphasis of this study is on the FTLD-MND spectrum; however, a brief review of the clinical aspects of other types of FTLD will be performed.

1.1.2.1 Behavioural variant frontotemporal dementia (bvFTD)

The most pronounced early symptoms of this type of FTD include personality changes, disinhibition and apathy. The behavioural disinhibition can result in socially inappropriate behaviour and/or impulsive or careless actions. It can also include the development of new criminal behaviours, for example, theft, and a tendency to make embarrassing personal remarks. The decreased inhibition can also lead to inappropriate fiscal decisions that can result in financial ruin. Further, patients usually have reduced libido, although they may make inappropriate sexual comments. Apathy can be mistaken for depression, since it manifests as a decreased interest in social interaction, work, hobbies and hygiene. Patients also show lower responsiveness to emotions and the needs of other people as well as a loss of sympathy and empathy towards their relatives and friends. Additionally, they can show stereotyped behaviours such as repetitive movements or the repetitive use of verbal phrases. Increased consumption of sweet foods or binge eating can be a reflection of hyperorality in patients with the behavioural variant of FTD. The course of this disease type is very slow, with the progression of the cognitive deficit taking years and normal positron emission tomography (PET) and magnetic resonance imaging (MRI) scans often being seen at the outset. Some of these patients suffer primary psychiatric disorders, while others may have a slow sporadic or genetic form of FTLD. The pathogenesis of the behavioural type of FTD mainly involves the right temporal lobe (Bang et al., 2015, Kipps et al., 2010).

1.1.2.2 Primary progressive aphasia (PPA)

The initial phase of this type of FTD includes a gradual, progressive decline in linguistic skills. During the first few years, the language deficit can impact the naming of objects, language production, syntax or word understanding as detected through conversations or language assessment, which has a significant detrimental effect on daily living activities. If the patient presents with visuospatial or episodic visual memory impairments, then Alzheimer's disease should be considered. Patients usually show no behavioural disturbance during the initial phase of this type of FTD (Mesulam, 2001, Bang et al., 2015).

1.1.2.2.1 Semantic variant primary progressive aphasia (svPPA)

Semantic dementia is a syndrome characterised by semantic aphasia and associative agnosia, which is an inability to interpret sensations and therefore an inability to identify objects (Neary et al., 1998). The semantic loss leads to impaired word finding and comprehension, which mainly results from the asymmetrical degeneration of the anterior temporal lobes and amygdala (Seeley et al., 2005). The left temporal lobe (semantic) variant is approximately three times more common than the right temporal (behavioural) type of FTD. During the initial phase of the disease, the other language domains are spared and patients retain fluent speech and correct grammar. Further, the people and object recognition deficits extend beyond the visual and tactile domain to olfactory and gustatory clues. With disease progression, behavioural changes may manifest, including emotional withdrawal, irritability, insomnia and strict or selective eating. In the left temporal lobe variant, the right side functions are heightened. Therefore, patients will develop visual compulsions, for example, repetitive playing with puzzles and painting. Yet, patients with the right lobe variant can develop verbal compulsions involving words and symbols, such as writing telephone numbers and letters or playing solitaire (Bang et al., 2015).

1.1.2.2.2 Non-fluent variant primary progressive aphasia (nfvPPA)

The main characteristic of this type of FTD is laboured, slow and stuttered speech production with the misuse or omission of grammar. Speech and sound errors are often made by patients, including substitutions, insertions, deletions, transposition and distortion. Although patients experience no trouble in understanding simple sentences, they can misunderstand sentences with complex syntactic constructions. Intact writing is maintained in some patients despite the

prominent impairment in terms of the spoken language. Object knowledge and single word recognition are not affected in this type of FTD (Bang et al., 2015, Gorno-Tempini et al., 2011).

1.1.2.3 Frontotemporal dementia with motor neuron disease (FTLD-MND)

Dementia in MND patients has been intermittently reported over the last 100 years. However, the concept of an FTLD-MND interrelationship has only fully emerged during the last decade as more pathological and genetic discoveries have enforced their specific association. Nowadays, FTLD-MND is recognised as a dementia syndrome that presents a unique set of diagnostic and management challenges. Some 10–15% of MND patients are diagnosed with FTD, although mild cognitive impairment can be recognised in a higher proportion of MND patients (Burrell et al., 2016, Mitsuyama and Inoue, 2009). Further, 40% of FTD patients develop mild MND symptoms (Burrell et al., 2011). MND symptoms arise more frequently in patients with the behavioural variant of FTD when compared to the semantic or non-fluent variant primary progressive aphasia. Typically, patients will present with upper and lower motor neuron signs. The upper motor neuron signs include hyperreflexia, spasticity and extensor plantar response, while the lower motor signs include muscular atrophy, weakness and fasciculation. FTD patients also present with clinical features of corticobasal syndrome, which is characterised by asymmetrical parkinsonism, sensory-motor cortical dysfunction, dystonia and alien-limb syndrome. In addition, FTD patients can display the clinical features of supranuclear palsy syndrome, which is characterised by postural instability with a tendency for falling and decreased eye movement velocity. Apathy, impulsivity and executive behavioural dysfunction are all common in FTLD-MND patients (Burrell et al., 2011, Bang et al., 2015, Hsieh et al., 2016). The diagnostic criteria for the FTD clinical subtypes are summarised in Figure 1, which is adapted from (Bang et al., 2015).

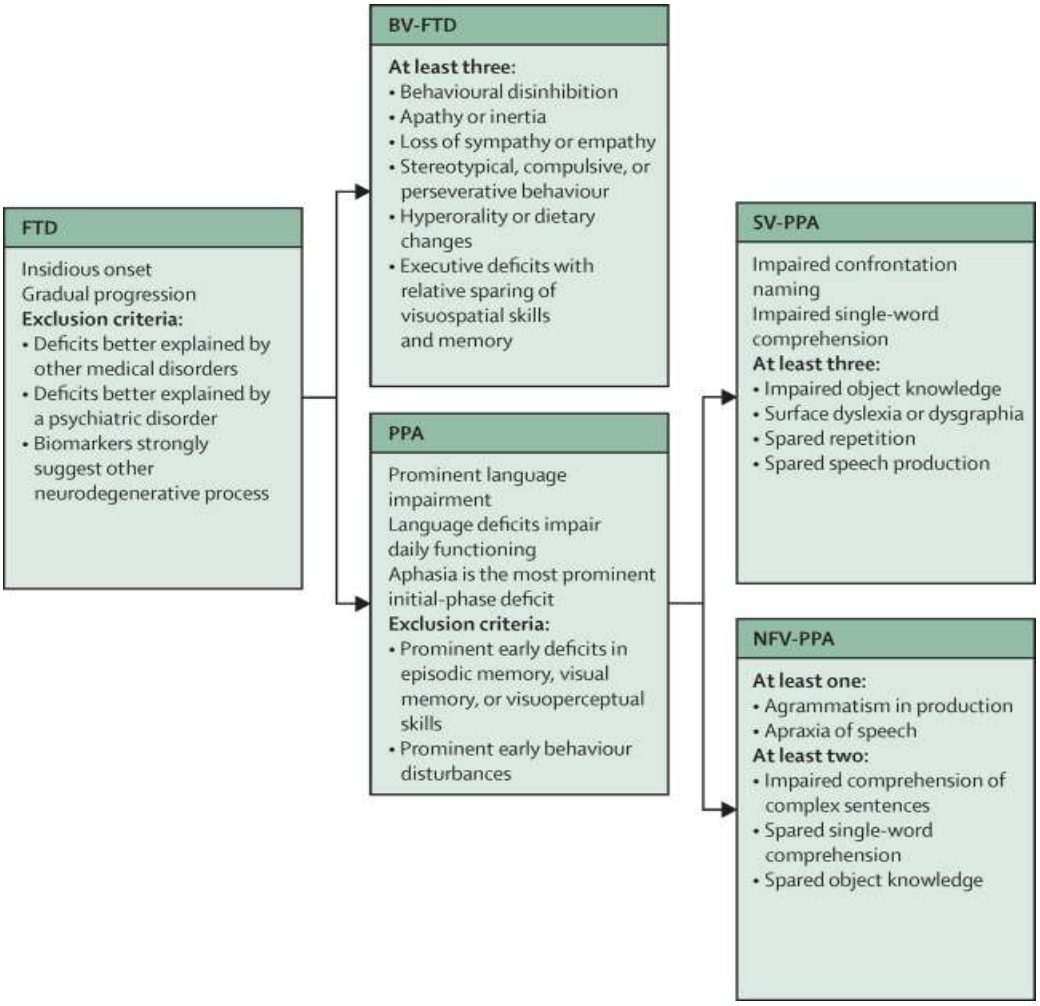

Figure 1: Diagnostic criteria for the clinical diagnosis of FTD (Bang et al., 2015).

1.1.3 Pathological subtypes of FTLD

Neuronal loss, microvacuolar changes and gliosis of the frontal lobes, anterior temporal lobes, insular cortex and anterior cingulate gyrus represent the common gross anatomy characteristics of FTLD. Advances in immunohistochemistry and molecular biology techniques have led to the further classification of the FTLD spectrum disorders according to the predominant neuropathological protein deposition in the brain of FTLD patients. Three main pathological categories of FTLD have been identified. The majority of FTLD cases are characterised by cytoplasmic aggregates containing the microtubule-associated protein tau (MAPT) (FTLD-Tau),

the TAR DNA-binding protein with a molecular weight of 43 kDa (TDP-43) (FTLD-TDP) or, more rarely, the protein fused in sarcoma (FUS) (FTLD-FUS). A very small proportion of FTLD cases have a ubiquitin-only or p62-only positive pathology or even lack aggregate pathology altogether. Some 40% of FTLD cases are familial, with one-third to one-half of the familial cases following an autosomal dominant inheritance pattern. A number of mutations that are linked to FTLD have been identified, including within the following genes: *MAPT, TARDBP, VCP, CHMP2B* and *C9orf72* (DeJesus-Hernandez et al., 2011b, Renton et al., 2011, Kabashi et al., 2008, Baker et al., 2006, Cruts et al., 2006a, Johnson et al., 2010, Skibinski et al., 2005). The pathological subtypes of FTLD will be briefly reviewed in this chapter, although a more detailed review of FTLD-TDP will be presented in Chapter 4. The continuum of ALS and FTD is represented according to their overlapping symptoms, common genetic mutations and underlying pathology in Figure 2.

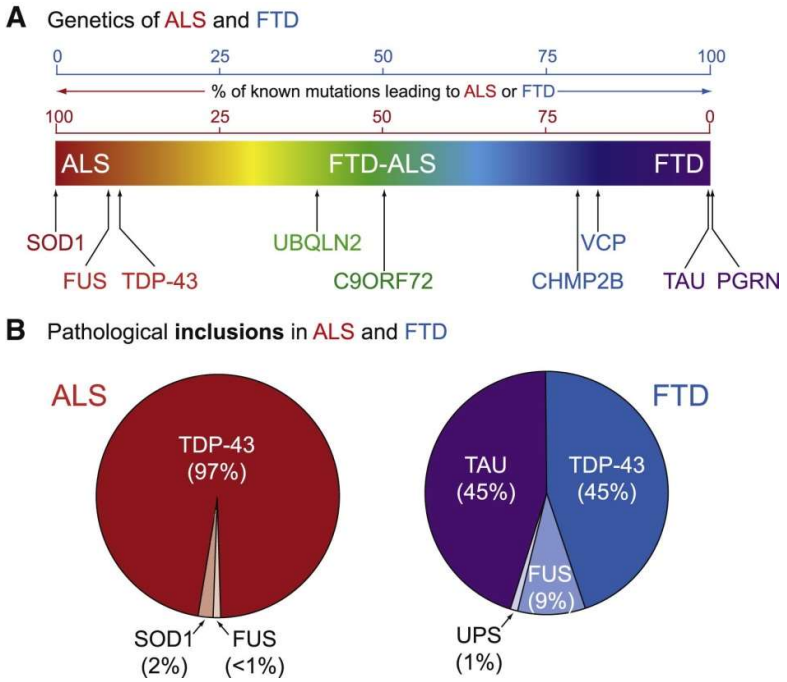

Figure 2: (A) Represents the continuum of ALS and FTD as a broad neurodegenerative disorder spectrum, with the disorders presenting as extremes of a spectrum of overlapping clinical symptoms (ALS in red and FTD in purple). The major identified genetic causes of ALS and FTD are plotted according to the ratio of known mutations that give rise to ALS or FTD. (B) Represents the proportion of pathological protein inclusions in ALS and FTD according to the major protein aggregation. The inclusions of TDP-43 and FUS/TLS in ALS and FTD reflect the pathological overlap between ALS and FTD. The figure is adapted from (Ling et al., 2013).

1.1.3.1 FTLD-Tau

Tau is a microtubule-associated protein coded by the *MAPT* gene on chromosome 17q21 and some 36–50% of FTLD cases show tau pathology (Bang et al., 2015, Ling et al., 2013). Tau promotes the assembly and stability of the microtubules, thereby maintaining neuronal integrity and axoplasmic transport (Lee and Leugers, 2012). Low levels of tau are expressed in the glial cells; however, it is predominantly expressed in the axons. The tau gene contains 16 exons, while there are six tau isoforms expressed in the adult human brain via the alternative splicing of exons 2, 3 and 10. The accumulation of abnormal hyperphosphorylated tau characterises a group of neurodegenerative diseases referred to as the tauopathies, which include FTLD-Tau. The tau aggregates differ in terms of the isoform content and the degree of phosphorylation among the tau disorders, which is believed to explain the variation in the morphology of inclusions and cellular specificity (Lee and Leugers, 2012). The most common subtypes of FTLD-Tau are Pick's disease, progressive supranuclear palsy (PSP) and corticobasal degeneration (CBD). Pick's disease constitutes 5% of all dementia cases and 30% of all FTLD-Tau cases. Pick's disease is characterised by the knife-edge atrophy of the frontal, temporal and cingulate gyrus, while the parietal lobe is better preserved (Bang et al., 2015); (Mackenzie and Neumann, 2016, Lee and Leugers, 2012). Pick's disease more commonly presents as the behavioural variant of FTD or the non-fluent variant of primary progressive aphasia and it is usually not accompanied by MND (Piguet, 2013). The histological characteristics of Pick's Disease include severe neuronal loss, swollen neurons (Pick cells) and large spherical argyrophilic cytoplasmic inclusions in the neurons (Pick bodies). Pick bodies are most numerous in layers 2 to 4 of the neocortex and they mainly contain the 3R tau isoform. Pick bodies can also be detected in the granule and pyramidal cells of the hippocampus (Kovacs et al., 2012).

CBD accounts for about 35% of all FTLD-Tau cases and it mainly presents with bvFTLD, nfvPPA or both (Kim et al., 2012, Bang et al., 2015). It is characterised by bradykinesia, dystonia, rigidity, alien-limb phenomenon, apraxia and cortical sensory signs. Asymmetrical and focal cerebral cortex atrophy, depigmentation of the substantia nigra and atrophy of the globus pallidus are the typical gross features of a CBD patient's brain. The main histopathological feature is the presence of ring-shaped collections of short cell processes, which are known as astrocytic plaques, due to the accumulation of pathological tau in the distal processes of the astrocytes (Sha et al., 2006). In addition, the pathology shows various nuclear and cytoplasmic inclusions, abundant thread

pathology, coiled bodies and ramified astrocytes to be characteristic of CBD. The pathology is predominant in the cerebral cortex and white matter and it is restricted to the basal ganglia, diencephalon and midbrain in the subcortical regions (Dickson et al., 2002).

PSP accounts for approximately 31% of all cases of FTLD-tau (Josephs et al., 2011). The cortical atrophy is milder than in CBD, although the subcortical atrophy is more severe in PSP at subcortical levels, specifically the globus pallidus, subthalamic nucleus and brainstem nuclei. The histopathological characteristics include neuronal granular inclusions, globose tangles and tufted astrocytes (Rebeiz et al., 1968, Bang et al., 2015).

Globular glial tauopathy (GGT) is a rare 4R tauopathy, which has previously been reported under a variety of different terminologies, including sporadic multiple system tauopathy with dementia. Clinically, GGT may present as bvFTLD with or without extrapyramidal signs, primary lateral sclerosis or as a combination of the two (Ahmed et al., 2013). The tau pathology in GGT is widespread in the white matter, with oligodendrocyte and astrocyte inclusions that have a distinctive globular morphology. The tau pathology in the neurons is mainly represented by diffuse immunoreactivity or globular inclusions (Mackenzie and Neumann, 2016).

Argyrophilic grain disease (AGD) is a sporadic 4R tauopathy that usually presents as mild amnestic dementia, slowly progressive dementia and late onset dementia (Tolnay and Frank, 2007). AGD patients rarely present with bvFTD despite the presentation of the kind of emotional and personality changes that are common in AGD (Tsuchiya et al., 2001, Ishihara et al., 2005). The histopathological hallmark in AGD is the presence of small dot-like spindle-shaped structures (grains) that are tau immunoreactive and argyrophilic. The grains are most abundant in the temporal limbic neocortex and amygdala; however, they may extend to the adjacent temporal neocortex. The grain structures are thought to represent degenerating dendrites (Mackenzie and Neumann, 2016).

Another type of FTLD-Tau is caused by *MAPT* mutations, which result in autosomal dominant FTLD and parkinsonism associated with chromosome 17 (FTLD-17). About 10% of all familial FTLD cases are caused by *MAPT* mutations. The mutations are either deletions or missense in exons 1, 9, 10, 11, 12 or 13 or in the intron following exon 10. FTLD-17 patients usually present with atypical parkinsonism with a combination of personality and behavioural changes and cognitive dysfunction. The neuropathological hallmark of FTLD-17 is the presence of glial hyperphosphorylated tau inclusions in the cortical and subcortical grey and white matter. The

inclusion morphology, biochemistry and anatomical distribution overlap with those of the sporadic tauopathies, as do the clinical features among families in relation to specific mutations (Wszolek et al., 2006, Ghetti et al., 2011). Generally, mutations in exons 9, 11, 12 and 13 cause dementia and they are predominantly neuronal inclusions in the form of either Pick bodies with 3R tau composition or AD-like neurofibrillary tangles (NFT) with both 3R and 4R tau isoforms. In contrast, mutations affecting the alternative splicing of exon 10 lead to neuronal and glial pathology that resembles PSP and CBD with a relatively increased 4R tau isoform. The clinical presentation is commonly associated with prominent parkinsonism (Mackenzie and Neumann, 2016).

1.1.3.2 FTLD-TDP

Aggregates containing the transactive response DNA-binding protein with a molecular weight of 43 kDa (TDP-43) account for approximately 50% of all cases of FTLD (FTLD-TDP). TDP-43 is a 414 amino acid DNA/RNA-binding protein that is involved in multiple aspects of RNA processing, including transcription, splicing, transport and RNA stabilisation (Buratti et al., 2010). TDP-43 has been identified as the major component of the ubiquitin-positive, tau-negative inclusions detected in FTLD cases referred to as FTLD-U and most cases of ALS (Arai et al., 2006); (Neumann et al., 2006b). The pathological aggregates of TDP-43 show abnormal modifications of TDP-43 that include ubiquitination, hyperphosphorylation and N-terminal truncation (Neumann et al., 2006b); Hasegawa et al., 2008; (Neumann et al., 2009a, Hasegawa et al., 2008). The major pathological hallmark of FTLD-TDP is the loss of the normal diffuse nuclear staining of TDP-43 and the presence of TDP-43-immunoreactive neuronal cytoplasmic inclusions (NCI) and dystrophic neurites (DN). TDP-43 neuronal intranuclear inclusions (NII) can also be present, particularly in cases with a positive familial history due to progranulin mutations. In addition, TDP-43 inclusions are ubiquitin- and p62-immunoreactive in the absence of other proteins associated with other neurodegenerative diseases. Furthermore, the TDP-43 pathology demonstrates glial cytoplasmic inclusions (GCI) in the oligodendrocytes (Neumann et al., 2007a), delicate wispy neurites (Hatanpaa et al., 2008) and diffuse neuronal cytoplasmic staining (pre-inclusions) (Brandmeir et al., 2008). Typically, TDP-43 inclusions are abundant in the frontotemporal neocortex and the granule cells of the dentate gyrus of the hippocampus; however, subcortical pathology is not uncommon (Geser et al., 2009, Josephs et al., 2009). Figure 3 demonstrates the identified pathology of TDP-43 in the ubiquitin-positive, tau-negative inclusions in the frontal cortex and

hippocampus of FTLD-U cases. Figure 4 shows the biochemical signature of pathological TDP-43 as discovered by Neumann et al. (2006).

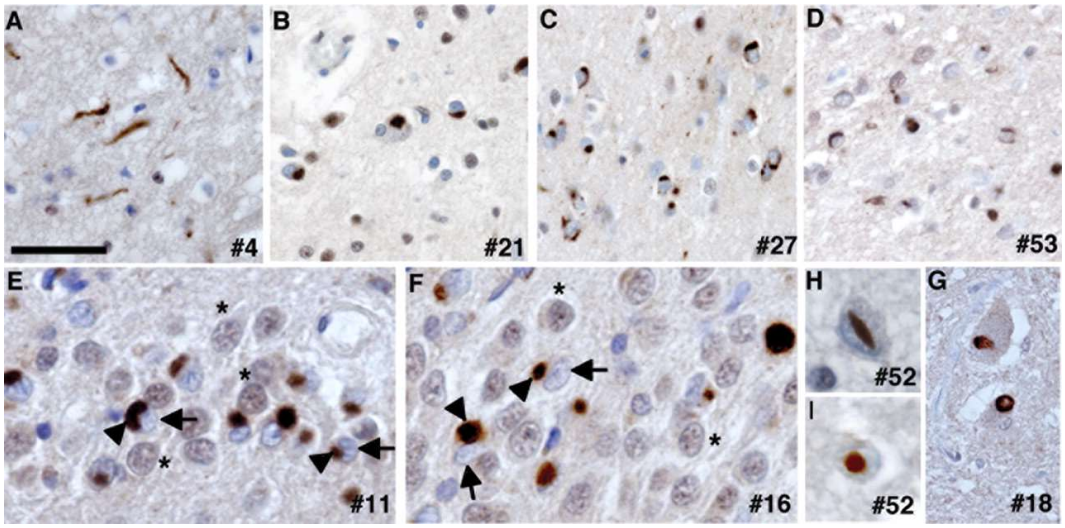

Figure 3: Spectrum of FTLD-U neuropathology as detected by anti-TDP-43 in the frontal cortex of different types of FTLD-U (A–D). TDP-43 strongly stains the ubiquitin inclusions in the hippocampal dentate granule neurons (E and F). The clearing of nuclear TDP-43 (arrows) in ubiquitin-bearing neurons when compared to that of normal neurons (*) (E and F). TDP-43 lentiform inclusion (H), round TDP-43 inclusion (G) and intranuclear TDP-43-positive inclusion and Lewy body-like round inclusions in the motor neurons of the spinal cord (I). Scale bar in (A) corresponds to 50 µm [(A) to (D) and (G)], 25 µm [(E) and (F)] and 20 µm [(H) and (I)]. (Neumann et al., 2006b).

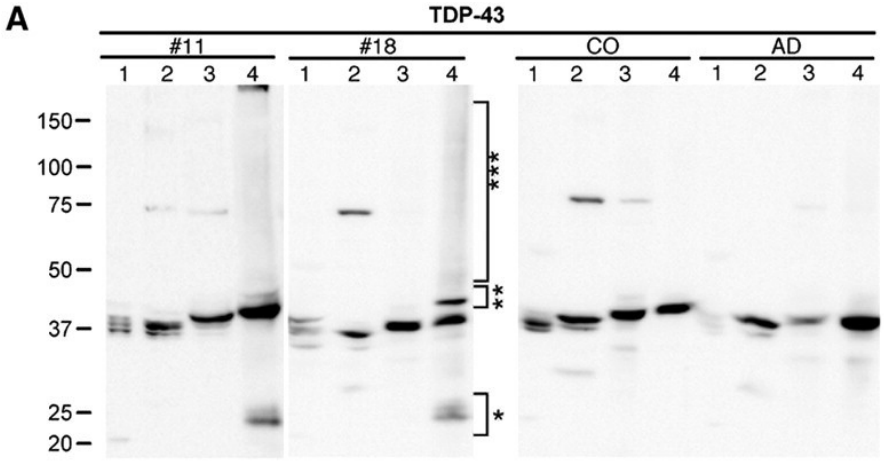

Figure 4: The biochemical signature of pathological TDP-43 in sporadic and familial FTLD-U. (A) Immunoblots of sequential extracts from the frontal cortex of FTLD-U types 1 and 2 with rabbit anti-TDP-43 showed pathologic ~25-kD bands (*), 45-kD bands (**), and high M_r smear (***) in the urea fraction. Lane 1, low salt; 2, high salt with Triton x-100; 3, sarkosyl; and 4, urea (Neumann et al., 2006b).

The variation in the morphology and cortical laminar distribution of the TDP-43 inclusions led to the further classification of FTLD-TDP into four major subtypes (types A, B, C and D) (Sampathu et al., 2006, Mackenzie et al., 2011b). The histopathological classification of FTLD-TDP was described by two different groups depending on the morphology and distribution of the ubiquitin-positive, tau-negative inclusions in FTLD cases (Sampathu et al., 2006, Mackenzie et al., 2006). In 2011, a new harmonised classification was proposed by the authors of the original papers (Mackenzie et al., 2011b). Briefly, type A FTLD-TDP is characterised by crescentic or oval NCI and numerous short DN that are primarily concentrated in layer 2 of the neocortex. Lentiform NII can be seen; however, they are not a consistent feature of this subtype. Type B FTLD-TDP is characterised by a moderate number of NCI throughout all the cortical layers and very few DN. Type C has very few NCI and elongated DN in the upper cortical layers. Type D FTLD-TDP refers to the pathology associated with *VCP* mutations and it is characterised by frequent lentiform NII and numerous short DN (Mackenzie et al., 2011b). The pathological subtypes of FTLD-TDP cases have been correlated with the clinical phenotypes of FTLD-TDP. In addition, the identified genetic mutations provided a good marker for the underlying pathology seen in the distinguished FTLD-TDP subtypes (Sieben et al., 2012a). Table 2 summarises the correlation between the FTLD-TDP pathological subtypes, clinical phenotypes and genetic mutations identified as underlying causes of FTLD-TDP.

Table 2: Correlation between the FTLD-TDP subtypes' neuropathological characteristics, clinical phenotypes and genetic mutations (Sieben et al., 2012a)

Subtypes of FTLD-TDP	Associated gene mutation	Associated clinical phenotype	Neuropathological findings
Type A	*GRN*, *C9orf72*	bvFTD (PNFA)	Many NCI and DN in superficial cortical layers (layer II) NII in superficial cortical layers GCI.
Type B	*C9orf72*	FTD-MND bvFTD	NCI throughout the entire cortical thickness. NCI in the hypoglossal nucleus and ventral horn of the spinal cord. Pre-inclusions.
Type C		SD (bvFTD)	Long DN in superficial cortical layers. Few NCI and NII.
Type D	*VCP*	IBMPFD	Many NII and DN throughout the entire cortical thickness. Few NCI.

The presentation of FTD varies among the FTLD-TDP subtypes. FTLD-TDP is considered to be the most common FTLD molecular subtype, accounting for approximately 50% of all FTLD cases. Some 50% of all nfvPPA and 25% of all CBD cases were recognised as type A FTLD-TDP. Type

A represents only a small proportion of the bvFTD cases with or without MND. Yet, two-thirds of nfvPPA and 25% of bvFTD cases were identified as FTLD-TDP type B based on the pathology (Seeley et al., 2008, Kim et al., 2012). Approximately 90% of all svPPA (left temporal involvement) or temporal variant bvFTD (right temporal involvement) cases were recognised as type C FTLD-TDP (Mackenzie et al., 2011b, Rohrer et al., 2010). Figure 5 summarises the relationship between the clinical FTD presentation and the underlying neuropathology.

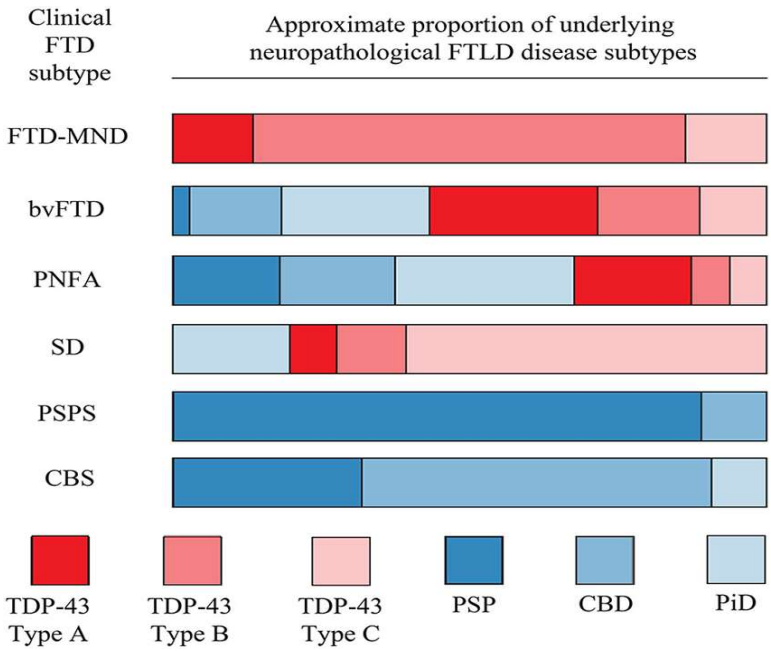

Figure 5: Relationship between the clinical FTD presentation and the underlying FTLD neuropathology. For each clinical subtype on the left, the bar is divided to show the approximate proportion of cases that are underpinned by the indicated disease neuropathology. Profound neuropathological heterogeneity exists for many clinical subtypes, particularly bvFTD and PNFA. This figure is based on data from Josephs et al. (2011). The diagram is adapted from (D'Alton and Lewis, 2014).

1.1.3.2.1 Granulin gene mutation (GRN)

Progranulin is a secreted growth factor with many functions that is cleaved in order to generate the pro-inflammatory granulin subunits (De Muynck and Van Damme, 2011). Mutations in the *GRN* gene were identified in 2006 as the cause of 5–20% of all FTLD cases and they form the basis of families with autosomal-dominant FTLD linked to chromosome 17 that are not due to *MAPT* mutations (Cruts et al., 2006b). The *GRN* pathogenic mutations all result in null alleles, which leads to decreased levels of functional progranulin (haploinsufficiency). The clinical presentation varies significantly, even among members of the same family. Patients with *GRN* mutations commonly present with bvFTLD or nfvPPA with some degree of parkinsonism. ALS is

exceptionally rare with *GRN* mutations (Mackenzie, 2007a). The TDP-43 pathology is consistent with FTLD-TDP type A with abundant subcortical pathology, particularly in the striatum, and it is often associated with hippocampal sclerosis and numerous delicate DN (Cairns et al., 2007, Mackenzie, 2007a).

1.1.3.2.2 C9orf72 expansion mutations

The abnormal expansion of a GGGGCC (4G2C) hexanucleotide repeat in a non-coding region of the *C9orf72* gene was identified in 2011 as the most common genetic cause of familial and sporadic forms of both FTD and ALS, as well as the basis of most families in which both FTLD and ALS are present (DeJesus-Hernandez et al., 2011a, Renton et al., 2011). The clinical presentation is commonly associated with bvFTLD; however, a wide range of neurological features are now recognised, including memory deficits, extrapyramidal movement disorders, psychosis and nfvPPA (Hsiung et al., 2012). The clinical features may vary tremendously among members of the same family, with carriers of the *C9orf72* expansion mutation presenting with the typical features of ALS or FTLD or a combination of both. The pattern of neocortical TDP-43 pathology is most commonly type B (Figure 2g and h); however, a subset of cases (usually older patients without clinical ALS) show features more consistent with FTLD-TDP type A or a combination of types A and B (Hsiung et al., 2012, Mann et al., 2013). *C9orf72* cases demonstrate a unique and highly specific feature in addition to the TDP-43 pathology, namely the presence of NCI and NII that are negative for TDP-43; however, they are immunoreactive for ubiquitin and p62 (DeJesus-Hernandez et al., 2011a, Al-Sarraj et al., 2011). These inclusions are now known to be the result of the unconventional repeat-associated non-ATG-initiated (RAN) translation of the hexanucleotide repeat, which is triggered when it is massively expanded (Mori et al., 2013a, Gendron et al., 2013). Five different dipeptide repeat proteins (DPR) are generated by various reading frame translations that occur in the sense and anti-sense RNA strands: glycine-alanine (GA), glycine-arginine (GR), glycine-proline (GP), proline-alanine (PA) and proline-arginine (PR). GP is generated by translation in both directions. All the TDP-43-negative inclusions in all *C9orf72* cases are labelled by antibodies to the DPRs; however, the GA, GP and GR peptides generated from the sense transcripts are more abundant, while the PA and PR, which are generated from the antisense transcripts, are relatively rare (Davidson et al., 2016, Gomez-Deza et al., 2015, Schludi et al., 2015). The anatomical distribution of the DPR inclusions shows no correlation with

the regional pattern of TDP-43 pathology and it is highly consistent among cases regardless of the clinical features. The DPR pathology, including NCI, dot-like NII and short DNs, is abundant in all regions of the cerebral neocortex, limbic cortex and cerebellar cortex, whereas it is more variable and modest in the thalamus, basal ganglia and upper brainstem.

The DPR pathology is extremely rare in the lower brainstem and spinal cord (Schludi et al., 2015, Mackenzie et al., 2013, Davidson et al., 2014). An additional consistent feature of *C9orf72* expansion cases is the presence of intracellular RNA aggregates. These RNA foci are present in the nuclei of approximately 50% of neurons in specific anatomical regions and they are rarely seen in the cytoplasm of neurons or in glial cells. The RNA foci are composed of sense and antisense DPR transcripts; however, the role of these RNA foci in the pathogenesis of *C9orf72* FTLD-TDP remains unclear. Further, the relative significance of TDP-43 in relation to DPR in the pathogenesis of FTLD-TDP in *C9orf72* expansion cases is a source of much debate (Davidson et al., 2014, DeJesus-Hernandez et al., 2011a, Mackenzie and Neumann, 2016, Lee et al., 2013b).

1.1.3.2.3 Valosin-containing protein (VCP) mutations

VCP is a member of the AAA-ATPase gene superfamily, which functions as a molecular chaperone in specific cellular activities that are directly or indirectly regulated by the UPS. Mutations in the *VCP* cause a rare familial syndrome in which inclusion body myopathy, Paget's disease of the bone and FTD with variable penetrance are seen (IBMFD) (Kimonis et al., 2008). The pathology of TDP-43 in cases with *VCP* mutations is specific to FTLD-TDP type D and it is characterised by numerous NII and DN in the neocortex as well as an absence of pathology in the hippocampus (Mackenzie and Neumann, 2016).

1.1.3.2.4 TARDBP mutations

Transactive response DNA-binding protein *(TARDBP*) is the gene encoding the TDP-43 protein. Many different mutations in the *TARDBP* have been identified in many populations with different geographical origins (Sreedharan et al., 2008, Van Deerlin et al., 2008). Over 40 pathogenic mutations in the *TARDBP* have been identified; however, they are considered to be rare causes of the disease because they comprise only about 4% of familial ALS (fALS) cases and 1.5% of sporadic ALS (sALS) (Gendron et al., 2013). Most of these mutations are missense in exon 6 and

they cause single amino acid substitutions in the C-terminus that alter the protein-protein interaction and hence do not affect nucleic acid binding (Mackenzie et al., 2010b). The *TARDBP* mutations are mostly linked to a pure-ALS clinical presentation; however, they have been found in familial and sporadic FTLD cases (with and without MND), in bvFTLD associated with supranuclear palsy and in parkinsonism. Although *TARDBP* mutations have been reported in cases of clinical FTLD presentation, most of these reports lack a neuropathological evaluation. The pattern of TDP-43 pathology in cases with *TARDBP* mutations is unusual, with complete sparing of the hippocampal dentate fascia and the presence of NCI, NII and DN predominantly in the subcortical regions, while DN are mostly present in the neocortex (Borroni et al., 2009, Kovacs et al., 2009, Mackenzie and Neumann, 2016).

1.1.3.2.5 Other mutations associated with FTLD-TDP

Mutations in many other genes that have been identified as rare causes of ALS have also been identified in FTLD patients, including *sequestosome 1* (Kovacs et al., 2016), *ubiquilin-2* (Deng et al., 2011), *TANK-binding kinase 1* (Gijselinck et al., 2015) and *optineurin* (Shen et al., 2015). There are currently insufficient data concerning the pattern of TDP-43 pathology with these mutations; however, it was reported that the TDP-43 pathology for a patient with a *TANK-binding kinase 1* mutation is inconsistent with FTLD-TDP type A or B (Mackenzie and Neumann, 2016).

1.1.3.3 Fused in sarcoma FTLD (FTLD-FUS)

FTLD-FUS accounts for 5–10% of all FTLD cases. It is predominantly associated with early-onset FTLD with severe disinhibition and, in some cases, with psychosis and behavioural abnormalities; however, language deficits are absent in FTLD-FUS patients (Mackenzie et al., 2011a). Anatomically and histopathologically, FTLD-FUS is characterised by severe striatal atrophy and abundant FUS-immunoreactive inclusions in the dentate gyrus (Roeber et al., 2008). FUS was initially discovered as a component of the fusion oncogenes, which cause specific types of human cancer. FUS belongs to the heterogeneous nuclear ribonucleoprotein (hnRNP) family and it is involved in many aspects of RNA and DNA processing, including transcription and transport (Calvio et al., 1995, Chaudhury A, 2010). The normal physiological functions of FUS in the brain are not yet fully understood; however, functional studies have suggested that it is involved in RNA transcript regulation, which is important for neuronal structure, dendritic integrity and plasticity.

Mutations in the FUS were discovered in 2009 to cause a small percentage of ALS cases (ALS-FUS) (Vance et al., 2009, Kwiatkowski et al., 2009). The clinical and pathological overlap between FTLD and ALS as well as the high level of similarity in the functional homology between TDP-43 and FUS suggested FUS as a candidate pathological protein in the 5–10% of FTLD cases that are not characterised by tau or TDP-43. Several subsequent studies showed that the characteristic cellular inclusions seen in the majority of the tau/TDP-negative FTLD subtypes were FUS-immunoreactive (Neumann et al., 2009b). In addition, FUS was also recognised in neuronal intermediate filament inclusion disease (NIFID) (Neumann et al., 2009c), basophilic inclusion body disease (BIBD) and atypical FTLD-U (aFTLD-U) (Munoz et al., 2009). Subsequently, it was demonstrated that FUS inclusions can also contain Ewing's sarcoma (EWS) and TATA-binding protein-associated factor 15 (TAF15) (collectively, FUS, EWS and TAF15 are known as the FET protein family). FTLD-FUS inclusions have also been shown to contain transportin 1 (TRN1), which is the protein responsible for the nuclear import of the FET proteins (Brelstaff et al., 2011, Neumann et al., 2011, Neumann et al., 2012). Indeed, it has been suggested by one research group that aFTLD-U, NIFID and BIBD could be classified under the broad nomenclature of FTLD with FET-positive inclusions (FTLD-FET) (Rademakers et al., 2012). Recently, evidence has been provided that the accumulated FET proteins in FTLD are modified after they are translated, which may be related to the pathogenesis of FTLD-FET. The most common abnormal post-translation modifications include the reduced methylation of the arginine residue in the arginine-glycine rich region, which is adjacent to the nuclear localisation signal and results in the abnormal binding of FET to TRN1 (Dormann et al., 2012) and may hence explain why the FET proteins colocalise with FUS in FTLD. Yet, mutations that selectively disrupt the nuclear localisation signal of FUS result in the weak binding of FUS to TRN1, which in turn results in the abnormal accumulation of FUS in the cytoplasm in ALS-FUS (Dormann et al., 2010, Neumann et al., 2011). The role of the post-translation modification of FET proteins in FTLD cases is currently unknown (Mackenzie and Neumann, 2016).

1.2 TDP-43 and TDP-43 Proteinopathy

1.2.1 Background

TDP-43 is a 414 amino acid nuclear factor protein with a molecular weight of 43 kDa, which is encoded by the *TARDBP* gene on ch1p36.2. It consists of five coding exons and one non-coding exon. Structurally, it is characterised by two RNA recognition motifs known as RRM1 and RRM2 (RRM1: ~aa 106–175 and RRM2: ~aa 191–262) that have the capability to bind nucleic acids. TDP-43 also has a nuclear localisation sequence (NLS) and a nuclear export signal. In addition, it contains a glycine-rich C-terminal region (~aa 274–413), which allows it to bind single-stranded DNA, RNA and proteins (Mackenzie et al., 2010b, Hasegawa et al., 2011, Ayala et al., 2005). The C-terminal tail of TDP-43 resembles that of the heterogeneous ribonucleoproteins and it interacts with other hnRNP proteins. The C-terminal domain is essential for the exon skipping and splicing inhibitory function of TDP-43. TDP-43 is widely expressed, highly conserved and predominantly localised to the nucleus; however, it is continuously shuttling between the nucleus and cytoplasm. This process is partly regulated by the nuclear export signal motifs and nuclear localisation signal (Winton et al., 2008, Da Cruz and Cleveland, 2011, Warraich et al., 2010, Sephton et al., 2012). TDP-43 can regulate the stability of its own mRNA, which provides an autoregulation mechanism for its own levels. In addition, TDP-43 influences diverse cellular functions by means of regulating the splicing and stability of many other transcripts (Polymenidou et al., 2012, Ayala et al., 2011b). A schematic presentation of human TDP-43 is provided in Figure 6.

Initially, TDP-43 was cloned as a human protein that binds the TAR DNA of human HIV-1 acting as a transcription repressor (Ou et al., 1995). Subsequently, it was identified as part of a complex involved in splicing the cystic fibrosis transmembrane conductance regulator gene as well as the apoA-II gene (Buratti et al., 2001, Mercado et al., 2005). Nuclear TDP-43 plays an important role in the regulation of RNA splicing and microRNA biogenesis modulation (Xu, 2012). In addition, it has been suggested that TDP-43 is also involved in other cellular processes such as cell division and apoptosis (Braun RJ, 2011). Approximately 30% of cellular TDP-43 resides in the cytoplasm with nuclear efflux, which is regulated by stress and activity. TDP-43 is an important component of the neuronal dendritic and somatodendritic RNA transport granules; therefore, it plays a key

role in neuronal plasticity through regulating local protein production in the dendrites (Diaper et al., 2013, Alami et al., 2014).

Under cellular stress, TDP-43 is involved in the production of stress granules through the formation of complexes in order to sequester mRNAs redundant for survival (Colombrita et al., 2009, Scotter et al., 2015). It is crucial to more fully understand the normal functions and interactions of TDP-43, since these could prove the key to understanding the pathogenesis of disease and hence lead to the development of effective therapeutic targets.

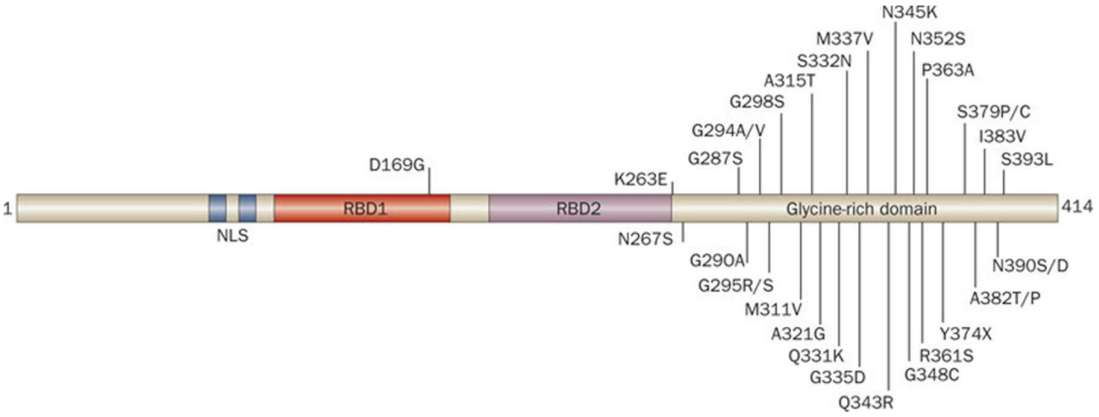

Figure 6: Schematic presentation of human TDP-43, which comprises four known functional domains: a nuclear localisation sequence, two RNA recognition motifs known as RRM1 and RRM2 and a C terminal glycine-rich domain that mediates protein-protein interactions (Chen-Plotkin et al., 2010).

1.2.2 TDP-43 proteinopathy

TDP-43 was identified as the major component of the ubiquitinated neuronal inclusions in ALS and FTLD in 2006 (Neumann et al., 2006b). Subsequently, TDP-43-positive inclusions were shown to be present in 97% of familial or sporadic ALS cases, except for those caused by mutations in the *SOD1* or *FUS* (Mackenzie, 2007b, Maekawa et al., 2009, Suzuki et al., 2012). The abnormally accumulated TDP-43 in ALS and FTLD-TDP cases is detergent resistant, hyperphosphorylated, ubiquitinated and cleaved (Arai et al., 2006, Neumann et al., 2006b). Five abnormal phosphorylation sites were identified at serine residues in the C-terminal region (Hasegawa et al., 2008). The neuropathological examination of FTLD-TDP and ALS cases has revealed the clearance of nuclear TDP-43 and the accumulation of both hyper-phosphorylated full-length TDP-43 and TDP-43 fragments of 18-26kDa (Hasegawa et al., 2011). The TDP-43 proteinopathy can spread from the spinal cord, cortical motor neurons and glia to other cortical regions, which can be used as the staging for disease progression (Brettschneider et al., 2014).

1.2.3 Role of TDP-43 in neurodegeneration

The precise mechanism by which TDP-43 mislocalisation and aggregation causes neurodegeneration has not yet been fully elucidated. The shift of TDP-43 from the nucleus to the cytoplasm suggests that the loss of normal TDP-43 nuclear function may be a key mechanism leading to the degeneration of neurons. Knockdown studies support this hypothesis in terms of the induced morphological nuclear defects, dysregulation of the cell cycle, increased cell death and altered neurite outgrowth (Mackenzie et al., 2010b, Lagier-Tourenne et al., 2010, Strong et al., 2007).

In vitro studies have suggested that the accumulation of TDP-43 in cellular inclusions can also induce a toxic gain of function, which is independent of the normal biological function of the protein (Johnson et al., 2008). Several studies have shown that the C-terminal fragment of TDP-43 is more insoluble than full-length TDP-43, with a tendency to aggregate and become ubiquitinated, phosphorylated and toxic to cells (Igaz et al., 2009, Zhang et al., 2009). However, one study suggested that the cytoplasmic aggregates bind the full-length TDP-43, leading to depletion from the nucleus (Nonaka et al., 2009). Yet, a pure toxic effect has been suggested by one research group due to the retention of normal nuclear expression (Zhang et al., 2009). In vitro studies expressing the mutant TDP-43 in cultured cells support the toxic effect of the C-terminal accumulation hypothesis (Sreedharan et al., 2008, Barmada et al., 2010). The pathogenic mechanism of TDP-43 proteinopathy remains unresolved due to the inconsistencies found among the available in vivo and in vitro models as well as the fact that none of these models properly replicate all the features of the human disease. Indeed, current results suggest multiple disease mechanisms are likely to contribute to neuronal death (Scotter et al., 2015). Further discussion concerning TDP-43 will be presented in forthcoming chapters (Chapters 3, 4 and 5).

1.3 hnRNPs

The term ‘heterogeneous nuclear ribonucleoproteins’ is a collective term for the proteins that associate with the pre-mRNAs (also known as heterogeneous nuclear RNAs according to their size heterogeneity and cellular location). The hnRNAs or pre-mRNAs are the products of the primary protein-coding transcripts produced by RNA polymerase II. Although the hnRNP proteins bind the hnRNAs, they are not stable components of the other classes of RNP complexes, for example, small nuclear RNA proteins (snRNPs) (Dreyfuss, 1993, Shyu and Wilkinson, 2000). At least 20 major hnRNPs along with other minor hnRNPs have been found in human cells (HeLa cells). The major hnRNPs are designated hnRNP-A1 through hnRNP-U and they have a molecular weight range from 34–120 kDa. The definition of hnRNPs does not distinguish between the different proteins according to their structure, function, tissue specificity, abundancy, steady state sub-nuclear localisation or the time they join the complexes. Therefore, splicing factors as well as traditional hnRNPs such as hnRNP A1 or H are components of the hnRNP complex so long as they bind directly and co-purify with the same hnRNAs. In this context, the hnRNP complexes are usually large and diverse and they contain numerous proteins that are highly dynamic and show various protein abundances (Markovtsov et al., 2000, Dreyfuss, 1993). Structurally, the hnRNP proteins contain one or more of a small number of RNA-binding motifs, which are also known as RNA recognition motifs (RRM), in addition to one or more protein-protein interaction and protein localisation domains and KH domains (Burd, 1994). The hnRNPs play important roles in several cellular functions, including transcription regulation, gene splicing, telomere-length maintenance and RNA processing (Michelotti et al., 1996, Hoek et al., 1998). Further discussion concerning the hnRNPs can be found in the following chapters (Chapters 3, 4 and 5).

1.4 Aims of this Study

The present study aims to:

1. Investigate the expression of potential TDP-43 binding partners in brain and spinal cord tissue from neurodegenerative disease cases with TDP-43 pathology using immunohistochemistry.
2. Further examine the expression of any proteins that show potential interaction with TPD-43 in other neurodegenerative disease cases in order to confirm whether their expression is specifically linked to TDP-43 pathology or is also seen in other neurodegenerative mechanisms.
3. Explore the regional specificity of any specific protein pathology by conducting immunohistochemistry in several regions of the brain.
4. Investigate the relationship and possible colocalisation between the identified proteins and TDP-43 aggregates using double immunofluorescence techniques.
5. Biochemically characterise the identified proteins in the brain tissue of TDP-43 cases using the solubility fractionation of brain tissue and Western blotting.
6. Investigate the interaction between the identified proteins and TDP-43 in cell lines using molecular biology techniques.

Chapter 2 Materials and Methods

2.1 Human Tissue Samples

2.1.1 Case selection and tissue preparation

Post-mortem brain tissue was obtained from the MRC London Neurodegenerative Diseases Brain Bank at the Institute of Psychiatry, Psychology and Neuroscience, King's College London (KCL). For each case, at the time of donation, one brain hemisphere was fixed in buffered formalin. Then, a neuropathological diagnosis was performed and the tissue was processed as formalin-fixed paraffin-embedded (FFPE) blocks for histopathological studies. The neuropathological assessment was performed according to the standard criteria. The other hemisphere was sectioned and specific brain areas were isolated by an expert before being placed individually into plastic bags, then labelled and sealed appropriately and stored at -80˚C.

Post-mortem brain tissue was obtained from 111 cases: 30 cases of FTLD with TDP-43 aggregates (FTLD-TDP) without the *C9orf72* expansion (comprising 15 FTLD-TDP type A, six FTLD-TDP type B and nine FTLD-TDP type C). Additionally, 23 FTLD-TDP cases with the *C9orf72* expansion were used (of which 15 were identified as FTLD-TDP subtype B and three as subtype A, the remainder could not be accurately subtyped). In addition, four FTLD/ALS with tau aggregates (FTLD-Tau, ALS-Tau), four Pick's disease, one FTLD with ubiquitin and progranulin mutations (FTLD-U-PRGN), three ALS with the FUS mutation (FUS-ALS), three ALS with the SOD1 mutation, 13 sporadic ALS (sALS), one ALS with P62 aggregates, two FTLD/ALS with the *TARDBP* mutation, one ALS with chronic inflammatory demyelinating polyneuropathy (CIDP), two dementia with Lewy bodies (DLB), one argyrophilic grain disease (AGD), one spinocerebellar ataxia (SCA), one Huntington's disease, and seven Alzheimer's disease cases were examined. Fourteen healthy controls without a history of neurological problems or psychiatric disorders and without any significant pathology (matched for gender, age and post-mortem delay) were also used. The demographic details concerning all the cases used in this study are presented in Table 3.

Table 3: Demographic details concerning all the cases used in this study, including the experiments each case was involved with (PMD: post-mortem delay, IHC: immunohistochemistry, dIF: double immunofluorescence)

Ref	Case	MRC ID	Diagnosis	Sex	Age at death (yrs)	PMD (hrs)	Fixation time (weeks)	IHC Exp	dIF	Western blotting
1	025/11	BBN_1085	FTLD-TDP A	M	87	40.5	12	hnRNP-E2, UBQLN2, hnRNP-M, hnRNP-C1/C2, hnRNP-Q		hnRNP-E2/PCBP2, TDP-43
2	029/09	BBN_15298	FTLD-TDP A	M	69	42	5	UBQLN2, hnRNP-M, hnRNP-C1/C2, hnRNP-Q, hnRNP-G/RBMX	hnRNP-E2 vs TDP-43 and hnRNP-E2 vs ubiquitin	hnRNP-E2/PCBP2, TDP-43
3	037/12	BBN_10599	FTLD-TDP A	F	79	56	6	hnRNP-E2		hnRNP-E2/PCBP2, TDP-43
4	063/12	BBN_4568	FTLD-TDP A	M	59	36	4	hnRNP-E2		
5	120/11	BBN_15306	FTLD-TDP A	M	71	14	8	hnRNP-E2		
6	172/12	BBN_10245	FTLD-TDP A	M	87	31	10	hnRNP-E2, UBQLN2, hnRNP-M, hnRNP-C1/C2, hnRNP-Q		
7	205/07	BBN_9863	FTLD-TDP A	M	73	24.5	8	hnRNP-E2		hnRNP-E2/PCBP2, TDP-43
8	229/03	BBN_15281	FTLD-TDP A	F	67	15	7	hnRNP-E2		hnRNP-E2/PCBP2, TDP-43
9	103/08	BBN_15294	FTLD-TDP C	F	85	24	11	hnRNP-E2, UBQLN2, hnRNP-M, hnRNP-C1/C2, hnRNP-Q		hnRNP-E2/PCBP2, TDP-43
10	294/13	BBN_19697	FTLD-TDP A	F	78	72	8	hnRNP-E2		hnRNP-E2/PCBP2, TDP-43
11	334/09	BBN_15302	FTLD-TDP A	M	81	11	24	hnRNP-E2		
12	033/08	BBN_15292	FTLD-TDP A	F	56	35	10	hnRNP-E2, UBQLN2, hnRNP-M, hnRNP-C1/C2, hnRNP-Q		
13	047/07	BBN_15287	FTLD-TDP A	F	74	70	8	hnRNP-E2		
14	097/09	BBN_16282	FTLD-TDP A	M	78	n/a	n/a	hnRNP-E2		
15	099/08	BBN_15293	FTLD-TDP A	M	70	7	n/a	hnRNP-E2		

16	030/06	BBN_6230	FTLD-TDP B	M	71	43.5	n/a	hnRNP-E2		
17	157/12	BBN_4249	FTLD-TDP B	M	86	45	6	hnRNP-E2, UBQLN2, hnRNP-M, hnRNP-C1/C2, hnRNP-Q		
18	169/11	BBN_9950	FTLD-TDP B	M	72	38	12	hnRNP-E2, UBQLN2, hnRNP-M, hnRNP-C1/C2, hnRNP-Q		hnRNP-E2/PCBP2, TDP-43
19	058/12	BBN_4590	FTLD-TDP B	F	73	54	8	hnRNP-E2, UBQLN2, hnRNP-M, hnRNP-C1/C2, hnRNP-Q		
20	244/07	BBN_15289	FTLD-TDP B	M	68	46	4	hnRNP-E2		
21	432/12	BBN_11067	FTLD-TDP B	M	81	31	8	hnRNP-E2, UBQLN2, hnRNP-M, hnRNP-C1/C2, hnRNP-Q		
22	013/10	BBN_15303	FTLD-TDP C	M	69	6	12	hnRNP-E2, UBQLN2, hnRNP-M, hnRNP-C1/C2, hnRNP-Q, hnRNP-G/RBMX	hnRNP-E2 vs TDP-43 and hnRNP-E2 vs ubiquitin	hnRNP-E2/PCBP2, TDP-43
23	022/07	BBN_15286	FTLD-TDP C	M	68	120	7	hnRNP-E2, hnRNP-G/RBMX	hnRNP-E2 vs TDP-43 and hnRNP-E2 vs ubiquitin	
24	061/13	BBN_15200	FTLD-TDP C	M	69	16	11	hnRNP-E2, UBQLN2, hnRNP-M, hnRNP-C1/C2, hnRNP-Q		
25	301/10	BBN_15304	FTLD-TDP C	M	80	45	20	hnRNP-E2,UBQLN2, hnRNP-M, hnRNP-C1/C2, hnRNP-Q, hnRNP-G/RBMX	hnRNP-E2 vs TDP-43 and hnRNP-E2 vs ubiquitin	
26	350/08	BBN_15295	FTLD-TDP C	M	82	14	16	hnRNP-E2, hnRNP-G/RBMX	hnRNP-E2 vs TDP-43 and hnRNP-E2 vs ubiquitin	
27	409/08	BBN_15297	FTLD-TDP C	M	78	n/a	12	hnRNP-E2, UBQLN2, hnRNP-M, hnRNP-C1/C2, hnRNP-Q		
28	163/07	BBN_15288	FTLD-TDP C	M	80	6.5	12	hnRNP-E2, UBQLN2, hnRNP-M, hnRNP-C1/C2, hnRNP-Q		
29	295/07	BBN_15290	FTLD-TDP C	M	66	54	8	hnRNP-E2		
30	101/09	BBN_15299	FTLD-TDP A	M	88	31	n/a	hnRNP-E2		hnRNP-E2/PCBP2, TDP-43
31	088/00	BBN_15270	FTLD-TDP *C9orF72* B	F	57	16	n/a	hnRNP-E2,UBQLN2, hnRNP-M, hnRNP-C1/C2, hnRNP-Q		hnRNP-E2/PCBP2, TDP-43

32	403/08	BBN_15296	FTLD-TDP *C9orF72* B	F	70	15.5	12	hnRNP-E2	
33	019/95	BBN_16651	FTLD-ALS *C9orF72* B	M	51	64	7	hnRNP-E2	
34	050/98	BBN_16458	FTLD-ALS *C9orF72* B	M	70	40	n/a	hnRNP-E2	
35	068/05	BBN_6227	FTLD-ALS *C9orf72* B	M	55	76	31	hnRNP-E2, UBQLN2, hnRNP-M, hnRNP-C1/C2, hnRNP-Q	
36	069/02	BBN_6198	FTLD-ALS *C9orf72* B	M	58	11	15	hnRNP-E2	
37	095/05	BBN_10306	FTLD-ALS *C9orf72* B	M	64	68	11	hnRNP-E2	
38	112/99	BBN_16438	FTLD-ALS *C9orf72* A	F	58	12	61	hnRNP-E2	
39	117/91	BBN_16969	FTLD-ALS *C9orf72* B	F	57	12	12	hnRNP-E2	
40	141/06	BBN_6232	FTLD-ALS *C9orf72*	M	70	38	12	hnRNP-E2	hnRNP-E2/PCBP2, TDP-43
41	144/12	BBN_4253	FTLD-ALS *C9orf72* B	F	59	21	10	hnRNP-E2, UBQLN2, hnRNP-M, hnRNP-C1/C2, hnRNP-Q	hnRNP-E2/PCBP2, TDP-43
42	151/08	BBN_6251	FTLD-ALS *C9orf72 B*	M	62	73.5	14	hnRNP-E2	
43	156/95	BBN_16615	FTLD-ALS *C9orf72 B*	F	64	44	4	hnRNP-E2, hnRNP-G/RBMX	hnRNP-E2/PCBP2, TDP-43
44	157/04	BBN_15713	FTLD-ALS *C9orf72* B	M	57	22.5	35	hnRNP-E2, UBQLN2, hnRNP-M, hnRNP-C1/C2, hnRNP-Q	hnRNP-E2/PCBP2, TDP-43
45	163/09	BBN_15300	FTLD-ALS *C9orf72 A*	M	79	35	5	hnRNP-E2,UBQLN2, hnRNP-M, hnRNP-C1/C2, hnRNP-Q	
46	174/08	BBN_6252	FTLD-ALS *C9orf72* B	F	43	69	14	hnRNP-E2	
47	205/99	BBN_15641	FTLD-ALS *C9orf72*	F	70	60	37	hnRNP-E2, hnRNP-G/RBMX	hnRNP-E2/PCBP2, TDP-43

48	223/08	BBN_6254	FTLD-ALS *C9orf72* B	M	53	82	10	hnRNP-E2	hnRNP-E2/PCBP2, TDP-43
49	229/06	BBN_16380	FTLD-ALS *C9orf72*	F	59	34.5	17	hnRNP-E2	
50	290/10	BBN_16223	FTLD-ALS *C9orf72*	M	55	19	17	hnRNP-E2	
51	311/07	BBN_6242	FTLD-ALS *C9orf72*	F	39	69.5	18	hnRNP-E2, hnRNP-G/RBMX	
52	315/07	BBN_15291	FTLD-ALS *C9orf72* A	M	56	18.5	11	hnRNP-E2	
53	400/08	BBN_16304	FTLD-ALS *C9orf72* B	M	59	46	10	hnRNP-E2	
54	008/10	BBN_9933	Alzheimer's disease	F	98	25	9	hnRNP-E2	
55	012/10	BBN_9934	Alzheimer's disease	M	70	60	19	hnRNP-E2	
56	200/10	BBN_4182	Alzheimer's disease	F	81	23	18	hnRNP-E2	
57	207/10	BBN_4183	Alzheimer's disease	F	79	40	8	hnRNP-E2	
58	247/05	BBN_9801	Alzheimer's disease	F	90	23	20	hnRNP-E2	
59	315/09	BBN_9927	Alzheimer's disease	F	90	35	18	hnRNP-E2	
60	346/09	BBN_9930	Alzheimer's disease	M	101	48	12	hnRNP-E2	
61	347/08	BBN_2924	AGD	M	82	20	8	hnRNP-E2	
62	247/07	n/a	CIDP ALS	M	70	5days	14	hnRNP-E2	
63	020/08	BBN_16337	DLB	M	85	29.5	18	hnRNP-E2	
64	263/05	BBN_10290	DLB	M	78	41	25	hnRNP-E2	
65	155/06	BBN_15283	FTLD-U-PRGN	M	70	57	22	hnRNP-E2	
66	063/08	BBN_6245	FUS ALS	F	35	13	5	hnRNP-E2	
67	086/01	BBN_6189	FUS ALS	F	35	24	39	hnRNP-E2	
68	203/12	BBN_10244	FUS ALS	F	23	37	12	hnRNP-E2	

69	420/12	BBN_11070	HUNTINGTON'S DIS	M	65	36	8	hnRNP-E2
70	237/12	BBN_10214	P62-ALS	M	65	33	10	hnRNP-E2
71	008/06	BBN_10282	Pick's dis	M	72	6	19	hnRNP-E2
72	009/06	BBN_10281	Pick's dis	M	61	23	21	hnRNP-E2
73	048/02	BBN_15776	Pick's dis	M	66	17	3	hnRNP-E2
74	258/06	BBN_15285	Pick's dis	M	67	16.5	7	hnRNP-E2
75	058/08	BBN_6244	sALS	M	55	33	22	hnRNP-E2
76	059/01	BBN_6187	sALS	M	70	73	75	hnRNP-E2
77	075/06	BBN_10272	sALS	M	87	70	22	hnRNP-E2
78	091/08	BBN_6248	sALS	M	66	38	8	hnRNP-E2
79	148/04	BBN_15715	sALS	M	74	34	40	hnRNP-E2
80	226/03	BBN_6219	sALS	M	49	32.5	33	hnRNP-E2
81	249/09	BBN_6267	sALS	M	68	5	18	hnRNP-E2
82	142/06	BBN_16392	SOD1 ALS	F	61	13.5	21	hnRNP-E2
83	284/13	BBN_19995	*TARDBP* mutation	M	57	48	9	hnRNP-E2
84	151/10	BBN_6273	Tau-ALS	F	75	38	3	hnRNP-E2
85	067/00	BBN_15268	Tau-FTLD	F	58	31	13	hnRNP-E2
86	074/00	BBN_15269	Tau-FTLD	M	67	35	9	hnRNP-E2
87	247/06	BBN_15284	Tau-FTLD	F	62	30.5	9	hnRNP-E2
88	348/08	BBN_6257	TDP-ALS	F	69	64	14	hnRNP-E2
89	329/07	BBN_6243	sALS	M	67	70	11	hnRNP-E2
90	136/02	BBN_15766	SCA	F	74	33	53	hnRNP-E2
91	034/06	BBN_10276	SOD 1 ALS	M	47	13.5	18	hnRNP-E2
92	101/96	BBN_16553	SOD1 ALS	F	46	5	14	hnRNP-E2
93	204/03	BBN_6217	sALS	F	56	39	56	hnRNP-E2

94	251/09	BBN_6268	sALS	M	78	2	18	hnRNP-E2	
95	257/11	BBN_6280	sALS	M	75	38	9	hnRNP-E2	
96	274/05	BBN_10285	sALS	M	42	41	23	hnRNP-E2	
97	194/06	BBN_16384	sALS	F	57	15.3	23	hnRNP-E2	hnRNP-E2/PCBP2, TDP-43
98	047/02	BBN_15777	CNT	F	87	21.5	150	hnRNP-E2	
99	047/03	BBN_15753	CNT	M	64	70.5	53	hnRNP-E2, UBQLN2, hnRNP-M, hnRNP-C1/C2, hnRNP-Q	hnRNP-E2/PCBP2, TDP-43
100	048/09	BBN_16291	CNT	M	81	18	17	hnRNP-E2, UBQLN2, hnRNP-M, hnRNP-C1/C2, hnRNP-Q	hnRNP-E2/PCBP2, TDP-43
101	063/10	BBN_16242	CNT	F	90	50	19	hnRNP-E2,hnRNP-G/RBMX	hnRNP-E2/PCBP2, TDP-43
102	066/00	BBN_15621	CNT	M	61	53	14	hnRNP-E2	
103	077/00	BBN_16429	CNT	M	68	53	4	hnRNP-E2, UBQLN2, hnRNP-M, hnRNP-C1/C2, hnRNP-Q	hnRNP-E2/PCBP2, TDP-43
104	123/09	BBN_16280	CNT	M	78	24	8	hnRNP-E2	hnRNP-E2/PCBP2, TDP-43
105	130/09	BBN_16277	CNT	M	54	30	8	hnRNP-E2, hnRNP-G/RBMX	
106	149/01	BBN_15791	CNT	M	95	44	20	hnRNP-E2	
107	150/01	BBN_15790	CNT	M	40	40	25	hnRNP-E2	
108	272/09	BBN_16256	CNT	M	62	~80	18	hnRNP-E2, hnRNP-G/RBMX	
109	308/09	BBN_16251	CNT	M	66	52	7	hnRNP-E2, UBQLN2, hnRNP-M, hnRNP-C1/C2, hnRNP-Q	
110	158/14	BBN_22991	CNT	F	73	27	6	hnRNP-E2, UBQLN2, hnRNP-M, hnRNP-C1/C2, hnRNP-Q	
111	278/96	BBN_16525	CNT	F	77	29	14	hnRNP-E2	

Paraffin sections were obtained from the frontal cortex, temporal lobe, hippocampus, cerebellum and spinal cord. After the tissue selection, 7 µm sections were cut using a microtome. The sections were floated in a 37˚C water bath and then mounted onto glass slides (Superfrost™). Each slide was labelled with the case number and the region of the brain or spinal cord used. The slides were left to dry on a 37˚C hot plate. Once dry, the slides were incubated in a 60˚C oven overnight and then kept in a 37˚C oven until used for immunohistochemistry or double-labelling immunofluorescence experiments.

2.1.2 Immunohistochemistry (IHC)

The sections were dewaxed by twice submerging them into fresh xylene for 5 minutes each time. Then, they were dehydrated by twice submerging them into absolute ethanol for 5 minutes each time. The endogenous peroxidase enzymes were blocked by placing the sections in 200 ml of methanol containing 5 ml of 30% aqueous hydrogen peroxide solution for 30 minutes. The blocking of the endogenous enzymes is essential for reducing the interaction with the ABC/HRP solution used later in the protocol. The slides were washed for 10 minutes under running tap water, then rinsed with distilled water for 2 minutes and placed into 1x TBS (Tris-buffered saline). The TBS stock was made by mixing 604.5 g of Trizma base and 900 g of sodium chloride in 10 L distilled water. The pH was adjusted to 7.6 using 1M HCL.

The antigen retrieval step is important for recovering the antigens that may have been altered by the fixation process. The antigen retrieval step was performed using the extended citrate method. The slides were submerged in a citrate buffer containing 14.7 g of sodium citrate diluted in 5 L distilled water with a pH of 6.0. The slides were microwaved on full power for 8 minutes followed by being simmered twice for 6 minutes each time. Afterwards, the slides were cooled down under running tap water and washed in TBS twice for 5 minutes each time. A piece of wax was used to circle around the sections, creating a hydrophobic barrier to ensure the solutions stayed on the sections during the incubations. Normal serum blocking was carried out to block non-specific binding as follows. For the primary polyclonal antibodies raised in rabbits, the sections were incubated in normal swine serum (NSS) diluted with TBS (1:10) for 20 min. For the monoclonal antibodies raised in mice, the sections were incubated with normal rabbit serum (NRS) diluted with TBS (1:10) for 20 min. The sections were then drained and the primary antibody applied

according to the optimal dilution obtained via the optimisation experiments (with 1:100 NSS for the polyclonal antibodies or 1:100 NRS for the monoclonal antibodies in TBS). 250 µl was added to each section and they were incubated overnight at 4˚C. Details concerning the primary antibodies used throughout the study and the optimal dilutions for each specific experiment are provided in Table 4. A negative control slide was incubated in each experiment with 1:100 NSS or NRS (depending on the antibody used) in TBS.

Table 4: Details of the antibodies used for the screening of TDP-43 binding partners in FTLD-TDP cases and specific optimal experimental dilutions

Antibody	Source	Experiment/Optimal dilution
TDP-43 10782-2-AP (Proteintech)	Rabbit polyclonal	WB/1:1000 dIF/1:250
UBQLN2 (M03), clone 5F5 (Abnova #H00029978-M03)	Mouse monoclonal	IHC/1:500, dIF/1:150
hnRNP-M 95-RE36 (Santa Cruz. sc-134360)	Mouse monoclonal	IHC/1:500
hnRNP-C1/C2 (H-105) sc-15386, Santa Cruz	Rabbit polyclonal	IHC/1:500
hnRNP-Q (I8E4) sc-56703, Santa Cruz	Mouse monoclonal	N/A
hnRNP-E2-23 G: (sc-101136, Santa Cruz)	Mouse monoclonal	IHC/1:500, dIF/1:250, WB/1:500
PCBP2 (WH0005094M7 - clone 5F12 Sigma-Aldrich) (hnRNP E2)	Mouse monoclonal	IHC/1:500, dIF/1:250
hnRNP-E2/PCBP2 (M07), clone 5F12 Abnova (H00005094-M07)	Mouse monoclonal	IHC/1:500, WB/1:500
RBMX (H-80): (sc-48796, Santa Cruz) (hnRNP G)	Rabbit polyclonal	IHC/1:500
hnRNP-E1 (E-2) (sc-137249, Santa Cruz)	Mouse monoclonal	IHC/1:500
Ubiquitin (Dako, z0458)	Rabbit polyclonal	dIF/1:200
Phosphorylated pTDP-43 (pS409/410-2); 1:1500, Cosmo Bio Ltd, Tokyo, Japan)	Rabbit polyclonal	dIF/1:250, WB/1:2000

IHC: immunohistochemistry, dIF: double-labelling immunofluorescence, WB: Western blotting.

On the second day, the slides were washed twice in TBS for 5 min each wash. The secondary antibodies were applied as follows. For the polyclonal rabbit primary antibodies, swine-anti-rabbit biotinylated immunoglobulin (SAR) obtained from Dako Ltd and diluted in TBS 1:100 was applied at 250 µl/section for 45 minutes. For the monoclonal mouse primary antibodies, rabbit anti-mouse biotinylated immunoglobulin (RAM) obtained from Dako Ltd and diluted in TBS 1:100 was applied at 250 µl/section for 45 minutes. The avidin-biotin complex horseradish peroxidase (ABC) solution was prepared by adding 2 drops of reagent (A) and 2 drops of reagent (B) (ABC kit obtained from Vectastain) to 5 ml of TBS. The slides were washed twice in TBS for 5 minutes each wash and then the ABC solution was added to the sections and incubated for 45 minutes. During this time, the 3,3'-diaminobenzidine tetrahydrochloride (DAB) solution was prepared by adding 1 DAB tablet (Sigma D5905) to 20 ml of TBS and allowing to dissolve. The solution was filtered and then

activated by adding 10 µl of 30% H_2O_2 (once activated, DAB should be used within 2 hours). The sections were washed twice in TBS (5 min each wash) and the activated DAB solution was added in order to allow visualisation by chromogenic precipitation of the oxidised DAB. This serves as an amplification of the antigen signal in the tissue. The sections were incubated with DAB for up to 10 minutes. The sections were washed in running tap water for 10 minutes and then counter-stained with haematoxylin for 20 seconds to visualise the nuclei and the overall structure of the tissue. Next, they were washed in running tap water again before being dipped into acid alcohol (2 sec intervals) and returned to running tap water. The sections were then washed in distilled water for 2 minutes. The sections were dehydrated by submerging the slides into a series of different concentrations of ethanol: 70% alcohol for 2 minutes, followed by 2 minutes in 95% ethanol and then absolute alcohol twice for 2 minutes. The slides were submerged into fresh xylene four times for 2 minutes each time, before coverslips were added using Ralmount glue (formulation Raymond A. Lamb, BDH).. The sections were visualised using a bright field microscope with an attached camera (Zeiss Axioplan microscope and AxioCam MRc 5 megapixel Zeiss camera) and the images were captured using AxioVision software (AxioVision Rel. 4.7. Carl Zeiss).

2.1.3 Double-labelling immunofluorescence

In this study, a double-labelling immunofluorescence (dIF) method was used to detect the colocalisation of two antigens in the same tissue. The experiments were conducted according to a modified protocol supplied by the Brain Bank at KCL. The dewaxing and antigen retrieval steps were similar to those of the IHC protocol detailed above. The normal serum blocking was performed by incubating the sections with normal goat serum (NGS) diluted 1:10 in phosphate buffer saline (PBS) solution.

All the primary antibodies were diluted in PBS with a pH of 7.4 and then incubated for 60 minutes. The primary antibodies for both antigens were mixed in the diluted solution; however, they had to be raised in different species, that is, one antibody is monoclonal and raised in mice, while the second antibody is polyclonal and raised in rabbits. The details of the primary antibodies used in this study and their optimal dilutions will be described in the following chapters. The sections were washed with PBS twice for 5 minutes each wash. Then, the sections were incubated with fluorophore secondary antibodies for 45 minutes.

The secondary antibodies used were Alexa Fluor® goat anti-rabbit, which was used to label the polyclonal primary antibodies, and Alexa Fluor® goat anti-mouse, which was used to label the monoclonal primary antibodies (Alexa Fluor® 488 Goat Anti-Mouse IgG [Invitrogen] and Alexa Fluor® 568 Goat Anti-Rabbit IgG [Invitrogen]). The colour of the fluorescence was chosen as green (488 nm) or red (568 nm) for each antibody. The sections were covered with foil in order to protect them from light and avoid the activation of the fluorescence. Following incubation, the sections were washed three times in PBS (5 min each wash). Next, the sections were incubated with Sudan Black for 10 minutes to quench the natural autofluorescence seen in human brain tissue. The Sudan Black was prepared by adding 0.15 g to 50ml of 70% ethanol (prepared at least 45 min in advance with constant mixing and filtering). The sections were washed eight times with PBS, for 5 minutes each wash. The slides were mounted using Vectashield with DAPI (Vector Laboratories Ltd, Petersfield, UK) and then coverslipped. All the sections were visualised using an inverted fluorescence microscope (Zeiss Axiovert S100, Gottingen, Germany). There were further modifications made for some experiments, which will be discussed alongside the results of each experiment.

2.1.3.1 Inclusions counting

Slides were visualised using the inverted fluorescence microscope (Zeiss Axiovision). TDP-43, ubiquitin and hnRNP-E2 inclusions were counted in the frontal cortex sections from 1 FTLD-TDP type A case (case #2) and 4 FTLD-TDP type C cases (case #22, #23, #25 and #26). Depending on the section size, 8-10 fields from each slide were selected and the number of inclusions were counted in each field (the number of inclusions seen in the red channel were counted manually using a hand-held counter, the fluorescence channel was then switched to green and the number of inclusions seen counted, the number of these inclusions that colocalised was also recorded). Further details about the number of inclusions and percentage calculations will be provided in the result section in chapter 4.

2.1.4 Western blotting

2.1.4.1 Human brain tissue fractionation for Western blotting

The aim of this fractionation protocol is to determine whether the protein forms soluble or insoluble aggregates. Different detergents of increasing strengths were used to release different cellular components. Two fractionation protocols were used. One uses sarkosyl detergent, while the other uses RIPA detergent for protein extraction. For both protocols, approximately 100 mg of frozen cortical grey matter from the frontal cortex (Brodmann area 9) of each case was dissected from the white matter and meninges at 4°C.

RIPA Protocol: Each brain tissue sample was homogenised using approximately 30 strokes of the glass douncer in 1 ml of ice-cold high-salt buffer containing 750 mM of NaCl, 10 mM of NaF and 'complete protease inhibitor cocktail tablets' (Roche, 1 tablet per 50 ml of buffer). 200 µl of the homogenate was retained as the lysate fraction of the sample. The remaining homogenate was transferred into ultrafuge tubes and then spun for 30 minutes at 44,000 rpm in the ultrafuge at 4°C (Beckman Ultrafuge). The supernatant was removed and stored at -20°C as the high-salt fraction of the sample. The pellet was washed twice by resuspension in 1 ml of the high-salt buffer and then spun at 44,000 for 20 minutes at 4°C. The previous steps were repeated using a Triton buffer containing 750 mM of NaCl, 10 mM of NF and 1% Triton X-100 (supernatant saved as the Triton fraction) and then an RIPA (radioimmunoprecipitation assay) buffer containing 1% NP-40, 0.5% sodium deoxycholate and 0.1% SDS (supernatant saved as the RIPA fraction). The RIPA buffer is effective for protein extraction because it contains three non-ionic and ionic detergents; however, this detergent combination may prove relatively incompatible with certain downstream applications. Finally, the pellet was resuspended in a urea buffer containing 7 M of urea, 2 M of thiourea, 4% CHAPS, 30 mM of Tris-HCL pH 8.5 and vortex for 15 minutes. All the buffers were made up in 250 ml of stock buffer containing 50 mM of Tris-HCL, 150 mM of NaCl and 5 mM of EDTA with a pH of 7.4. All the fractions were stored at -20°C until used for Western blotting.

Sarkosyl Protocol: The brain sample from each case was homogenised using approximately 30 strokes of the glass douncer in 1 ml of ice-cold low-salt (LS) buffer, which contained 10 M of Tris pH 7.5, 5 M of EDTA (ethylenediaminetetraacetic acid), 1 M of dithiothreitol, 10% sucrose and a cocktail of protease inhibitors (Roche, 1 tablet per 50 ml of buffer). The homogenate was transferred into ultrafuge tubes and then spun for 30 minutes at 18,000 rpm in the ultrafuge at 4°C (Beckman Ultrafuge). Next, 2x the sample buffer (0.5 m of Tris-HCL pH 6.8, 2% SDS, 10%

glycerol and 100 mg of bromophenol blue diluted in dH2O) was added to the supernatant and the samples were vortexed for 10 seconds, boiled for 10 min at 100°C and then saved at -20°C. The pellet was washed twice by resuspension in 1 ml of the same buffer and spun at 44,000 for 20 minutes at 4°C. The supernatant was discarded. The pellet was resuspended in 1 ml of ice-cold high-salt Triton buffer that exhibited the same composition as the LS buffer with the addition of 1% Triton X-100 and 0.5 M of NaCl. The samples were sedimented at 44,000 rpm for 30 min at 4°C. The supernatant was saved with 2x the sample buffer, vortexed and boiled for 10 min at 100°C and then saved at -20°C as the HS fraction. The pellet was washed twice in the HS buffer as per the previous washes. The pellet was resuspended in 1 ml of ice-cold Triton buffer that contained 30% sucrose made up by adding 3 g of sucrose to 10 ml of Triton X-100. The supernatant was saved as the TX fraction at -20°C after adding 2x the sample buffer and boiling at 100°C for 10 min. The pellet was resuspended in the sarkosyl buffer containing the LS buffer plus 1% N-Lauroylsarcosine and 0.5 M of NaCl. The samples were sonicated for a few seconds and then vortexed for 1 hour at room temperature. The samples were sedimented at 44,000 rpm for 30 min at 4°C and the supernatant was saved as the SARK fraction. The remaining pellet was resuspended in 200 µl of urea buffer containing 7 M of urea, 2 M thiourea, 4% 3[(3cholamidopro-pyl)dimethylammonio]-1-propanosulphonate (CHAPS) and 30 M of Tris-HCLpH8.5. The samples were vortexed for 20 min at room temperature. Some 200 µl of 2x the sample buffer was added to each sample and centrifuged at 14,000 rpm for 10 min at 10°C. The supernatant was saved as the urea fraction at -20°C (without boiling).

2.1.4.2 Gel electropheresis

Specific proteins were detected using the Western blotting technique, which uses gel electrophoresis to separate proteins by their electrophoretic mobility according to their size, conformation, length and change of molecules. The Western blotting technique is comprised of three steps. The first step is size separation, while the second step involves the transfer of the proteins from the gel to a nitrocellulose or polyvinylidene difluoride (PVDF) membrane. Finally, the proteins are marked with an appropriate primary antibody, which is later probed with a fluorescent secondary antibody. The fluorescence is then visualised digitally (LI-COR Odyssey®) or via enhanced chemiluminescence (ECL).

The Western blots were performed using an SDS-PAGE polyacrylamide gel NuPAGE R Novex R 10% Bis-Tris buffering agent. This specific gel has a neutral pH, which minimises any protein modification. It is also the best option for the separation of medium- to small-sized proteins under denaturing conditions. The NuPAGE R Novex R gel comes in either 26 or 12 loading wells. The number of wells was chosen according to the sample number used for each experiment.

The gel separation range depends on the buffer solution used for the Western blot. The MOPS (morpholino propanesulphonic acid) running buffer was used for the Western blots in this study. The composition of the 20x NuPAGE R MOPS SDS running buffer includes 50 mM of Tricine, 50 mM of Tris base and 1% SDS (pH 8.24). The 20x MOPS running buffer was diluted to 1x using double distilled water and then added to the gel tank. Although the MOPS buffer is designed to resist the high temperatures the gel encounters, ice was used in the tank to cool the gel down during the electrophoric separation.

For the RIPA fractionation protocol, the samples were diluted into 2x sample buffer before loading onto the gel. The 2x sample buffer was comprised of the following: 62.5 mM of Tris-HCL pH 6.8, 2% SDS, 10% glycerol and 0.01% bromophenol blue in 50 ml of distilled water. The total lysate and HS fractions were prepared by adding 25 µl of each sample to 25 µl of the HS buffer and 50 µl of the 2x sample buffer (1:5 dilution). The Triton and RIPA fractions were prepared by adding 50 of µl of the sample to 50 of µl the 2x sample buffer (1:1 dilution). The urea fraction was prepared by using 10 µl of the sample with 10 µl of the 2x sample buffer (1:1 dilution).

The sarkosyl samples were allowed to thaw at room temperature and the urea fraction was spun for 15 min at 14,000 rpm at 4°C before loading into the gels. Some 1–2 µl of protein ladder (Bio-Rad) was loaded into a separate well on the gel as a reference for the protein sizes. The ladder contained ten Strep-tag® recombinant proteins that ranged in size from 10 kDa to 250 kDa. Figure 7 presents an illustrative image of the protein ladder used throughout the experiments. The gel ran for approximately 90 min at 150–190 volts.

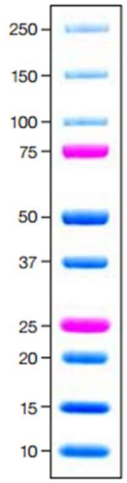

Figure 7: Representative blot of Precision Plus Protein™ Dual Color Standards (Bio-Rad).

2.1.4.3 Protein transfer to the nitrocellulose membrane (iBlot)

The samples can be visualised on the gel as they are diluted in the bromophenol blue sample buffer. The samples should travel in equal lines from each well down to the gel. Once the line reaches the bottom of the gel (after approximately 90 minutes), the run is stopped and the gel is transferred onto a nitrocellulose membrane so the proteins can be probed with specific antibodies for band detection.

The nitrocellulose membrane is composed of 100% pure nitrocellulose with approximately 0.2 µm pores (Invitrogen). The gel was equilibrated into a 2x diluted transfer buffer (Invitrogen) for 5 min at room temperature on a plate shaker. The transfer buffer (Invitrogen) contained 5 mM of Bicine, 25 of mM Bis-Tris (free base) and 1 mM of EDTA (pH 7.2) all dissolved in 100 ml of ultrapure water. The transfer buffer was diluted down to 2x containing 10% methanol with double-distilled water. Approximately 25 ml was used for each gel.

The Invitrogen (iBlot_R) transfer device was used for the gel transfer. The device utilises high field energy, high currents and shortened distance electrodes to transfer the proteins from the gel to the nitrocellulose membrane. The device runs for 7 min, during which the proteins are transferred by hydrophobic and electrostatic interactions to the membrane.

2.1.4.4 Protein detection on the blot

Ponceau S staining was applied to the membrane following the transfer. Ponceau S staining is designed for the rapid, reversible staining of any protein band on the nitrocellulose membrane, which allows for confirmation that the proteins were transferred to the membrane from the gel. Any excess Ponceau stain was removed by washing in water and the membrane was taken for antigen blocking. To reduce the non-specific binding of the proteins on the blot, antigen blocking was carried out using 5% skimmed milk, which was comprised of 2.5 g of skimmed milk powder (FLUKA Skim Milk Powder for microbiology #70166) in 50 ml of 1x TBS-T containing 0.01% Tween-20 (Calbiochem). The blocking milk solution was added to the blot in a plastic bottle and then left on a roller for 20 min at room temperature.

The primary antibodies were diluted in 1% skimmed milk in 1x TBS-T and the blot was incubated overnight on a roller at 4°C. The primary antibodies used in this study were the polyclonal rabbit TDP-43 10782-2-AP (Proteintech) and the PCBP2 mouse monoclonal (M07) clone 5F12 (Abnova). The next day, the blot was washed three times with TBS-T (10–20 min each wash) on a roller at room temperature. The blot was then incubated with the secondary antibodies obtained from Thermo Scientific (Goat anti-Rabbit IgG [H+L] Secondary Antibody, DyLight 680 conjugate, and Pierce Goat anti-Mouse IgG [H+L] Secondary Antibody, DyLight 800 conjugate) diluted to 1:5000 in 1% milk for 2–3 hours on a roller at room temperature (tubes covered in tin foil to protect the blot from light). The blot was then washed three times with TBS-T as previously described. The blot was visualised using the LI-COR Odyssey® scanner and the bands were analysed according to both the sample fraction and the band size. The blots were also probed with a loading control antibody in order to ensure that the increase or decrease in the size of the bands seen in the individual cases was not due to differences in the sample loading. The loading control used was rabbit GAPDH (Sigma, G8795). The density of the bands was measured using ImageJ 1.47v software, which will be described in the next section.

2.2 Cell Biology

2.2.1 Cell lines and tissue culture

Two cell lines were used in this study. Human embryonic kidney 293 (HEK-293T) cells were used for the overexpression, knockdown and immunoprecipitation experiments, while HeLa cells (derived from cervical cancer cells) were used for the immunocytochemistry experiments in order to investigate the accumulation of TDP-43 and hnRNP-E2 in stress granules. The HeLa cells were chosen for this purpose because they have a larger cytoplasm and they show better survival for the co-transfection and stress experiments than other cell lines, for example, SHSY5Y and CV1 cells.

The cells were grown in vitro in 75 cm^2 cell culture flasks with 8 ml of growing media. The growing media used was DMEM (Dulbecco's modified Eagle's medium) with GlutaMAX and high glucose (4.5 g/L), which was obtained from Life Technologies. Foetal bovine serum (FBS) was added to the media to make up a final concentration of 10% FBS. Antibiotics were added to the media as 100 U/mL of penicillin and 100 µg/mL of streptomycin so as to protect the cells from bacterial infections. The cells will continue to grow in this media until they cover the available surface area (confluence) or the growing media is depleted of nutrients. Therefore, the cells were subcultured to prevent them from dying. In order to subculture the cells, they needed to be in a suspension. All the reagents and media used for the subculturing were warmed in a water bath to 37ºC. After aspirating the media from the flask completely, the cells were washed with 4 mL of DPBS (Dulbecco's phosphate-buffered saline) obtained from Life Technologies to wash off the media and any dead floating cells. After aspirating the DPBS, 1 mL of the protease enzyme (trypsin) was added to the cells and incubated for 2 minutes at 37ºC. Trypsin will release the adherent cells from the surface of the flask in order to allow them to be resuspended in fresh media. Once the cells fell off the surface, they were resuspended in 7 mL of fresh warm media. Some 1 mL of the cell suspension was passaged into a new flask and 7 mL of fresh warm media was added. The flask was labelled with the passage number and date and then placed back in the incubator. The rest of the cell suspension was used for the planned experiments as needed or else discarded appropriately. The cells' transfection for overexpression and knockdown will be detailed in Chapter 5.

2.2.2 Western blotting

The cells were harvested in 1x SDS load buffer (50 mM of Tris-HCl pH 6.8, 2% SDS, 10% glycerol and 12.5 mM of EDTA without bromophenol blue or reducing agents) with 1x complete proteinase inhibitor (PI) (Roche) and 1x phosphatase inhibitors (PhosSTOP) and then boiled for 10 minutes. The protein concentrations within the harvested cell samples were quantified using the Bio-Rad DC protein assay (Bio-Rad, Hemel Hempstead, UK) against a bovine serum albumin (BSA) standard. After analysing the sample's concentration, only 5 µg of proteins from each sample was loaded onto the polyacrylamide gel electrophoresis (PAGE) for Western blotting. The samples were diluted to 5 µg using the harvesting buffer and 2x the loading buffer (125 mM of Tris-HCL pH 6.8, 4% SDS, 20% glycerol and 0.02% bromophenol blue dissolved in double-distilled water with 1 mM of dithiothreitol [DTT]). Fresh PI and PhosSTOP were added to the loading buffer.

The PAGE Western blotting technique was used to separate the different sized proteins in the samples. The NuPAGE_R Novex_R 10% Bis-Tris (buffering agent) gel was used in this study. Further, 20x MOPS composed of 50 mM of Tricine, 50 mM of Tris base and 1% SDS (pH 8.24) was used as the gel running buffer. The MOPS was diluted to 1x with distilled water and then added to the Western blotting tank. Ice was also added to reduce the temperature during the gel running.

The samples were loaded onto the gel and 1–2 µl of the Bio-Rad ladder (Precision Plus Protein™ Dual Color Standards #161-0374) was added to the gel as a reference for detecting the protein sizes. The gel was run at 150 mV for approximately 90 minutes. When the samples reached the bottom of the gel, the Western blot was stopped and the gel was removed. The gel was then incubated for 5 minutes in a transfer buffer on a plate shaker at room temperature. The transfer buffer was made up by diluting the Invitrogen transfer buffer, which contains 25 mM of Bicine, 25 mM of Bis-Tris (free base) and 1 mM of EDTA pH 7.2, to 2x NuPAGE_R containing 10% methanol with distilled water. The gels were then transferred onto nitrocellulose membrane (Invitrogen) using the iBlot gel transfer system (Life Technologies iBlotTM).

The blots were stained with Ponceau S rapid stain to ensure the protein was successfully transferred from the gel to the membrane. The Ponceau S staining was then washed off using tap water. The blots were blocked in TBS with 0.05% Tween 20 (TBS-T) and 5% non-fat dried milk (NFDM, Sigma-Aldrich) for 20 min. The blots were probed overnight at 4°C with the primary antibodies. The blots were then washed with 1x TBS-T three times (15–20 minutes each wash)

on a roller at room temperature. The secondary antibodies (IRDye® 800CW Goat anti-Mouse IgG [H + L], 925-32210, and VRDye™ 549 Goat anti-Rabbit IgG [H + L], 926-54020, LI-COR Biotechnology, Cambridge, UK) were added at a 1:5000 dilution in TBS-T plus 1% NFDM and then incubated while rolling for 3 hours at room temperature. After the 3 hours, the blots were washed with 1x TBS-T three times for 15–20 minutes each wash. The blots scanned on the LI-COR Odyssey® gel scanner (LI-COR Biotechnology).

The quantitative analysis of the blots was performed by measuring the density of the lanes and bands using ImageJ 1.47v software. In order to measure the density of the bands using ImageJ, a rectangular shape should be drawn around the band. The shape, size and location of the first selection will serve as a guide for the rest of the lanes on the gel. The density of the bands is plotted as curves. The peak of each band was detected by a straight line connecting the start and the end of the curve peak. The area underneath each curve was measured using the wand tracing tool in the ImageJ 1.47v software and presented as a number. Figure 8 presents an example of the band density quantification using ImageJ 1.47v.

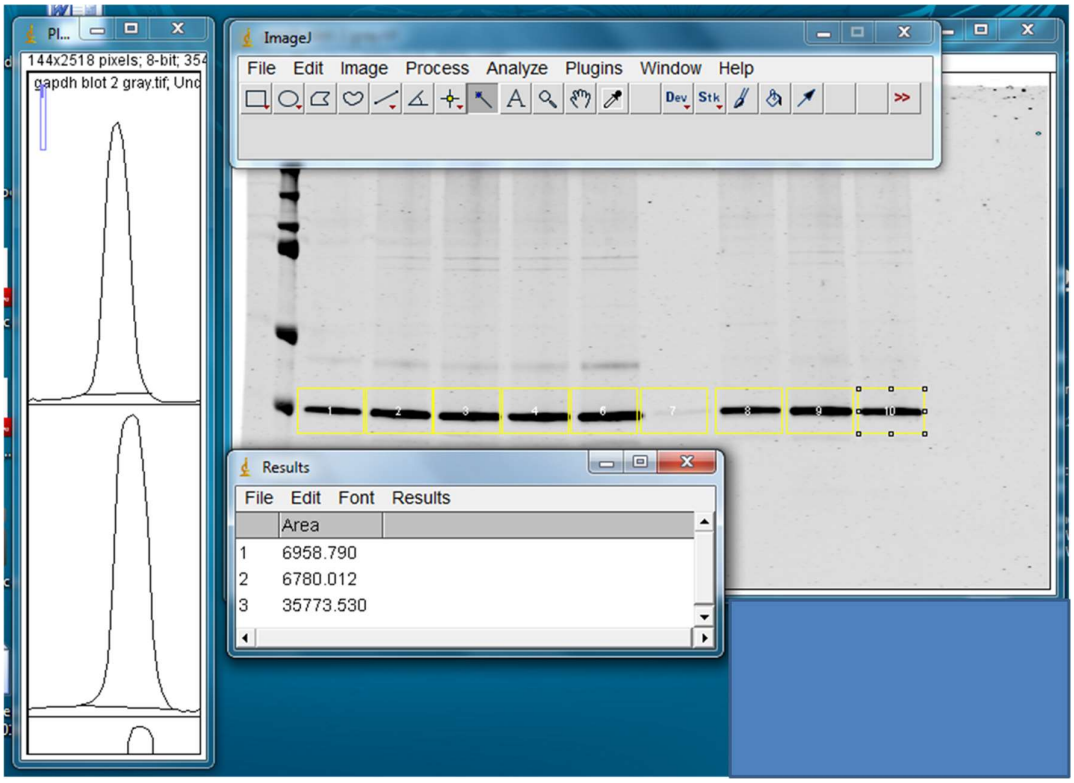

Figure 8: An illustrative example of the Western blot band quantification using the ImageJ 1.47v software. A rectangular shape is drawn around the bands and the density of the bands is presented as curves. The area underneath the peaks of the curves is measured using the selected tool and then translated into numbers.

2.2.3 Immunocytochemistry and stress experiments

Coverslips were added to a 24-well plate and then coated with poly-D-lysin (PDL) by incubating for 1 hr. The coverslips were rinsed twice with 500 µl of PBS before the cells were plated. The HeLa cells were plated on coverslips at 50,000 cells/well and left in the incubator to recover for 24 hrs. After this time, the cells were transfected with non-transgenic Flag-tagged hnRNP-E2 and HA-tagged (wild type) WT TDP43 plasmids, which will be described further in Chapter 5. After 48 hrs transfection time, the cells were exposed to different stress conditions in order to encourage the formation of stress granules. Some cells were treated with 0.5 mM of sodium arsenite for 30 minutes, while some were treated with 600 mM of sorbitol for 1 hr and others were treated with both 600 mM of sorbitol for 1hr and 0.5 mM of sodium arsenite for 30 minutes. As a control condition, other transfected cells were not exposed to any stressful conditions. The sodium arsenite and sorbitol were diluted in DMEM and then added to the cells after removing the media from the wells. Once the incubation time was up, the cells were fixed by removing the media and adding 500 µl/well of 4% PFA (paraformaldehyde) for 10 minutes and then replacing it with PBS.

The primary antibodies were diluted in an immunobuffer, which contained PBS with 1% donkey serum and 0.2% Triton TX-100. The primary antibodies were added to the coverslips as required for each experiment and then incubated on a plate rocker overnight at 4ºC. Next, the primary antibodies were removed and the coverslips were washed three times with PBS. The secondary fluorescent antibodies used were donkey anti-mouse 488 and donkey anti-rabbit 549 (Life Technologies). They were diluted in the same immunobuffer and then added to the coverslips and incubated for 3 hours on a plate rocker at room temperature. They were covered in order to protect them from the light. The secondary antibodies were removed and the coverslips were washed by adding and removing 500 µl/well PBS during each wash. DAPI (1.25 ug/ml) was added to the coverslips for 30 seconds and then washed with PBS. The coverslips were mounted using Fluorescence Mounting Medium (Dako Omnis) on microscopic slides and left to dry underneath an opaque object to prevent light exposure. The Leica confocal SP system was used to visualise high-resolution images. The processing of the images was performed using ImageJ 1.47v software.

2.2.4 Immunoprecipitation (pull-downs)

The cells were transfected as further described in Chapter 5. The cells were harvested using ice-cold IP buffer that contained 50 mM of Tris pH 7.4, 150 mM of NaCl and 1% Triton TX-100 with protease and phosphatase inhibitors. The samples were centrifuged for 30 seconds at 14,000 rpm at 4ºC. The supernatant was transferred into new tubes and the pellets were discarded. Some of the supernatant was saved as lysate to be used as an input for each sample. For the IP, the primary antibodies were added to each sample as required (with 20 µl of Invitrogen Protein G Dynabeads) and incubated on a roller at 4ºC for 4 hrs. Afterwards, the Eppendorf tubes containing the samples were attached to a magnet in order to allow the migration of the magnetic beads to the side of the Eppendorf tube. Some 20 µl of the supernatant was removed as the flow-through (FT), which was diluted with 20 µl of the 2x loading buffer containing 62.5 mM of Tris-HCL pH 6.8, 2% SDS, 10% glycerol and 0.01% bromophenol blue with 1 mM of dithiothreitol (DTT), proteinase inhibitors (1 tablet per 50 mL) and PhosSTOP (1 tablet per 50 mL). The samples were boiled for 10 minutes. The rest of the supernatant was discarded and the beads were washed three times with 500 µl of IP buffer by removing the Eppendorf tubes from the magnet, inverting them and spinning them in a pulse centrifuge for a few seconds. For the final wash, a 10 µl pipette was

used to ensure all the grit was removed. Following the washes, 20 µl of the 2x loading buffer with DTT was added to the beads and boiled for 10 minutes. The samples were loaded onto gels for Western blotting as previously described. The volume of the samples loaded onto the gels was as follows: 4 µl of the lysate and flow-through and 12 µl of the IP buffer in a 26-well gel or 9 µl of the lysate and flow-through and 15 µl of the IP buffer in a 12-well gel.

Chapter 3 Screening for TDP-43-Binding Proteins

3.1 Introduction

In 2006, TDP-43 was identified as the major component of the ubiquitinated protein aggregates in FTLD (FTLD-U), FTLD-U with MND (FTLD-MND) and ALS (Neumann et al., 2006a). Many studies have examined the role of TDP-43 in neuronal degeneration in order to understand the pathology of these diseases and establish appropriate therapeutic targets. TDP-43 belongs to the hnRNP family of proteins; therefore, it interacts with many proteins involved in the biogenesis of mRNA and other cellular and nuclear functions. A list of candidates TDP-43 interacting proteins was previously established in our lab using the stable isotope labelling with amino acids in cell culture (SILAC) method (Stalekar et al., 2015). The aim of the SILAC project was to identify the proteins down- and up-regulated by TDP-43 RNAi knockdown and overexpression in order to define the associated network pathways involved in TDP-43 pathology. The SILAC method depends on the incorporation of amino acids with substituted stable isotopic nuclei (e.g.13C, 15N), which allows the direct comparison of changes in protein expression between two samples (Mann, 2006, Ong et al., 2002). The SILAC method involves growing two populations of cells in two different media, one containing normal amino acids (light medium) and the other containing a heavy amino acid, for example, ^{13}C instead of ^{12}C. After the incorporation of either the light or heavy amino acids into the peptides, the SILAC method distinguishes two proteomes by the molecular weight of the light or heavy amino acid that is used during the growth of the two cell populations. The SILAC method's amino acid replacement would be achieved after five cell doublings in all proteins, including proteins with insignificant turnover. Therefore, there will ultimately be two populations of cells, namely population A labelled with light amino acids and population B labelled with heavy amino acids. At this point, a perturbation is introduced to one population of cells, which in this case was a knockdown of TDP-43. Then, cells from both populations (i.e. A and B) are mixed and their proteomes extracted and measured by means of mass spectrometry. Each peptide appears as a pair in the mass spectra and the ratio of the peak intensities in the mass spectrometer provides the ratio of the proteins in population A versus that in population B. If there is no change in the abundance of a particular protein due to the knockdown of TDP-43, then it will appear in a 1:1 ratio. Therefore, the SILAC method represents

a powerful approach for identifying multiple targets in a single experiment (Ong et al., 2002, Mann, 2006, Stalekar et al., 2015). Figure 9 illustrates the concept of the SILAC method.

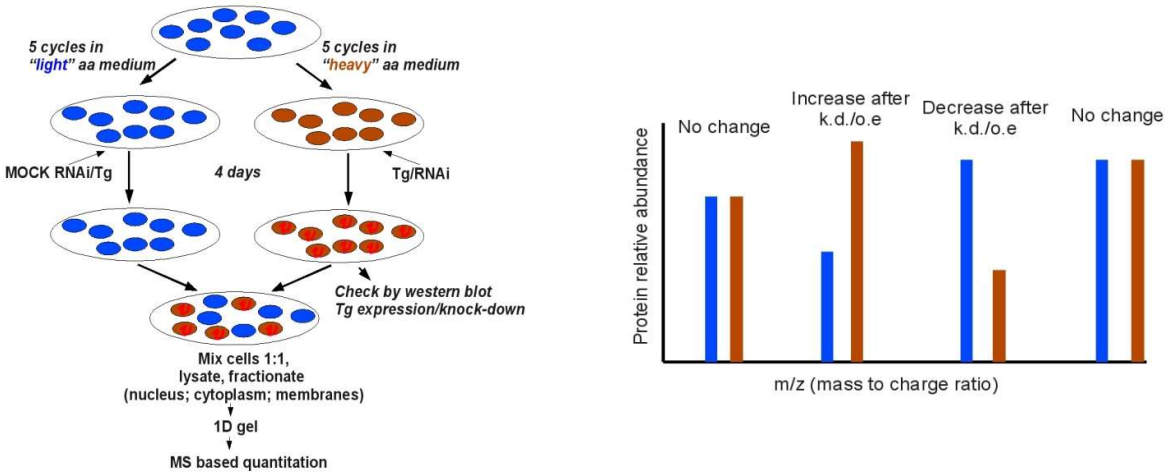

Figure 9: An illustration of the SILAC method. The left-hand side presents a diagrammatic explanation of the two cell populations, while the right-hand side is a representative illustration of the peptide presentation by means of spectrometry.

The result of the SILAC experiment was recently published (Stalekar et al., 2015). In brief, the spectrum counts of the peptides were compared in control fractions and fractions of TDP-43 knocked-down cells. The cells were fractionated into nuclear and cytoplasmic fractions. Some 106 differentially abundant candidate proteins were identified in the nuclear fraction, 65 of them being increased and 50 decreased due to the TDP-43 knockdown. Further, 167 proteins were identified in the cytoplasmic fraction, of which 73 were increased and 94 decreased because of the TDP-43 knockdown. A list of all the identified proteins can be found in (Stalekar et al., 2015). The majority of the differentially expressed proteins are involved in RNA processing and intracellular transport (Stalekar et al., 2015).

In this study, the expression of a number of the identified proteins and their potential role in the disease mechanism was investigated using post-mortem human brain and spinal cord samples from FTLD and ALS cases with TDP-43 pathology. An initial screening for those proteins in the FTLD and ALS brain and spinal cord tissue was performed by IHC, which is recognised as an important tool for elucidating a differential diagnosis that cannot be determined by conventional analysis. It is considered to be a purely descriptive method, which presents a picture of the situation that occurs in vivo. The discovery of antigen retrieval methods allowed for its application

in fresh and fixed tissue, which increased its applicability in the diagnosis of pathological anatomy (Huang et al., 1976, de Matos et al., 2010). The contribution of IHC to the field of neurodegeneration research has advanced far beyond the identification of specific diseases from a differential clinical diagnosis. The discovery of protein depositions within degenerating neurons taken from the post-mortem tissues of patients has opened a window of opportunity for better understanding the underlying pathological mechanisms (Duraiyan et al., 2012, de Matos et al., 2010). Based on the level of change observed in the SILAC study as well as other previous research publications detailing their cellular functions, a number of proteins that could potentially interact with TDP-43 pathology were selected for investigation in the present study. The selected proteins were RANBP1, ubiquilin-2, hnRNP-M, hnRNP-C1/C2, hnRNP-Q and hnRNP-E2.

3.1.1 RANBP1

Ran-binding protein 1 regulates the RanGTPase system. Ran is a small GTPase that is predominantly located in the nuclear membrane (Ren et al., 1995). The RanGTP gradient controls the transport of proteins and other biomolecules through the nuclear envelope. RANBP1 binds directly to RanGTP and stimulates its conversion to RanGDP (Melchior et al., 1993) (Bischoff et al., 1995). RanBP1 was found to be downregulated by TDP-43 knockdown in the SILAC experiment (Stalekar et al., 2015). The downregulation of RanBP1 by TDP-43 knockdown was also reported in SK-Hep1 cells, with the same study suggesting that TDP-43 regulation could be a possible target for metabolic regulation in hepatic cell carcinoma (Park et al., 2013). TDP-43 was also reported to promote the silencing of exon 5 in the RanBP1 transcript (Tollervey et al., 2011b). The depletion of RanBP1 increases the RanGTP in cells, which can arrest protein transport through the nuclear envelope (Tedeschi et al., 2007). The loss of RanBP1 is embryonically lethal to mice and it is associated with microcephaly by disrupting the cortical projection of developing neurons selectively in layers 2/3, which is a critical area for behavioural impairments (Paronett et al., 2015).

3.1.2 Ubiqulin-2

Ubiquilin-2 belongs to the ubiquilin family of proteins that regulate the degradation of ubiquitinated proteins. It is encoded by the *UBQLN2* gene, which is located on the X chromosome. Five missense mutations have been identified in the *UBQLN2* gene that are linked to ALS and FTLD.

One mutation was found in a large X-linked dominant ALS-dementia family (Deng et al., 2011), while two mutations were found in single patients from two small families with classic ALS. The other two mutations segregated with the disease in multigenerational ALS-FTD families. Ubiquilin-2 pathology was described as a component of spinal cord inclusions in a subset of sporadic ALS, familial ALS and ALS with dementia cases (Deng et al., 2011, Williams et al., 2012, Fecto and Siddique, 2011). Functional studies have shown that defects in ubiquilin-2 cause the impaired degradation of misfolded proteins, which implies a common pathogenic mechanism in neurodegenerative diseases (Deng et al., 2011).

3.1.3 hnRNPs

TDP-43 belongs to the very large family of nuclear factors known as hnRNPs (Buratti and Baralle). hnRNP is a collective term for the proteins that associate with the pre-mRNAs (hnRNAs). There are more than 20 major hnRNPs found in human cells, which are designated hnRNP-A1 to hnRNP-U (Table 5) (Chaudhury et al., 2010, Dreyfuss et al., 2002, Ghosh et al., 2008, Weighardt et al., 1996). The binding of hnRNPs to hnRNAs strongly affects the fate and processing of hnRNAs to mRNAs by influencing their structure and interactions. Steady-state hnRNPs are normally localised in the nucleus; however, they shuttle continuously between the nucleus and the cytoplasm, which indicates that they play a role in transducing signals between the nucleus and the cytoplasm as well as in mRNA export and function in the cytoplasm (Pinol-Roma and Dreyfuss, 1992). hnRNPs are important proteins for the nucleocytoplasmic transport of mRNAs as well as mRNA localisation, translation and stability. They also play an important role in transcription regulation, gene splicing, telomere length maintenance, immunoglobulin gene recombination, pre-ribosomal-RNA processing and 3'-end processing (Hoek et al., 1998, Michelotti et al., 1996, Mayeda and Krainer, 1992, Tomonaga and Levens, 1995). Several other hnRNP proteins were found to interact with TDP-43 in the SILAC experiment (Stalekar et al., 2015). Therefore, the hnRNPs represent potential TDP-43 interacting proteins in ALS and FTLD cases. In the search for TDP-43 candidate partners in ALS and FTLD, a number of hnRNPs that were either identified by the SILAC experiment or selected based on other research studies were included in the screening section of this study. The investigated hnRNPs were hnRNP-C1/C2, hnRNP-M, hnRNP-Q and hnRNP-E2.

Table 5: Characterisation of hnRNPs and other mRNA proteins (Dreyfuss et al., 2002)

Proteins	Domain structure	kDa*	Possible functions	Shuttling	References
A1	2XRBD, RGG	34	mRNA splicing mRNA export Telomere biogenesis	+	8,24–26,29,35 43,44 20,22
A2/B1	2XRBD, RGG	36/38	mRNA splicing mRNA localization	+	1,2 45,49
C1/C2	1XRBD	41/43	mRNA splicing mRNA stability	–	1,2 56
D(AUF1)	2XRBD, RGG	44–48	Telomere biogenesis mRNA stability Recombination	+	19,21 55,59,60 23
E1/E2 (αCP1,2 or PCBP1,2)‡	3XKH	38,39	mRNA stability Translational control	+	54,57 50,51,53
F	3XRBD	53	mRNA splicing	N/K§	27
H/H'(DSEF-1)	3XRBD	56	mRNA splicing Polyadenylation	N/K§	31,33 40
I (PTB)	4XRBD	59	mRNA splicing mRNA localization Polyadenylation	+	28,30 47 38
K	3XKH, RGG	62	Transcription Translational regulation	+	16–18 10,50,51,53
L	4XRBD	68	mRNA export mRNA stability	N/K§	7 42
Q	3XRBD, RGG	55–70	mRNA splicing	N/K§	34
U	RGG	120	Nuclear retention	–	1,2
PABPI	4XRBD	72	mRNA translation and stability	+	64–67
HuR	3XRBD	36	mRNA stability mRNA export	+	109 44
Yra1	1XRBD	27	mRNA export	–	123,124
Npl3/Nop3	2XRBD, RGG	60	mRNA export Pre-rRNA processing	+	41 36
Hrp1/Nab4	2XRBD, RGG	73	Polyadenylation	+	37
Squid/hrp40	2XRBD, RGG	40	mRNA localization	N/K§	46
ASF/SF2 (SRp30a)	2XRBD, RS domain	30	mRNA splicing	+	63
SC35 (SRp30b)	1XRBD, RS domain	30	mRNA splicing	–	63
SRp20	1XRBD, RS domain	20	mRNA splicing mRNA export	+	63 116
9G8	1XRBD, RS domain	35	mRNA splicing mRNA export	+	63 116
magoh	N/Hǁ	17	EJC/mRNA localization	(+)¶	79,83,127,128
Y14	1XRBD	24	EJC/NMD mRNA localization	+	78–80 90,91
Aly/REF	1XRBD	32	EJC/mRNA export	+	79,82,88
RNPS1	1XRBD, RS domain	50	mRNA splicing EJC/NMD	+	81 79,89
DEK	N/Hǁ	60	EJC/mRNA splicing	–	79,87
Upf3	1XRBD	66	EJC/NMD	+	85,86,89
SRm160	RS domain	160	EJC/mRNA splicing	–	77,79

*Molecular mass (kDa) is estimated from SDS-polyacrylamide gel electrophoresis.
‡Although αCP1/PCBP1 and αCP2/PCBP2 have been identified as hnRNP E1/E2 proteins, it has not been verified that these proteins are identical to hnRNP E proteins in the human hnRNP complexes[1,2].
§N/K, not known.
ǁN/H, no significant homology to other known motifs.
¶This protein is strongly proposed to shuttle[79,83], but it has not been proved.

3.1.3.1 hnRNP-M

hnRNP-M is present in four isoforms (hnRNP-M1-4), which arise from two variable mRNAs by means of the alternative splicing of single pre-mRNA and differ in terms of a stretch of 39 amino acids. hnRNP-M contains three RRM, a glycine/methionine-rich region and a methionine/arginine-

rich repeat motif (Dreyfuss et al., 2002, Datar et al., 1993, Kafasla et al., 2002. hnRNP-M depletion from nuclear extracts inhibits splicing in early spliceosome assembly {Aidinis,1995 #2193). The alternative splicing of transcripts generated from fibroblast growth factor receptor 2 (FGFR2) and other mini-genes was found to be regulated by hnRNP-M (Park et al., 2011, Hovhannisyan and Carstens, 2007). The splicing regulation function of hnRNP-M can be influenced by interactions with specific binding partners (Marko et al., 2010, Lleres et al., 2010).

One component of the hnRNP-M interaction network is the association of hnRNP-M with the Ewing sarcoma protein (EWS). EWS belongs to the highly related RNA/ssDNA-binding proteins and transcription factors known as the FET family of proteins (FUS/TLS, EWS and TAF15) (Pahlich et al., 2009, Tan and Manley, 2009). The FET family of proteins was initially discovered as components of the fusion oncogenes that cause human cancers. The proteins' normal function is predicted to include roles in RNA transcription, processing and transport, microRNA processing and DNA repair (Kovar, 2011, Law et al., 2006). Mutations in the FUS/TLS gene have been reported to cause of 3% of familial ALS and 1% of sporadic ALS (Mackenzie et al., 2010b, Vance et al., 2009). ALS with FUS mutations (ALS-FUS) is characterised by abnormal cytoplasmic neuronal and glial inclusions that are immune-reactive for FUS. FUS inclusions were also detected in several subtypes of FTLD designated as FTLD-FUS. However, no FUS mutations have been reported in any of the FTLD-FUS cases to date (Mackenzie et al., 2010a, Urwin et al., 2010, Snowden et al., 2011). Interestingly, the abnormal accumulation of all three FET proteins in pathological inclusions has been reported as a consistent and specific feature of all subtypes of FTLD-FUS. This contrasts with the situation of ALS-FUS, where only FUS was detected in the pathological inclusions in all investigated cases, which raises the possibility of subtle differences in the pathogenic pathways involved in the different FTLD-FUS subtypes (Neumann et al., 2011). Moreover, a study by Marko et al. (2014) reported that hnRNP-M interacts with FUS/TLS and TAF15 as well as EWS. However, the selective preferences of the hnRNP-M isoforms associate with different FET proteins. Indeed, FUS/TLS preferably interacted with the relatively more abundant lower molecular weight hnRNP-M1/2 isoform, while TAF15 showed a greater preference for associating with the higher molecular weight hnRNP-M3/4. The complex formation of hnRNP-M with FET proteins was found to be based on protein-protein interactions rather than RNA-based interactions (Marko et al., 2014). Furthermore, hnRNP-M was found to promote SMN2 exon 7 pre-mRNA inclusions in spinal muscular atrophy due to directly contacting an

enhancer on exon 7 (Cho et al., 2014). Together, the reported interactions of hnRNP-M suggest that it may have involvement in the underlying mechanisms of neurodegeneration, which renders it worthy of further investigation in FTLD and ALS cases.

3.1.3.2 hnRNP-C1/C2

hnRNP-C1/C2 are two alternative splice translation products of the human *hnRNP-C1/C2* gene (Burd, 1994). hnRNP-C1 is created by the excision of 13 amino acids from the hnRNP-C1/C2 coding sequence, which makes hnRNP-C1 the smaller of the two variants (Rech et al., 1995, McAfee et al., 1996). hnRNP-C1/C2 form the core elements of an hnRNP complex – along with hnRNP-A1, hnRNP-A2, hnRNP-B1 and hnRNP-B2 – that acts to handle RNA transcripts for intracellular destruction or translation. hnRNP-A, B and C form heterotetrameric complexes that assemble as an anti-parallel 4-helix coiled coil on nascent transcripts in order to regulate their splicing, turnover and polyadenylation (Dreyfuss et al., 2002). hnRNPC1/C2 were found to interact with dengue virus RNA and vimentin (which is an intermediate filament supporting cellular integrity) (Dechtawewat et al., 2015). The hnRNP-C1/C2 complex was also identified as a competitor with the normally functioning VDR-retinoid X receptor (RXR) dimer for binding to the vitamin D response element (VDRE), which causes vitamin-D-resistant rickets (Chen et al., 2006). hnRNP-C1/C2 have also been reported to exhibit nuclear actions, including splicing, telomere regulation, nuclear retention of hnRNAs, mRNA biogenesis and transport, protein translation and nuclear matrix stability (Orphanides and Reinberg, 2000). Both hnRNP-C1 and C2 contain an RNA recognition motif and a leucine zipper-like RNA-binding motif. Under basal conditions, hnRNP-C1/C2 reside mainly in the nucleus; however, they translocate to the cytoplasm during certain cellular conditions such as mitosis, apoptosis and viral infection (Dreyfuss, 1993, Kim et al., 2003, Gustin and Sarnow, 2002). The important functions of hnRNPC1/C2 in pre-mRNA packaging and processing render them possible candidates for TDP-43 partnership.

3.1.3.3 hnRNP-Q

hnRNP-Q has three isoforms, which are generated by alternative splicing. hnRNP-Q1 is the major isoform and it contains an acidic residue-rich domain at the N terminus. It also contains three RNA recognition motifs (RRMs) in the central region and an arginine/glycine (RG)-rich domain at the C terminus. hnRNP-Q2 has a truncated RRM2 and an extended C-terminal region. hnRNP-

Q3 only differs from hnRNP-Q1 in terms of its C-terminal extension, which is the same as that seen for hnRNP-Q2, making it the longest isoform (Chen et al., 2008a). hnRNP-Q has been reported to play a role in mRNA splicing and mRNA stability (Mourelatos et al., 2001, Grosset et al., 2000). In the neurons, hnRNP-Q was found to be a component of the cytoplasmic mRNA granules and it has been suggested that it acts with the survival motor neuron (SMN) gene in mRNA trafficking (Rossoll et al., 2003, Rossoll et al., 2002). Interestingly, a clinical study reported elevated expression levels of hnRNP-Q in spinal muscular atrophy (SMA) patients with mild symptoms as well as in their unaffected siblings, which suggests a severity modulation role of hnRNP-Q (Helmken et al., 2003). SMA is a common inherited neuromuscular disorder caused by the homozygous loss of function of the *SMN1* gene. At least one copy of the *SMN2* gene, which is highly identical to the *SMN1* gene, is carried by all SMA patients. A critical nucleotide change resulting in alternative splicing and the exclusion of exon 7 is seen in the majority of SMN2 mRNA, which results in a lower level of production of the functional SMN protein (Chen et al., 2008a, Yuo et al., 2008). The involvement of hnRNP-Q in the pathology of SMA makes it an interesting candidate for screening in FTLD and ALS.

3.1.3.4 hnRNP-E2

The hnRNP-E proteins belong to the hnRNP-K protein family with triple KH domains designated KH1, KH2 and KH3. Each of the KH domains is able to interact independently with a target RNA sequence, which provides these proteins with a potentially high number of complex-specific RNA interactions. They are highly expressed in human tissues and they can bind both poly(C) regions and low-C mRNAs. hnRNP-E1 and E2 are the most highly expressed and well-characterised isoforms of the hnRNP-E proteins. They have 89% amino acid similarity. It is believed that hnRNP-E1 is encoded by an intronless gene that is a product of a retrotransposition event of a fully processed minor isoform of hnRNP-E2 (Makeyev and Liebhaber, 2002, Makeyev et al., 1999, Woolaway et al., 2007). Woolaway et al. (2007) investigated the effects of the overexpression and depletion of hnRNP-E1 and E2 on HIV-1 gene expression. They demonstrated that the depletion of either hnRNP-E1 or E2 led to the increased production of the HIV-1 structural proteins. Yet, the overexpression of hnRNP-E1 but not of E2 can inhibit the expression of the Rev-dependent RNAs encoding gp120 and p24. Therefore, despite the high degree of sequence similarities between the hnRNP-E1 and E2 isoforms, they have distinct non-redundant cellular

functions. Work conducted by other research groups has corroborated these findings by demonstrating the higher affinity of hnRNP-E1 for hnRNP-D than hnRNP-E2 (Kiledjian et al., 1999). It has also been reported that hnRNP-E1 and E2 exhibit differential regulation in response to the hypoxic stress of cortical neurons (Zhu et al., 2002).

3.1.4 Aims of this chapter

This chapter aims to identify the proteins in human brain and spinal cord tissue that could be interacting with TDP-43 pathology by using immunohistochemistry on FTLD-TDP tissue (of different pathological subtypes) and control cases.

3.2 Methods

3.2.1 Immunohistochemistry

Sections were obtained from FTLD cases with identified TDP-43 pathological subtypes. Formalin-fixed, paraffin-embedded tissue sections from the frontal cortex of the brain of five subtype A, four subtype B, five subtype C, five TDP-43 cases with the *C9orf72* expansion and five control cases were examined using immunohistochemistry (tissue from the TDP-43 subtype D could not be obtained due to its rarity). IHC was performed as described in section 2.1.1 using antibodies directed against the proteins selected as candidate TDP-43-binding proteins based on the results of the SILAC experiment.

Initially, each antibody was optimised for use in the IHC technique by testing a number of dilutions (and, if necessary, pretreatment techniques) of each antibody on control and FTLD sections. The utilised antibodies are detailed in section 2.2.2.

3.2.2 Double-labelling immunofluorescence

Double-labelling immunofluorescence was conducted as described in section 2.2.3. The primary antibodies were the TDP-43 polyclonal antibody (Proteintech) at a 1:250 dilution and the ubiquilin-2 monoclonal antibody (Abnova) at a 1:150 dilution. The experiment was performed on FTLD-TDP cases #2 and #22, which showed ubiquilin-2 inclusions by IHC.

3.3 Results

3.3.1 Initial screening of TDP-43-binding candidate proteins on human brain tissue

Immunohistochemistry was utilised to screen for the candidate TDP-43-binding proteins identified in the SILAC experiment (Stalekar et al., 2015) in the frontal cortex tissue from FTLD-TDP cases and controls. Initially, two control cases and two FTLD-TDP cases were used to optimise the antibodies and then further investigation was conducted using a number of cases from different FTLD subtypes and control cases.

3.3.1.1 RANBP1

RANBP1 was tested at dilutions of 1:75, 1:100 and 1:200, with the 1:200 dilution being demonstrated to be optimal.

The results of the RANBP1 antibody optimisation are demonstrated in Figure 10. The immunostaining of RANBP1 at a 1:200 dilution in the frontal cortex of the control case (A) showed strong nuclear reactivity when compared to the frontal cortex of the FTLD-TDP subtype B case (B). The cytoplasmic staining looked similar in both the control (A) and the case (B), with only very minimal background staining. There were no RANBP1 aggregates detected in any region of the frontal cortex of the FTLD-TDP case.

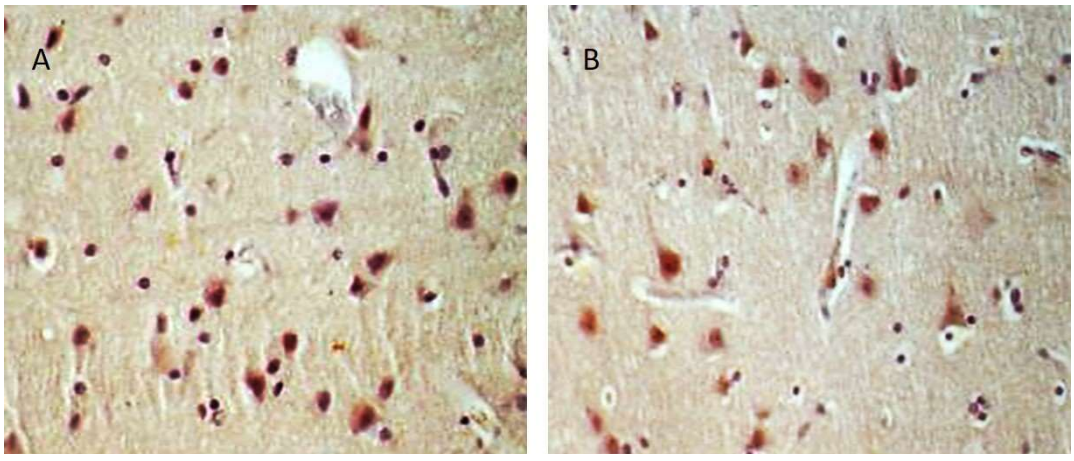

Figure 10: RANBP1 IHC at 1:200 in the frontal cortex of a control case (A) and an FTLD subtype B case (B). Strong nuclear staining in the control as compared to weak nuclear labelling in FTLD-TDP.

Further IHC for RANBP1 was not performed due to time limitations. We focused on the hnRNPs because of the increasing body of evidence regarding their interaction with TDP-43.

3.3.1.2 Ubiquilin-2

The ubiquilin-2 antibody was tested at dilutions of 1:100, 1:250 and 1:500 (all with citrate buffer pretreatment). The optimal dilution was found to be 1:500, with diffuse and very weak cytoplasmic staining and stronger nuclear staining being seen in the motor neurons in the frontal cortex of a control case (Figure 11A). In the frontal cortex of the FTLD-TDP type B case (Figure 11B), striking ubiquilin-2-positive inclusions were detected in the motor neurons' cell bodies and neurites.

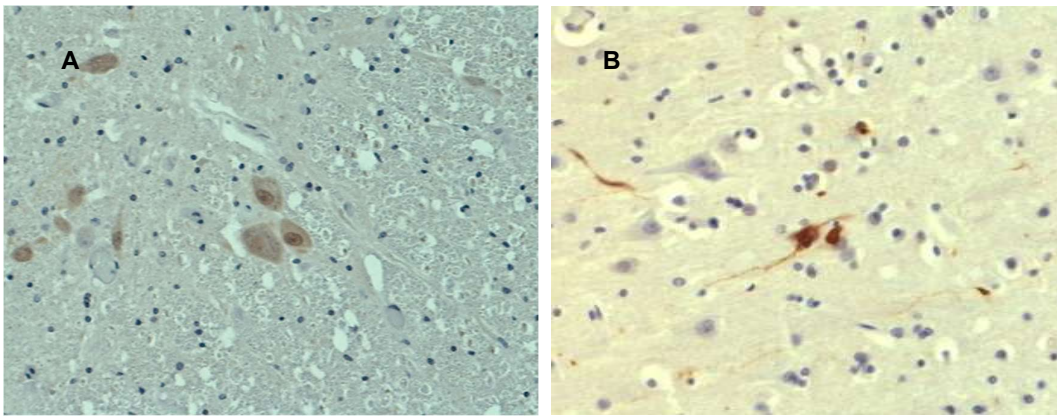

Figure 11: Ubiquilin-2 staining in the frontal cortex of a control case (A) and an FTLD-TDP case (type B) (B). Diffuse weak cytoplasmic and strong nuclear staining are seen in the motor neurons of the control case, whereas inclusions were noted in the FTLD-TDP case.

The pattern of ubiquilin-2 staining in the different FTLD subtypes was then further investigated using the optimal 1:500 dilution. The results from five FTLD type A, four FTLD type B, five FTLD type C, five *C9orf72* expansion-positive cases and five controls are shown in Table 6 and Figure 12. Ubiquilin-2 inclusions were detected in the FTLD-TDP subtype B and FTLD-C9orf72 expansion-positive cases, but not in the other groups.

Table 6: UBQLN2 IHC results

Case Ref.	*Case No.*	*Diagnosis*	*Subtype*	*UBQLN2 IHC*
9	103/08	FTLD-TDP	A	Diffuse cytoplasmic and strong nuclear staining
12	033/08	FTLD-TDP	A	Diffuse cytoplasmic and strong nuclear staining
2	029/09	FTLD-TDP	A	Diffuse cytoplasmic and strong nuclear staining – some neurites seen
1	025/11	FTLD-TDP	A	Diffuse cytoplasmic and strong nuclear staining
6	172/12	FTLD-TDP	A	Weak cytoplasmic and strong nuclear staining
21	432/12	FTLD-TDP	B	Nuclear staining only
19	058/12	FTLD-TDP	B	Nuclear staining only
17	157/12	FTLD-TDP	B	Strong staining with inclusions
18	169/11	FTLD-TDP	B	Strong nuclear staining, inclusions and dendrites
22	013/10	FTLD-TDP	C	Strong nuclear staining
25	301/10	FTLD-TDP	C	Strong nuclear
28	163/07	FTLD-TDP	C	Diffuse cytoplasmic and nuclear
24	061/13	FTLD-TDP	C	Weak overall – some positive dendrites
27	409/08	FTLD-TDP	C	Weak nuclear staining
31	403/08	FTLD-ALS *C9orf72*	B	Strongly nuclear positivity, inclusions seen
35	069/02	FTLD-ALS *C9orf72*	B	Weaker overall but strong nuclear and inclusions seen
41	151/08	FTLD-ALS *C9orf72*	B	Strongly nuclear positivity, inclusions seen
44	163/09	FTLD-ALS *C9orf72*	A	Strongly nuclear positivity, inclusions seen
45	174/08	FTLD-ALS *C9orf72*	n/a	Strongly nuclear positivity, inclusions seen
109	158/14	Control	n/a	Weak nuclear and cytoplasmic staining
110	278/96	Control	n/a	Weak nuclear and cytoplasmic staining
99	048/09	Control	n/a	Weak nuclear and cytoplasmic staining
100	063/10	Control	n/a	Weak nuclear and cytoplasmic staining
103	123/09	Control	n/a	Weak nuclear and cytoplasmic staining

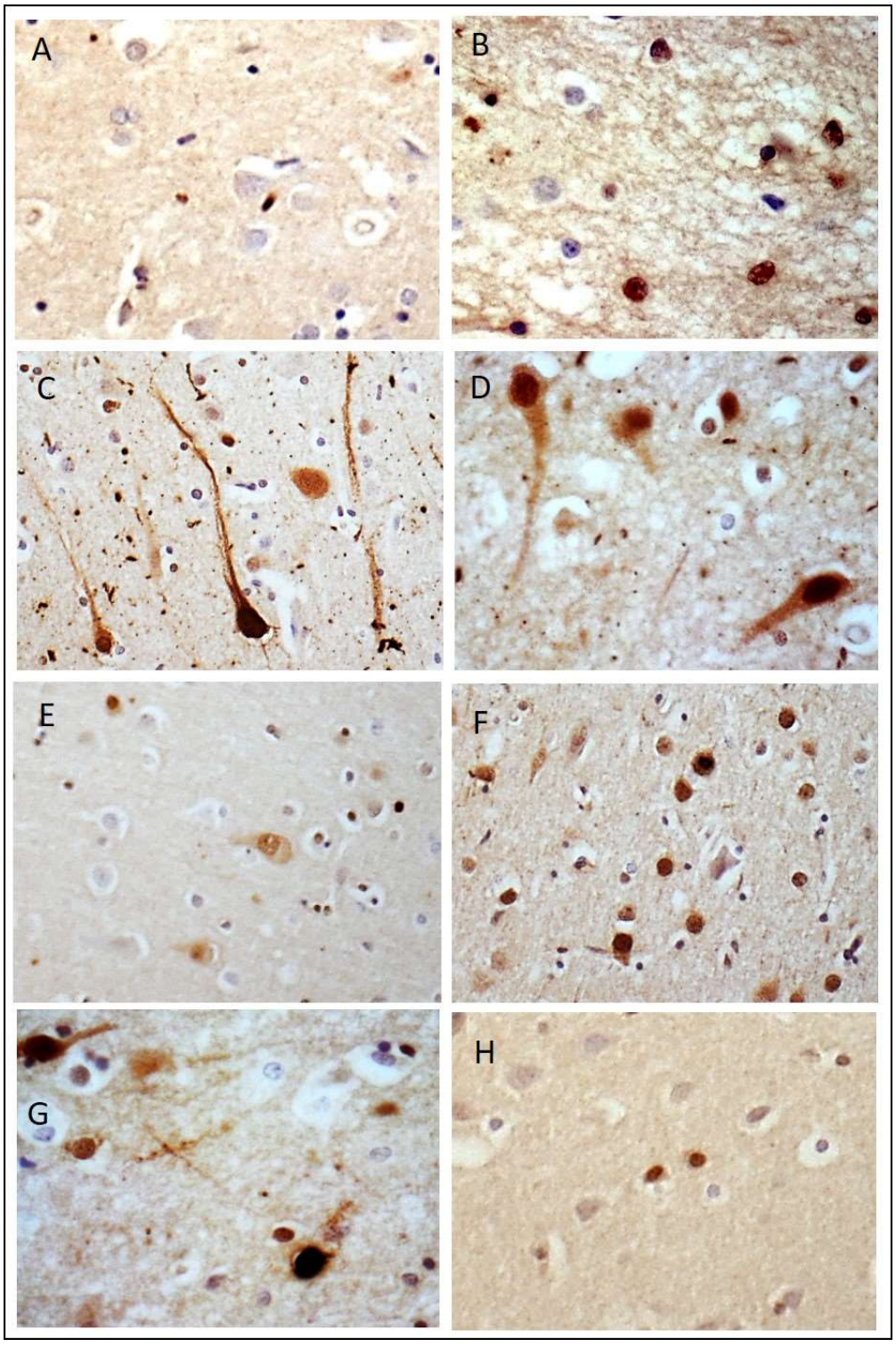

Figure 12: IHC for ubiquilin-2 shown in FTLD-TDP cases: subtype A, case ref. 2, 20x (A) and 40x (B), subtype B, case ref. 17, 20x (C) and 40x (D), subtype C, case ref. 28, 20x (E), *C9orf72* expansion-positive, case ref. 45, 20x (F) and 40x (G) and control, case ref. 99, 20x (H). Cytoplasmic staining and strong nuclear positivity are seen in both the FTLD-TDP and control cases. Striking inclusions can be seen in C, D, F and G.

3.3.1.3 hnRNP-E2

The hnRNP-E2 IHC showed weak diffuse staining in the cytoplasm and stronger nuclear staining in the frontal cortex of the control case (Figure 13A). In the frontal cortex of two FTLD-TDP cases, the hnRNP-E2 IHC showed striking crescentic perinuclear and dystrophic neurite inclusions (B). The inclusions were detected with all three tested dilutions (i.e. 1:100, 1:250 and 1:500), although 1:500 was chosen as the optimum dilution.

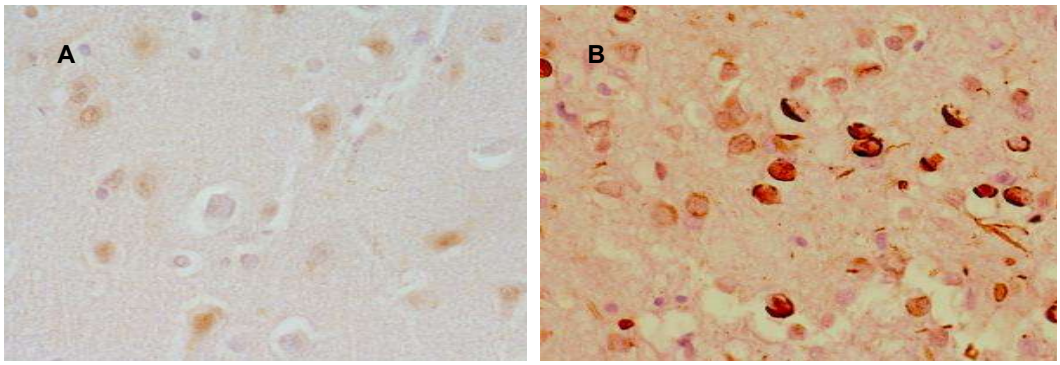

Figure 13: hnRNP-E2 immunohistochemistry. Weak staining in the cytoplasm and stronger nuclear staining in the frontal cortex of the control case (A, left). In the frontal cortex of two FTLD-TDP cases, hnRNP-E2 IHC showed striking crescentic perinuclear and dystrophic neurites inclusions (B, right).

Table 7: hnRNP-E2 IHC results

Case Ref.	*Case No.*	*Diagnosis*	*Subtype*	*hnRNP E2 Inclusions*
9	103/08	FTLD-TDP	A	+
12	033/08	FTLD-TDP	A	+
2	029/09	FTLD-TDP	A	+
1	025/11	FTLD-TDP	A	-
6	172/12	FTLD-TDP	A	+
21	432/12	FTLD-TDP	B	-
19	058/12	FTLD-TDP	B	-
17	157/12	FTLD-TDP	B	-
18	169/11	FTLD-TDP	B	-
22	013/10	FTLD-TDP	C	+
25	301/10	FTLD-TDP	C	+
28	163/07	FTLD-TDP	C	+
24	061/13	FTLD-TDP	C	+
27	409/08	FTLD-TDP	C	+
31	403/08	FTLD-ALS *C9orf72*	B	-
35	069/02	FTLD-ALS *C9orf72*	B	-
41	151/08	FTLD-ALS *C9orf72*	B	-
44	163/09	FTLD-ALS *C9orf72*	A	-
45	174/08	FTLD-ALS *C9orf72*	n/a	-
109	158/14	Control	n/a	-
110	278/96	Control	n/a	-
99	048/09	Control	n/a	-
100	063/10	Control	n/a	-
103	123/09	Control	n/a	-

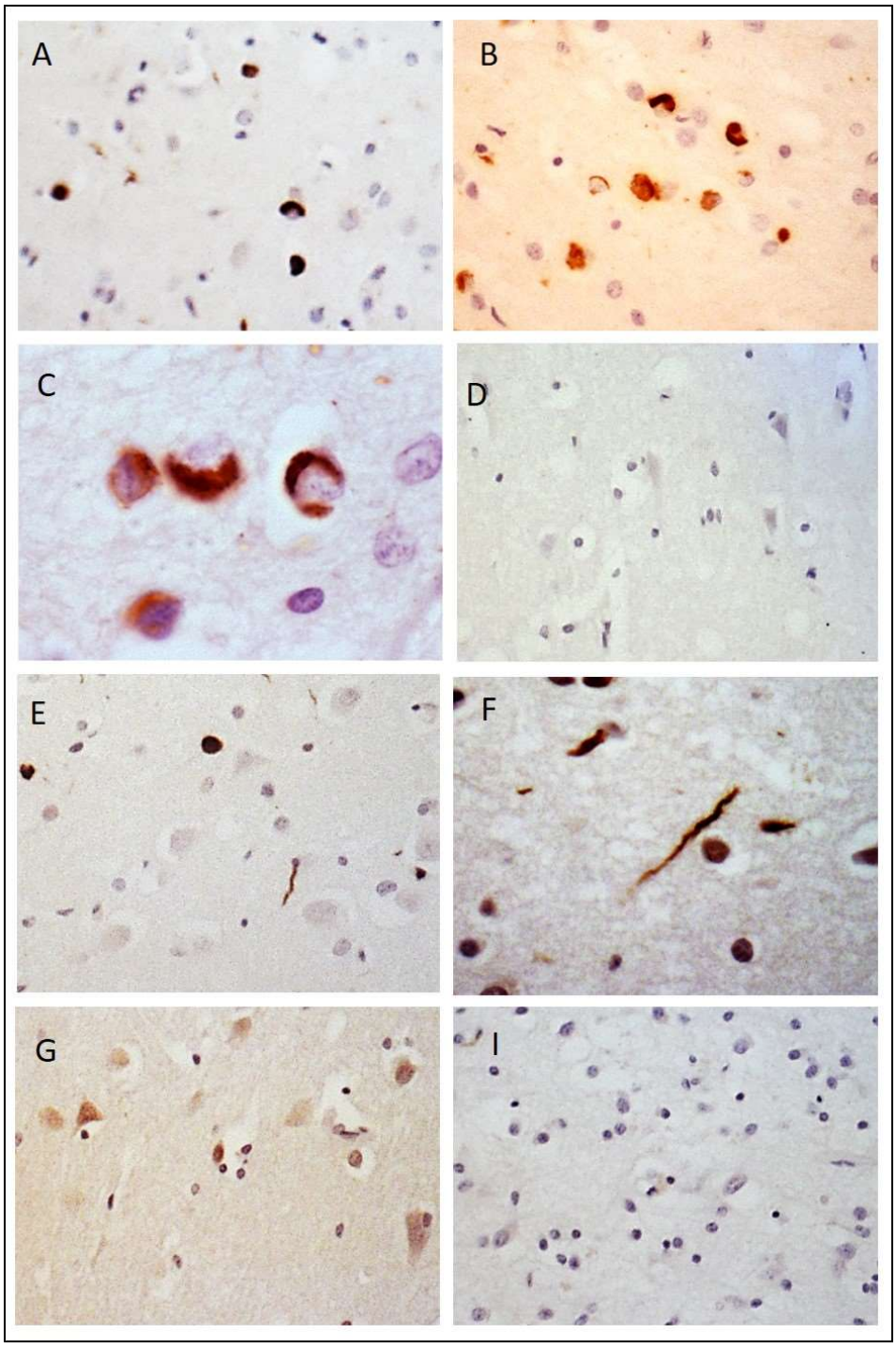

Figure 14: IHC for hnRNP-E2 shown in FTLD-TDP cases: subtype A, case ref. 2, 20x (A), 40x (B) and 100x (C). Subtype B, case ref. 17, 20x (D). Subtype C, case ref. 25, 20x (E) and 40x (F). *C9orf72* expansion-positive, case ref. 31, 20x (G). Control, case ref. 109, 20x (I). Weak cytoplasmic staining is seen in both the FTLD-TDP and control cases. Inclusions matching the pattern of TDP-43 pathology can be seen in subtypes A and C.

.

3.3.1.4 hnRNP-M

hnRNP-M was tested at dilutions of 1:100, 1:200 and 1:500, with 1:500 being selected as the optimal dilution. The IHC of hnRNP-M in the frontal cortex of the FTLD-TDP case (Figure 15A–D) showed nuclear immunoreactivity, which did not differ from the frontal cortex staining of the control case (Figure 15E).

Table 8: hnRNP-M IHC results

Case Ref.	*Case No.*	*Diagnosis*	*Subtype*	*hnRNP-M IHC*
9	103/08	FTLD-TDP	A	Nuclear staining
12	033/08	FTLD-TDP	A	Weak nuclear and cytoplasmic staining
2	029/09	FTLD-TDP	A	Nuclear and cytoplasmic staining
1	025/11	FTLD-TDP	A	Weak nuclear staining
6	172/12	FTLD-TDP	A	Weak nuclear staining
21	432/12	FTLD-TDP	B	Weak cytoplasmic staining
19	058/12	FTLD-TDP	B	Nuclear staining
17	157/12	FTLD-TDP	B	Nuclear staining
18	169/11	FTLD-TDP	B	Nuclear and cytoplasmic staining
22	013/10	FTLD-TDP	C	Nuclear and cytoplasmic staining
25	301/10	FTLD-TDP	C	Weak cytoplasmic staining
28	163/07	FTLD-TDP	C	Nuclear staining
24	061/13	FTLD-TDP	C	Nuclear staining
27	409/08	FTLD-TDP	C	Weak nuclear staining
31	403/08	FTLD-ALS *C9orf72*	B	Nuclear staining
35	069/02	FTLD-ALS *C9orf72*	B	No positivity
41	151/08	FTLD-ALS *C9orf72*	B	Nuclear staining
44	163/09	FTLD-ALS *C9orf72*	A	Nuclear and cytoplasmic staining
45	174/08	FTLD-ALS *C9orf72*	n/a	Nuclear and cytoplasmic staining
109	158/14	Control	n/a	Nuclear staining
110	278/96	Control	n/a	Weak nuclear staining
99	048/09	Control	n/a	Weak nuclear staining
100	063/10	Control	n/a	Weak nuclear staining
103	123/09	Control	n/a	Weak nuclear staining

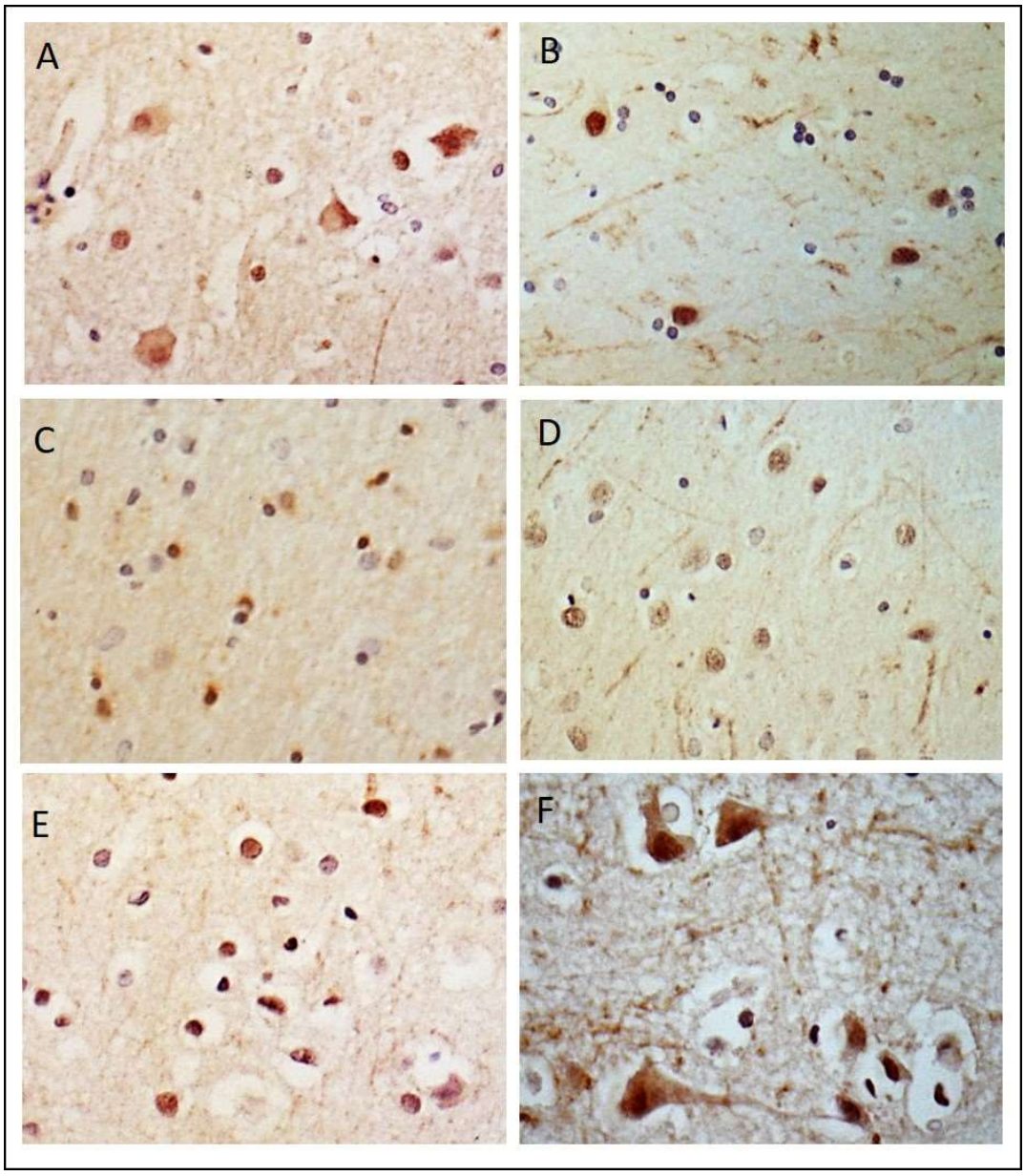

Figure 15: IHC for hnRNP-M shown in FTLD-TDP cases: subtype A, case ref. 4, 20x (A), subtype B, case ref. 11, 20x (B), subtype C, case ref. 2, 20x (C), *C9orf72* expansion-positive, case ref. 41, 20x (D), control, case ref. 103, 20x (E). Control, case ref. 109, 40x (F). Cytoplasmic staining and nuclear positivity are seen in all the FTLD-TDP subgroups and control cases. There was no obvious difference between the subtype groups.

3.3.1.5 hnRNP-C1/C2

hnRNP-C1/C2 were tested at concentrations of 1:100, 1:200 and 1:500, with 1:500 being selected as the optimal dilution. Strong staining in the nucleus was detected by the hnRNP-C1/C2 in the frontal cortex of both the control (Figure 16A) and the FTLD-TDP case (Figure 16 B).

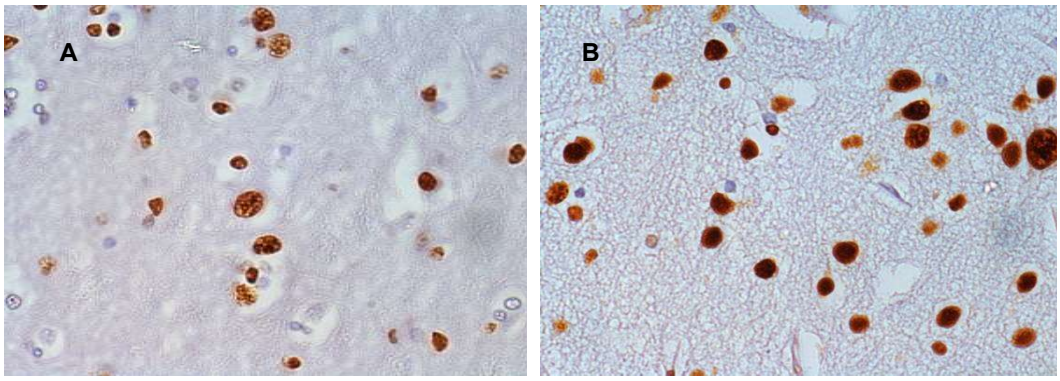

Figure 16: hnRNP-C1/C2 immunohistochemistry. Strong staining in the nucleus was detected in the frontal cortex of both the control (A, left) and the FTLD-TDP case (B, right).

Table 9: hnRNP-C1/C2 IHC results

Case Ref.	*Case No.*	*Diagnosis*	*Subtype*	*hnRNP-C1/C2 IHC*
9	103/08	FTLD-TDP	A	No immuno-positivity
12	033/08	FTLD-TDP	A	Nuclear staining
2	029/09	FTLD-TDP	A	Strong nuclear staining
1	025/11	FTLD-TDP	A	Nuclear staining
6	172/12	FTLD-TDP	A	Nuclear staining
21	432/12	FTLD-TDP	B	Nuclear staining
19	058/12	FTLD-TDP	B	Nuclear staining
17	157/12	FTLD-TDP	B	Nuclear staining
18	169/11	FTLD-TDP	B	Strong nuclear staining
22	013/10	FTLD-TDP	C	Nuclear staining
25	301/10	FTLD-TDP	C	No positivity
28	163/07	FTLD-TDP	C	Nuclear staining
24	061/13	FTLD-TDP	C	Nuclear staining
27	409/08	FTLD-TDP	C	No positivity
31	403/08	FTLD-ALS *C9orf72*	B	Nuclear staining
35	069/02	FTLD-ALS *C9orf72*	B	No positivity
41	151/08	FTLD-ALS *C9orf72*	B	Nuclear staining
44	163/09	FTLD-ALS *C9orf72*	A	Nuclear staining
45	174/08	FTLD-ALS *C9orf72*	n/a	Nuclear staining
109	158/14	Control	n/a	Nuclear staining
110	278/96	Control	n/a	Weak nuclear staining
99	048/09	Control	n/a	Weak nuclear staining
100	063/10	Control	n/a	Weak nuclear staining
103	123/09	Control	n/a	Weak nuclear staining

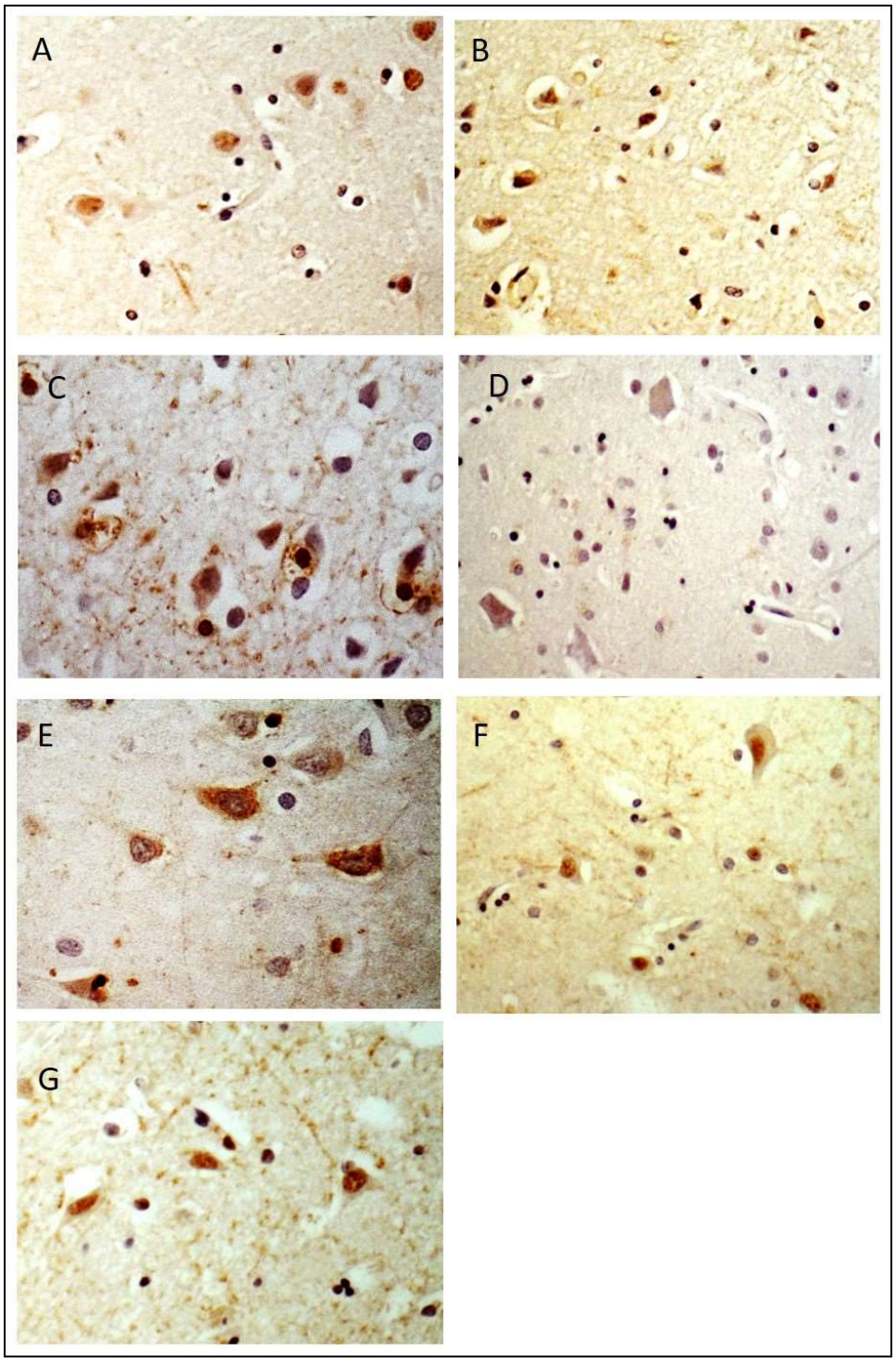

Figure 17: IHC for hnRNP-C1/C2 shown in FTLD-TDP cases: subtype A, case ref. 12, 20x (A). Subtype B, case ref. 19, 20x (B) and 40x (C). Subtype C, case ref. 22, 20x (D) and 40x (E). *C9orf72* expansion-positive, case ref. 45, 20x (F). Control, case ref. 109, 20x (G). Diffuse cytoplasmic staining and strong nuclear positivity are seen in all the FTLD-TDP subgroups and control cases. There was no obvious difference between the subtype groups.

3.3.1.6 hnRNP-Q

hnRNP-Q IHC at all dilutions (1:50, 1:250 and 1:500) showed no immunoreactivity in either the frontal cortex of the control (Figure 18A) or the frontal cortex of the FTLD-TDP case (Figure 18B).

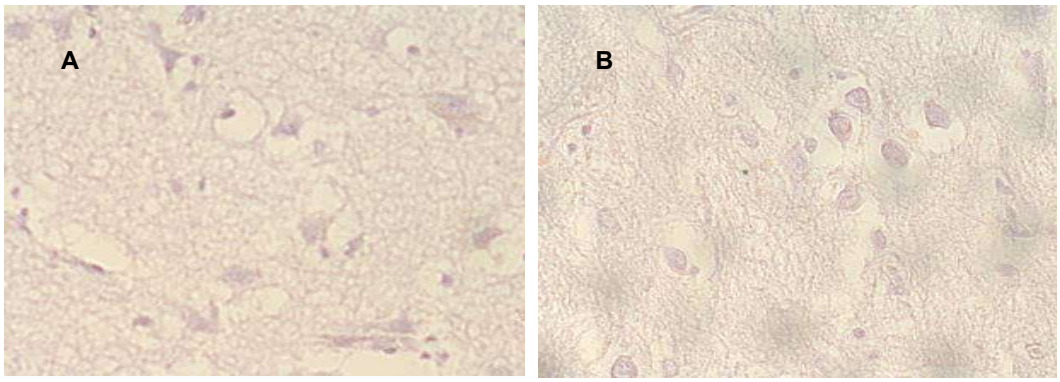

Figure 18: hnRNP-Q IHC. No immunoreactivity is detectable.

3.3.2 Localisation of ubiquilin-2 within TDP-43 aggregates

The colocalisation of TDP-43 and ubiquilin-2 was detected in the frontal cortex of FTLD-TDP cases #2 and #5. Panel A in Figure 19 shows the colocalisation of ubiquilin-2 within round TDP-43 inclusions in subtype A FTLD-TDP (case ref. 2). Ubiquilin-2 also colocalised within neuritic TDP-43 inclusions in the frontal cortex of subtype C FTLD-TDP (case ref. 22), as depicted in Figure 19 (B1–B3).

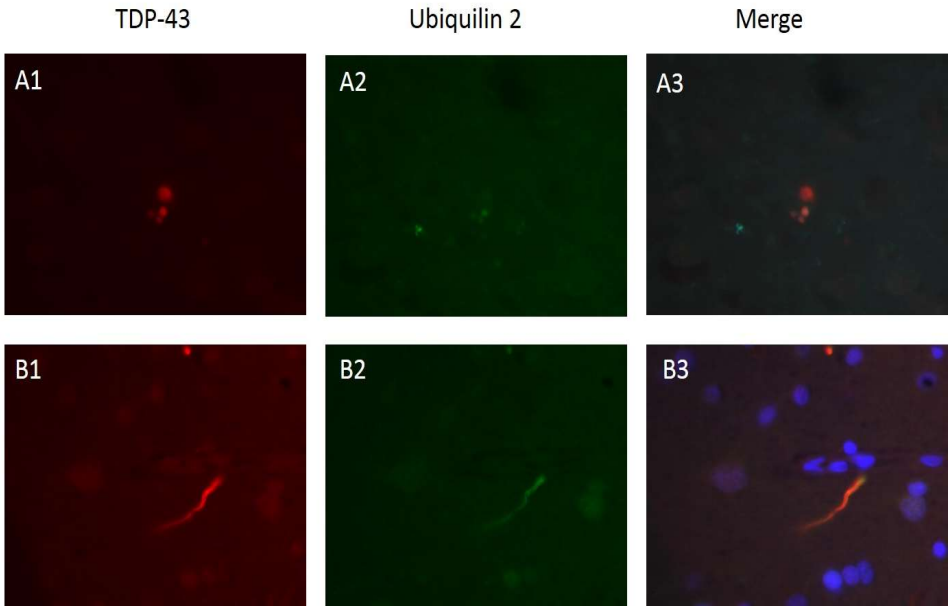

Figure 19: dIF of TDP-43 and ubiquilin-2 in FTLD-TDP subtype B, case ref. 2, (A1–A3) and in FTLD-TDP subtype C, case ref. 22, (B1–B3).

3.4 Discussion

The accumulation and aggregation of misfolded proteins is a hallmark of various neurological and systemic diseases. The difference between cell types arises from the different protein expressions of the genes rather than from the genes themselves, which results in the production of specific sets and amounts of proteins for each cell type and often accounts for cellular specificity in disease (Venter et al., 2001, Fagerberg et al., 2011). The amino acid sequences of an individual protein determine its specific three-dimensional structures. The hydrophobic parts of the protein fold, meeting other hydrophobic parts in the sequence internally and leaving their hydrophilic residues on the outside, which allows for their interaction with charged residues of different polarity (Tyers and Mann, 2003). The precise organisation of protein complexes and/or individual proteins maintains the integrity of cellular function. The correct activity of a network of thousands of proteins is essential for cells to function properly. The functions of a protein depend on its structure, which is determined by its amino acid sequence, as well as the chaperone proteins, which supervise the folding process of proteins (Soto, 2003). A wide range of neurodegenerative diseases have been characterised, sub-classified and diagnosed via the identification of misfolded protein aggregates, including Alzheimer's disease, Parkinson's disease, motor neuron disease and frontotemporal dementia. The aggregated proteins share some structural and morphological staining characteristics; however, they may have distinct biological or biochemical features (Martin, 1999a). The involvement of misfolded protein aggregates in the neuron death process has been supported by a significant amount of evidence. The first step towards understanding the cellular mechanisms and/or pathological pathways underlying protein aggregation and neurodegeneration is to identify the aggregated proteins, their functions and their interaction partners in certain organelle or cellular compartments (Fagerberg et al., 2011, Alberts, 2002). The identification of proteins in human tissues involves a variety of techniques, including IHC, microarray IHC, Western blotting and immunofluorescence. IHC has become a routine tool for the specific detection and quantification of abnormal protein inclusions in post-mortem human tissues since antibodies against specific proteins have become commercially available (Duraiyan et al., 2012). Since the identification of TDP-43 as the major component of protein aggregates in MND and FTLD, TDP-43 has been subject to thorough investigation in order to understand its role in the neuronal degeneration process. The identification of TDP-43-interacting networks of proteins would represent a step forward in understanding its pathological mechanism and pathway. A list of candidate TDP-43-binding proteins was generated in the SILAC experiment described earlier in this chapter. The expression of a number of these proteins was investigated in FTLD-TDP brain tissue. The proteins were selected according to the results of the SILAC

experiment, while the cases were selected according to the TDP-43 pathological subtype. The optimal dilution for each antibody was detected by testing three different dilutions within the range recommended by the manufacturer. The dilution that resulted in less background staining and clear cellular staining was used for the rest of the experiments.

Despite the close relationship between RanBP1 and TDP-43 and its downregulation by TDP-43 knockdown in the SILAC experiment, there were no aggregates detected in the FTLD-TDP and ALS cases (Stalekar et al., 2015). The interaction of RanBP1 with TDP-43 was also demonstrated by several other studies, as mentioned in the introduction to this chapter (Park et al., 2013, Tollervey et al., 2011a, Tedeschi et al., 2007, Paronett et al., 2015). However, the absence of RanBP1 from the TDP-43 aggregates does not exclude it from the TDP-43 interaction network, which has been described by other studies (Tollervey et al., 2011a).

Ubiquilin-2 inclusions were detected in the FTLD cases with subtype B pathology and cases with the *C9orf72* expansion. The inclusions were seen in both the cell body and the neurites. In addition, the colocalisation of ubiquilin-2 with TDP-43 inclusions was detected using double-labelling immunofluorescence techniques. Previously, Brettschneider and colleagues reported that ubiquilin-2 pathology provides a characteristic neuropathological signature distinguishing FTLD-TDP cases with and without *C9orf72*. Their study suggested a pathophysiological link between UBQLN pathology and *C9orf72* expansion (Brettschneider et al., 2012). Our findings correlate with those of Brettschneider et al.'s (2012) report; however, we found UBQLN inclusions in FTLD-TDP subtype B without the *C9orf 72* mutation, which suggests that it is more related to the TDP pathological pattern than *C9orf72* expansion. Alternatively, these two cases could contain a *C9orf72* expansion that was not identified during in-house screening. Further dIF experiments could provide a clearer answer regarding the possible relation between UBQLN pathology and TDP-43 pathology in FTLD-TDP cases, which could not be conducted in the present study due to time limits. In addition, the focus of this study is on hnRNPs, although the UBQLN interaction with TDP-43 in FTLD-TDP cases could be the focus of future studies.

The hnRNP-M and hnRNP-C1/C2 immunoreactivity in the FTLD-TDP cases did not differ from that of the control cases. No reactivity for hnRNP-Q was detected using any concentration of the available antibody. All three hnRNPs share similar functions with TDP-43 in terms of RNA processing and splicing control. The reported interaction of hnRNP-M with FUS/TLS may explain the absence of hnRNP-M from the TDP-43 cases (Marko et al., 2014). hnRNP-M was not investigated in the FUS cases in this project. hnRNP-C1/C2 clearly have a strong nuclear presence, as expected in basal conditions. However, in the FTLD-TDP cases there was

weak staining of the cytoplasm around the nuclei when compared to the control case. It has been reported that hnRNP-C1/C2 translocate to the cytoplasm during certain cellular conditions such as apoptosis. Despite the absence of aggregates, the cytoplasmic presence of hnRNP-C1/C2 may indicate that cells are undergoing apoptosis (Dreyfuss, 1993, Kim et al., 2003, Gustin and Sarnow, 2002). Interestingly, hnRNP-Q has a close relation to MND, specifically with SMA, as discussed in the introduction to this chapter. The complete absence of immunoreactivity could be related to a faulty antibody, which could be investigated further in the future.

The results of the hnRNP-E2 IHC revealed striking perinuclear and neuritic inclusions in the FTLD-TDP subtypes A and C cases, but not in the subtype B or *C9orf72* expansion-positive cases. Based on these striking results, further investigations were carried out to examine the specificity and pathological importance of this finding, which will be detailed in the following chapters (Helmken et al., 2003, Chen et al., 2008a, Yuo et al., 2008).

3.5 Conclusion

The role of TDP-43 in the neurodegenerative process is not yet fully understood despite the intensive study of TDP-43 over the past decade. Screening for TDP-43 binding partners and identifying TDP-43 protein networks may enhance our understanding of the pathological mechanisms that could lead to TDP-43 aggregation and ultimately cause neuronal death. A list of candidate proteins was generated based on those that were influenced by the TDP-43 knockdown in a SILAC experiment previously published by our laboratory. A number of these proteins were probed using immunohistochemistry in human brain tissue. Inclusions were detected with two proteins, namely ubiquilin-2 and hnRNP-E2. Ubiquilin-2 inclusions were seen selectively in the subtype B and *C9orf72* expansion-positive cases, whereas E2 inclusions were seen specifically in the subtype A and C FTLD-TDP cases. The interaction of ubiquilin-2 and TDP-43 in the *C9orf72* expansion cases was detected by our group in experiments that were running parallel to this project. Therefore, hnRNP-E2, its interaction with TDP-43 and its potential mechanistic role in pathology were selected as the next focus of this project.

Chapter 4 Investigation of hnRNP-E2 in FTLD and MND Human Brain Tissue

4.1 Introduction

In 2006, two large-scale studies recognised three distinct histopathological patterns according to the anatomical distribution and morphology of the neuronal ubiquitin inclusions in FTLD-U brains (Sampathu et al., 2006, Mackenzie et al., 2006). The two studies were conducted independently and simultaneously, which led to the non-matching numbering of the subtypes; however, the pathological features that defined the subtypes were almost identical (Table 10). Shortly afterwards, the Sampathu group reported the identification of TDP-43 as the major protein component of the ubiquitin inclusions in most FTLD-U cases as well as the majority of sporadic and some familial ALS (sALS and fALS) cases (Neumann et al., 2006b). Subsequently it was reported by other groups that most of their FTLD-U cases exhibited the same pathological pattern of TDP-43 (Cairns et al., 2007, Davidson et al., 2007). A fourth FTLD-U subtype was described during the same period, which was specifically associated with mutations in the valosin-containing protein (*VCP*) gene. The *VCP* mutation type of FTLD represents the familial syndrome of Paget's disease of bone with inclusion body myopathy and frontotemporal dementia (Forman et al., 2006). This type of FTLD-U also shows TDP-43 pathology, which led to the recommendation by Mackenzie et al. (2009) that all FTLD-U cases with TDP-43 pathology be designated as FTLD-TDP (Neumann et al., 2007b, Mackenzie et al., 2009).

Both Mackenzie et al.'s (2006) and Sampathu et al.'s (2006) classification systems were widely accepted and repeatedly validated; however, the use of both systems was a source of confusion. Therefore, the principal authors of the original two papers proposed a new harmonised classification of FTLD-TDP pathology to replace the previously used classification systems (Mackenzie et al., 2011b). The new classification system took into consideration the frequency of the subtypes, with "A" being the most common subtype of FTLD-TDP. It also recommended replacing the numbers and orders of the subtypes in the previous two systems with letters to avoid confusion. Table 10 summarises the classification systems, while Figure 20 provides an illustration of the pathological pattern of the TDP-43 inclusions identified in each subtype. In this study, the new classification system will be used for all pathology descriptions.

Table 10: FTLD harmonised classification proposed by Mackenzie et al. (2011)

New system	Mackenzie et al.	Sampathu et al.	Cortical pathology	Common phenotype	Associated genetic defects
Type A	Type 1	Type 3	Many NCI Many short DN Predominantly layer 2	bvFTD PNFA	*GRN* mutations
Type B	Type 3	Type 2	Moderate NCI Few DN All layers	bvFTD MND with FTD	Linkage to *C9orf72* expansion
Type C	Type 2	Type 1	Many long DN Few NCI Predominantly layer 2	SD bvFTD	
Type D	Type 4	Type 4	Many short DN Many lentiform NII Few NCI All layers	Familial IBMPFD	*VCP* mutations

bvFTD: behavioural variant frontotemporal dementia, *DN*: dystrophic neurites, *GRN*: progranulin gene, *IBMPFD*: inclusion body myopathy with Paget's disease of bone and frontotemporal dementia, *MND*: motor neuron disease, *NCI*: neuronal cytoplasmic inclusions, *NII*: neuronal intra-nuclear inclusions, *PNFA*: progressive non-fluent aphasia, *SD*: semantic dementia, *VCP*: valosin-containing protein gene (Mackenzie et al., 2011b).

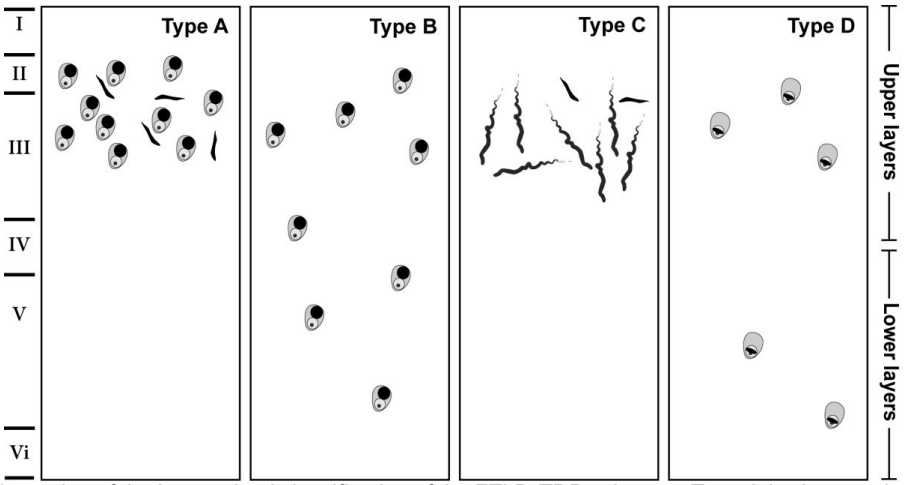

Figure 20: An illustration of the harmonised classification of the FTLD-TDP subtypes. Type A is characterised by moderate to numerous TDP43-immunoreactive NCI and short DN predominantly in the upper cortical layers II/III. Type B cases typically show moderate to numerous TDP43-immunoreactive NCIs and sparse DNs across all cortical layers. Type C cases' main characteristic is the presence of long dystrophic neurites predominantly in the upper cortices and NCIs. Type D cases present with numerous lentiform NII (Tan et al., 2013).

Many genetic mutations have been reported to be linked to familial FTLD-TDP, as detailed in Chapter 1. In brief, mutations have been reported in the granulin gene (*GRN), VCP, TARDBP* and, most recently, the abnormal expansion of a GGGGCC hexanucleotide repeat in a non-coding region of the *C9orf72* gene, which is considered to be the most common genetic cause of sporadic and familial forms of FTLD and ALS (DeJesus-Hernandez et al., 2011a, Kaivorinne et al., 2014). The understanding of the molecular basis of FTLD has advanced remarkably due to the substantial pathological and genetic findings over the past decade. However, there still exists a gap in our understanding of the exact molecular mechanisms that underlie the identified pathology. The purpose of this study is to investigate the TDP-43 pathology in FTLD and ALS in order to further understand the TDP-43 pathophysiology through its interaction with other proteins. From the screening results detailed in the previous chapter, hnRNP-E2 inclusions were detected in the frontal cortex of FTLD subtypes A and C cases, but not in subtype B or *C9orf72* expansion cases. Therefore, a series of experiments were conducted in an effort to characterise the hnRNP-E2 pathology seen in the FTLD-TDP brain tissue utilising both human brain tissue and cell biology techniques. This chapter will present the pathological findings concerning hnRNP-E2 and its relation to TDP-43 and ubiquitin in human brain tissue from FTLD-TDP cases and other neurodegenerative diseases.

As a first step in confirming this result, different antibodies for hnRNP-E2 were purchased and optimised on the same cases as those featured in the screening results. In Chapter 1, details regarding hnRNP-E2 belonging to the hnRNP-K subfamily of hnRNPs and its great number of similarities with other members of that family were given. It has been reported that hnRNP-E2 and hnRNP-E1 share 89% structural homology. It is further believed that hnRNP E1 is encoded by an intronless gene that is a product of a retrotransposition event of a fully processed minor isoform of hnRNP E2 (Valverde et al., 2008, Waggoner and Liebhaber, 2003, Makeyev and Liebhaber, 2002, Woolaway et al., 2007). In addition, Wang et al. (2011b) found that hnRNP-E2 interacts with the SRp75/hnRNP-G complex to regulate exon 10 splicing. The misregulation of exon 10 splicing results in the FTLD-type associated with tau (Wang et al., 2011b). Therefore, it was important that the cases that exhibited positive hnRNP-E2 immunoreactivity were screened for hnRNP-E1 and hnRNP-G in order to exclude any interaction with the hnRNP-E2 antibody.

Second, the disease specificity of hnRNP-E2 was investigated by assessing a large number of cases in order to include more TDP-43-related cases as well as other neurodegenerative disease cases and controls. At the time of this study, there were 30 FTLD-TDP cases without the *C9orf72* mutation and 22 FTLD-TDP cases

carrying the *C9orf72* mutation identified in the Brain Bank at the Institute of Psychiatry, Psychology and Neuroscience, King's College London.

In addition, to investigate whether hnRNP-E2 plays a general role in neurodegeneration or whether it is specific to FTLD, a number of cases of various other neurodegenerative diseases were screened for hnRNP-E2 pathology. Furthermore, the areas of the brain screened for hnRNP-E2 aggregates were increased to include the frontal cortex, hippocampus and spinal cord. For the other neurodegenerative cases, areas with the most prominent pathology were selected for screening, which mostly involved the frontal or frontotemporal cortices. In cases where there was motor neuron involvement, sections from the spinal cord were investigated. The cases and section details are presented in the results section of this chapter.

Third, the functionality of a protein can be examined by characterising its interactions with other proteins (Rao et al., 2014). One way of studying protein-protein interaction in vitro utilises double-labelling immunofluorescence of the proteins of interest. Therefore, the colocalisation of hnRNP-E2, TDP-43 and ubiquitin was investigated in human brain sections using the dIF technique. Cases that showed positive immunoreactivity for hnRNP-E2 in IHC were used and the inclusions of hnRNP-E2, TDP-43 and ubiquitin were counted, then the percentage of colocalisation was calculated. The main issue needing to be overcome in this experiment was the natural autofluorescence seen in the human brain, which was solved by means of multiple washing and the preparation of fresh Sudan Black for each experiment. Higher power magnification images of the inclusions were captured using the confocal microscope in order to closely examine the colocalisation of hnRNP-E2 with TDP-43 and ubiquitin in FTLD-TDP cases.

The biochemical signature of pathological TDP-43 in FTLD-TDP cases was identified by Neumann et al. (2006b). They sequentially extracted the grey matter from FTLD-TDP brains with buffers of increasing strength and ran Western blots of the samples. The hallmark of the pathology described by Neumann et al. (2006b) was the presence of detergent-resistant insoluble TDP-43 in the urea fraction, including the presence of the 45 kDa band, the high molecular weight smear and the presence of the C-terminal cleavage product at 25 kDa. Thus, the final experiment performed utilising human brain tissue in this study aimed to biochemically characterise hnRNP-E2 in FTLD-TDP cases using the Neumann et al.'s (2006 protocol for brain tissue fractionation. Four groups of cases were used for this experiment: 1) healthy control brains (control), 2) FTLD-TDP cases with negative immunoreactivity to hnRNP-E2 (FTLD-TDP -ve hnRNP-E2), 3) FTLD-TDP cases with positive hnRNP-E2 immunoreactivity (FTLD-TDP +ve hnRNP-E2) and 4) FTLD-TDP with *C9orf72* expansion cases (*C9orf72*). Several issues developed in relation to the Western blots, specifically concerning

the TDP-43 immunoreactivity on the blots and the consistency of hnRNP-E2 immunoblots with the IHC results. Several repeats of the tissue fractionation and Western blots were performed using both the SARK fractionation protocol (adopted from Neumann et al. (2006) and the RIPA fractionation protocol (developed by Dr Jackie Mitchell for mouse brain fractionation). Different antibodies were used for the TDP-43 on some of the samples in order to check the specificity of the TDP-43 antibodies, with the results being presented in Appendix C.

4.1.1 Aims of this chapter

The present chapter aims to:

1. Confirm the screening results concerning hnRNP-E2 through the application of several commercially available hnRNP-E2 antibodies.
2. Investigate the specificity of the hnRNP-E2 antibodies by applying hnRNP-E1 and hnRNP-G to the cases previously identified to have positive hnRNP-E2 inclusions.
3. Investigate hnRNP-E2 pathology in further brain regions of FTLD-TDP cases and to investigate the correlation of hnRNP-E2 pathology with the TDP-43 pathological subtypes and other demographic factors. The hnRNP-E2 immunoreactivity was also investigated in other neurodegenerative diseases in order to establish the disease specificity of hnRNP-E2 pathology.
4. Investigate the colocalisation of hnRNP-E2 with TDP-43 and ubiquitin inclusions in the brain tissue of FTLD-TDP cases.
5. Characterise the biochemical signature of hnRNP-E2 in the brain tissue of FTLD-TDP cases.

4.2 Methods

4.2.1 Immunohistochemistry

4.2.1.1 hnRNP-E2 antibody optimisation and confirmation

Three hnRNP-E2/PCBP2 antibodies obtained from three different companies were tested at different dilutions on the same cases (both control and FTLD-TDP cases). The first antibody was the mouse monoclonal antibody raised against recombinant hnRNP-E2 of human origin (hnRNP-E2 [23 G] code no. sc-101136, Santa Cruz). The second antibody was the mouse monoclonal PCBP2 (hnRNP-E2 code no. WH0005094M7, clone 5F12, Sigma-Aldrich). The third antibody was the Abnova mouse monoclonal PCBP2 monoclonal antibody (M07, clone 5F12, Abnova #H00005094-M07). All the antibodies were tested at dilutions of 1:50, 1:250 and 1:500. The IHC procedure was performed as described in Chapter 2.

4.2.1.2 Cases and brain region selection

The hnRNP-E2 IHC was performed on all the cases listed in section 2.1.1. For the FTLD cases, the frontal cortex and hippocampus were examined, as well as the spinal cord where available. For the other neurodegenerative disease cases, the regions were selected according to the prominent pathology of each disease. The results section of this chapter provides the full case details.

4.2.2 Double-labelling immunofluorescence

Double-labelling immunofluorescence was performed on several cases that showed hnRNP-E2-positive inclusions by IHC in order to check for colocalisation with TDP-43 and ubiquitin. The experiments were performed as described in Chapter 2. The primary antibody used to detect hnRNP-E2 was the mouse monoclonal antibody hnRNP-E2 (Santa Cruz), which was chosen for ease of experimental design as TDP and ubiquitin are polycolonal. Some experiments were performed using the hnRNP-E2 (Abnova) antibody to confirm the results. All the hnRNP-E2 antibodies were used at a 1:250 dilution. The TDP-43 antibody was the rabbit polyclonal (Proteintech), which was used at a 1:250 dilution. The ubiquitin antibody was the rabbit polyclonal anti-ubiquitin obtained from Dako (code no. Z045801), which was used at a 1:100 dilution. All the sections were incubated with fluorophore secondary antibodies for 45 minutes in the dark. The secondary antibodies used were Alexa Fluor® goat anti-rabbit, which was used to label the polyclonal primary antibodies, and Alexa Fluor® goat anti-mouse, which was used to label the monoclonal primary antibodies (Alexa Fluor® 488 Goat Anti-Mouse IgG [Invitrogen] and Alexa Fluor® 568 Goat Anti-Rabbit IgG [Invitrogen]). The colour of

the fluorescent signal was chosen as green (488 nm) or red (568 nm) for each antibody. Following incubation, the sections were washed in PBS and incubated with Sudan Black for 10 min. The sections were washed multiple times with PBS and the slides were mounted using Vectashield with DAPI and then coverslipped. All the sections were visualised using an inverted fluorescence microscope (Zeiss Axiovision) and high-resolution images were obtained using the Leica confocal SP system. The processing of the images was performed using ImageJ 1.47v software.

4.2.3 Western blotting

hnRNP-E2 insolubility in the brain tissue was investigated using the Western blotting technique. A 100 mg sample was dissected from the frozen frontal cortex grey matter (Brodmann area 9) of each case and the tissue was fractionated using the Sarkosyl fractionation protocol as described in Chapter 2. Details concerning the cases used for Western blotting are presented in Table 1.

Table 11: Details of the FTLD-TDP cases and control cases used for Western blotting and the hnRNP-E2 IHC results

Ref	Case	Diagnosis	Sex	Duration (months)	PMD (hrs)	Fixation time (weeks)	hnRNP-E2 (FCx)
2	029/09	FTLD-TDP A	M	108	42	5	+
3	037/12	FTLD-TDP A	F	108	56	6	+
22	013/10	FTLD-TDP C	M	48	6	12	+
25	301/10	FTLD-TDP C	M	108	45	20	+
9	103/08	FTLD-TDP A	F	84	24	11	+
32	403/08*	FTLD-TDP *C9orf72* B	F	144	15.5	12	-
7	205/07	FTLD-TDP A	M	96	24.5	8	-
8	229/03	FTLD-TDP A	F	156	15	7	-
1	025/11	FTLD-TDP A	M	48	40.5	12	-
10	294/13	FTLD-TDP A	F	24	72	8	-
18	169/11	FTLD-TDP B	M	180	38	12	-
5	101/09	FTLD-TDP A	M	38	5	n/a	-
41	144/12	FTLD-ALS *C9orf72 B*	F	n/a	21	10	-
42	151/08	FTLD-ALS *C9orf72 B*	M	12	73.5	14	-
44	157/04	FTLD-ALS *C9orf72 B*	M	72	22.5	35	-
45	163/09	FTLD-ALS *C9orf72 A*	M	11	35	5	-
17	229/06	FTLD-ALS *C9orf72*	F	10	34.5	17	-
98	047/02	CNT	F	n/a	21.5	150	-
100	048/09	CNT	M	n/a	18	17	n/a
101	063/10	CNT	F	n/a	50	19	-
102	066/00	CNT	M	n/a	53	14	-
104	123/09	CNT	M	n/a	24	8	-
105	130/09	CNT	M	n/a	30	8	-

4.2.3.1 Gel electropheresis and Western blotting

The samples were thawed at room temperature for a few minutes and then spun in the centrifuge for a few seconds before loading onto the Western blot gels. Some 10 µl of each of the five fractions (i.e. lysate, low salt, Triton, SARK and urea) from each case were loaded onto the 26-well SDS-PAGE polyacrylamide gel NuPAGE R Novex R 10% Bis-Tris buffering agent with a neutral pH gel. Each gel was loaded with the five fractions of a control case, a FTLD-TDP case with hnRNP-E2 +ve inclusions, a FTLD-TDP with -ve hnRNP-E2 inclusions and an FTLD-TDP with the *C9orf72* expansion. The lysate and urea fractions of one case were also loaded onto all the gels as intra-gel controls. In addition to the samples, 1–2 µl of the protein ladder (Bio-Rad) was loaded onto the gels as a protein size reference. The gels ran at 150–190 volts for approximately 90 minutes. Once the line reached the bottom of the gel, the run was stopped and the gel was transferred onto a nitrocellulose membrane so the proteins could be probed with specific antibodies for band detection as described in Chapter 2. The blots were blocked with 5% skimmed milk for 20 minutes before the primary antibodies were added to the blots. The primary antibodies were diluted in 1% skimmed milk in 1x TBS-T and the blots were incubated overnight on a roller at 4°C. The brain blots were probed with the polyclonal rabbit TDP-43 10782-2-AP (Proteintech) and the PCBP2 mouse monoclonal (M07) clone 5F12 (Abnova). The next day, the blots were washed three times with TBS-T (10–20 min each wash) on a roller at room temperature. The blots were then incubated with the secondary antibodies obtained from Thermo Scientific (Goat anti-Rabbit IgG [H+L] Secondary Antibody, DyLight 680 conjugate, and Pierce Goat anti-Mouse IgG [H+L] Secondary Antibody, DyLight 800 conjugate), which were diluted to 1:5000 in 1% milk for 2–3 hours on a roller at room temperature in the dark. The blots were then washed three times with TBS-T as previously described. The blots were visualised using the LI-COR Odyssey® scanner and the bands were analysed according to both the sample fraction and the band size. The blots were also probed with loading control to ensure that any increase or decrease in the size of the bands seen in the cases was not due to differences in sample loading. The loading controls used were histone 3, lamin or GAPDH.

The protein quantification from the blots was performed using the ImageJ software as described in Chapter 2. The loading controls were not detected in the insoluble fraction (urea); therefore, the normalisation of the quantified results was conducted by taking the ratio of the insoluble/soluble (urea/lysate) fractions of each case separately and then calculating the average for each case group. The differences in the insoluble TDP-43 and hnRNP-E2 levels among the sample groups were determined using a one-way ANOVA followed by a Bonferroni post-hoc t-test with a significance level of $p < 0.05$. The t-test was a two-tailed t-test assuming equal

variance between the groups. The mean is presented as (Mean ± SE), with SE representing the standard error of the samples.

4.2.4 Correlation of demographic factors with hnRNP-E2 pathology

A total of 29 FTLD-TDP cases without the *C9orf72* mutation were examined for hnRNP-E2 pathology by means of IHC. At least two regions of the brain and/or spinal cord were examined for each case. The cases were subtyped according to the TDP-43 pathology into four subtypes as previously described. In order to identify the factors that may influence the IHC results, for example, the TDP-43 subtype pathology, post-mortem delay or fixation time, a Chi-square test was performed to identify any variable significance. All the analyses were carried out using SPSS software (IBM SPSS statistics 19).

Table 12: Details of the FTLD-TDP cases used in the statistical analysis

	Case	Diagnosis	Sex	PMD (hrs)	Fixation time (weeks)
1	025/11	FTLD-TDP A	M	40.5	12
2	029/09	FTLD-TDP A	M	42	5
3	037/12	FTLD-TDP A	F	56	6
4	063/12	FTLD-TDP A	M	36	4
5	120/11	FTLD-TDP A	M	14	8
6	172/12	FTLD-TDP A	M	31	10
7	205/07	FTLD-TDP A	M	24.5	8
8	229/03	FTLD-TDP A	F	15	7
9	103/08	FTLD-TDP C	F	24	11
10	294/13	FTLD-TDP A	F	72	8
11	334/09	FTLD-TDP A	M	11	24
12	033/08	FTLD-TDP A	F	35	10
13	047/07	FTLD-TDP A	F	70	8
14	097/09	FTLD-TDP A	M	n/a	n/a
15	099/08	FTLD-TDP A	M	7	n/a
16	030/06	FTLD-TDP B	M	43.5	n/a
17	157/12	FTLD-TDP B	M	45	6
18	169/11	FTLD-TDP B	M	38	12
19	058/12	FTLD-TDP B	F	54	8
20	244/07	FTLD-TDP B	M	46	4
21	432/12	FTLD-TDP B	M	31	8
22	013/10	FTLD-TDP C	M	6	12
23	022/07	FTLD-TDP C	M	120	7
24	061/13	FTLD-TDP C	M	16	11
25	301/10	FTLD-TDP C	M	45	20
26	350/08	FTLD-TDP C	M	14	16
27	409/08	FTLD-TDP C	M	n/a	12
28	163/07	FTLD-TDP C	M	6.5	12
29	295/07	FTLD-TDP C	M	54	8

4.3 Results

4.3.1 Immunohistochemistry

Immunohistochemistry was utilised to screen for candidate TDP-43-binding proteins on different areas of the human brain from cases of FTLD with positive TDP-43 inclusions, as described in Chapter 3. hnRNP-E2 showed strong positive cytoplasmic and neritic inclusions in the frontal cortex of a subset of FTLD-TDP cases. Details concerning these cases are presented in Table 3 (Chapter 2).

4.3.1.1 Antibody confirmation and optimisation

In order to confirm the positive results of the hnRNP-E2 IHC on FTLD-TDP cases, further IHC experiments were performed using the other two hnRNP-E2/PCBP2 antibodies on the same cases (ref. 2). Antibody optimisation was performed by testing gradual dilutions of 1:50, 1:250 and 1:500. The 1:500 dilution showed good immunopositivity with less background staining. Figure 21 shows the IHC results using the three different hnRNP-E2 antibodies at 1:500 dilutions. Details concerning the utilised antibodies are listed in Table 4 (Chapter 2). In the control frontal cortex (case ref. 108), the hnRNP-E2 staining was diffusely distributed between the nucleus and the cytoplasm; however, the nuclear staining was stronger than that seen in the cellular cytoplasm (Figure 21 A). In an FTLD-TDP type A case (case ref. 2), hnRNP-E2 (Santa Cruz) detected perinuclear and neuritic inclusions (Figure 21B). The Abnova hnRNP-E2/PCBP2 antibody detected the same structures; however, the background staining was much less than that seen for the previous Santa Cruz antibody (Figure 21C). The Sigma antibodies detected the same inclusions; however, they produced very strong background staining (Figure 21D). Therefore, the Santa Cruz and Abnova antibodies were selected for use in further experiments.

hnRNP-G IHC was performed on those cases with hnRNP-E2-positive inclusions due to the reported interaction between the two. The results showed hnRNP-G to be diffusely present in the nuclei and the cytoplasm. hnRNP-G did not detect any inclusions or similar structures to those detected with hnRNP-E2 (Figure 21E). Due to the similarities between hnRNP-E2 and hnRNP-E1, IHC was performed on the same FTLD-TDP cases that showed positive immunoreactivity to hnRNP-E2 in order to exclude any cross-reactivity. The hnRNP-E1 IHC (Figure 21F) on the frontal cortex of the FTLD-TDP case did not show similar aggregates to those detected with hnRNP-E2.

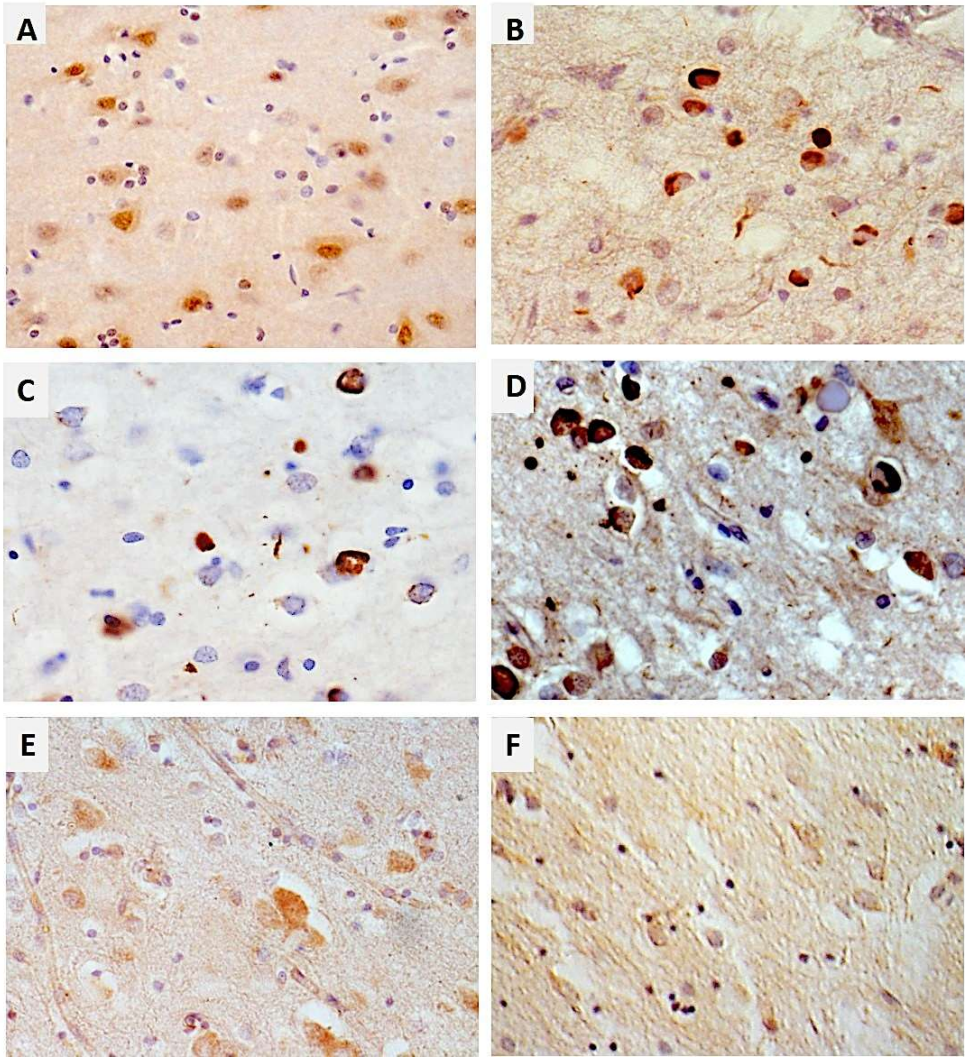

Figure 21: Optimisation and confirmation of the hnRNP-E2 IHC results using different antibodies on the frontal cortex of a type A FTLD-TDP case (case ref. 2). The results of the hnRNP-E2 Santa Cruz IHC on a control frontal cortex show hnRNP-E2 to be diffusely distributed between the nucleus and the cytoplasm, with a stronger nuclear presence than cytoplasmic (A) (case ref. 108). Round and ring-shaped perinuclear inclusions were detected in the frontal cortex of an FTLD-TDP case with the hnRNP-E2 Santa Cruz antibodies (B) (case ref. 2). The background staining is moderate with this antibody. The Abnova hnRNP-E2 antibody produced much less background staining and still detected similar inclusion structures to the previous antibody (C) (case ref. 2). The hnRNP-E2/PCBP2 Sigma antibodies produced very strong background staining yet detected the same inclusions as the previous two antibodies (D) (case ref. 2). The hnRNP-G/RBMX IHC on the frontal cortex of the same case did not detect any inclusions (E) (case ref. 2). The hnRNP-E1 IHC on the frontal cortex of the same case also did not detect any inclusions (F) (case ref. 2). All antibodies used at a 1:500 dilution.

4.3.1.2 hnRNP-E2 in different regions of the brain of a subset of FTLD-TDP cases

hnRNP-E2 was investigated in different regions of the brain of FTLD-TDP and MND cases without the *C9orf72* expansion. hnRNP-E2 inclusions were detected in the frontal cortex, hippocampus and spinal cord (Figure 22 and Figure 23). Figure 22 shows the hnRNP-E2 IHC in different regions of the brain and spinal cord of a type A FTLD-TDP case (case ref. 2). The frontal cortex pathology of hnRNP-E2 is predominant in the superficial layers, mainly in layer 2 of the neocortex, with numerous cytoplasmic perinuclear and intraneuronal inclusions and frequent neuritic inclusions (Figure 22A). In the hippocampus, hnRNP-E2 inclusions were detected within the granular cells (Figure 22B). No hnRNP-E2 inclusions were detected in the cerebellum in any FTLD-TDP cases without the *C9orf72* mutation (Figure 22C). In the spinal cord, sparse inclusions were detected in the grey matter of the anterior horn of the thoracic spinal cord region. The spinal cord inclusions were detected in only two cases (case ref. 2, Figure 22D–E, and case ref.16, Figure 22F).

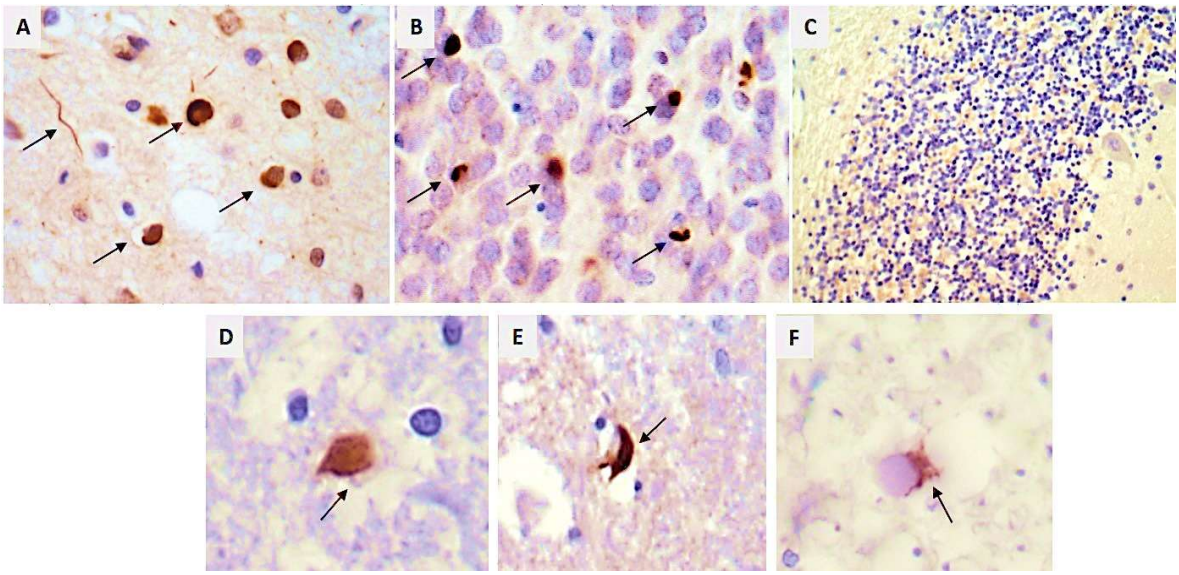

Figure 22: IHC of hnRNP-E2 in a type A FTLD-TDP case (ref. 2) (A–E). Numerous cytoplasmic perinuclear and intraneuronal inclusions and frequent neuritic inclusions were detected, mainly in layer 2 of the frontal cortex (A). Intracellular cytoplasmic inclusions were detected in the pyramidal cells of the hippocampus of the same case (B). In the cerebellum of the same case, there was no pathology detected in the granular layer, molecular layer or Purkinje cells (C). Sparse inclusions were detected in the grey matter of the anterior horn of the thoracic region of the spinal cord of the same case (ref. 2) (D and E). Sparse spinal cord inclusion was detected in another case (ref. 16) in the grey matter of the anterior horn.

In the type C FTLD-TDP cases, the long neuritic profiles of hnRNP-E2 inclusions were predominantly detected in the superficial layers of the frontal cortex (Figure 23A). They were also detected in the pyramidal layer of the hippocampus (Figure 23B). Round intracellular inclusions were detected in the granular layer of the dentate gyrus in the hippocampus in type C FTLD-TDP cases (Figure 23C). The abundance of the inclusions among the positive cases varied from case to case. Figure 24 shows hnRNP-E2 inclusions in the frontal cortex of four different cases of FTLD-TDP type C.

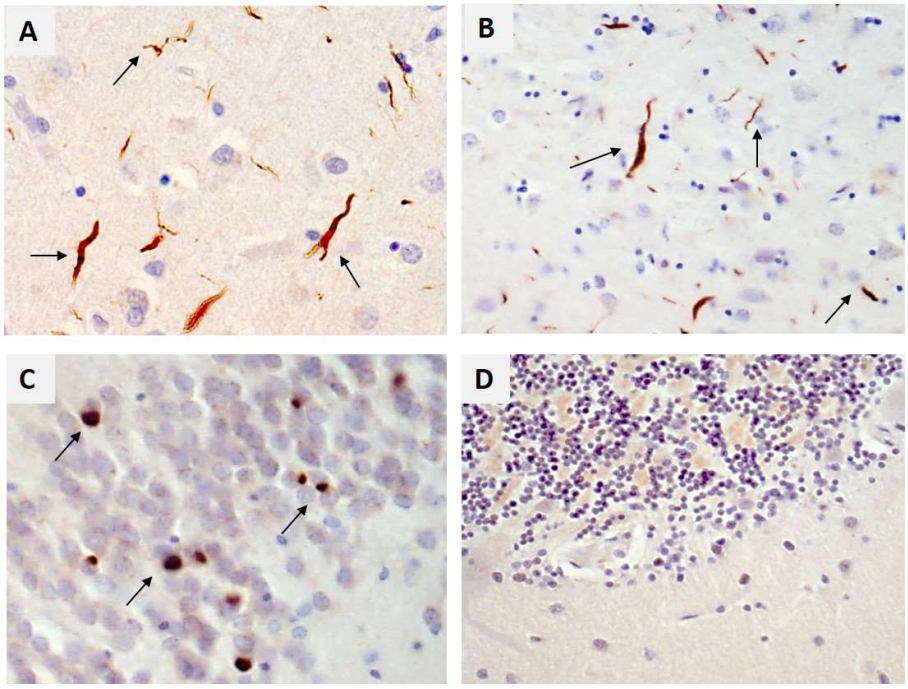

Figure 23: hnNRP-E2 IHC from a type C FTLD-TDP case (ref. 22). Frequent long neuritic inclusions of hnRNP-E2 were predominantly detected in the superficial layers of the frontal cortex (A). They were also detected in the granular layer of the hippocampus (B). In the dentate gyrus of the hippocampus, round intracellular inclusions were detected (C). No pathology was detected in the cerebellum (D).

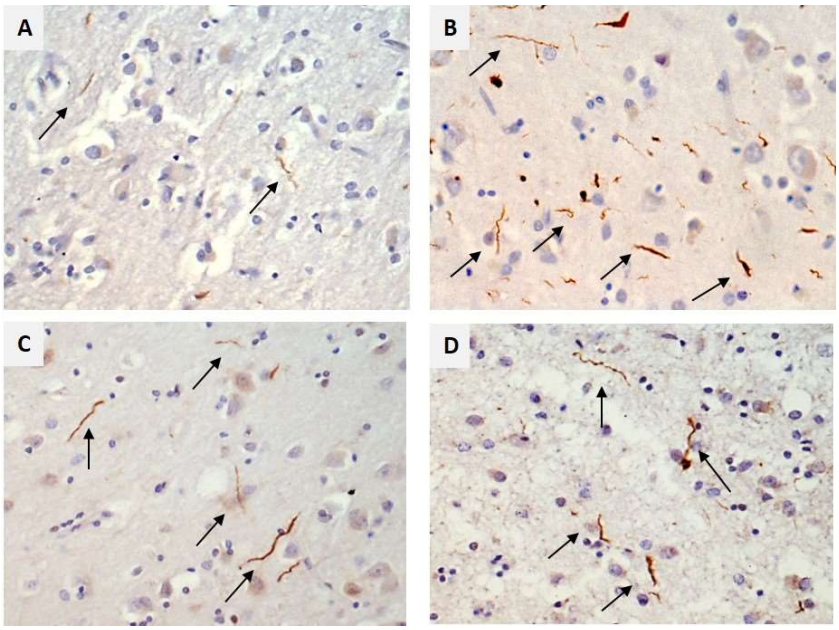

Figure 24: hnRNP-E2 IHC of the frontal cortex from four different type C FTLD-TDP cases showing the variation in the hnRNP-E2 abundancy in each case. Very few inclusions were detected in case (A) (ref .25) when compared to the other cases in (B) ref. 22, (C) ref. 9 and (D) ref. 27.

Example IHC results of hnRNP-E2 in the *C9orf72* FTLD-TDP cases are presented in Figure 25. Strong nuclear staining of the hnRNP-E2 with diffuse cytoplasmic staining was detected in the frontal cortex of the *C9orf72* FTLD-TDP cases (Figure 25A), which did not differ from the frontal cortex staining detected in the control cases (Figure 25C). In the cerebellum, diffuse staining within the Purkinje neurons was detected in the *C9orf72* FTLD-TDP cases (Figure 25B), which resembled that detected in the control cerebellum (Figure 25D). No inclusions were detected in the molecular layer or the granule cell layers of the cerebellum (Figure 25). Details concerning the FTLD-TDP cases, including the *C9orf72* expansion cases, are presented in Table 13. To conclude, hnRNP-E2 inclusions were detected in one or more regions of the brain and spinal cord in 16 out of the 30 cases, which represents 53.3% of the FTLD-TDP cases without the *C9orf72* expansion. Six out of 15 subtype A FTLD-TDP cases showed hnRNP-E2 inclusions in the frontal cortex and hippocampus, while two cases had inclusions in the spinal cord (40% of FTLD-TDP A cases had hnRNP-E2 inclusions). One subtype B case out of a total of six showed hnRNP-E2-positive inclusions in both the frontal cortex and the spinal cord (16.6%). Seven out of eight subtype C FTLD-TDP cases showed hnRNP-E2 inclusions in the frontal cortex (87.5%).

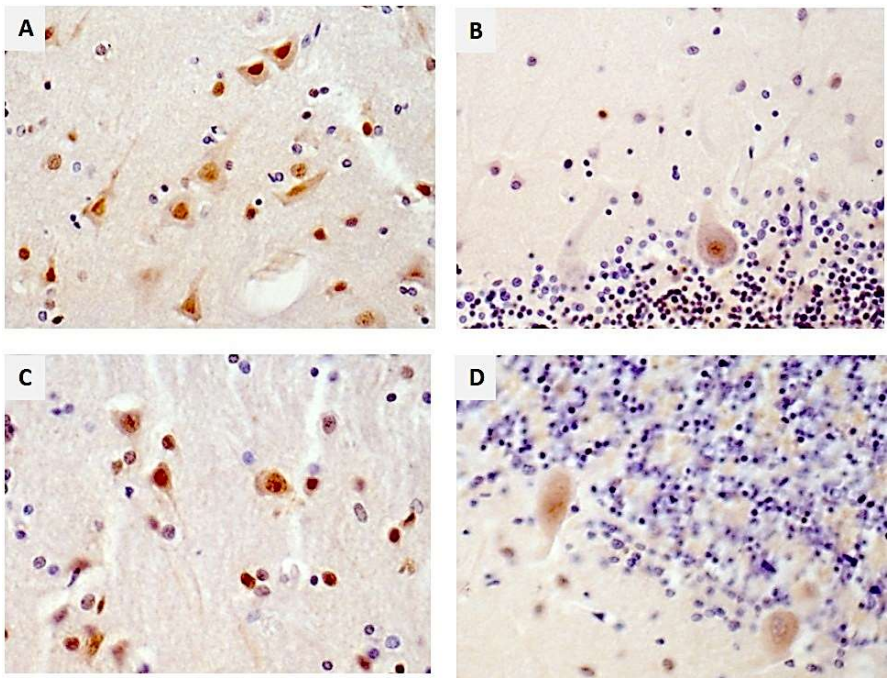

Figure 25: hnRNP-E2 IHC on the frontal cortex and cerebellum of control case ref. 105 (A and B) and on an FTLD-TDP case (ref. 42) with the *C9orf72* expansion (C and D).

Table 13: Details of the hnRNP-E2 IHC results for all the FTLD-TDP cases representing the regions investigated forhnRNP-E2 immunoreactivity. (+: inclusions detected, -: inclusions not detected, FCx: frontal cortex, HC: hippocampus, SC: spinal cord)

Ref	Case	Diagnosis	hnRNP-E2/PCBP2 IHC		
			FCx (E2)	HC (E2)	SC (E2)
1	025/11	FTLD-TDP A	-	-	n/a
2	029/09	FTLD-TDP A	+	+	+
3	037/12	FTLD-TDP A	+	-	n/a
4	063/12	FTLD-TDP A	+	+	+
5	120/11	FTLD-TDP A	-	-	-
6	172/12	FTLD-TDP A	+	-	-
7	205/07	FTLD-TDP A	-	-	n/a
8	229/03	FTLD-TDP A	-	-	n/a
9	103/08	FTLD-TDP A	+	+	n/a
10	294/13	FTLD-TDP A	-	-	n/a
11	334/09	FTLD-TDP A	-	-	n/a
12	033/08	FTLD-TDP A	+	-	n/a
13	047/07	FTLD-TDP A	-	-	n/a
14	097/09	FTLD-TDP A	-	-	-
15	099/08	FTLD-TDP A	-	-	n/a
16	030/06	FTLD-TDP B	+	-	+

17	157/12	FTLD-TDP B	-	-	-
18	169/11	FTLD-TDP B	-	-	n/a
19	058/12	FTLD-TDP B	-	-	n/a
20	244/07	FTLD-TDP B	-	-	n/a
21	432/12	FTLD-TDP B	-	-	-
22	013/10	FTLD-TDP C	+	+	-
23	022/07	FTLD-TDP C	+	+	-
24	061/13	FTLD-TDP C	+	+	-
25	301/10	FTLD-TDP C	+	+	-
26	350/08	FTLD-TDP C	+	+	+
27	409/08	FTLD-TDP C	+	+	n/a
28	163/07	FTLD-TDP C	+	-	-
29	295/07	FTLD-TDP C	-	-	-
30	101/09	FTLD-TDP A	-	-	n/a
31	088/00	FTLD-TDP *C9orF72 B*	-	-	-
32	403/08	FTLD-TDP *C9orF72 B*	-	-	-
33	019/95	FTLD-ALS *C9orF72*	-	n/a	n/a
34	050/98	FTLD-ALS *C9orF72*	-	n/a	n/a
35	068/05	FTLD-ALS *C9orf72*	-	n/a	-
36	069/02	FTLD-ALS *C9orf72 B*	-	n/a	-
37	095/05	FTLD-ALS *C9orf72*	-	n/a	-
38	112/99	FTLD-ALS *C9orf72*	-	n/a	n/a
39	117/91	FTLD-ALS *C9orf72*	-	-	n/a
40	141/06	FTLD-ALS *C9orf72*	-	n/a	-
41	144/12	FTLD-ALS *C9orf72*	-	n/a	-
42	151/08	FTLD-ALS *C9orf72 B*	-	-	n/a
43	156/95	FTLD-ALS *C9orf72 B*	-	n/a	n/a
44	157/04	FTLD-ALS *C9orf72*	-	n/a	n/a
45	163/09	FTLD-ALS *C9orf72 A*	-	-	n/a
46	174/08	FTLD-ALS *C9orf72*	-	n/a	n/a
47	205/99	FTLD-ALS *C9orf72*	-	n/a	n/a
48	223/08	FTLD-ALS *C9orf72*	-	-	n/a
49	229/06	FTLD-ALS *C9orf72*	-	n/a	-
50	290/10	FTLD-ALS *C9orf72*	-	n/a	n/a
51	311/07	FTLD-ALS *C9orf72*	-	n/a	-
52	315/07	FTLD-ALS *C9orf72 A*	-	n/a	n/a
53	400/08	FTLD-ALS *C9orf72*	-	n/a	-
31	088/00	FTLD-TDP *C9orF72 B*	-	-	-
32	403/08	FTLD-TDP *C9orF72 B*	-	-	-
33	019/95	FTLD-ALS *C9orF72*	-	n/a	n/a
34	050/98	FTLD-ALS *C9orF72*	-	n/a	n/a
35	068/05	FTLD-ALS *C9orf72*	-	n/a	-
36	069/02	FTLD-ALS *C9orf72 B*	-	n/a	-
37	095/05	FTLD-ALS *C9orf72*	-	n/a	-

38	112/99	FTLD-ALS *C9orf72*	-	n/a	n/a
39	117/91	FTLD-ALS *C9orf72*	-	-	n/a
40	141/06	FTLD-ALS *C9orf72*	-	n/a	-
41	144/12	FTLD-ALS *C9orf72*	-	n/a	-
42	151/08	FTLD-ALS *C9orf72 B*	-	-	n/a
43	156/95	FTLD-ALS *C9orf72 B*	-	n/a	n/a
44	157/04	FTLD-ALS *C9orf72*	-	n/a	n/a
45	163/09	FTLD-ALS *C9orf72 A*	-	-	n/a
46	174/08	FTLD-ALS *C9orf72*	-	n/a	n/a
47	205/99	FTLD-ALS *C9orf72*	-	n/a	n/a
48	223/08	FTLD-ALS *C9orf72*	-	-	n/a
49	229/06	FTLD-ALS *C9orf72*	-	n/a	-
50	290/10	FTLD-ALS *C9orf72*	-	n/a	n/a
51	311/07	FTLD-ALS *C9orf72*	-	n/a	-
52	315/07	FTLD-ALS *C9orf72 A*	-	n/a	n/a
53	400/08	FTLD-ALS *C9orf72*	-	n/a	-
41	144/12	FTLD-ALS *C9orf72*	-	n/a	-
42	151/08	FTLD-ALS *C9orf72 B*	-	-	n/a
43	156/95	FTLD-ALS *C9orf72 B*	-	n/a	n/a
44	157/04	FTLD-ALS *C9orf72*	-	n/a	n/a
45	163/09	FTLD-ALS *C9orf72 A*	-	-	n/a
46	174/08	FTLD-ALS *C9orf72*	-	n/a	n/a
47	205/99	FTLD-ALS *C9orf72*	-	n/a	n/a
48	223/08	FTLD-ALS *C9orf72*	-	-	n/a
49	229/06	FTLD-ALS *C9orf72*	-	n/a	-
50	290/10	FTLD-ALS *C9orf72*	-	n/a	n/a
51	311/07	FTLD-ALS *C9orf72*	-	n/a	-
52	315/07	FTLD-ALS *C9orf72 A*	-	n/a	n/a
53	400/08	FTLD-ALS *C9orf72*	-	n/a	-
49	229/06	FTLD-ALS *C9orf72*	-	n/a	-

4.3.1.3 hnRNP-E2 in neurodegenerative diseases

The involvement of hnRNP-E2 in all types of neurodegeneration was investigated in a broad range of neurodegenerative diseases, including Pick's disease, DLB, Alzheimer's disease and Huntington's disease. Other types of FTLD cases were also examined for hnRNP-E2 pathology, including FTLD with tau aggregates (FTLD-Tau), FTLD with ubiquitin only inclusions (FTLD-U) and FTLD with the *progranulin* mutation (FTLD-U-PRGN). Due to the close relation between FTLD and ALS, sporadic ALS cases, ALS with the *FUS* mutation, ALS with the *SOD1* mutation and ALS with the *TARDBP* mutation were also investigated for hnRNP-E2 immunoreactivity by IHC. In addition, argyrophilic grain disease (AGD) and spinocerebellar ataxia (SCA) cases were included.

The results of the hnRNP-E2 IHC on all the cases mentioned above did not reveal any pathological aggregates in the brain or spinal cord in any disease other than FTLD-TDP, with all the sections appearing similar to the controls. Figure 26 shows the IHC of hnRNP-E2 on the frontal cortex of a control case (case ref. 105) (A), a dementia with Lewy bodies case (B) (case ref. 63), an FTLD case with tau (*MAPT* mutation) (C) (case ref. 86) and an Alzheimer's disease case (D) (case ref. 55). hnRNP-E2 showed diffuse nuclear and cytoplasmic staining in all the cases and controls, with no intracellular or extracellular inclusions. The negative control slide is also presented in Figure 26 (F). Details of all the cases can be found in Table 3 (Chapter 2).

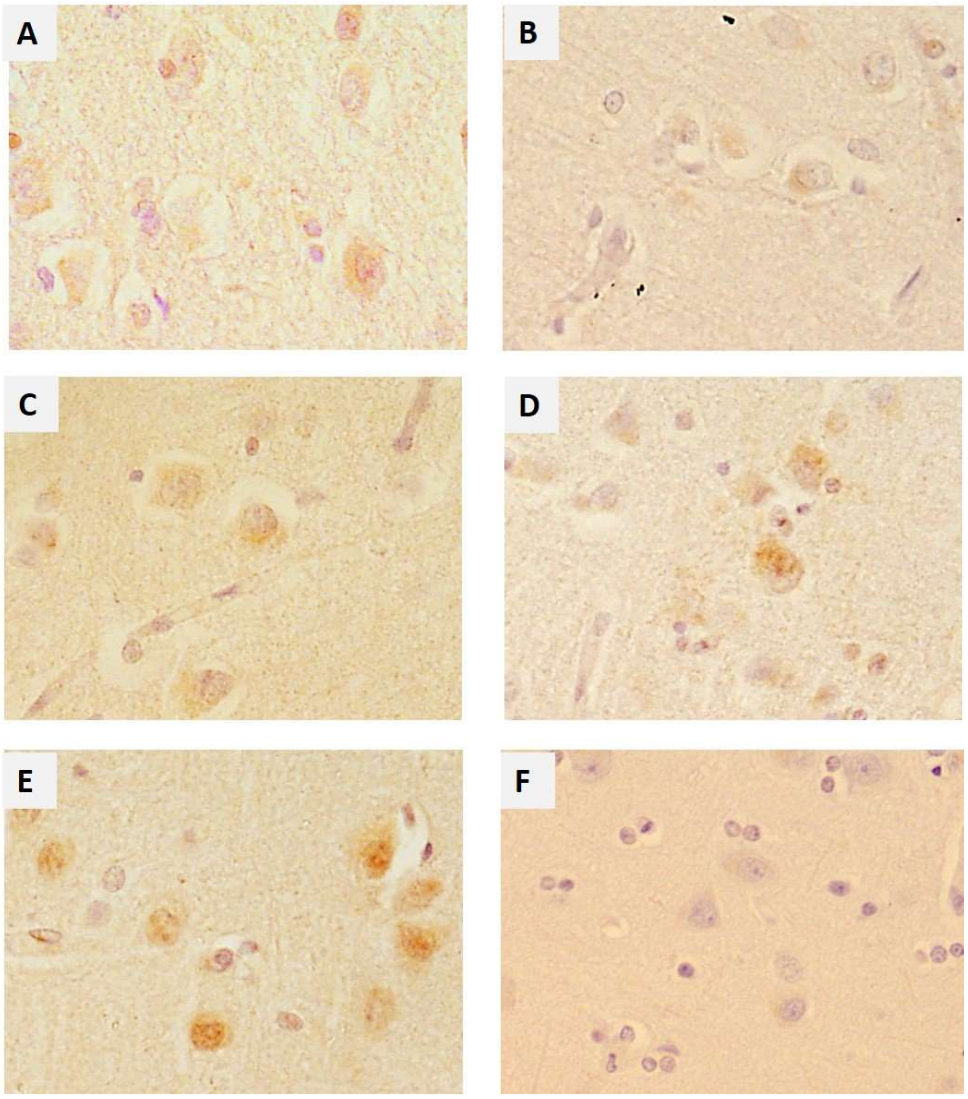

Figure 26: hnRNP-E2 (Santa Cruz, 1:500) IHC on the frontal cortex of control and neurodegenerative cases. Control case (A, ref. 105), dementia with Lewy bodies case (B, ref. 63) an FTLD with tau case (*MAPT* mutation, C, ref. 86), an Alzheimer's disease case (D, ref. 55) and a Pick's disease case (E, ref. 72). F represents the negative control slide.

4.3.2 Double-labelling immunofluorescence

4.3.2.1 Colocalisation of TDP-43 and hnRNP-E2 in human brain tissue

In order to examine the relationship of hnRNP-E2 with TDP-43 pathology, double-labelling immunofluorescence was performed to investigate any colocalisation within the TDP-43 inclusions. Inclusions were counted as described in the methods chapter (Chapter 2). A total of 465 TDP-43 inclusions and 393 hnRNP-E2 inclusions were registered from 1 FTLD-TDP type A case (case #2) and 4 FTLD-TDP type C cases (case #22, #23, #25 and #26). The percentage of the inclusions that colocalised was calculated. It was found that hnRNP-E2 colocalised with ~84.5% of TDP-43 inclusions. Figure 27 is a low magnification image showing the density and distribution of TDP-43 (red) and hnRNP-E2 (green) and the ratio of their colocalisation in the frontal cortex of an FTLD-TDP case. Figure 27A, A1 and A2 represent the dIf of both TDP-43 and hnRNP-E2 in the frontal cortex of a control case, showing that the normal nuclear localisation of TDP-43 and hnRNP-E2 appears to be shuttling between the nucleus and the cytoplasm, which is a normal distribution (Figure 27A and A1). The merged image (Figure 27A2) shows that there is some nuclear colocalisation of TDP-43 and hnRNP-E2 in some cells. hnRNP-E2 does not follow the same distribution of TDP-43 in all the cells in the frontal cortex in the control case (Figure 27). As previously mentioned, different types of inclusions were detected with hnRNP-E2, while similar results were detected with dIF for both TDP-43 and hnRNP-E2. Higher magnification images of individual cells were obtained using a confocal microscope, which show the complete colocalisation of both TDP-43 and hnRNP-E2 in the perinuclear and neuritic inclusions (Figures 28 and 29). Figure 28 also shows the colocalisation of both TDP-43 and hnRNP-E2 in the frontal cortex of an FTLD-TDP type A case where both perinuclear and neuritic inclusions are present. The colocalisation was absolute in both inclusions types (Figure 28). Images were also obtained from a type C FTLD-TDP case where mainly TDP-43 neuritic inclusions are detected in the frontal cortex (Figure 29). Again, the colocalisation of hnRNP-E2 with TDP-43 in the neuritic inclusions was detected. It is clear that hnRNP-E2 is related to TDP-43 through its course in the neurites (Figure 29G, H, I, J, K and L).

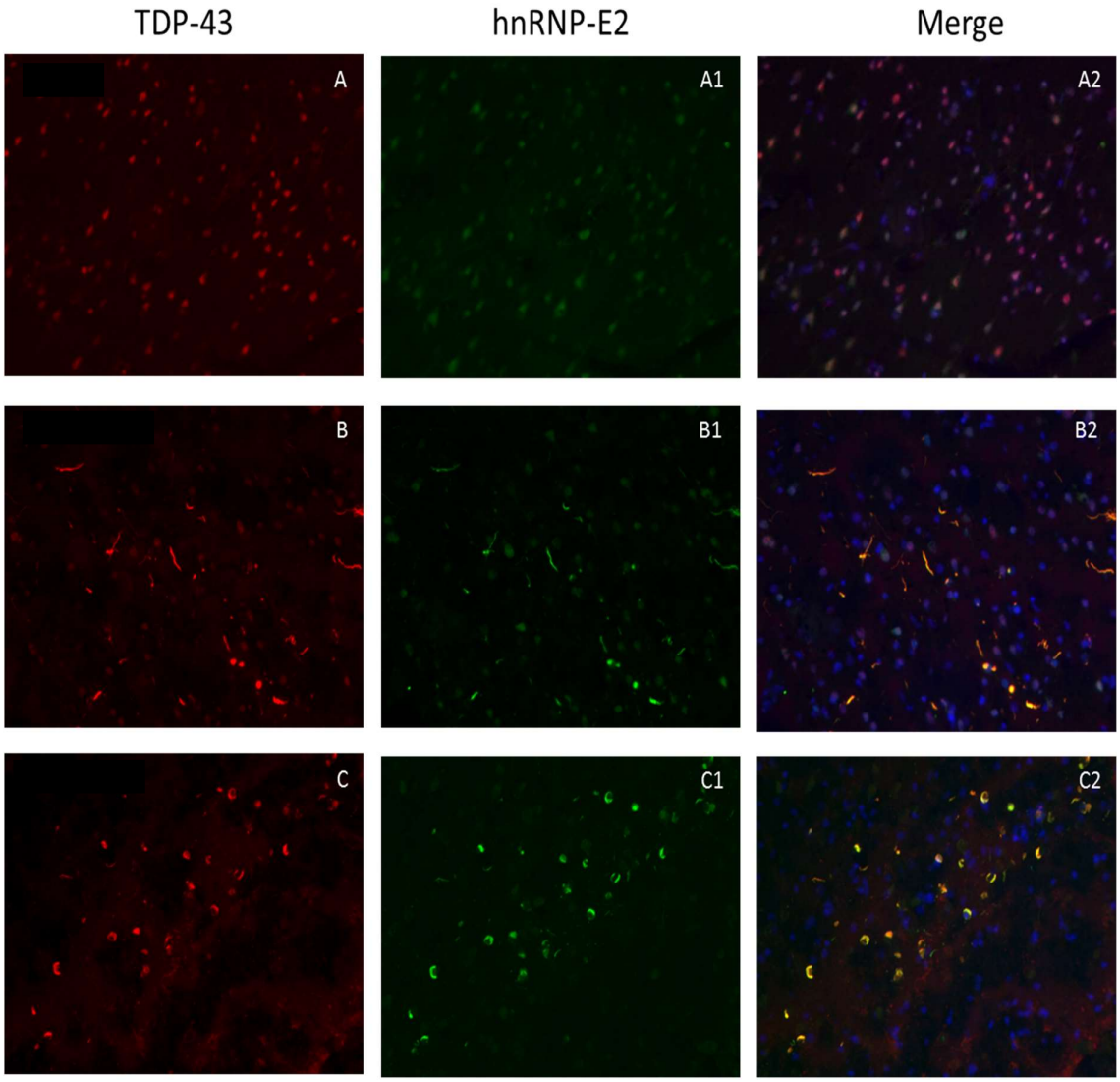

Figure 27: Double-labelling immunofluorescence of TDP-43 (red) and hnRNP-E2 (green) in the frontal cortex of a control case (A, A1 and A2), case ref. 104, which shows mainly nuclear staining of TDP-43. The shuttling of hnRNP-E2 between the cytoplasm and the nucleus is clear because it does not colocalise with TDP-43 in the nuclei of all cells. TDP-43 and hnRNP-E2 inclusions were detected in the frontal cortex of a type C FTLD-TDP case (B, B1 and B2, ref. 22) and s type A case (C, C1 and C2, ref. 2).

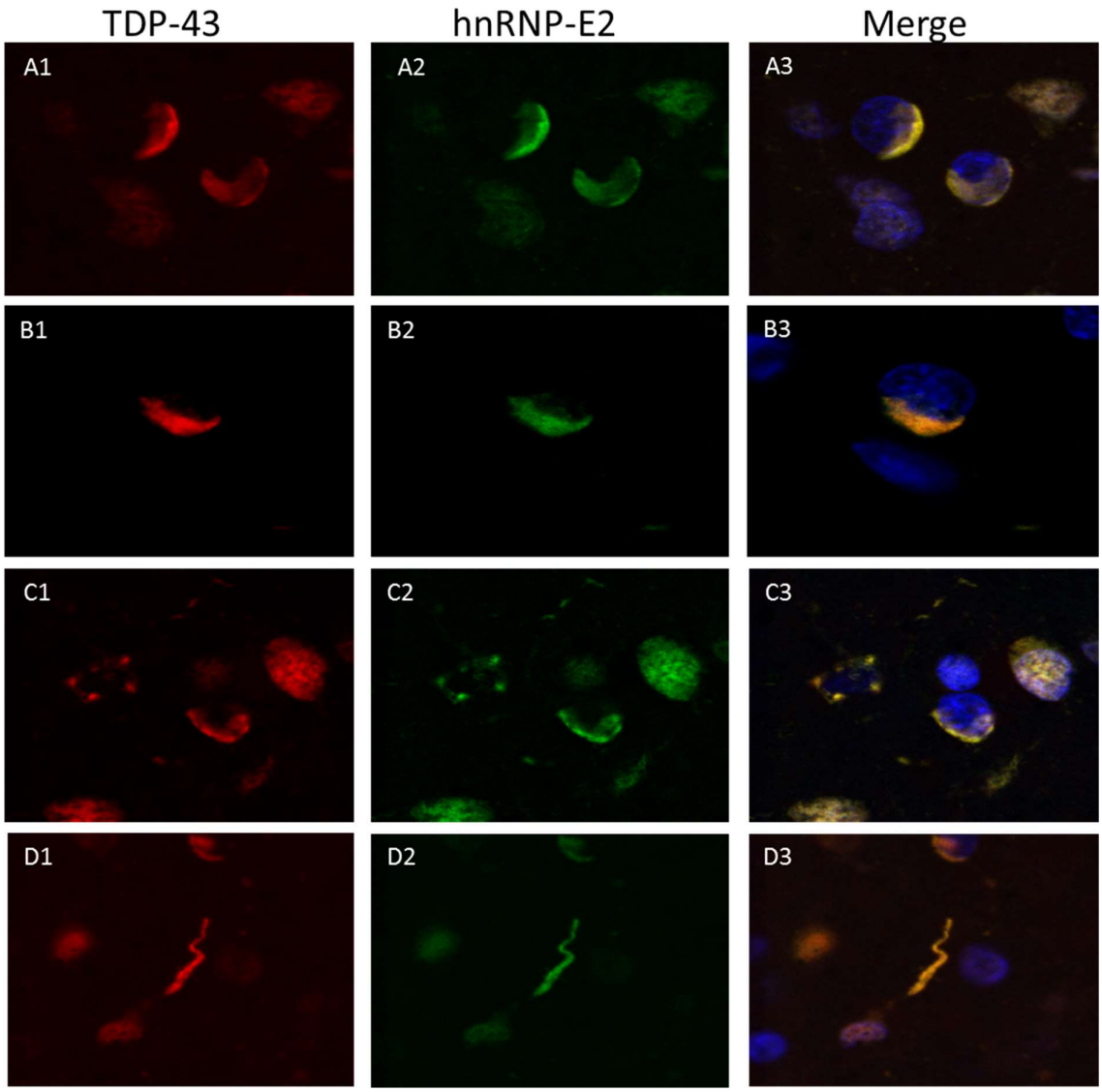

Figure 28: Confocal images from the frontal cortex of a type A FTLD-TDP case (ref. 2), which show TDP-43 (A1, B1, C1 and D1) and hnRNP-E2 (A2, B2 C2 and D2). The colocalisation of hnRNP-E2 within the TDP-43 inclusions is very clear in the merged images (A3, B3, C3 and D3).

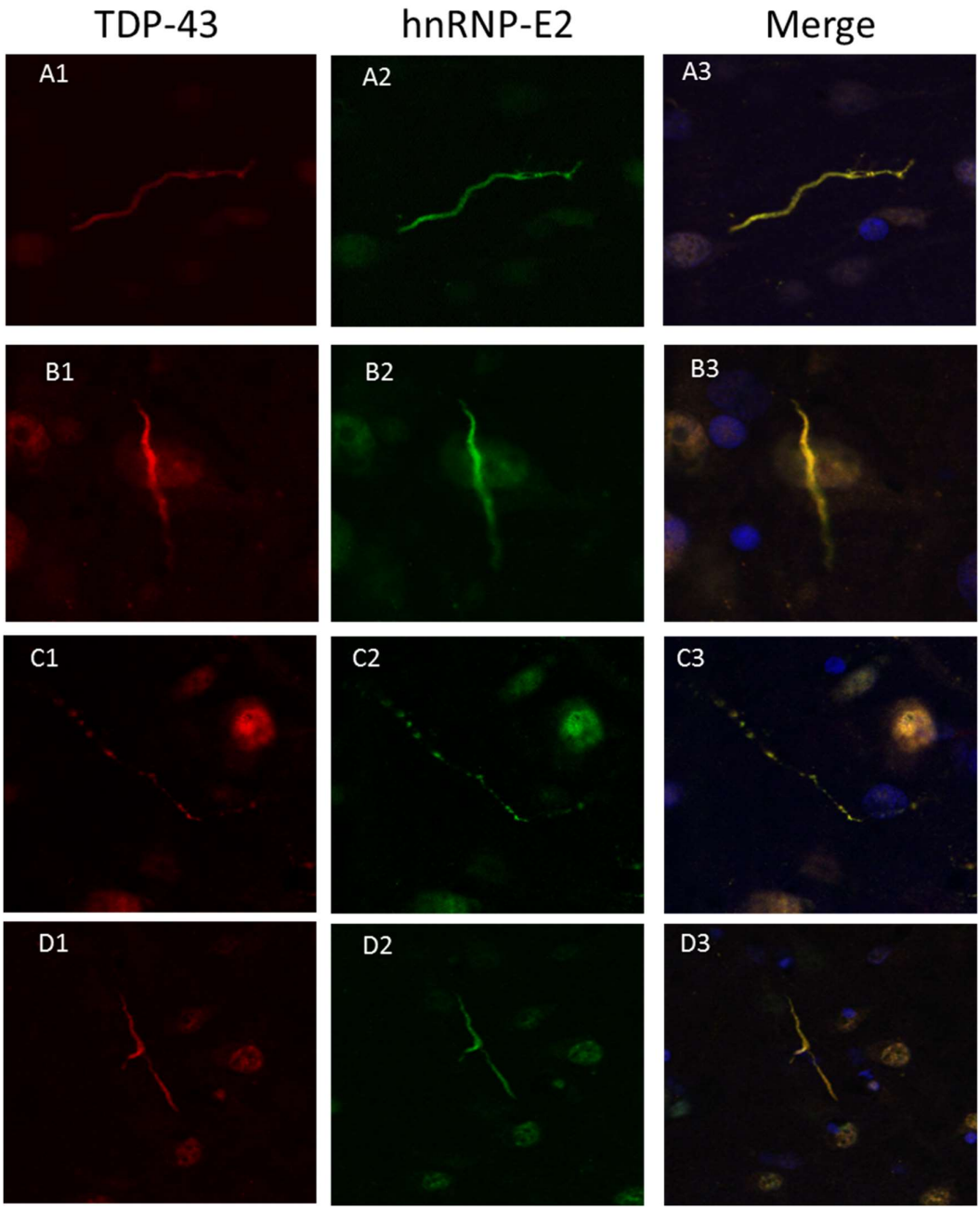

Figure 29: Confocal images from the frontal cortex of a type C FTLD-TDP case (ref. 22), which show TDP-43 (A1, B1, C1 and D1) and hnRNP-E2 (A2, B2, C2 and D2). Immunofluorescence shows the absolute colocalisation of hnRNP-E2 with TDP-43 along the neuronal exons (A3, B3, C3 and D3).

4.3.2.2 Colocalisation of ubiquitin and hnRNP-E2 in human brain tissue

hnRNP-E2 colocalisation with ubiquitin was also investigated. A total of 551 ubiquitin inclusions and 374 hnRNP-E2 inclusions were counted from 1 FTLD-TDP type A case (case #2) and 4 FTLD-TDP type C cases (case #22, #23, #25 and #26) as described in the methods chapter (Chapter 2). The colocalisation of hnRNP-E2 with ubiquitin in the frontal cortex of FTLD-TDP cases accounted for 67% of all ubiquitin inclusions. Figure 30 shows the distribution of both ubiquitin and hnRNP-E2 in the frontal cortex of a type A FTLD-TDP case. It is clear from Figure 30 that not all the ubiquitin inclusions colocalised with hnRNP-E2 and vice versa. It is also clear from Figure 30 (B1–C3) that hnRNP-E2 and ubiquitin do not exhibit absolute colocalisation within the inclusions such as that seen with TDP-43 and hnRNP-E2 inclusions. Figure 31 shows closer images of the ubiquitin and hnRNP-E2 inclusions in the frontal cortex of other type A and type C FTLD-TDP cases.

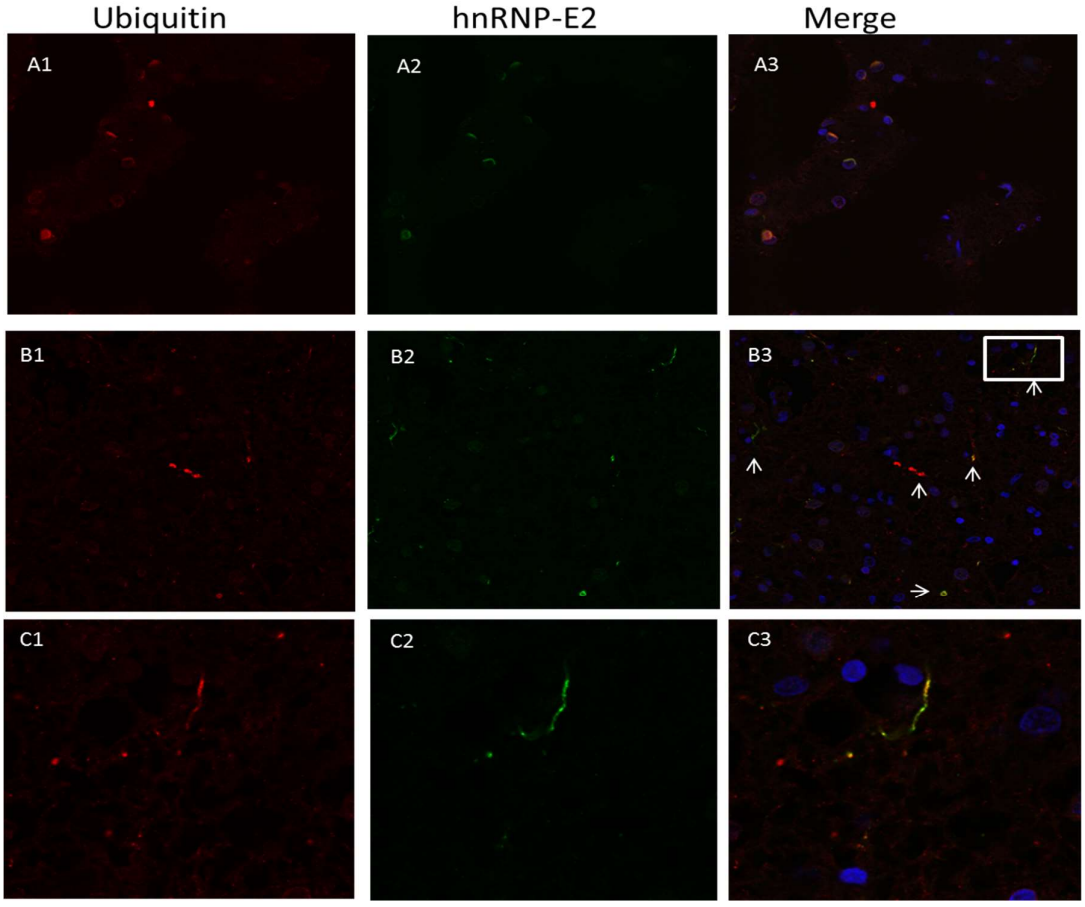

Figure 30: The distribution of ubiquitin (A1, B1 and C1) and hnRNP-E2 (A2, B2 and C2) inclusions in the frontal cortex of a type C FTLD-TDP case (ref. 22). A3 and B3 show that there are some ubiquitin inclusions that do not have hnRNP-E2, while some inclusions have hnENP-E2 but not ubiquitin. C1–3 are magnified images of the box area in B3. The colocalisation of hnRNP-E2 within the ubiquitin inclusions is not absolute (C3).

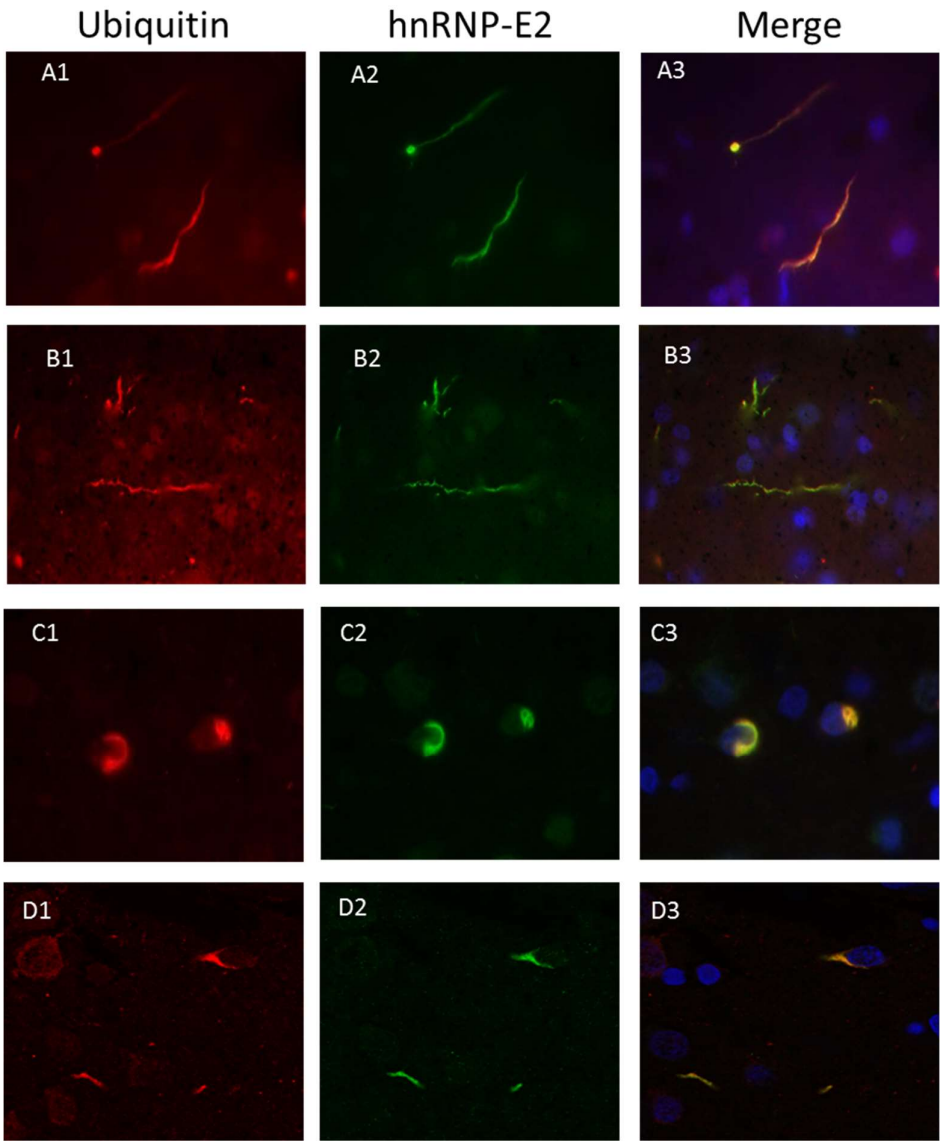

Figure 31: Closer images of ubiquitin (A1, B1, C1 and D1) and hnRNP-E2 (A2, B2, C2 and D2) in the frontal cortex of type C cases (ref. 22, A1–A3) and (ref. 26, B1-B3) and a type A case (ref. 2, C1–D3).

4.3.3 Western blotting

The levels of insoluble hnRNP-E2 were examined in FTLD-TDP cases using Western blotting techniques. Results were obtained from FTLD-TDP cases without the *C9orf72* expansion, which showed positive hnRNP-E2 inclusions in IHC. In addition to the control cases, FTLD-TDP cases with *C9orf72* that did not show any hnRNP-E2 inclusions on IHC were also tested. Figure 32 presents the details of the cases used in the Western blotting. Six cases in each group were used (i.e. six FTLD-TDP with hnRNP-E2-positive inclusions in IHC, six FTLD-TDP without hnRNP-E2 inclusions in IHC, six FTLD-TDP with the *C9orf72* expansion that were all negative for hnRNP-E2 in IHC and six control cases). The *C9orf72* cases were included to check whether there was any insoluble hnRNP-E2 that could be detected with Western blotting not with IHC. All the blots were probed with the rabbit polyclonal TDP-43 (Proteintech) antibody and the mouse monoclonal hnRNP-E2 (Abnova) antibodies. The fractionation protocol is detailed in section 2.1.4.1.

4.3.3.1 hnRNP-E2 Western blots in FTLD-TDP cases and controls

All the samples were fractionated according to the SARK fractionation protocol described in Chapter 2. The Abnova mouse hnRNP-E2 antibody was used at 1:500 dilutions to label the Western blots for hnRNP-E2. The hnRNP-E2 bands were detected on the Odyssey® system's mouse channel at the expected size of ~37kDa. The quantification of the blots was performed using the ImageJ software and the graphs were plotted using GraphPad software (Figure 32). All five fractions of each case were loaded onto the gels so that each blot had a control case, an FTLD-TDP with hnRNP-E2 +ve IHC, an FTLD-TDP with hnRNP-E2 -ve IHC and an FTLD-TDP with the *C9orf72* mutation.

The presence of the hnRNP-E2 insoluble band was not consistent with all the IHC results; therefore, a definite conclusion regarding hnRNP-E2 insolubility could not be drawn by inspecting the Western blots. In Blot A, Figure 32, the control case 66/00 had a moderate band of hnRNP-E2 in its urea fraction; however, the hnRNP-E2 +ve case 13/10 showed a very strong insoluble band of hnRNP-E2 in its urea fraction, which is consistent with the IHC results for this particular case. In Blot B, Figure 32, the hnRNP-E2 -ve case showed a stronger band for hnRNP-E2 in the urea fraction when compared to the hnRNP-E2 +ve case. In Blots C, D and F, Figure 32, all the cases and controls showed a similar moderate hnRNP-E2 band in the urea fraction. In Blot E, there is a strong band of insoluble hnRNP-E2 in the urea fraction of the hnRNP-E2 +ve case and a moderately strong band in the *C9orf72* case when compared to the control and hnRNP-E2 -ve case on the same blot (Figure 32).

The levels of hnRNP-E2 for all the cases were quantified as described in Chapter 2 using ImageJ software and the average for each group of cases was plotted. The levels of insoluble hnRNP-E2 in the urea fractions were normalised to the soluble levels in the lysate fraction for each case. The average of the hnRNP-E2 levels for each group of cases was calculated and a statistical analysis was performed. A one-way ANOVA test was performed to compare the insoluble hnRNP-E2 levels in all the case groups. The ANOVA test showed no significant difference in the insoluble hnRNP-E2 levels among the case groups: control cases (0.82 ± 0.21), hnRNP-E2 +ve cases (2.26 ± 0.65), hnRNP-E2 -ve cases (2.05 ± 0.55) and *C9orf72* cases (1.11 ± 0.27) (one-way ANOVA, $F = 1.12$, df. = 3 and 20, $p = 0.37$, $P > 0.05$) (Figure 33).

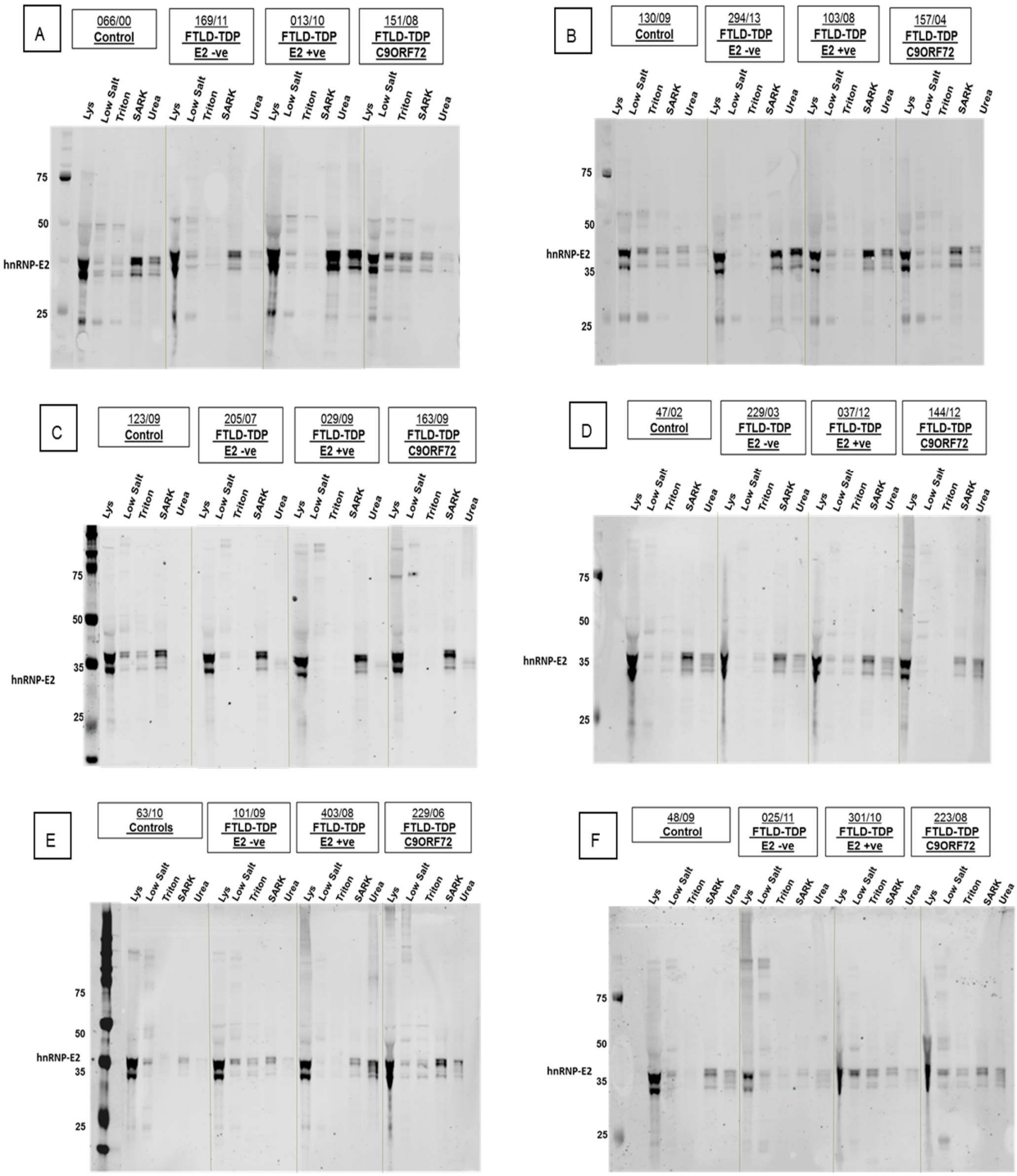

Figure 32: Western blots of hnRNP-E2. Each blot has a control case, an hnRNP-E2 -ve case, an hnRNP-E2 +ve case and an FTLD-TDP case with *C9orf72* expansion. The five fractions of each case were loaded, starting with the lysate fraction followed by the low salt, Triton, SARK and, finally, the insoluble urea fraction. The hnRNP-E2 bands were detected at 37 KDa using the mouse hnRNP-E2 antibodies (Abnova).

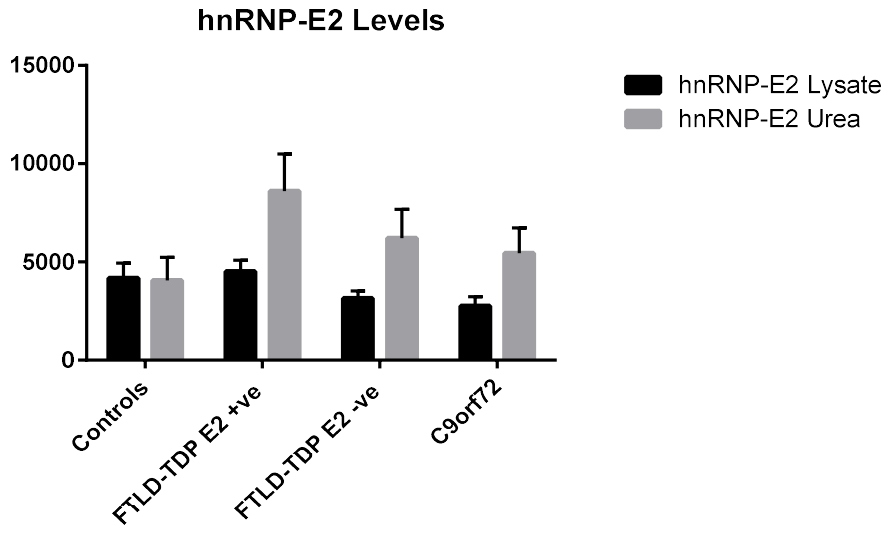

Figure 33: Levels of soluble hnRNP-E2 in the lysate fraction and the insoluble levels of hnRNP-E2 in the urea fraction in the control cases, FTLD-TDP E2 +ve cases, FTLD-TDP E2 -ve cases and FTLD-TDP with *C9Orf72* expansion cases.

4.3.3.2 TDP-43 Western blots on FTLD-TDP cases and controls

The same blots were labelled for TDP-43 using the full-length Proteintech TDP-43 rabbit antibody. The TDP-43 bands were detected on the Odyssey® system's rabbit channel at the expected size of ~43 kDa. The quantification of the TDP-43 bands was performed using the ImageJ software and the graphs were plotted using GraphPad software. All five fractions of each case were loaded onto the gels so that each blot had a control case, an FTLD-TDP with hnRNP-E2 +ve IHC, an FTLD-TDP with hnRNP-E2 -ve IHC and an FTLD-TDP with the *C9orf72* mutation case.

The pathological hallmark in TDP-43 proteinopathies is the presence of the insoluble band of TDP-43 in the urea fraction of brain lysate. The smearing of TDP-43 in the urea lane is another pathological hallmark of TDP-43 proteinopathy. The TDP-43 blots were used as a reference in this study in order to try to spot any differences between the cases in correlation with hnRNP-E2 pathology. In Blot A, Figure 34, the FTLD-TDP E2 +ve case 13/10 showed a strong band of TDP-43 at 43 kDa; however, there was no difference in the band seen in the other FTLD-TDP cases or the control (Figure 34). By looking at Blots B and C, it is clear there is no band of insoluble TDP-43 in the urea fraction in the control case. Furthermore, the FTLD-TDP E2 +ve case has a stronger band when compared to the FTLD-TDP E2 -ve and FTLD-TDP *C9orf72* cases on the same blots. In Blot D, Figure 34, a band of insoluble TDP-43 was detected in the control case; however, there was no smearing when compared to the other three FTLD-TDP cases in the blot. Blot E, Figure 34, showed a faint

insoluble TDP-43 band in the control case, which is slightly less intense than the band detected in the FTLD-TDP E2 -ve case. The FTLD-TDP E2 +ve case showed a stronger insoluble TDP-43 band and smearing in comparison to the FTLD-TDP *C9orf72* case on the same blot. Yet, Blot F, Figure 34, showed a stronger band of insoluble TDP-43 in the control case when compared to the FTLD-TDP E2 -ve and E2 +ve cases on the same blot. However, the band was larger and stronger in the FTLD-TDP *C9orf72* case on the same blot. As the presence of the insoluble band was not conclusive, the quantification and statistical analysis of the TDP-43 insolubility was performed in order to detect any significant results.

The levels of TDP-43 in all the cases were quantified as described in Chapter 2 using ImageJ software and the average for each group of cases was plotted. The levels of insoluble TDP-43 in the urea fractions were normalised to the soluble levels in the lysate fraction for each case. The average of the TDP-43 levels for each group of cases was calculated and a statistical analysis was performed. A one-way ANOVA test was conducted to compare the insoluble TDP-43 levels in all the case groups. The ANOVA test showed no significant difference in the insoluble TDP-43 levels among the case groups: control cases (1.03 ± 0.27), hnRNP-E2 +ve cases (1.91 ± 0.57), hnRNP-E2 -ve cases (1.56 ± 0.47) and *C9orf72* cases (2.1 ± 0.72) (one-way ANOVA, $F = 1.23$, df. = 3 and 20, $p = 0.32$, $P > 0.05$) (Figure 35).

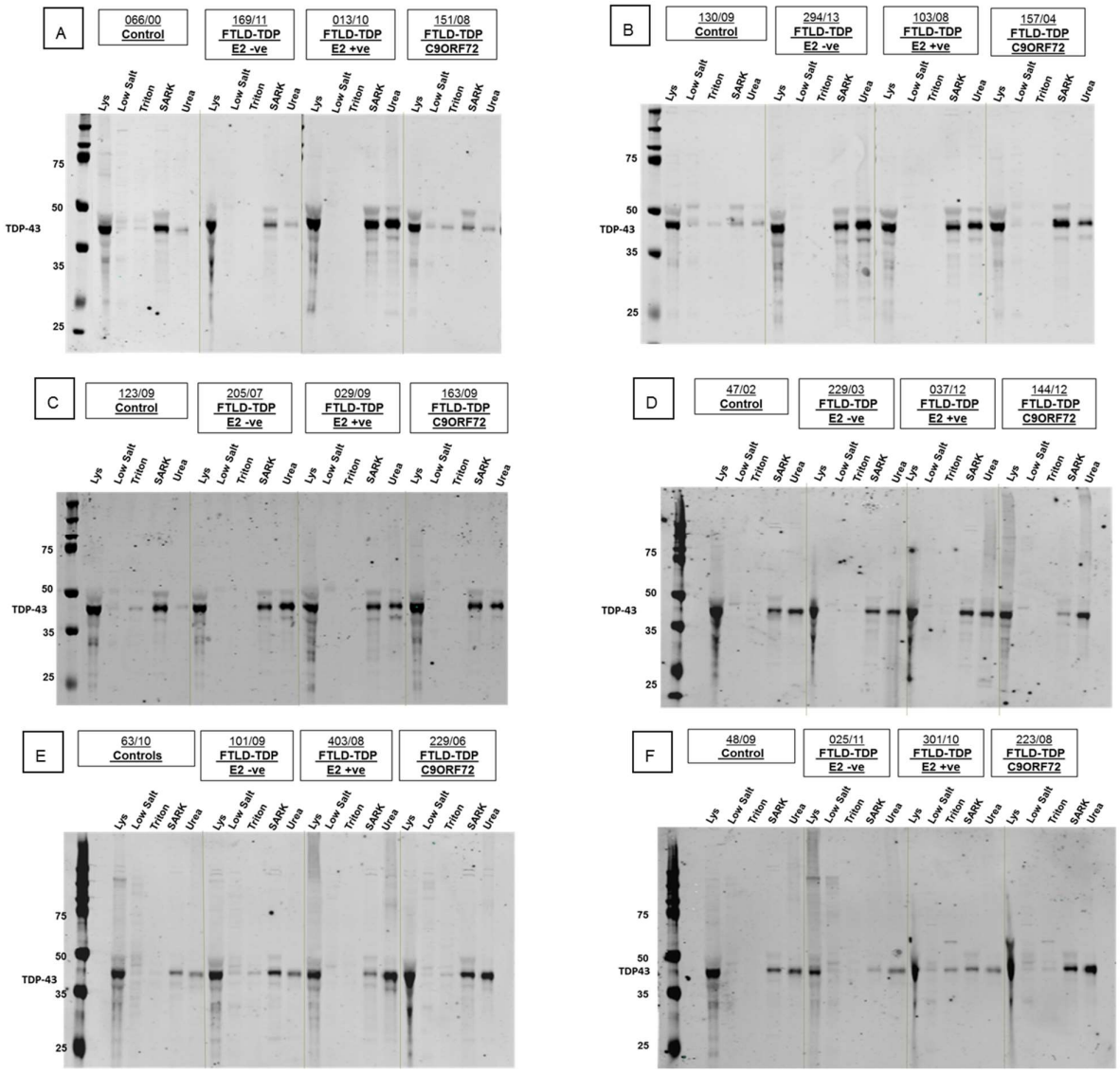

Figure 34: Western blots of TDP-43. Each blot has a control case, an hnRNP-E2 -ve case, an hnRNP-E2 +ve case and an FTLD-TDP case with *C9orf72* expansion. The five fractions of each case were loaded, starting with the lysate fraction followed by the low salt, Triton, SARK and, finally, the insoluble urea fraction. TDP-43 bands were detected at 43 KDa using the rabbit TDP-43 antibodies (Proteintech).

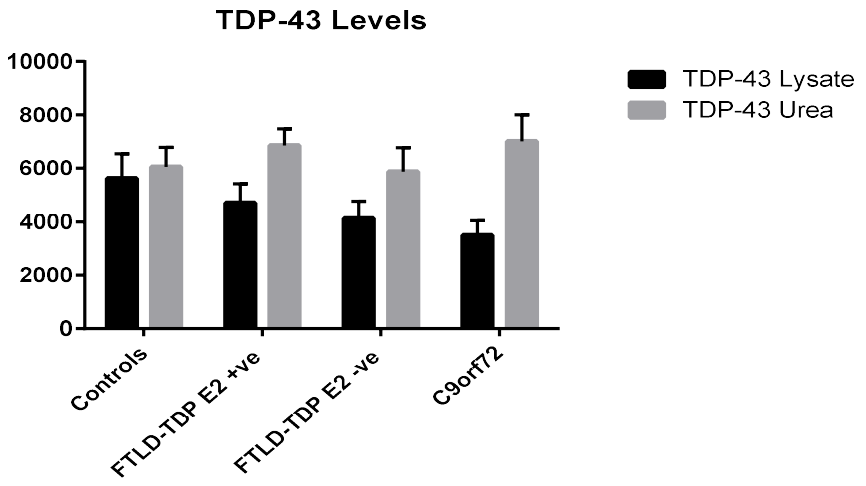

Figure 35: Levels of soluble TDP-43 in the lysate fraction and the insoluble levels of TDP-43 in the urea fraction in the control cases, FTLD-TDP E2 +ve cases, FTLD-TDP E2 -ve cases and FTLD-TDP with *C9orf72* expansion cases.

4.3.3.3 Detection of the 25 kDa band of TDP-43 with the phospho TDP-43 antibody

A comparison of the different TDP-43 antibody signatures on the Western blots was carried out by running the samples from the frontal cortex of FTLD-TDP cases fractionated by the SARK protocol Western blot gels as previously described. The blots were labelled with the phospho-TDP antibody (Figure 36A) as well as with the Proteintech TDP-43 antibody (Figure 36B). The principal difference was the detection of the TDP-43 pathological 25 kDa band by the phospho TDP antibody, which was absent when the full-length TDP-43 Proteintech antibody was used (Figure 36A).

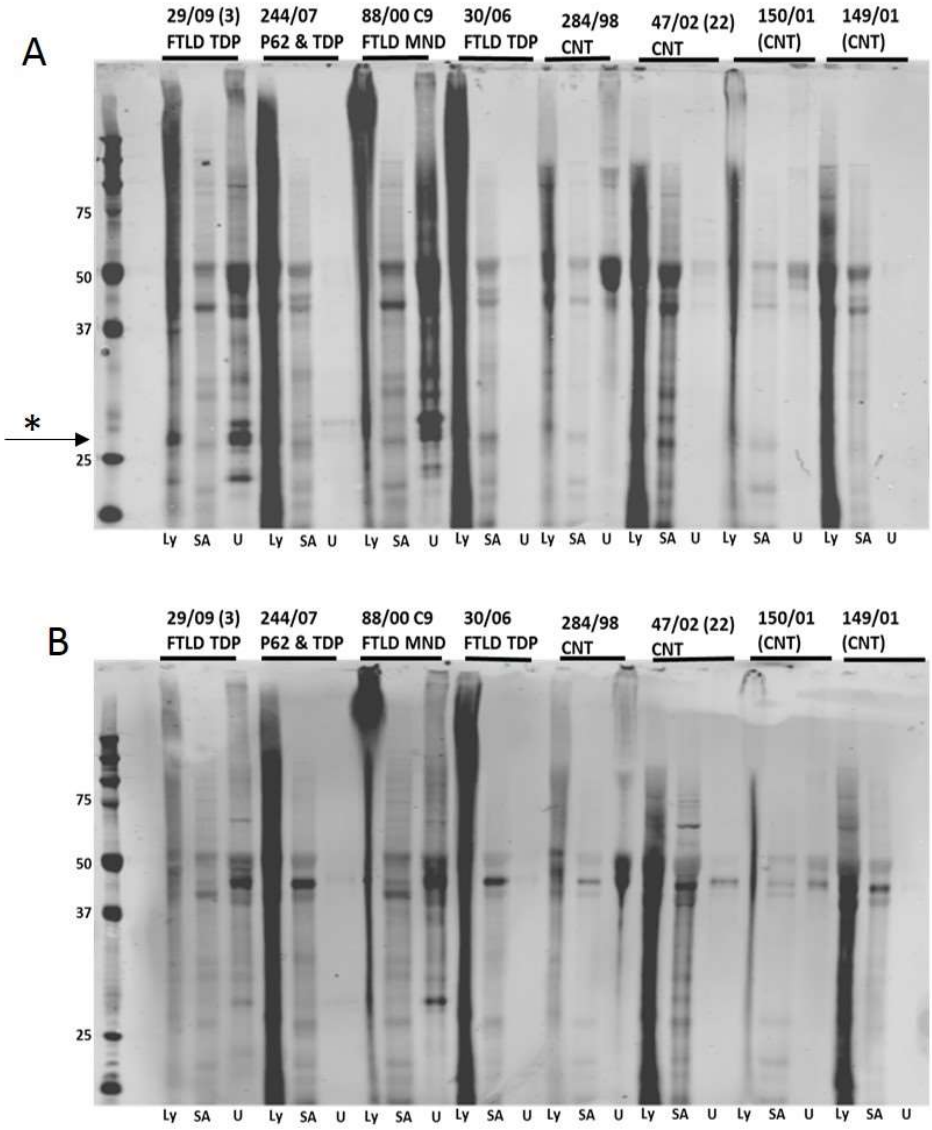

Figure 36: Western blot of the soluble and insoluble fractions from the frontal cortex of FTLD-TDP cases. A) Represents the results with the anti-phospho TDP-43 antibodies at 1:1000. The arrow indicates the pathological ~25 kDa of TDP-43 in the urea fraction. B) The same blot was probed by the Proteintech TDP-43 full-length antibodies lacking the ~25 kDa of TDP-43.

4.3.4 Statistical analysis of hnRNP-E2 pathology and demographic data concerning the cases

4.3.4.1 FTLD-TDP subtypes

A Chi-square test of independence was performed to examine the relation between the FTLD-TDP pathological subtypes and hnRNP-E2 pathology. The relation between these variables was found to be significant (X^2 [2, N = 29] = 6.139, p < 0.05). hnRNP-E2 pathology depends significantly on the subtype of TDP-43 pathology in FTLD cases. FTLD-TDP subtype A and subtype C have a greater frequency of hnRNP-E2 pathology than subtype B (Figure 37).

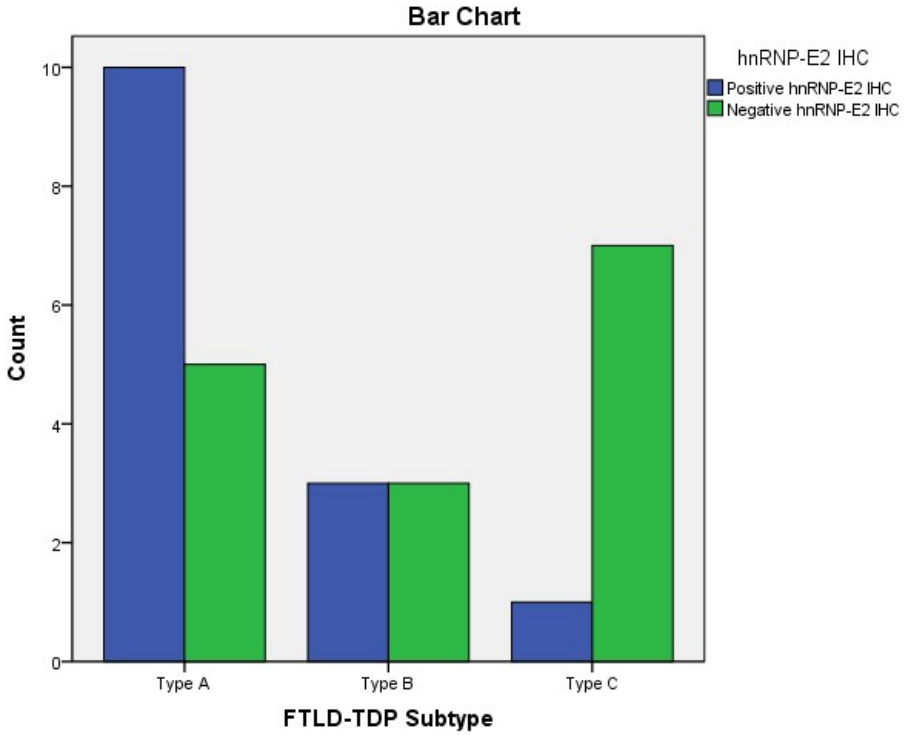

Figure 37: FTLD-TDP subtype A and subtype C have a greater frequency of hnRNP-E2-positive immunoreactivity than that seen with subtype B.

4.3.4.2 Gender, dementia duration, PMD and fixation time

hnRNP-E2 pathology is independent of both gender and dementia duration (X^2 [1, N = 29] = 1.98, p > 0.05). The PMD (X^2 [22, N = 27] = 23, p > 0.05) and fixation time (X^2 [10, N = 26] = 9.85, p > 0.05) also failed to affect hnRNP-E2 pathology in FTLD-TDP cases.

4.4 Discussion

hnRNP-E2 inclusions in FTLD-TDP brain tissue were first detected during the hnRNPs screening experiment discussed in Chapter 3. Confirmation of this finding was achieved through several experiments conducted on human brain tissues utilising IHC, dIF and WB. hnRNP-E2 is an RNA-binding protein that belongs to the hnRNP-K family of proteins. They are characterised by triple KH domains that can interact independently with target RNA sequences, which allows this protein family to potentially form highly complex-specific RNA interactions. hnRNP-E2 shares 89% amino acid similarity with hnRNP-E1; therefore, it was important to confirm that the antibody detecting hnRNP-E2 did not also detect E1. The IHC of hnRNP-E1 performed on the same cases with positive hnRNP-E2 immunoreactivity did not detect any inclusions similar to those detected by the hnRNP-E2 antibodies. The presence of hnRNP-E2 in the inclusions seen in the FTLD-TDP patients' brain tissue indicates its possible involvement in the underlying pathology of neurodegeneration.

hnRNP-E2's disease specificity was investigated by applying hnRNP-E2 IHC to a wide range of neurodegenerative cases. The results showed hnRNP-E2 inclusions in a subset of FTLD-TDP cases that do not carry the *C9orf72* mutation. Of the 30 FTLD-TDP cases, hnRNP-E2 was positive in 16 cases, which represented 53.3% of the investigated FTLD-TDP cases. The cases' demographic data was statistically analysed in order to check the dependency of hnRNP-E2 pathology on any of the demographic variables. The only significant dependence was found in relation to the TDP-43 pathological subtype. FTLD-TDP subtypes A and C have a significantly higher frequency of hnRNP-E2 immunoreactivity than subtype B. Indeed, in subtype B, there was only one positive case for hnRNP-E2. Alternatively, this case could come under another subtype because of difficulties in subtyping.

Due to the reported relation between hnRNP-E2 and hnRNP-G, an additional experiment was designed to investigate the presence of hnRNP-G in hnRNP-E2 inclusions as well as to confirm hnRNP-E2's antibody specificity. It has been reported that hnRNP-E2 contributes to the regulation of exon 10 by interacting with hnRNP-G and SRp75 (Wang et al., 2011a). The same study suggested that the exon 10 inclusions seen in FTLD-17 are due to the weakened binding of hnRNP-E2/hnRNP-G with SRp75, which promotes it as a possible strategy for correcting the imbalance in the exon 10 ratio seen in tauopathies (Wang et al., 2011a). Tau is a microtubule-associated protein that aggregates in multiple neurodegenerative diseases. The splicing misregulation of the adult-specific exon 10 of tau leads to the

expression of abnormal ratios of tau isoforms seen in FTDP-17 and AD (Niblock and Gallo, 2012, Broderick et al., 2004b, Wang et al., 2011a).

hnRNP-G, which is also known as RBMX, is X-linked and it has a different set of co-factors and targets from its Y-linked paralogue, RBMY. In this study, the possibility of hnRNP-E2 presenting as a complex with hnRNP-G was investigated by applying the IHC of hnRNP-G to the hnRNP-E2-positive cases. The results showed that hnRNP-G is not part of the hnRNP-E2 inclusions seen in FTLD-TDP brains. In addition, the absence of hnRNP-E2 from other neurodegenerative diseases, including tauopathies such as AD, supports the notion that it is more closely related to TDP-43 pathology. Furthermore, the hnRNP-E2 inclusions followed the course of the TDP-43 inclusions in FTLD-TDP brains according to the new pathological classification of FTLD established by Mackenzie et al. (Mackenzie et al., 2011b). Although there is no established association between TDP-43 and tau (Robinson et al., 2014), the presence of hnRNP-E2 in the TDP-43 inclusions and its identified role in the regulation of tau exon 10 emphasise its role in neurodegeneration and the search for new mechanisms.

The dIf results revealed a strong relation between TDP-43 and hnRNP-E2, with 84.5% of the TDP-43 inclusions being found to harbour hnRNP-E2. hnRNP-E2 was also present in 67% of the ubiquitin inclusions in the same cases. Examining the inclusions with a high resolution revealed that hnRNP-E2 showed colocalisation within the TDP-43 aggregates. In relation to ubiquitin, hnRNP-E2 was partially ubiquitinated, as shown by the high resolution images of the hnRNP-E2/ubiquitin inclusions. A question arose at this point concerning whether hnRNP-E2 deposition has any implications for TDP-43's suggested pathological mechanisms and why it is only seen in a subset of FTLD-TDP cases. The possible mechanisms of colocalisation will be discussed later in this section.

Insoluble hnRNP-E2 was detected in the urea fraction of some FTLD-TDP cases; however, the Western blotting results were not conclusive for several reasons. The hnRNP-E2 insoluble band was not consistent with all the IHC results. The hnRNP-E2 insoluble band in the urea fraction was detected in some of the hnRNP-E2-negative cases by IHC, except for the FTLD-TDP cases with the *C9orf72* expansion. hnRNP-E2 was absent from some of the hnRNP-E2-positive FTLD-TDP cases determined by IHC. Therefore, hnRNP-E2's insolubility in brain tissue is not certain. This could be related to the abundant variation of the hnRNP-E2 inclusions among the cases or simply the fact that it is present in soluble and insoluble forms in different cases. The quantitative results were also inconclusive, which could be due to the small number of cases used for fractionation.

Several issues arose in relation to the TDP-43 Western blotting. The full-length TDP-43 antibody used did not detect the C-terminal fragment at the 25 kDa. However, it was detected with the phospho TDP antibodies, as described in Figure 36. A small amount of insoluble TDP-43 was detected in some of the control cases; however, the pathological high molecular weight smear was absent from those controls. The quantitative results were again not conclusive, which could again be due to the small number of cases used. The amount of TDP-43 varied among the FTLD-TDP cases. Interesting, an increasing amount of evidence is emerging regarding the heterogeneity of TDP-43 in the brain of FTLD-TDP and ALS-TDP patients (Tsuji et al., 2012, Takeuchi et al., 2016, Armstrong et al., 2010). TDP-43 can exist as different species with variable solubility, microscopical appearance and mobility profiles, which may explain the variation seen among the cases as well as the presence of small amounts of insoluble TDP-43 in control tissue (Scotter et al., 2015). Additional differences in the TDP-43 pathological bands in the Western blots were detected among the different types of FTLD-TDP (Tsuji et al., 2012). Furthermore, a recent study investigated the TDP-43 inclusions in the brain of ALS patients, characterising them according to the location and abundancy of the TDP-43 aggregates in the brain of ALS patients (Takeuchi et al., 2016). The present results of the hnRNP-E2 and TDP-43 Western blotting may suggest that there exist different conformations of TDP-43 and hnRNP-E2, which could correspond to the pathological phenotype of FTLD-TDP or the histological subtypes of FTLD-TDP.

Further insight into the functions of hnRNP-E2 could provide an explanation for the colocalisation of hnRNP-E2 with TDP-43 and ubiquitin inclusions; however, a definite answer will require rigorous investigations. Most prior studies have focused on the post-transcriptional and translational controls of hnRNP-E2 in RNA viruses such as poliovirus, rhinovirus and coxsackievirus (Sean et al., 2008, Zell et al., 2008, Walter et al., 1999). hnRNP-E2 plays a role in mRNA stability and translation regulation through its ability to bind to the poly(C) stretches of both DNA and RNA. It was also reported to bind to the 3' and 5' UTR of the hepatitis C virus (Tingting et al., 2006). Like other hnRNPs, hnRNP-E2 participates in protein-protein interactions and it is essential for mouse foetal development, although not all of its functions and interactions have yet been identified (Ghanem et al., 2015).

Both TDP-43 and hnRNP-E2 are present with ubiquitin in FTLD-TDP cases, as shown in the results discussed above. Thus, it is possible that ubiquitin could be the link explaining the colocalisation of TDP-43 and hnRNP-E2. Scotter et al. (2014) suggested that an impaired cellular ubiquitin proteasome system (UPS) results in misregulated soluble TDP-43 levels, which then act as a nucleation for

aggregates. The cascade of ubiquitin-mediated protein degradation involves the stepwise action of three enzymes, namely the ubiquitin-activating enzyme (E1), the ubiquitin-conjugating enzyme (E2) and the ubiquitin ligase enzyme, which provided substrate specificity (E3). E3 ubiquitin ligase recruits the ubiquitin-loaded conjugating enzyme E2, recognises a protein substrate and either directly catalyses or assists with the transfer of ubiquitin from E2 to the protein substrate (Hershko and Ciechanover, 1998). hnRNP-E2 was identified as an adapter between the ubiquitin ligase E3 ITCH and the mitochondrial antiviral-signalling protein (MAVS) in cellular studies (You et al., 2009). The overexpression of hnRNP-E2 led to the degradation of MAVS and abolished the cellular response to viral infection, while the knockdown of hnRNP-E2 had the opposite effect. hnRNP-E2 is not a ligase enzyme; however, it performs a ligase-enzyme-adapting activity, which recruits the conjugating enzyme to its substrate (You et al., 2009). Moreover, a ubiquitin ligase complex has been recently identified by Uchida et al. (2016) that is involved in TDP-43 degradation. The ligase complex consists of the von Hippel-Lindau protein (VHL), which is a tumour suppressor protein, and the cullin-2 (CUL2) RING, which belongs to the hydrophobic family of proteins that provides a temporary complex for ubiquitin ligase E3. The CUL2 combines with the RING proteins, which contain a zinc-finger domain. VHL was identified as the substrate binding part of the complex, which showed the preferential recognition site of Glu246 in the RRM2 of misfolded TDP-43. Interestingly, when VHL is overloaded in the cytoplasm, it tends to stabilise and aggregate with TDP-43. VHL was detected in TDP-43 inclusions in motor neurons in the spinal cord of ALS patients. This suggested that the imbalance between VHL and CUL2 is the key to TDP-43 aggregation and highlighted the CUL2 E3 ligase as a potential therapeutic target for TDP-43 proteinopathies (Uchida et al., 2016). Whether or not hnRNP-E2 could be a component or an adaptor of this ligase complex is a question requiring further investigation.

Based on recent studies, another possible explanation for the colocalisation of hnRNP-E2 with TDP-43 is hnRNP-E2's apoptosis regulation function. Evidence of neuronal apoptosis was reported in ALS and FTLD cases through elevated levels of activated caspase-3 in the patients' spinal cord and brain tissue when compared to the controls (Martin, 1999b, Su et al., 2000). Moreover, caspase-3 was identified as the protease responsible for TDP-43 fragmentation (Zhang et al., 2007b). More interestingly, caspase-3 downregulates TDP-43 in glioma cells (Nan et al., 2014). Many studies have linked hnRNP-E2 to caspase-3 activation. hnRNP-E2 is upregulated in human glioma tissue, while the knockdown of hnRNP-E2 inhibited glioma growth through the induction of caspase-3-mediated apoptosis and the

inhibition of cell-cycle progression (Han et al., 2013). Additionally, it has been reported that the overexpression of hnRNP-E2 induces apoptosis in human oral cancer tissue (Roychoudhury et al., 2007). The reported data provided preliminary evidence of hnRNP-E2's involvement in neuronal apoptosis, which was investigated by Mao et al. (2016) in cases of acute spinal cord injury (SCI). Following SCI, both hnRNP-E2 and caspase-3 were upregulated in the neurons (Mao et al., 2016). The knockdown of hnRNP-E2 decreased the expression of caspase-3 in the primary neurons. However, the levels of cyclin D1 did not change after the hnRNP-E2 knockdown, which suggested that hnRNP-E2-induced neuronal apoptosis is independent of cell cycle activation (Mao et al., 2016). The detailed mechanism of hnRNP-E2 in modulating caspase-3 activity and apoptosis has not yet been clarified. It is possible that this mechanism may mediate TDP-43 aggregation; however, this does not appear to be true in all cases of FTLD-TDP. Hence, the implications of hnRNP-E2 in TDP-43 pathology and FTLD/ALS require further investigation.

Another possible link could be established through microRNAs (miRNA). miRNAs are small non-coding RNAs that possess gene expression regulatory functions. Nuclear and cytoplasmic TDP-43 were identified as modulators of miRNAs maturation and it was found that they promote neuronal outgrowth by facilitating miRNAs production (Kawahara and Mieda-Sato, 2012). Interestingly, hnRNP-E2 expression was found to be regulated by miRNA-214; however, the regulatory pathway still needs to be determined (Tang et al., 2015). The stress response is another possible explanation for the colocalisation of hnRNP-E2 and TDP-43 in the FTLD-TDP brain, which will be discussed in the next chapter.

4.5 Conclusion

Striking hnRNP-E2 inclusions were detected in a subset of FTLD-TDP brain tissue using the IHC technique and the colocalisation with TDP-43 was then confirmed using dIF. The hnRNP-E2 inclusions were highly specific for FTLD-TDP cases that do not carry the *C9orf72* mutation. hnRNP-E2 pathology in FTLD-TDP cases is highly dependent on the TDP-43 pathological subtype, showing a significantly higher frequency in subtypes A and C. hnRNP-E2 colocalised with 84.5% of TDP-43 inclusions in FTLD-TDP brain tissue and with 67% of ubiquitin inclusions in the same cases. hnRNP-E2 was not detected in any of the other neurodegenerative diseases tested, which suggests that it could be closely related to the TDP-43 pathological mechanism. However, the fact that E2-positive inclusions were not detected

in any FTLD-TDP cases with the *C9orf72* mutation (despite the TDP-43 pathology seen in these cases) is intriguing and may suggest the occurrence of different disease mechanisms. hnRNP-E2 has several functions in the UPS and programmed cell death, which could directly or indirectly contribute to TDP-43 pathology. The results presented here emphasise the importance of further investigations into the role of hnRNP-E2 in TDP-43 proteinopathy, specifically in FTLD-TDP cases.

Chapter 5 Utilising Cell Biology to Investigate the Relationship Between hnRNP-E2 and TDP-43

5.1 Introduction

The human brain tissue results in this study provided strong evidence of a relationship between hnRNP-E2 and TDP-43 in a subset of FTLD-TDP cases without the *C9orf72* expansion. Indeed, we detected immunoreactive hnRNP-E2 inclusions in the frontal cortex, hippocampus and spinal cord in 53.3% of FTLD-TDP cases without the *C9orf72* expansion. Furthermore, in these cases, abundant hnRNP-E2 was detected in 84.5% of TDP-43 inclusions, as identified by double-labelling immunofluorescence. In addition, the hnRNP-E2 inclusions followed the morphological pattern of TDP-43 inclusions seen in different pathological types of FTLD-TDP. Moreover, there was a significant dependence between hnRNP-E2 pathology and the TDP-43 pathological subtypes. Increased hnRNP-E2 insolubility was detected in those cases according to the Western blotting results presented in Chapter 4. Therefore, it was important to further investigate the relationship and possible interactions between hnRNP-E2 and TDP-43 by utilising cell biology techniques in order to add to our understanding of the TDP-43 pathological mechanisms in FTLD and MND pathology.

Since the discovery of TDP-43 as the major component of the ubiquitin inclusions in FTLD and ALS (Neumann et al., 2006b), the identification of the pathological mechanisms triggered by its aggregation has been the focus of a major research effort. The abnormal TDP-43 aggregates form the basis of an extensive network of neurodegenerative diseases that are collectively referred to as TDP-43 proteinopathies (Geser et al., 2009). TDP-43 represents the master protein in this type of pathological mechanism; however, there are other RNA-binding proteins that could be mutated and/or aggregated in diseased brains, including FUS/TLS and other hnRNP proteins (Buratti and Baralle, 2012). Investigating the pathological mechanism of TDP-43 is complicated by its involvement in a massive number of RNA-processing events (Neumann et al., 2006a, Janssens and Van Broeckhoven, 2013). As TDP-43 is an RNA-binding protein that belongs to the hnRNP family, most of its functional properties are mediated by binding to specific RNA target sequences (Tollervey et al., 2011a, Buratti and Baralle, 2001). In addition, several proteomic studies have indicated that TDP-43's interaction with other hnRNP proteins is important for RNA maturation (Freibaum et al., 2010). These studies support the nuclear loss of function suggested to drive the role of TDP-43 in neurodegeneration (Dewey et al., 2012, Wang

et al., 2008)); however, other studies have suggested that cytoplasmic TDP-43 aggregation drives the neurodegeneration process through a toxic gain of function (Johnson et al., 2008, Winton et al., 2008). More evidence is emerging regarding the involvement of hnRNP proteins in TDP-43 pathology, specifically in FTLD and ALS. Recently, hnRNP-A3 was identified as a component of some of the p62-positive/TDP-43-negative hippocampal inclusions seen in a subset of FTLD/ALS cases with the *C9orf72* expansion. It was also shown to be component of the RNA foci and it has been suggested that it binds to the 4G2C repeats in *C9orf72* transcripts (Mori et al., 2013b); however, its pathogenic role still needs to be determined. In addition, the recent implication of hnRNP-A2/B1 and hnRNP-A1 in ALS and multisystem proteinopathy supports the hypothesis of a physical and functional interaction between TDP-43 and other hnRNPs (Romano et al., 2014, Calini et al., 2013, Kim et al., 2013). Therefore, the relative expression of a specific protein within the TDP-43 interaction network may have a significant impact on the function of TDP-43, either through direct interaction or independently by acting on the same cellular targets (Mohagheghi et al., 2016, Hanson et al., 2010, Buratti et al., 2013). Accordingly, an experiment was designed to knockdown and overexpress hnRNP-E2 and TDP-43 in HEK293T cells in order to investigate how changes in the level of one protein affect the levels of the its protein partner. The knockdown and overexpression experiments also aimed to determine whether hnRNP-E2 is upstream or downstream of TDP-43 pathology. In order to further confirm the interaction, co-immunoprecipitation was performed; however, the results were not conclusive due to technical issues. Several studies have suggested that TDP-43 is a stress responsive protein, although it remains unclear whether the TDP-43 aggregates arise from stress granules (SGs) (Wang et al., 2008, Liu-Yesucevitz et al., 2010, Colombrita et al., 2009). SGs are defined as transient cytoplasmic structures that are formed in response to cellular stress and they are believed to act as a sorting station for mRNAs (Dewey et al., 2012). TDP-43 was recruited into the SGs in the motor neuronal cell line NSC34 by oxidative assault using 0.5 mM of arsenite for 30 min. Exposure to low concentrations of oxidative stress for longer periods of time also resulted in the accumulation of TDP-43 in the SGs (Colombrita et al., 2009). It was further shown that osmotic stress can recruit TDP-43 into the SGs in HEK293T cells and primary cultured glia. The osmotic stress was applied by elevating the sugar levels using sorbitol, an intermediate in the polyol pathway, which is an ATP-independent metabolic route that generates fructose from glucose (Dewey et al., 2011). The same study reported that WT-TDP-43 takes a longer time to get into the SGs when compared to the mutant forms of TDP-43. In addition, WT-TDP-43 formed

more SGs over time than the mutant forms and those granules were relatively smaller and their sizes remained relatively unchanged over time (Dewey et al., 2011). The composition and morphology of SGs varies according to the cell and stress type. There are core components of SGs such as the T-cell intracellular antigen-1 (TIA-1) and the poly(A)-binding protein 1 (PABP1); however, the incorporation of other RNA-binding proteins differs according to the cell and stress type (Anderson and Kedersha, 2008). Despite the finding that TDP-43 colocalised with TIA-1 in NSC34 cells and with other SG markers in HEK293T cells, there was no colocalisation detected in the brains of MND patients (Colombrita et al., 2009). Another study reported the presence of TIA-1 and PABP1 in the RNA-positive basophilic inclusions seen in patients with adult-onset atypical MND (Fujita et al., 2008). Therefore, it is important to characterise the SGs' role in the pathology of neurodegeneration, specifically in relation to TDP-43 and its possible binding partners. Moreover, the SGs offer a relative model for investigating the toxic cytoplasmic gain of function hypothesis concerning TDP-43 pathology by investigating its incorrect accumulation within the cytoplasm inside the SGs (Dewey et al., 2011).

It was also reported that hnRNP-E2 is a novel component of SGs and P-bodies in HeLa cells following a yeast two-hybrid screen against TIA-1, while the interaction between hnRNP-E2 and TIA-1 was validated by double-labelling immunofluorescence (Fujimura et al., 2008). Both TDP-43 and hnRNP-E2 are reported to incorporate within SGs under stress conditions and there is evidence of their interactions with SG markers such as TIA-1 in different cell lines. As a result, an experiment was designed to investigate their interaction in SGs induced within HeLa cells. The HeLa cells were exposed to either oxidative or osmotic stress, or a combination of both conditions, and ICC was applied to detect both TDP-43 and hnRNP-E2 incorporation within the SGs. In addition, the interaction of both TDP-43 and hnRNP-E2 with the SG marker PABP1 was investigated under the same stress conditions.

5.2 Methods

In order to explore any potential physical interactions between the two proteins, hnRNP-E2 was overexpressed or knocked down and the resulting changes in the TDP-43 expression levels were examined. The same experiment was conducted to examine the impact of TDP-43 overexpression or knockdown on the hnRNP-E2 levels. Both TDP-43 and hnRNP-E2 were overexpressed and the cells stressed in order to encourage SGs to form and allow the examination of colocalisation between TDP-43 and hnRNP-E2 in the SGs.

5.2.1 Plasmid cloning

The HEK293T cells were plated at 50,000 cells/well in 500 µl of media in a 24-well plate and then incubated overnight at 37ºC. For the hnRNP-E2 overexpression, the cells were transfected with an N-terminal FLAG-tagged hnRNP-E2 plasmid. The FLAG-tagged non-transgenic hnRNP-E2 (FLAG-NT-hnRNP-E2) plasmid was generated in house by Dr Emma Scotter. Briefly, the hnRNP-E2 (transcript 1, isoform A) was amplified from normal human cDNA using primers containing AttB sites, with the forward primer also encoding a FLAG-tag.

Forward: 5'-GGGGACAAGTTTGTACAAAAAAGCAGGCTTGGCCACCATGGACTATAAAGATGATGATGATAAAATGGACACCGGTGTGATT-3'

Reverse: 5'-GGGGACCACTTTGTACAAGAAAGCTGGGTCTAGCTGCTCCCCATGCCACC-3'

The resulting amplicon was gel purified using the "freeze and squeeze" method (Tautz and Renz, 1983). It was cloned into Gateway® pDONR221 and then the Gateway® pT-Rex™-DEST30 plasmid vector using one tube format Gateway® cloning according to the manufacturer's directions (Thermo Fisher Scientific). DNA was prepared from the resulting bacterial clones using a NucleoSpin® plasmid miniprep kit (Macherey Nagel, Düren, Germany) and it was sequenced in-house using BigDye® Terminator v1.1 on an ABI3130 genetic analyser (Applied Biosystems Pty Ltd, Warrington, UK) (Heiner CR, 1998).

HA-TDP43-WT was used for all the experiments, except for the immunoprecipitation experiment in which GFP-TDP43-WT was used. The N-terminal EGFP-tagged TDP-43 wild type (WT) cDNA was previously cloned into the 4.7 kb pEGFP-C1 vector (ClonTech Laboratories Inc.) with *Bam*HI and *Xho*I by Dr Agnes Nishimura (Nishimura et al., 2010). The HA-tagged TDP-43 WT (HA-TDP43-WT) cDNA

was previously cloned by Dr Hazel Urwin into the 4.7 kb Gateway® pDONRTM221 vector (Thermo Fisher Scientific). The cells were also transfected with the pDEST30 vector and the GFP vector as a control for each experiment.

The DNA was transfected into the HEK293T cells using FuGENE® (Promega) according to the manufacturer's directions. Briefly, 125 ng of DNA was mixed with the OptiMEM medium and FuGENE® using a DNA to FuGENE® ratio of 1 µg:3 µL. The transfection mixtures were then left at room temperature for 15 minutes in order to form liposome complexes before being added to the cells. Antibiotic-free media we added to the cells prior to transfection, followed by the introduction of transfection mixtures and incubation for 6 hours at 37°C in 5% CO_2. The media were then replaced with new antibiotic-free media and the plates were returned to the incubator. The cells were harvested or fixed after 48–72 hours of transfection.

5.2.2 hnRNP-E2 and TDP-43 knockdown

For the knockdown experiments, the HeLa cells were transfected with specific small interfering RNA (siRNA) using the Lipofectamine™ 2000 (Thermo Fisher Scientific) transfection protocol according to the manufacturer's instructions. The cells were transfected with non-human targeted sequence (scrambled sequence [Scr]) or siRNAs targeting hnRNP-E2 or *TARDBP*. The hnRNP-E2-specific siRNA (sihnRNP-E2) was a 27-mer purchased from Eurogentec (Hampshire, UK) and previously validated to selectively knockdown hnRNP-E2 but not hnRNP-E1 (Woolaway et al., 2007). The siRNA sequences were as follows:

Scrambled sequence: 5'-CUUCCUCUCUUUCUCUCCCUUGGA-3'.

sihnRNPE2 sequence: 5'-AGACUGUUGCAUUGCCAACUGGUGCAG-3'.

Human siRNAs targeting endogenous TDP-43 were obtained from Thermo Fisher Scientific (Carlsbad, USA. HSS118767) and will be referred to here as siTDP-43 (Invitrogen Stealth). The scrambled non-targeting sequence for TDP-43 was also obtained from the same supplier (scrTDP; Invitrogen Stealth, low GC content) (Nishimura et al., 2014).

si TARDBP sequence: 5'-GAAAGATCTTAAGACTGGTCATTCA-3'.

Different concentrations of siRNAs (30 nM, 50 nM and 100 nM) were added to the cells in order to determine a dose response curve. As described above, the liposome complexes were formed by combining the siRNAs, Lipofectamine™ 2000 and OptiMEM media as directed by the manufacturer's

protocol. The transfection mixture was then left at room temperature for 20 minutes to allow the formation of DNA-Lipofectamine™ 2000 complexes before being added to the cells.

After 6 hrs, the media on the cells were replaced with fresh antibiotic-free media. After 48 hrs of transfection, the cells were harvested into a harvesting buffer. The sample quantification, Western blotting and analysis were performed as described earlier in this chapter (section 5.2.2) and in Chapter 2.

5.2.3 Protein quantification and statistical analysis of cell samples

For the protein quantification, the cells were harvested in 1x SDS loading buffer with PIs and PhoSTOP. The protein concentrations were quantified from the cellular lysates using the Bio-Rad DC Protein Assay (Bio-Rad, Hemel Hempstead, UK). Approximately 5 µg of total protein was prepared for each sample and then loaded onto PAGE Western blot in order to separate the different sized proteins in the samples as described in Chapter 2.

The relative quantitative analysis of the Western blot bands was performed by measuring the density of the bands using ImageJ 1.47v software. The quantification values were expressed as a ratio of the desired band density to the loading control band in each sample. The protein loading control in this experiment was glyceraldehyde-3-phosphate dehydrogenase (GAPDH), which is a housekeeping gene whose expression remains constant in the cells and tissues under investigation. GAPDH is a 36 kDa protein and it plays many roles in cellular function, including transcription regulation and apoptosis. It is integral for glycolysis and it exhibits stable and ubiquitous expression (Barber et al., 2005). It is important to use a loading control, not only for the protein quantification, but also to determine equal sample loading across all the wells and provide confirmation of the effective transfer of protein during Western blotting. The blots were probed with rabbit GAPDH (rGAPDH) after they were scanned for rTDP-43 and mhnRNP-E2 because the size of GAPDH is very similar to that of hnRNP-E2.

In order to measure the band density using ImageJ 1.47v, a rectangular shape should be drawn around the band. The shape, size and location of the first selection serves as a guide for the rest of the lanes on the gel. The density of the bands was plotted as curves. The peak of each band was detected by a straight line connecting the start and the end of the curve's peak. The area underneath each curve was measured using the wand tracing tool in the ImageJ software and then presented as a number. Figure 8 provides an example of band density quantification using ImageJ 1.47v.

Each band value was normalised to its loading control band in the same sample and the averages for each sample were determined from three or four independent experiment repeats.

The difference in the TDP-43 and hnRNP-E2 endogenous levels among the groups was determined using a one-way ANOVA followed by a Bonferroni post-hoc t-test with a significance level of $p < 0.05$. The t-test was a two-tailed t-test assuming equal variance between the groups. The mean is presented as (Mean ± SE), with SE representing the standard error of the samples.

5.2.4 Immunocytochemistry

To visualise the physical presence of TDP-43 and hnRNP-E2 in the SGs, the immunocytochemistry technique was utilised under basal and stressed conditions. Coverslips were added to a 24-well plate and coated with poly-D-lysine (50 µg/ml) for 1 hr in the incubator. The coverslips were rinsed twice with PBS before the cells were plated. The HeLa cells were plated on coverslips at 50,000 cells/well and then left in the incubator to recover for 24 hrs. The cells were transfected with the same FLAG-NT-hnRNP-E2 and HA-TDP43-WT plasmids as described in the overexpression section of this chapter. Some 48 hrs post-transfection, the cells were treated with different stress conditions to encourage the formation of SGs. Different combinations of sodium arsenite (0.5 mM) and/or sorbitol (600 mM) were diluted in fresh DMEM media as illustrated in Figure 38. The cells were incubated with stressors for 30 min before the sorbitol media were removed from the wells, where both sorbitol and arsenite stress was to be applied, and the arsenite media were added to them. Arsenite media were also added to the wells wherein the cells were exposed to only arsenite stress. The cells were then returned to the incubator for another 30 minutes. The cells were fixed by adding 4% PFA (paraformaldehyde) for 10 minutes and then replacing it with PBS. Immunocytochemistry was performed immediately or else the plates were left at 4°C for later use.

All the primary antibodies were diluted 1:500 in immunobuffer as detailed in Chapter 2. Immunocytochemistry was performed as follows. The cells transfected with only HA-TDP43-WT were stained with mouse TDP-43 (Santa Cruz sc-10087) and rabbit PABP1 (Abcam ab69110). The cells that were transfected with Flag-hnRNP-E2 were stained with mouse hnRNP-E2 (Abnova) and rabbit PABP1 (Abcam). The cells that were co-transfected with both HA-TDP-43-wt and Flag-hnRNP-E2-wt were stained with polyclonal TDP-43 (Proteintech) and monoclonal hnRNP-E2. The primary antibodies were added to the coverslips as detailed above for each specific well and then incubated on a plate rocker

overnight at 4ºC. Figure 38 illustrates the stress experiment plan and the antibodies used for each condition in the 24-well plate.

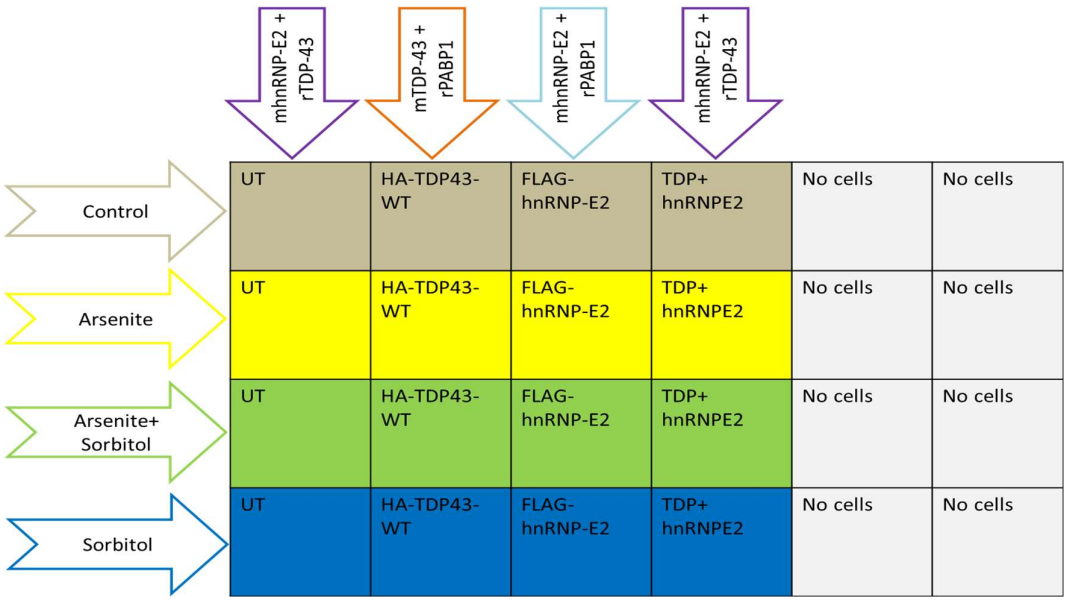

Figure 38: A 24-well plate with HeLa cells plated on glass coverslips and transfected with either HA-TDP-43-WT, Flag-hnRNP-E2- or a combination of the two. The top arrows demonstrate the antibody combination for each well in the column. The arrows on the left represent the stress condition applied to each row.

Next, the primary antibodies were removed and the coverslips were washed three times with PBS. The secondary fluorescent antibodies used were donkey anti-mouse 488 and donkey anti-rabbit 549 (Thermo Fisher Scientific). These antibodies were diluted in immunobuffer at 1:500 then added to the cells and incubated for 3 hr on a plate rocker at room temperature in the dark. Then, the secondary antibodies were removed and the coverslips were washed with 500 µl per well PBS. DAPI (Sigma) (1.25 ug/ml) was added to the coverslips for 30 seconds before removal and the coverslips were washed with PBS. The coverslips were mounted using mounting media (Dako Fluorescent Mounting Media) on microscopic slides and left to dry prior to visualisation using the Leica confocal SP system for high-resolution imaging. The images were processed and merged using ImageJ 1.47v software.

5.3 Results

5.3.1 Quantification of hnRNP-E2 and TDP-43 levels after gene overexpression and knockdown

In order to explore the mechanistic connection between TDP-43 and hnRNP-E2 as well as the possible role of this interaction in TDP-43 pathogenesis, we used cell biology techniques. Both TDP-43 and hnRNP-E2 were overexpressed or knocked down in HEK293T cells. The cell lysate was collected after successful transfection and the proteins were quantified in each sample. Western blotting was performed to detect both TDP-43 and hnRNP-E2 in the samples. The Western blots were analysed as described in the method section of this chapter and the quantification values were expressed as a ratio of the integral of band density in a sample to the loading control band in the same sample. The results were statistically analysed in order to assess the difference in TDP-43 or hnRNP-E2 levels among the control group and the experimental groups.

5.3.2 Statistical analysis of TDP-43 and hnRNP-E2 overexpression results

5.3.2.1 Changes in endogenous hnRNP-E2 levels according to TDP-43 overexpression

First, the endogenous levels of hnRNP-E2 were measured in three different sample groups from four repeated experiments. The untransfected cells and the PDest30-transfected cells both represent sample controls. The experimental group in this analysis was the HA-TDP43-WT-transfected cell group. A one-way ANOVA test was performed to compare the effect of HA-TDP43-WT overexpression on the endogenous level of hnRNP-E2 when compared to the two control groups.

The ANOVA showed that the WT-HA-TDP43 overexpressed cell samples (0.61 ± 0.15 $n = 4$) had significantly decreased levels of endogenous hnRNP-E2 when compared to the untransfected sample (1.72 ± 0.14 $n = 4$) and the PDest30 vector only sample (0.14 ± 0.12 $n = 4$) (one-way ANOVA, $F = 26.1$, d.f. = 2 and 9, $p = 0.0001$; Bonferroni post-hoc test). The Bonferroni post-hoc t-test revealed that there was a significant difference between the HA-TDP43-WT expressed cell samples and the untransfected cell samples ($p = 0.001$). It also revealed that there was a significant reduction in the hnRNP-E2 levels in the PDest30 samples when compared to the untransfected samples ($p = 0.0003$). Yet, there was no significant difference in the endogenous hnRNP-E2 levels between the HA-TDP43-WT and PDest30 expressed samples ($p > 0.05$) (Figure 39). Thus, TDP-43 overexpression did not affect the endogenous hnRNP-E2 levels.

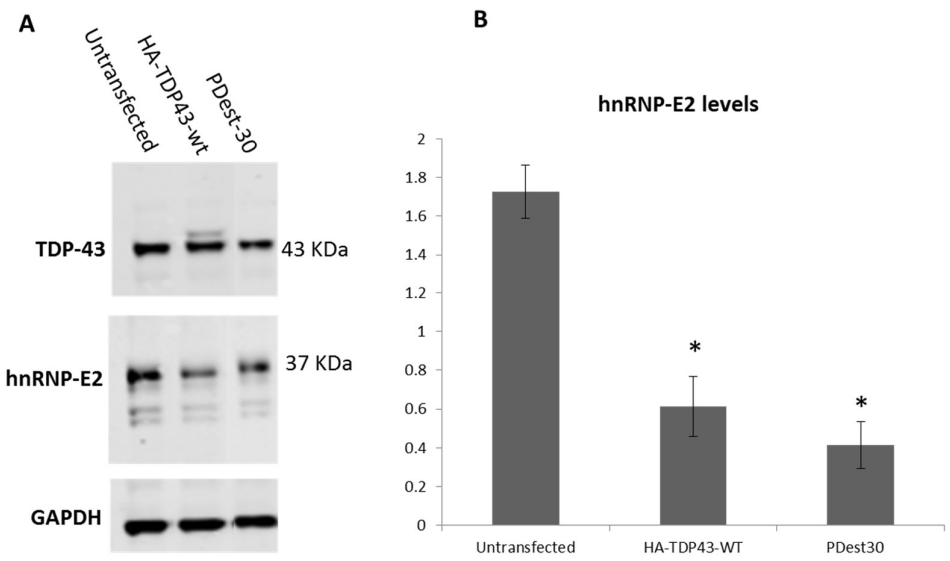

Figure 39: A) Representative Western blot of the HEK239T cell samples showing the levels of endogenous hnRNP-E2 in untransfected control cells, HA-TDP-43-WT-transfected cells and PDest30-transfected cells. B) The graph shows the statistical analysis performed using a one-way ANOVA among the three groups: HA-TDP43-WT (0.61 ± 0.15 n = 4), untransfected (1.72 ± 0.14 n = 4) and PDest30 (0.14 ± 0.12 n = 4), which revealed a significant difference in the hnRNP-E2 endogenous levels ($F = 26.1$, d.f. = 2 and 9, $p = 0.00018$). The Bonferroni post-hoc test revealed a significant difference in the hnRNP-E2 levels between the HA-TDP43-WT and untransfected samples ($p = 0.001$) and a significant difference in the hnRNP-E2 levels in the PDest30 samples when compared to the untransfected sample ($p = 0.0003$). However, there was no significant difference in the hnRNP-E2 levels between the PDest30- and HA-TDP43-WT-transfected cells ($p > 0.05$).

5.3.2.2 Changes in endogenous TDP-43 levels according to hnRNP-E2 overexpression

Second, the endogenous TDP-43 levels were measured in three different sample groups from four repeated experiments. The untransfected cells and the PDest30-transfected cells both represent sample control groups. The experimental group in this analysis was the Flag-hnRNP-E2-transfected cells. A one-way ANOVA was performed to compare the effect of Flag-hnRNP-E2 overexpression on the endogenous TDP-43 levels when compared to the two control groups.

The ANOVA showed that the cells with Flag-hnRNP-E2 overexpressed (0.27 ± 0.11 n = 4) had a significantly decreased level of endogenous TDP-43 when compared to the untransfected cells (0.96 ± 0.13 n = 4) and the pDEST30 vector only transfected cells (0.28 ± 0.14 n = 4) (one-way ANOVA, F = 9.88, d.f. = 2 and 9, p = 0.005; Bonferroni post-hoc test). The Bonferroni post-hoc t-test revealed that there was significant difference in the endogenous TDP-43 levels between the Flag-hnRNP-E2-expressed cell samples and the untransfected cell samples (p = 0.006). It also revealed that there was a significant reduction in the hnRNP-E2 levels in the pDEST30 samples when compared to the untransfected samples (p = 0.011), although there was no significant difference in the endogenous TDP-43 levels between the Flag-hnRNP-E2-transfected and PDest30 samples (p > 0.05) (Figure 40). Thus, hnRNP-E2 overexpression did not affect the endogenous TDP-43 levels.

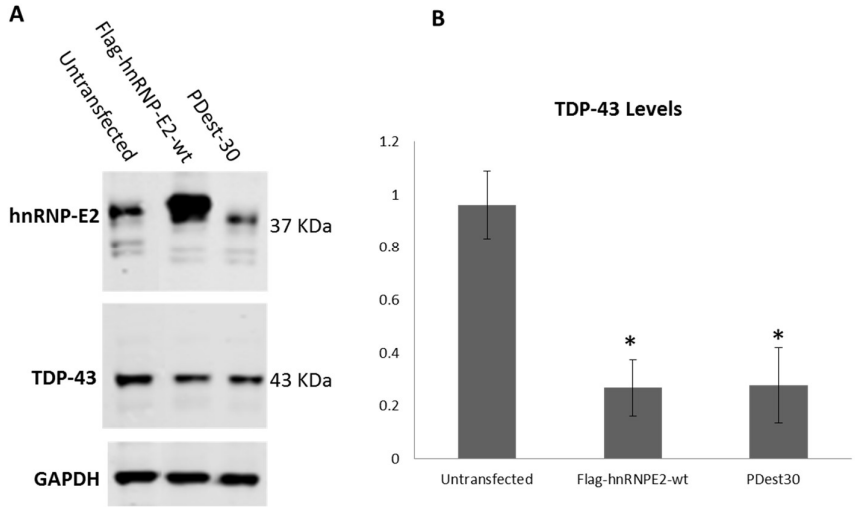

Figure 40: A) Representative Western blot of the HEK239T cell samples showing the levels of endogenous TDP-43 in untransfected control cells, Flag-hnRNP-E2-transfected cells and PDest30-transfected cells. B) The graph shows the statistical analysis performed using a one-way ANOVA among the three groups: Flag-hnRNP-E2 (0.27 ± 0.11 n = 4), untransfected (0.96 ± 0.13 n = 4) and PDest30 (0.28 ± 0.14 n = 4), which revealed a significant difference in the endogenous TDP-43 levels (F = 9.88, d.f. = 2 and 9, p = 0.005). The Bonferroni post-hoc test revealed a significant difference in the TDP-43 levels between the Flag-hnRNP-E2 and untransfected samples (p = 0.006) and a significant difference in the TDP-43 levels in the PDest30 samples when compared to the untransfected sample (p = 0.011). However, there was no significant difference in the hnRNP-E2 levels between the PDest30 and Flag-hnRNP-E2 overexpressed cells (p > 0.05).

5.3.3 Statistical analysis of TDP-43 and hnRNP-E2 knockdown results

5.3.3.1 hnRNP-E2 and TDP-43 knockdown

The HEK239T cells were treated with different concentrations (30 nM, 50 nM and 100 nM) of both SiRNA for TDP-43 and hnRNP-E2 as detailed in the methods section of this chapter. The cells were also transfected with scrambled sequences as a control for the knockdown of both TDP-43 and hnRNP-E2. The TDP-43 and hnRNP-E2 levels were measured using Western blotting. The blots were analysed using ImageJ software as described earlier. A one-way ANOVA test was performed, followed by a Bonferroni post-hoc two-tailed t-test to examine whether there was any significant difference in the TDP-43 and hnRNP-E2 levels.

The hnRNP-E2 knockdown resulted in a significant reduction in the TDP-43 levels when analysed using a one-way ANOVA among all the samples with different sihnRNP-E2 knockdown concentrations (one-way ANOVA, $F = 3.89$, d.f. = 4 and 10, $p = 0.037$; Bonferroni post-hoc test) (Figure 41). The Bonferroni post-hoc t-test revealed that there was significant difference in the endogenous TDP-43 levels between the untransfected cell samples (1.078 ± 0.074) and si hnRNP-E2 at 100 nM (0.56 ± 0.079) ($p = 0.009$); however, there was no significant difference detected between the other sample groups ($p > 0.05$) (Figure 41). The TDP-43 knockdown did not result in any significant changes in hnRNP-E2 (one-way ANOVA, $F = 0.51$, d.f. = 4 and 10, $p = 0.72$). The Bonferroni post-hoc two-tailed t-test also revealed no significant changes in hnRNP-E2 between all the sample groups ($p > 0.05$) (Figure 41). Thus, although these two proteins are known to interact and colocalise in a subset of FTLD cases, there is no evidence related to either the overexpression or knockdown to show that the levels of either protein are regulated by the levels of the other.

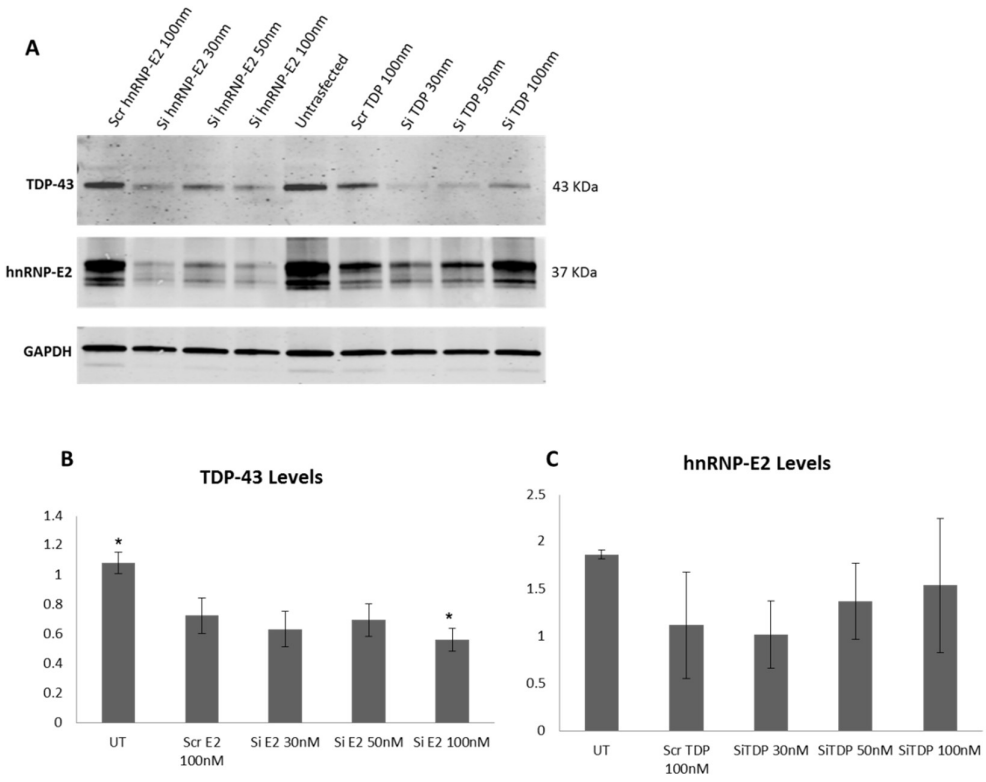

Figure 41: A) Representative Western blot of the HEK239T cell samples showing the levels of endogenous TDP-43 and hnRNP-E2 in untransfected (UT) control cells, gradual concentrations of si hnRNP-E2 (siE2) and si TDP-43 (SiTDP), and scrambled control samples for both hnRNP-E2 (Scr E2) and TDP-43 (Scr TDP). GAPDH was the loading control used in this experiment. B) The graph shows the statistical analysis performed using a one-way ANOVA among the sample groups to measure the endogenous TDP-43 levels in all sample groups UT (1.078 ± 0.074, n = 3), Scr E2 100 nM (0.722 ± 0.12, n = 3), SiE2 30 nM (0.63 ± 0.12, n = 3), SiE2 50 nM (0.69 ± 0.10 n = 3) and SiE2 100 nM (0.56 ± 0.08, n = 3). The endogenous TDP-43 levels were significantly decreased, as shown by the ANOVA test (one-way ANOVA, F = 3.89, d.f. = 4 and 10, p = 0.037; Bonferroni post-hoc test). The Bonferroni post-hoc two-tailed t-test revealed a significant difference in the endogenous TDP-43 levels (F = 9.88, d.f. = 2 and 9, p = 0.005). The Bonferroni post-hoc t-test also revealed a significant difference in the endogenous TDP-43 levels between the UT cells samples (1.078 ± 0.074) and SiE2 100 nM (0.56 ± 0.079) (p = 0.009); however, there was no significant difference in the TDP-43 levels between the other groups of SiE2, UT or Scr E2 (p > 0.05). C) The graph shows the statistical analysis performed using a one-way ANOVA among the sample groups in order to measure the endogenous hnRNP-E2 levels in all the sample groups: UT (1.86 ± 0.05 n = 3), Scr TDP 100 nM (1.11 ± 0.56, n = 3), SiTDP 30 nM (1.01 ± 0.35, n = 3), SiTDP 50 nM (1.36 ± 0.40, n = 3) and SiTDP 100 nM (1.53 ± 0.72, n = 3). There were no significant changes in the level of TDP-43 (one-way ANOVA, F = 0.51, d.f. = 4 and 10, p = 0.72) and the Bonferroni post-hoc test was also insignificant (p > 0.05).

5.3.4 Immunoprecipitation

In order to identify whether hnRNP-E2 directly interacts with TDP-43 as well as to determine whether they bind to each other to form a protein complex, co-IP experiments were performed. The HEK293T cells were co-transfected with GFP-TDP and Flag-hnRNP-E2 as described in the methods section. When the TDP-43 was immunoprecipitated using the Abcam rabbit GFP antibodies, there was no band detected for hnRNP-E2 using the Flag antibodies, which indicated that there was no interaction between TDP-43 and hnRNP-E2 (Figure 42A). A reverse experiment was also performed by immunoprecipitating

hnRNP-E2 using the Flag antibody and then immunoblotting with the rabbit TDP-43 antibody and mouse hnRNP-E2 antibody. Figure 42B shows a band of GFP-TDP-43, indicating the possible interaction between hnRNP-E2 and TDP-43 (Figure 42B). A further control experiment was performed to confirm that TDP-43 interacts with hnRNP-E2 rather than just the beads. The control experiment consisted of immunoprecipitating the just beads without any primary antibodies. The results showed a weak band for GFP-TDP, suggesting that either TDP-43 is binding to the beads or a contaminant protein was transferred into this fraction (Figure 42C). Therefore, the TDP-43 band seen with the hnRNP-E2 IP was not considered to be a true positive result and hence we found no evidence of protein-protein binding between hnRNP-E2 and TDP-43. Protein A Dynabeads were also tested (results not presented), which revealed the same false positive results.

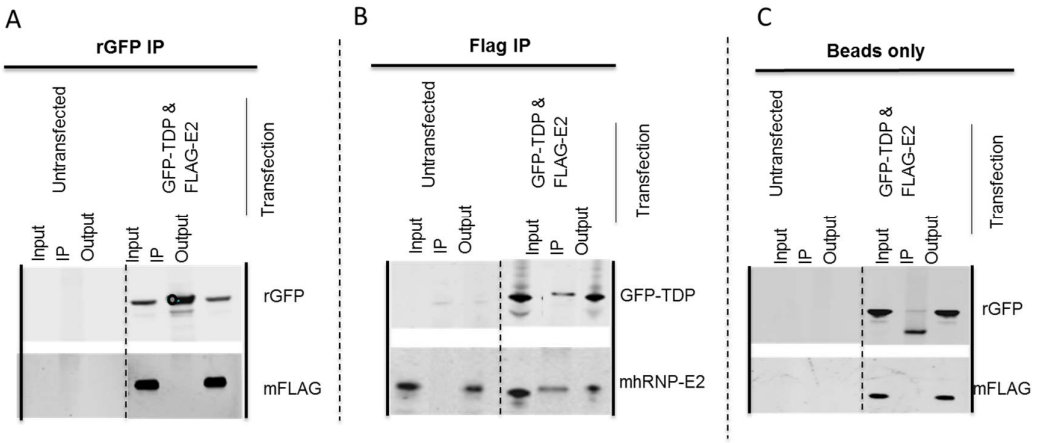

Figure 42: A) immunoprecipitation of GFP-TDP in untransfected and co-transfected cells using rabbit GFP antibodies. There was no band detected with the Flag antibodies for hnRNP-E2. (B) Immunoprecipitation of hnRNP-E2 using the rabbit Flag antibodies. The band for GFP-TDP was detected in the IP fraction; however, this was not considered to be a positive result. (C) Immunoprecipitation of beads only and labelled with rGFP and mFlag antibodies showing the GFP band in the IP fraction, which means that GFP-TDP sticks to the beads alone without antibodies.

5.3.5 Stress granules and immunocytochemistry

5.3.5.1 Both TDP43 and hnRNP-E2 colocalise with the SG marker PABP1

The HeLa cells were transfected with WT-HA-TDP43 as described in the methods section before stress was applied to the cells as previously described. Immunocytochemistry was carried out using the SG marker PABP1 and the rabbit TDP-43 antibodies. Figure 43A–C show untreated transfected cells without any SG formation, with the strong nuclear presence of TDP-43 and the absence of PABP1 from the nucleus. The transfected cells show strong nuclear TDP-43 staining and cytoplasmic PABP1 staining. The transfection rate with the WT-HA-TDP-43 was very low. In each coverslip, only 2–5 cells were transfected with WT-HA-TDP-43. When the cells were treated with 0.5 mM of sodium arsenite, small SGs were formed and the depletion of nuclear TDP-43 from the nucleus to the SGs was observed (Figure 43D, E and F). Treatment with sorbitol did not result in the formation of SGs (Figure 43G, H and I). The images obtained by confocal microscopy show large SG formation following exposure to both sorbitol and arsenite stress as well as clearly showing TDP-43 colocalised with the SG marker PABP1 (Figure 43J, K and L).

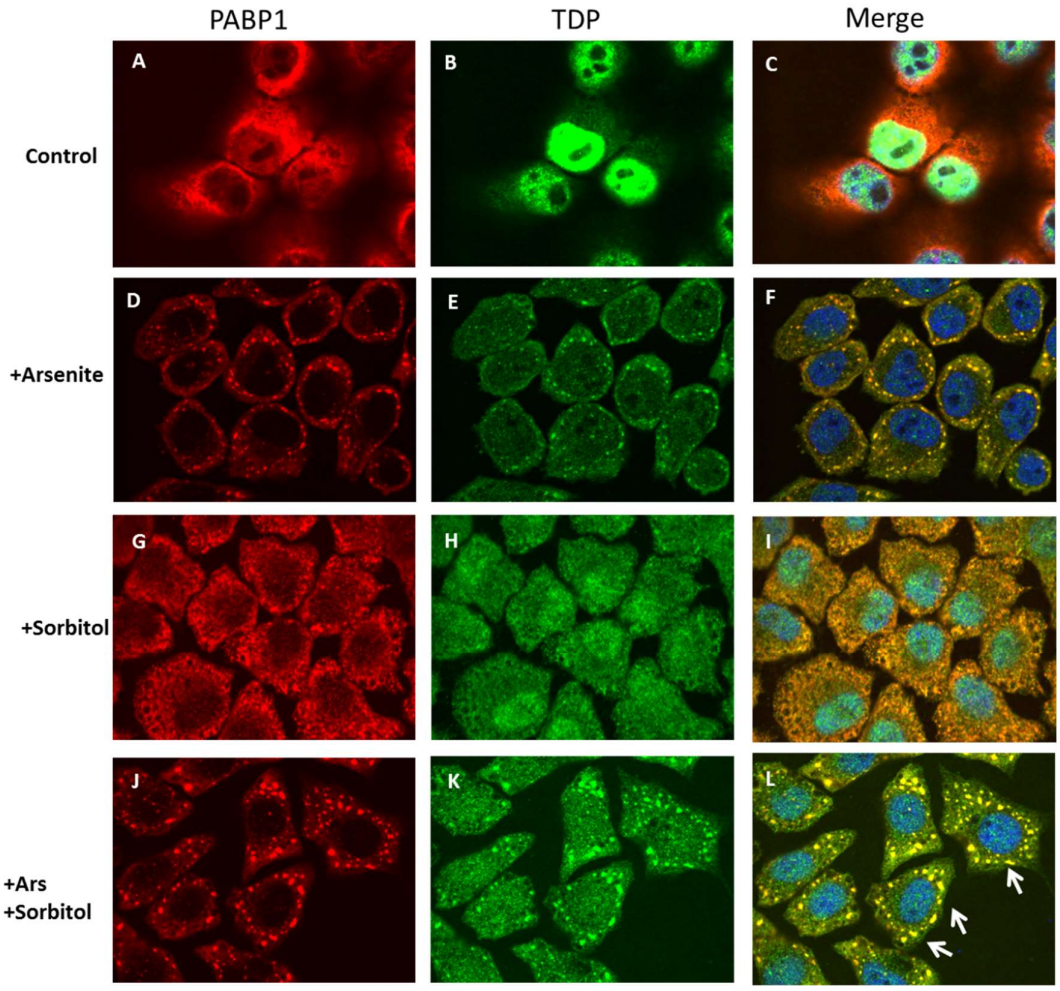

Figure 43: HA-TDP transfected HeLa cells untreated with any stress condition showing strong nuclear staining of TDP-43 (green) and normal cytoplasmic distribution of PABP1 (red) (A, B and C). The HA-TDP-transfected cells treated with 0.5 mM of sodium arsenite showing small SG formation and the recruitment of both PABP1 and TDP-43 into the SGs (D, E and F). HA-TDP-43-transfected cells treated for 60 minutes with 600 mM of sorbitol showed no SG formation and both PABP1 and TDP-43 were still within their normal cellular distribution (G, H and I). HA-TDP-43-transfected cells treated for both 60 minutes with 600 mM of sorbitol and 0.5 mM of sodium arsenite for 30 minutes (J, K and L). Immunocytochemistry for PABP1 (red) and TDP-43 (green) shows large SG formation in the cytoplasm of the cells and the colocalisation of both TDP43 and PABP1 within the SGs. The merged images include DAPI.

The HeLa cells were transfected with Flag-hnRNP-E2 before stress was applied as described previously. Figure 44 shows the hnRNP-E2-transfected cells without any stress, showing the cytoplasmic and nuclear distribution of hnRNP-E2 and the absence of PABP1 from the nuclei (Figure 44A, B and C). The transfection rate with Flag-hnRNP-E2 was higher than that seen with WT-HA-TDP-43. The application of arsenite stress for 30 minutes resulted in small SG formation and the accumulation of both PABP1 and hnRNP-E2 in the SGs (Figure 44D, E and F). Treatment with sorbitol alone for 1 hour did not result in SG formation; however, there was nuclear clearance of hnRNP-E2 (Figure 44G, H and I). The images obtained by confocal microscopy show large SG formation following exposure to both arsenite and sorbitol stress as well as clearly showing that hnRNP-E2 colocalised with the SG marker PABP1 (Figure 44J, K and L).

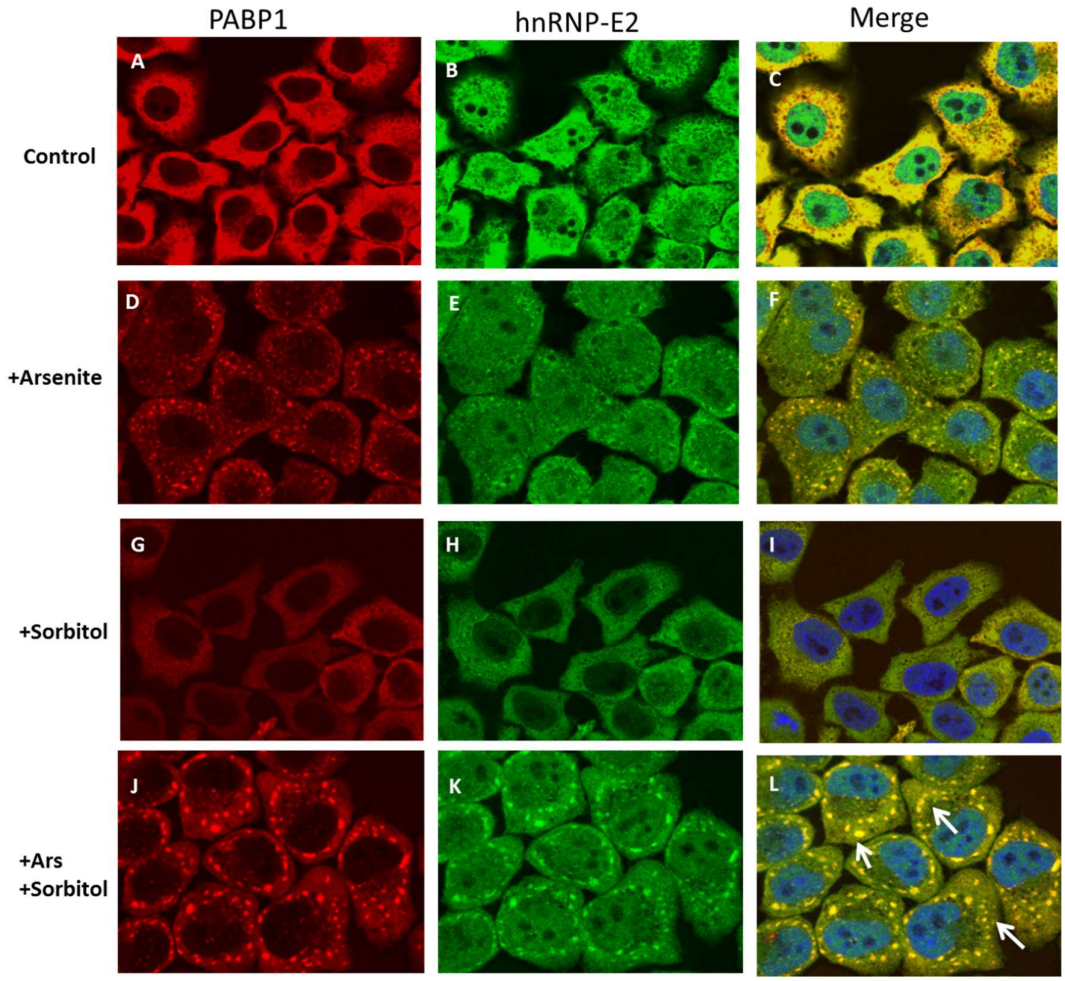

Figure 44: Flag-hnRNP-E2-transfected HeLa cells untreated with any stress condition showing strong nuclear staining of hnRNP-E2 (green) and normal cytoplasmic distribution of PABP1 (red) (A, B and C). The Flag-hnRNP-E2-transfected cells treated with 0.5 mM of sodium arsenite showing small SG formation and the recruitment of both PABP1 and hnRNP-E2 into the SGs (D, E and F). Flag-hnRNP-E2-transfected cells treated for 60 minutes with 600 mM of sorbitol showed no SG formation; however, hnRNP-E2 was cleared from the nucleus to the cytoplasm (G, H and I). Flag-hnRNP-E2-transfected cells treated for 60 minutes with 600 mM of sorbitol and 0.5 mM of sodium arsenite for 30 minutes (J, K and L). Immunocytochemistry for PABP1 and hnRNP-E2 shows large SG formation in the cytoplasm of the cells and the colocalisation of both hnRNP-E2 and PABP1 within the SGs. All merged images include DAPI.

5.3.5.2 Colocalisation of endogenous TDP-43 and hnRNP-E2 in SG

The untransfected HeLa cells were treated with different stress conditions in order to stimulate the formation of SGs as described in the methods section. Immunocytochemistry was performed to detect the endogenous TDP-43 and hnRNP-E2 proteins in the control and stress conditions. As expected, in the non-treated cells there was no formation of SGs, while TDP-43 and hnRNP-E2 were normally distributed in the cells (Figure 45A, B and C). The treatment of the cells with 0.5 of mM arsenite for 30 minutes resulted in the discrete formation of SGs, in which both TDP-43 and hnRNP-E2 were colocalised (Figure 45D, E and F). To determine whether osmotic stress interferes in the formation of SGs, the cells were treated with 600 mM of sorbitol for one hour and no formation of SGs was observed. However, the osmotic stress resulted in an increase in the cytoplasmic TDP-43 and hnRNP-E2 (Figure 45G, H and I). To increase the number of SGs, the cells were treated with sorbitol for one hour (to release TDP-43 and hnRNP-E2 into the cytoplasm) and, subsequently, the cells were treated with sodium arsenite (to recruit TDP-43 and hnRNP-E2 into the SGs). Virtually all the cytoplasmic TDP-43 and hnRNP-E2 was recruited into large SGs. Massive SGs were detected when the cells were treated with sorbitol followed by sodium arsenite. Clearly, both TDP-43 and hnRNP-E2 were recruited into the SGs and they both colocalised within them (Figure 45J, K and L).

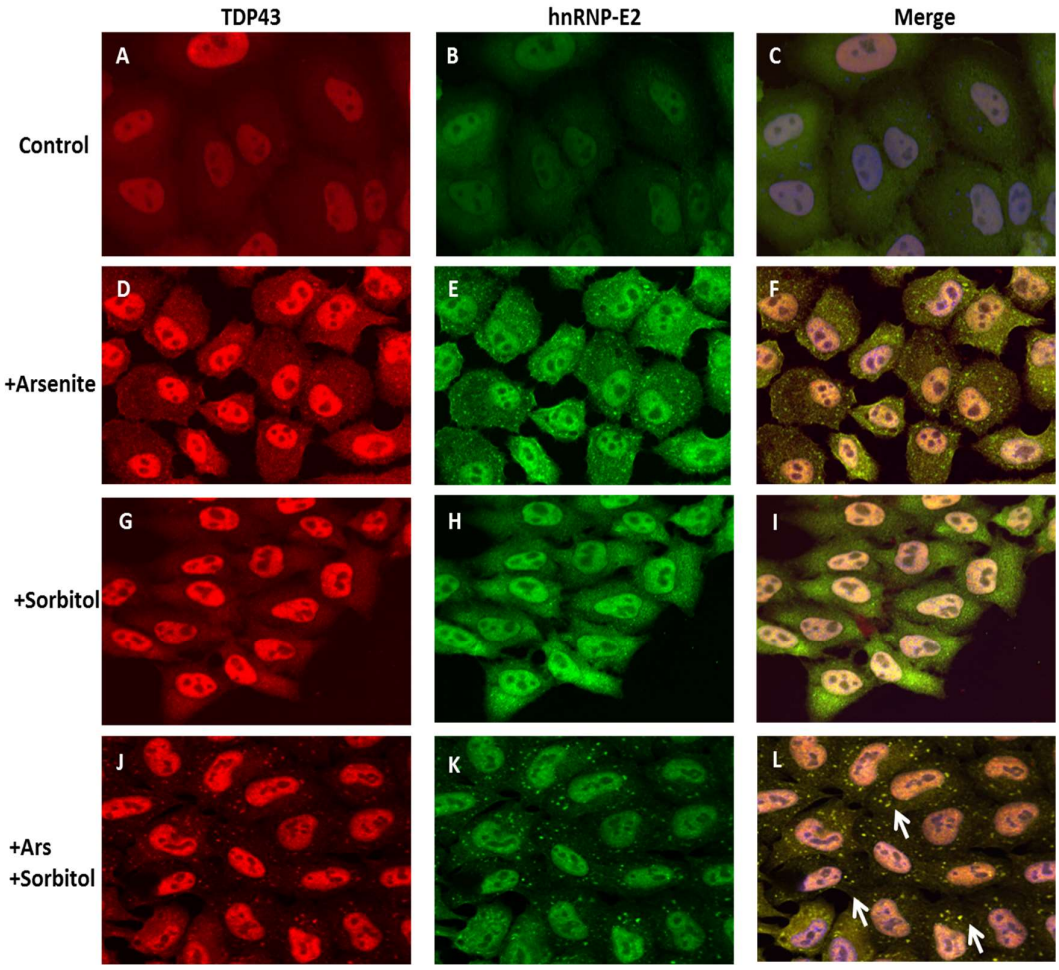

Figure 45: Untransfected HeLa cells were plated and left untreated. Immunocytochemistry with TDP43 and hnRNP-E2 shows the normal nuclear and cytoplasmic distribution of both TDP43 and hnRNP-E2 (A, B and C). Untransfected HeLa cells were treated for 30 minutes with 0.5 mM of sodium arsenite. Immunocytochemistry for TDP-43 (red) and hnRNP-E2 (green) showed SG formation and the colocalisation of both TDP43 and hnRNP-E2 within the SGs(D, E and F). When untransfected HeLa cells were treated with 600 mM of sorbitol for 60 minutes, the ICC showed no SG formation; however, the cell cytoplasm shows the formation of vacuoles due to the osmotic stress (G, H and I). Untransfected HeLa cells that were treated with both 600 mM of sorbitol for 60 minutes and 0.5 mM of sodium arsenite for 30 minutes showed very clear SG formation and both TDP-43 and hnRNP-E2 showed colocalisation within the SGs (J, K and L).

5.4 Discussion

TDP-43 is known to be one of the major components of the ubiquitin-positive inclusions seen in FTLD and MND (Neumann et al., 2006b). Following this discovery, the physiological and pathological characteristics of TDP-43 have been the focus of intense investigation in order to understand its role in the pathology of FTLD and MND. TDP-43 belongs to the hnRNP family of proteins and, like all the members of the hnRNP family, it possesses the ability to bind to RNA in a single-strand and sequence-specific manner. It also has the ability to bind to several proteins that modulate its RNA processing and, probably, its aggregation properties (Zhu et al., 2014, Zhang et al., 2013). Further, TDP-43 has the ability to bind to other hnRNPs as well as other RNA-binding proteins such as those implicated in SGs, for example, TIA-1 (Liu-Yesucevitz et al., 2010) (Buratti and Baralle, 2012).

We detected the colocalisation of hnRNP-E2 in 84.5% of TDP-43 inclusions in a subset of *C9orf72*-expansion-negative FTLD-TDP cases (Chapter 4). We sought to explore whether there was a link between TDP-43 and hnRNP-E2 that might explain this pathology by means of the co-regulation of protein levels or direct binding. We therefore used cell biology techniques to investigate this relationship and the possible implication of hnRNP-E2 aggregation in TDP-43 pathology.

In a network of interacting proteins, changes in the relative expression of a protein can have a significant impact on other proteins in the network, either directly or by affecting common cellular targets (Mohagheghi et al., 2016). Therefore, TDP-43 and hnRNP-E2 were overexpressed or knocked down in HEK293T cells and their relative expression was measured and statistically analysed by comparing it to controls. Their interaction was further investigated using co-immunoprecipitation to determine whether they form a protein complex as a result of their interaction. We also sought to determine whether the recruitment of TDP-43 and hnRNP-E2 into the SGs might play a role in their colocalisation within inclusions (Monahan et al., 2016, Liu-Yesucevitz et al., 2010, Dewey et al., 2012, Fujimura et al., 2008, Fujimura et al., 2009). Consequently, we examined the presence of TDP-43 and hnRNP-E2 in the SGs induced in HeLa cells with different stress conditions.

5.4.1 hnRNP-E2 could be upstream of TDP-43

The aim of this experiment was to determine whether the levels of TDP-43 and hnRNP-E2 were interdependent. WT-HA-TDP43 was overexpressed in HEK293T cells and the levels of endogenous hnRNP-E2 were measured. However, there was no significant difference found in the endogenous hnRNP-E2 between the WT-HA-TDP43-transfected and pDEST30-transfected cells ($p > 0.05$). When NT-Flag-hnRNP-E2 was overexpressed, no significant difference in the TDP-43 levels was detected between the pDEST30- and NT-Flag-hnRNP-E2-transfected cells.

The knockdown of hnRNP-E2 showed a significant decrease in the TDP-43 levels when a one-way ANOVA was performed among all the samples with different sihnRNP-E2 concentrations ($p < 0.05$). However, the Bonferroni post-hoc t-test corrected analysis revealed a significant difference in TDP-43 expression between the untransfected cell samples and sihnRNP-E2 at 100 nM ($p < 0.05$). Yet, TDP-43 knockdown did not result in any significant change in the hnRNP-E2 expression levels. The results suggest that hnRNP-E2 is upstream of TDP-43; however, it is not clear whether they interact directly or through indirect pathways.

To determine whether TDP-43 and hnRNP-E2 interact directly as part of a protein complex, we performed co-IP, wherein WT-GFP-TDP43 and NT-Flag-hnRNP-E2 were co-transfected into HEK293T cells. When WT-GFP-TDP-43 was pulled down, there was no indication of hnRNP-E2 precipitation using both the Flag and hnRNP-E2 antibodies in Western blots. When hnRNP-E2 was pulled down using Flag antibodies, a band for TDP-43 precipitation was detected. A beads alone control experiment was included to eliminate any possible interaction of the WT-GFP-TDP43 with the beads in the absence of any antibodies. The interaction of WT-GFP-TDP43 with the beads was detected using Protein G or Protein A Dynabeads. The interaction with the beads could be due to the GFP vector rather than TDP-43, since when the Western blots are labelled with TDP-43 antibodies, the band disappeared from the beads' IP. The TDP-43 antibodies did not detect a band of interaction when hnRNP-E2 was pulled down; however, this could be because the endogenous TDP-43 levels were not sufficient to appear on the Western blot when compared to the overexpressed levels. The results of the co-IP were not conclusive; however, if the TDP-43 band is confirmed, along with the results of the knockdown experiment, then hnRNP-E2 could be upstream of TDP-43. Otherwise, we can only conclude that under resting basal conditions TDP-43 and hnRNP-E2 do not directly interact with each other.

5.4.2 TDP-43 and hnRNP-E2 colocalise within stress granules

SGs are transient cytosolic structures that are formed when cells are exposed to stress such as hypoxia, heat, infection or oxidative stress (Anderson and Kedersha, 2008). They originate from polysomes and they store the mRNA of encoding housekeeping proteins as well as prioritising the selective translation of stress-response proteins (e.g. chaperons) and heat-shock proteins that are involved in damage repair. Therefore, SGs are considered to represent a sorting station wherein transcripts will be stored in a silent form for translation re-entry or to be degraded by cellular degradation systems (Bentmann et al., 2012). In addition to mRNAs, SGs also contain several RNA-binding proteins, some of which serve as specific markers for SGs, for example, PABP1 and TIA-1 (Dewey et al., 2012).

5.4.2.1 TDP-43 colocalises with PABP1 in HeLa cells under oxidative stress and combined oxidative and osmotic stress

TDP-43 has been reported to be a stress-responsive protein in several studies. Further, TDP-43 was described as a component of SGs in various cell lines under different stress conditions. The localisation of TDP-43 within SGs is determined by the stressor type and the cell type. Previous studies have reported that TDP-43 can be recruited into SGs in cell culture using oxidative stress, osmotic stress, heat shock, serum deprivation, ubiquitin-proteasome inhibition, endoplasmic reticulum stress and the herbicide Paraquat (Colombrita et al., 2009, Liu-Yesucevitz et al., 2010, Meyerowitz et al., 2011, Dewey et al., 2011, Freibaum et al., 2010, McDonald et al., 2011). TDP-43 was recruited into the SGs by osmotic stress and oxidative stress in mixed primary glial culture and HeLa cells (Dewey et al., 2011) as well as in vivo in axotomised mouse motor neurons (Moisse et al., 2009). However, TDP-43 failed to localise within SGs in HEK293T and the neural cell line (SH-SY5Y and Neuro2a) (Ayala et al., 2011a, Dewey et al., 2011). Bentmann et al. (2012) performed a thorough study on the requirements for TDP-43 recruitment into SGs. They analysed the effect of different *TARDBP* mutations seen in ALS on directing TDP-43 into the SGs. They also mapped the TDP-43 domains required for SG recruitment and investigated the presence of SG markers within TDP-43 inclusions in ALS/FTLD-TDP patients (Bentmann et al., 2012). They reported that both the RRM1 and the C-terminal glycine-rich domain are required for TDP-43 localisation within SGs. SG marker proteins such as TIA-1, eIF3 and PABP1 were reported to label the pathological TDP-43 inclusions in post-mortem brains of ALS and FTLD patients (Dormann et al., 2010, Bentmann et al., 2012, Colombrita et al., 2009, Kim et al., 2014). This could be

due to the presence of different TDP-43 species in the aggregates seen in various regions of the central nervous system, as Bentmann et al. (2012) suggested. Their data also suggested that the PABP1 labelling of TDP-43 inclusions depends on the presence of full-length TDP-43, which may explain the controversy surrounding the SG marker labelling within TDP-43 aggregates in human tissue (Bentmann et al., 2012). McGurk et al. (2014) detected PABP1 within TDP-43 inclusions in the spinal cord of ALS patients without mutations, as well as in ATXN2-ALS, FUS-ALS and *C9orf72* hexanucleotide repeat expansion ALS. They suggested that PABP1 tends to colocalise with mature TDP-43 inclusions rather than preinclusions. They also reported that it is more frequently present with TDP-43 in the spinal cord of *C9orf72* ALS patients than any other subset of ALS, which is consistent the findings of Bentmann et al. (Bentmann et al., 2012, McGurk et al., 2014). PABP1 was also reported to modulate TDP-43 toxicity in drosophila as well as to play an important role in mediating TDP-43 toxicity in model systems (Kim et al., 2014).

In this study, endogenous TDP-43 was recruited into the SGs in untransfected HeLa cells treated with arsenite (oxidative stress) and with combined stress treatment (oxidative and osmotic). This data are consistent with previously reported findings. The SGs were larger with the combined stress treatment when compared to the arsenite stress alone, since the osmotic stress recruits TDP-43 to the SGs, thereby allowing more protein to be incorporated within the SGs (Dewey et al., 2011).

In order to examine the transfection levels of WT-HA-TDP43 and NT-Flag-hnRNP-E2, as well as to confirm the localisation of TDP-43 and hnRNP-E2 within the SGs, labelling with the SG marker PABP1 was performed and the colocalisation was examined. The transfection rate for both WT-HA-TDP43 and NT-Flag-hnRNP-E2 was very low, with only 2–5 cells for WT-HA-TDP-43 and 4–10 cells for NT-Flag-hnRNP-E2 in each coverslip. However, the endogenous and overexpressed TDP-43 and hnRNP-E2 colocalised with the SG marker PABP1 under both stress conditions. Contrary to previous reports, osmotic stress on the HeLa cells failed to induce well-defined SGs formation; however, the combination of osmotic stress and stress caused by transfection increased the formation of vacuoles in the cytoplasm. Although there was a diffusion of TDP-43 from the nucleus into the cytoplasm, the loss of nuclear TDP-43 was less than that seen with oxidative stress.

Despite the evidence of TDP-43 interaction with multiple proteins within the SGs, not all of the proteins have been identified. As the TDP-43 C-terminal domain was reported to be a requirement for its localisation within SGs, protein-protein interactions could contribute to TDP-43 recruitment into SGs. Therefore, it is important to investigate the interaction of TDP-43 with other proteins in an effort to understand the process involved in TDP-43 pathology.

5.4.2.2 hnRNP-E2 colocalises with PABP1 in SGs under oxidative stress and combined oxidative and osmotic stress

hnRNP-E2 was first identified as a component of the α-complex of the human α-globin mRNA that enhances mRNA stability (Kiledjian et al., 1999). hnRNP-E2 plays an important role in biological processes such as transcription regulation and translation silencing. Further, hnRNP-E2 plays a central role in DNA repair, telomere biogenesis and cell signalling, which indicates its potential role in tumour development and progression (Eversole and Maizels, 2000). Currently, hnRNP-E2 is characterised as a facilitator of the internal ribosomal entry site (IRES)-mediated translation of both cellular and viral transcripts (Evans et al., 2003, Bedard et al., 2004). hnRNP-E2 was described as a shuttling protein between the nucleus and the cytoplasm; however, it was found to reside within a subset of processing bodies (P-bodies) in cells at a resting state. P-bodies are conserved cytoplasmic foci enriched with RNA-degrading enzymes, which serve as a storage site for mRNAs and could be involved in micro-RNA (miRNA)-dependent translational repression and short-interfering RNA (SiRNA) (Fujimura et al., 2009). Interestingly, hnRNP-E2 was not found in all the Dcp1a- and eIF4E-T-positive P-bodies, which suggests a specific mechanism that targets hnRNP-E2 into only certain P-bodies (Fujimura et al., 2009). In addition, it was reported that hnRNP-E2 localises to the SGs while still present within P-bodies. Yet, the knockdown of hnRNP-E2 did not affect the structural integrity of the SGs and P-bodies, while its overexpression does not affect the expression of the SG marker TIA-1. Fujimura et al. (2009) suggested that when cells are under stress, hnRNP-E2 shuttles between the P-bodies and SGs due to their close association. Additionally, they suggested that hnRNP-E2 may play an important role in transferring specific mRNA species from the SGs to P-bodies for degradation or mRNPs remodelling in SGs (Fujimura et al., 2009, Fujimura et al., 2008). They also investigated the important domains for hnRNP-E2 localisation within SGs and P-bodies, and they found that the KH1 domain is essential for hnRNP-E2 incorporation into the SGs. They also reported that the deletion of both KH2 and KH3 abolished

localisation to the P-bodies, although it did not affect the accumulation within the SGs (Fujimura et al., 2009)

The results of this study showed that hnRNP-E2 is recruited into the SGs, which was confirmed by the localisation of the SG marker PABP1 within HeLa cells under stress conditions. With oxidative stress, small SGs were formed when compared to those formed with the combined stress condition. More hnRNP-E2 was recruited into the SGs after the combined stress with both arsenite and sorbitol. The colocalisation of hnRNP-E2 with TDP-43 was further investigated in the HeLa cells after the application of stress conditions.

5.4.2.3 hnRNP-E2 colocalises with TDP-43 in SGs

The previous two experiments confirmed the presence of both TDP-43 and hnRNP-E2 within the SGs with the SGs marker PABP1. In this experiment, the colocalisation of endogenous TDP-43 with endogenous hnRNP-E2 within the SGs was confirmed in HeLa cells under various stress conditions. The SGs in this experiment appeared smaller and fewer than when TDP-43 or hnRNP-E2 was overexpressed in the HeLa cells. This could be due to the amount of both that was present endogenously being much less than in the case of overexpression.

Fujimura et al. (2009) also suggested that the presence of hnRNP-E2 is not important for SG formation and that it does not play a role in the structural basis of SGs and P-bodies. However, they did manage to demonstrate that the P-bodies that contain hnRNP-E2 are actively associated with the SGs and that hnRNP-E2 shuttles between the two. Their observations suggest the role of hnRNP-E2 in mRNA degradation. At this point in the present study, it is not clear how hnRNP-E2 interacts with TDP-43 within the SGs or whether hnRNP-E2 leads TDP-43 into the SGs.

Recently, Mao et al. (2016) reported the upregulation of hnRNP-E2 expression in the spinal cord after spinal cord injury in adult rats. They found that it modulates the caspase-dependent apoptosis pathway by interacting with caspase-3, since the knockdown of hnRNP-E2 resulted in a significant decrease in the caspase-3 expression in the primary neuronal cells. Furthermore, they reported that the knockdown of hnRNP-E2 inhibits the astrocyte proliferation and glutamate-induced apoptosis of the primary neurons in vitro. Their results support the hypothesis that hnRNP-E2 may be involved in neuronal apoptosis and cell cycle activation (Mao et al., 2016).

Given the results concerning the expression and Co-IP experiments, it appears that TDP-43 and hnRNP-E2 may interact indirectly, while the SG experiment suggests that hnRNP-E2 does not enhance the cellular toxic effect of the pathological TDP-43. Nevertheless, it suggests that TDP-43 could be escaping a clearance mechanism that is associated with hnRNP-E2. At this point, it remains unclear how and why hnRNP-E2 is colocalised with TDP-43 in a subset of FTLD-TDP cases as well as whether it is involved in the pathology of TDP-43. The study by Mao et al. (2016) provided evidence of its involvement in neuronal apoptosis, but at this stage, the mechanism of hnRNP-E2 in modulating neuronal repair remains unclear.

5.4.3 Conclusion

Our experiments manipulating the levels of TDP-43 and hnRNP-E2 showed that these two proteins do not interact or influence each other under basal conditions. Following oxidative stress, however, they are both recruited into the SGs. Once the stressor has resolved, the SGs are broken up and RNA-binding proteins and RNA are either released or degraded. It is possible that TDP-43 and hnRNP-E2 form aggregates that fail to be degraded and hence form a seed for further aggregation, which in turn either sequesters TDP-43 from the nucleus, thereby causing neurodegeneration by means of a loss of nuclear function mechanism, or implies that cytoplasmic aggregates are directly neurotoxic through a gain of function. At this point, it is not clear how and why hnRNP-E2 interacted with TDP-43 in a subset of FTLD-TDP cases, although our findings do provide further evidence for the role for SGs in acting as a seed for pathological protein aggregation in FTLD and ALS.

Chapter 6 Discussion and Conclusion

6.1 Discussion

FTLD is a clinically, genetically and pathologically heterogeneous group of disorders characterised by a change in language, behaviour and personality which can be accompanied by the signs of MND. FTLD is the second most common form of dementia with an onset before the age of 65 years and is characterised pathologically by atrophy of the frontal and anterior temporal lobes. The prevalence of FTLD is estimated to be between 10 and 30 per 100,000 and shows a strong familial component with 30-50% of patients reporting at least one family member with the same symptoms {Borroni, 2010 #983;Zarow, 2012 #700;Sieben, 2012 #709;Cairns, 2007 #1212}, with predominantly an autosomal dominant pattern of inheritance {Goldman, 2007 #2253}. Mutations in many different genes have been associated with FTLD, most of which also cause ALS. It is now recognised that FTLD and ALS share common genetic, clinical and pathological characteristics and are now considered to form the ends of a phenotypic spectrum. Mutations that exclusively or predominantly cause an FTLD phenotype include those in the genes *MAPT, GRN, VCP, CHMP2B* and the *G4C2* expansion in the *C9orf72* gene which is the most common mutation in FTLD and ALS. FTLD is a complex disorder and combined characterisation of the clinical and biological biomarkers is essential for diagnosis {Sieben, 2012 #709}. Clinically, FTLD is classified into three major types; progressive non-fluent aphasia, semantic dementia and frontotemporal dementia (FTD) {Mitsuyama, 2009 #1058}. FTLD is further classified pathologically based on the composition, morphology and distribution of the protein inclusions detected in the brain of FTLD patients. FTLD is classified into three major pathological subtypes; FTLD-Tau, FTLD-TDP and FTLD-FUS but a small proportion of cases show ubiquitin only, or p62 only, inclusions or show no aggregation pathology at all {Mackenzie, 2010 #227}. The identification of TDP-43 as the major component of the neuronal protein inclusions seen in FTLD and ALS provided a strong molecular link between the two syndromes. There is evidence that the mis-accumulation of TDP-43 is directly mechanistic in causing neurodegeneration however, the downstream events are not clearly understood. A major forward step in understanding the pathological mechanisms underlying the TDP-43 proteinopathies would be mapping out a network of its interacting proteins. This project aimed to identify TDP-43 binding partners in the brain and spinal cord tissues of FTLD and ALS patients. A list of candidate TDP-43 interacting proteins was previously generated by colleagues in our lab using the SILAC technique and the expression levels of a number of these proteins was examined in the brain

and spinal cord tissue of FTLD-TDP and ALS cases using the IHC technique, these proteins included; RanBP1, Ubiquilin-2, hnRNP-M, hnRNP-Q, hnRNP-C1/C2 and hnRNP-E2. Immunoreactive perinuclear inclusions and dystrophic neurites for Ubiquilin-2 and hnRNP-E2 were detected in the frontal cortex of FTLD-TDP cases. From this point forward hnRNP-E2 became the focus of the project and further experiments were designed to investigate the role of hnRNP-E2 in the pathogenesis of FTLD-TDP.

Ubiquilin-2 inclusions were detected in the frontal cortex of FTLD-TDP type B cases and *C9orf72* FTLD-TDP cases. Ubiquilin-2 pathology has since been reported to be characteristic for *C9orf72* pathology in FTLD-TDP cases {Brettschneider, 2012 #2272}. The findings of this project correlate with the reported study however, Ubiquilin-2 inclusions were also detected in 2 FTLD-TDP subtype B cases which do not carry the *C9orf72* expansion. This could mean that Ubiquilin-2 pathology is related more to the TDP-43 pathology subtype rather than the presence of the *C9orf72* expansion. There is also a possibility that the two subtype B cases have an unrecognised *C9orf72* expansion – or indeed a different mutation. Analysis of further numbers of FTLD-TDP subtype B cases could aid in determining the specificity of Ubiquilin-2 inclusions. From this point forward hnRNP-E2 became the focus of the project and further experiments were designed to investigate the role of hnRNP-E2 in the pathogenesis of FTLD-TDP.

6.1.1 hnRNPs in health and disease.

Neurons are non-dividing cells therefore they need tight mRNA homeostasis regulation as they are highly vulnerable to RNA binding protein dysfunction. hnRNPs, play a major role in gene expression regulation. The discovery of pathological mutations in many hnRNPs makes them the central focus in several neurodegenerative disorders such as ALS, FTLD and spinal muscular atrophy (SMA). Because of the growing repertoir of RNA binding proteins, it is still not clear how and when they are triggered to interact and complement each other's function. It has become clear that hnRNPs contribute to the development of many cancers as well as neurodegenerative disorders. However, the underlying patho-mechanisms for many hnRNPs remains to be explained and study of their common and specific disease related functions is needed. hnRNP dysfunction is also implicated in patients carrying the *C9orf72* repeat expansion as the sequestration of RNA binding proteins including hnRNP A3, F, H and K, which colocalise with intranuclear neuronal RNA foci in ALS/FTLD patient tissues {Mori, 2013 #19;Davidson,

2017 #2392;Cooper-Knock, 2014 #446;Lee, 2013 #2387}. Furthermore, mutations in several hnRNPs were identified as causative for ALS/FTLD which support the idea of altered RNA metabolism as the underlying patho-mechanism. Examples of identified mutations are hnRNP-A1 and A2/B1, TARDBP and FUS (which is also known as hnRNP-P2). Interestingly, most of the mutations in FUS are clustered around the NLS but for TDP-43, hnRNP-A1 and A2/B1 they are located in the low complexity, prion-like domain which increases its intrinsic tendency to self-aggregate {Kim, 2013 #18;Le Ber, 2014 #2395;Mohagheghi, 2016 #2396;Waibel, 2010 #2397;Gami-Patel, 2016 #2398}. In addition, *APP* mRNA translation was found to be regulated by hnRNP-C and fragile X mental retardation protein (FMRP), which both act competitively and influence APP translation in an opposing way. The cleavage product of APP is amyloid-beta, plaques of which are the hallmark of AD {Borreca, 2016 #2399}. Moreover, hnRNPs (A1, G, M, Q and R) are linked to SMN and shown to localize with TDP-43 and FUS in nuclear speckles which may function in spliceosome maintenance {Tsuiji, 2013 #23;Chen, 2008 #1818;Cho, 2014 #2184;Kashima, 2007 #2400;Moursy, 2014 #2401;Dombert, 2014 #2402}. Furthermore, hnRNPs are essential for coordinating the transport of stabilized mRNAs along the axonal skeleton to the presynaptic translation sites {Bekenstein, 2013 #2403}.

6.1.2 hnRNP-E2 in FTLD-TDP cases.

Characterisation of hnRNP-E2 in the brain and spinal cord of different FTLD-TDP subtypes and other neurodegenerative diseases was an essential step in identifying the specificity of hnRNP-E2 pathology. hnRNP-E2 IHC was performed on FTLD-TDP without the *C9orf72* expansion, FTLD-TDP with the *C9orf72* expansion, FTLD-Tau, FTLD-U-PRGN, ALS-FUS, ALS-SOD1, sALS, ALS with TDP-43 Mutation, CIDP, DLB, AGD, SCA, Pick's disease, Huntington's disease, Alzheimer's disease cases and healthy controls. hnRNP-E2 immuno-reactive inclusions were only detected in a subset of FTLD-TDP cases without *C9orf72* mutation but not in any of the other neurodegenerative disorders. This group of cases with positive hnRNP-E2 inclusions accounted for 53.3% of total FTLD-TDP cases without a *C9orf72* mutation. hnRNP-E2 pathology was detected in FTLD-TDP subtype A (6/15 cases) and subtype C (7/8 cases) and in one subtype B case. hnRNP-E2 inclusions were predominant in the superficial layers, particularly layer 2, of the neocortex with numerous perinuclear and intra-neuronal inclusions and frequent neuritic inclusions. hnRNP-E2 inclusions were also detected in the hippocampal pyramidal cells, dentate gyrus and in the grey matter of the anterior horn of the thoracic

region of the spinal cord. There were no inclusions detected in the cerebellum of any FTLD-TDP case with or without the *C9orf72* mutation.

These hnRNPE2 inclusions showed a similar pattern of inclusion type to the TDP-43 inclusions – indeed they were seen to colocalise with TDP-43 aggregates when analysed by double immunofluorescence labelling. hnRNP-E2 colocalised with 84.5% of TDP-43 inclusions and with 67% of the ubiquitin inclusions in the same cases. Closer examination of the inclusions by high resolution confocal microscope revealed absolute colocalisation of hnRNP-E2 with TDP-43, in contrast to the ubiquitin inclusions which suggest partial ubiquitination of hnRNP-E2. This strongly suggests that hnRNPE2 and TDP-43 are interacting, or depositing by the same mechanism. Why this is only seen in some of the FTLD-TDP subtypes is of interest and lends support to the hypothesis that the aggregation of TDP-43 in the different subtypes is occurring by different mechanisms. It also suggests that TDP-43 aggregation may not be the main biological event occurring in these diseases, but may be a reflection of neuronal dysregulation. The differing mechanisms of TDP-43 aggregation may also explain the clinical variability seen between the subtypes.

hnRNP-E2 was reported to regulate exon 10 splicing of the MAPT gene. Mis-splicing of exon 10 leads to an imbalance in the ratio of 3repeat and 4repeat tau, causing aggregation of 4repeat tau into neurofibrillary tangle-like structures linked to FTLD-tau, which is also known as FTDP-17 (Frontotemporal Dementia with parkinsonism linked to chromosome 17) {Broderick, 2004 #1428}. It was also reported that hnRNP-E2 interacts with SRp75/hnRNP-G complex to regulate the splicing of exon10 of the Tau gene. The authors of the paper suggested that a weak binding to the SRp75 might be the main reason behind the exon 10 inclusions in FTLD cases {Wang, 2011 #180}. Absence of hnRNP-E2 pathology in FTLD-tau cases (5 cases) and other tauopathy related cases in this study suggests that hnRNP-E2 is associated to TDP-43 pathology and that the imbalance in tau 3R and 4R ratio is not due to malfunctioning hnRNP-E2. Furthermore, hnRNP-E2 shares 89% structural homology with hnRNP-E1 which is believed to be encoded by an intron-less gene that is a product of a retrotransposon of a fully processed minor isoform of hnRNP-E2 {Valverde, 2008 #2019;Makeyev, 2002 #219;Woolaway, 2007 #185}. hnRNP-E1 and hnRNP-G involvement with hnRNP-E2 pathology was investigated in hnRNP-E2 positive cases. The IHC for both hnRNP-E1 and hnRNP-G revealed normal distribution compared to the control cases, which suggests the involvement of hnRNP-E2 is through a

different mechanistic pathway that could be more closely related to TDP-43, leading to its deposition in the brain of FTLD-TDP cases.

Characterisation of hnRNP-E2 insolubility in the brain of FTLD-TDP cases was carried out using WB on serially fractionated brain tissues from the following four groups; FTLD-TDP cases without *C9orf72* mutation with and without hnRNP-E2 inclusions, FTLD-TDP cases with *C9orf72* mutation as well as control cases. Bands of insoluble hnRNP-E2 were not detected in three FTLD-TDP cases with positive hnRNP-E2 inclusions. Moreover, an insoluble hnRNP-E2 band was detected in one FTLD-TDP case without the *C9orf72* expansion which was negative for hnRNP-E2 inclusions by IHC. This result could be due to the variation in the abundancy of hnRNP-E2 inclusions in the brain among cases or simply due to differences in the TDP-43 pathological signature within FTLD-TDP subtypes {Tsuji, 2012 #692;Armstrong, 2010 #239}. The inconsistency of the WB results with the IHC results made the biochemical characterisation of hnRNP-E2 in FTLD-TDP cases inconclusive. However, increasing the case number and carrying out further quantitative studies could give better insight into the biochemical characteristics of hnRNP-E2 in FTLD-TDP pathology.

The effect of gender, disease duration, PMD and fixation time were statistically analysed using a Chi-squared test to identify any significant variable effect among the hnRNP-E2 positive and hnRNP-E2 negative FTLD-TDP cases. None of the variables were shown to affect hnRNP-E2 positivity in FTLD-TDP cases. It would be interesting to further investigate the clinical presentation of disease in the E2 positive and negative cases to establish if there was a correlation with any specific clinical variable (above the general sub-type specific phenotype).

6.1.3 hnRNP-E2 role in neurodegeneration.

To date, there is little knowledge in the literature concerning specific hnRNP-E2 functions in the nervous system in health or neurodegenerative disease. There could be many possible explanations for hnRNP-E2 colocalisation with TDP-43 in degenerating neurons which could form the focus of future studies. Firstly, both TDP-43 and hnRNP-E2 may be present within ubiquitinated inclusions due to impairment of ubiquitin proteasome or autophagy pathways associated with aging, which lead to cytoplasmic TDP-43 accumulation and aggregation {Scotter, 2014 #2122;Uchida, 2016 #2112}. hnRNP-E2 is recognised to play a role as an adapter between the ubiquitin ligase E3 ITCH and the MAVS protein in cellular studies {You, 2009 #1487}. A recent study suggested that the key for TDP-43 aggregation is an imbalance between the substrate VHL and the ligase E3 CUL2 complex {Uchida, 2016 #2112}. hnRNP-E2 could provide a potential component or adapting activity for this complex which could be investigated in future studies. A second possible explanation of hnRNP-E2 colocalisation with TDP-43 is its involvement in the caspase-3 neuronal apoptosis pathway, which has been reported in ALS and FTLD cases {Martin, 1999 #2113;Su, 2000 #2116;Zhang, 2007 #1500;Han, 2013 #39}. Knockdown of hnRNP-E2 induces caspase-3 mediated apoptosis which was investigated in neuronal apoptosis after acute spinal cord injury and in primary neuronal cell lines. Levels of both hnRNP-E2 and caspase-3 were upregulated in neurons following acute spinal cord injury and when hnRNP-E2 was silenced in primary neurons, caspae-3 was down regulated {Mao, 2016 #1960}. The exact mechanism of hnRNP-E2 mediated neuronal apoptosis is not yet clear however, it provides a possible mechanism for TDP-43 aggregation in FTLD and ALS which could be a target for future studies. A third explanation is that miRNAs might form a link between TDP-43 and hnRNP-E2. TDP-43 is an identified modulator of miRNA maturation and it facilitates miRNA production to promote neuronal outgrowth {Kawahara, 2012 #786}. The levels of hnRNP-E2 expression were found to be regulated by miRNA-214 to supress proliferation and growth of glioma cells {Tang, 2015 #2125}. The exact regulatory mechanism has not been identified however, the regulatory functions of TDP-43 in miRNA production could be investigated in relation to hnRNP-E2 expression in the future. Furthermore, the cellular stress response could provide a possible explanation for TDP-43 and hnRNP-E2 aggregation in FTLD-TDP cases as both are reported to be stress responsive proteins {Colombrita, 2009 #1059;Dewey, 2012 #772;Moisse, 2009 #1955;Bentmann, 2013 #17}.

6.1.4 hnRNP-E2 and TDP-43 interaction.

The possible interaction between hnRNP-E2 and TDP-43 was investigated in this project through a series of cell biology experiments which aimed to determine whether hnRNP-E2 accumulation is upstream or downstream of TDP-43 accumulation and to investigate any physical interaction between hnRNP-E2 and TDP-43. Changes in the relative expression levels of one protein can have a significant impact on other proteins in its interacting network, either directly or indirectly by affecting common cellular targets {Mohagheghi, 2016 #1674}. To investigate if hnRNP-E2 is upstream of TDP-43 pathology, hnRNP-E2 was overexpressed and silenced in HEK293T cells and TDP-43 expression levels were measured and compared to controls. To investigate if hnRNP-E2 is downstream of TDP-43 pathology, a similar experiment was performed but with overexpressing and silencing TDP-43 and the levels of hnRNP-E2 were measured compared to controls. The knockdown of hnRNP-E2 showed a significant effect in reducing TDP-43 levels, in contrast knock down of TDP-43 did not affect hnRNP-E2 levels significantly. The overexpression experiments did not reveal significant changes either way. The results suggested that hnRNP-E2 is upstream of TDP-43 however, it is not clear if they are interacting directly or through an indirect pathway. To further investigate TDP-43 and hnRNP-E2 interaction, Co-IP was performed in HEK293T cells. The pull down of hnRNP-E2 showed a band for TDP-43 however it was shown that this band is due to the non-specific binding of GFP-TDP with the sepharose beads as it occurred in the absence of any antibodies. The IP results support the previous finding of hnRNP-E2 being upstream of TDP-43.

It was also shown that TDP-43 and hnRNP-E2 were both recruited into stress granules under stress conditions - as had previously been described by other groups {Fujimura, 2009 #224;Fujimura, 2008 #218;Dewey, 2011 #931;Monahan, 2016 #1921}. Following oxidative stress endogenous TDP-43 and hnRNP-E2 colocalised with each other within SGs as well as with the SG marker PABP1, an effect that was greatly enhanced by the sequential addition of an osmotic challenge. hnRNP-E2 has been identified as a facilitator of the IRES and to have an important role in remodelling mRNAs in the SGs and transferring specific mRNAs from SGs to P-bodies for degradation {Fujimura, 2009 #224;Fujimura, 2008 #218}. This study showed that TDP-43 and hnRNP-E2 colocalise within the SGs during cellular stress, however the exact mechanism of recruitment and evidence of direct/indirect interaction could not be deduced. The investigation of hnRNP-E2 and TDP-43 interaction in cell lines aimed to identify any direct or indirect interaction between hnRNP-E2 and TDP-43, initial results suggested that hnRNP-

E2 is upstream to TDP-43 pathology however, the results were not reproducible and therefore this part of the study was inconclusive. Under stress condition both proteins are recruited to stress granules, however further studies, including in vitro and in vivo models are required to fully explore the relationship of hnRNP-E2 to TDP-43 and its pathological significance.

6.2 Therapeutic Strategies for FTLD-TDP

FTD has traditionally been overshadowed by other neurodegenerative diseases, such as AD, in regard to therapeutic modifiers. Currently FTD treatment is based on symptom management rather than targeting the underlying cause of the neurodegeneration. Furthermore, the rational of using such therapeutics is based on efficacy in treating other neurodegenerative disorders or psychiatric conditions with similar behavioral phenotypes. Generally, FTD patients with behavioral disturbances are treated with serotonin or norepinephrine reuptake inhibitors and antipsychotics. However, there is no definitive treatment for FTD and there is an extreme need for novel therapeutics which target underlying pathological pathways {D'Alton, 2014 #2273}. The two pathological hallmarks of FTLD are hyperphosphorylated tau protein in neurons and glial cells (FTLD-tau) and TDP-43 inclusions which constitute 80-95% of FTLD-ubiquitin (FTLD-U) {Li, 2016 #2275}. The rapid advances in genetic and pathological discoveries over the past decade have provided a greater understanding of FTD and a potential approach for developing therapeutics. However, FTD remains a highly complex condition and the roles of tau and TDP-43 in the resulting neurodegeneration are still unclear {Sieben, 2012 #2276}.

6.2.1 FTLD-TDP genetics as driver for therapeutic strategies

FTD, is a clinically and pathologically heterogeneous condition and by the time the clinical phenotype and atrophy is diagnosed it is probably too late to reverse the neuronal changes already set in motion. Interestingly, structural and cognitive changes can be identified 5-10 years prior to presentation of symptoms in patients with a genetic FTD risk {Rohrer, 2015 #2277}. Therefore, understanding the presymptomatic stage and disease progression is crucial for future therapeutic development. As discussed earlier in this thesis, familial mutations in the *MAPT* gene encoding tau protein which explain a subset of FTLD cases also provide compelling evidence for the involvement of tau in sporadic cases which share some of the same pathological hallmarks {Hutton, 1998 #2278;Hutton, 1998 #2279}. However, TDP-43 genetics are more complicated in FTLD cases. *TARDBP* mutations are not found in

heritable FTLD despite it existing in familial ALS (which is considered to be at the opposite end of the disease spectrum to FTLD). Therefore, the connection seems justified on biological levels in addition to the reports of *TARDBP* mutations in sporadic FTLD cases {Borroni, 2009 #2280;Synofzik, 2014 #2281}. Familial FTLD has been linked to mutations in the *VCP*, *C9ORF72* and *GRN* genes. Other rare mutations have also reported to cause FTLD, including those in *CHMP2B, SQSTM1,* and *UBQLN2*.

6.2.1.1 TDP-43 and PGRN

Although *GRN* mutations are widely accepted as being related to TDP-43 pathology, the mechanisms connecting progranulin haploinsuffeciency and TDP-43 aggregation remain unclear. PGRN possesses neurotrophic activity and it has roles in the periphery including inflammation and wound healing {Ahmed, 2007 #2283;Laird, 2010 #2282}. Animal model studies provided some insight into TDP-43 pathology related to *GRN* mutations. Elevated levels of hyperphosphorylated full-length TDP-43 were recovered from detergent-insoluble brain fractions from *GRN* knockdown mice although phosphorylated TDP-43 was not detected in the ubiquitinated inclusions {Wils, 2012 #2377}. Reduction of PGRN enhances caspase-3 activation which make the neurons vulnerable to sublethal doses of N-methyl-D aspartic acid (NMDA) and hydrogen peroxide which may contribute to TDP-43 pathology. Some *GRN* knockdown mice do not exhibit accumulation of TDP-43 C-terminal fragments or only show TDP-43 accumulation at a late stage {Wils, 2012 #2377;Guo, 2010 #2378;Ahmed, 2010 #2379}. The current explanation is that TDP-43 pathological fragment aggregation may be a late event in FTLD pathogenesis or that the mice model cannot stimulate the full extent of the human pathology.

PGRN is a particularly attractive target for treatment development. The strategies targeting PGRN are mainly divided into two groups. The first group focuses on increasing the levels of PGRN and the second group focuses on targeting its receptors. An example of medications used to elevate PGRN level is Suberoylanilide hydroxamic acid (SAHA), a histone deacetylase inhibitor (HDACi) which has been identified as an enhancer of GRN transcription and subsequently shown to increase PGRN expression in a neuro-2a cell line derived from pathogenic GRN mutation carriers {Cenik, 2011 #2380}. Another example is Bafilomycin A1 (Baf A1), which is a vascular ATPase inhibitor shown to increase PGRN levels, however the exact mechanism remains undetermined {Capell, 2011 #2381}. Sortilin1 and TNF are examples of group two therapeutics targeting PGRN receptors, which reduce GRN-induced endocytosis resulting in increased PGRN levels {Hu, 2010 #2382;Tsai, 2014 #2383}. These

data suggest that the development of specific PGRN modulation compounds might be a key to treat TDP-43 pathologic FTLD.

hnRNP-E2 is reported to regulate caspase-3 levels and play a role in cellular apoptosis {Mao, 2016 #1960}. This study could have provided a further explanation if it considered hnRNP-E2 in FTLD-TDP with *GRN* mutation. Here, only one case with *GRN* mutation has been investigated by IHC which was negative for hnRNP-E2 inclusions. Increasing the cases number and running western blots on brain lysate could have advanced this study regarding PGRN role in FTLD-TDP pathology. Also investigating hnRNP-E2 in the *GRN* knockdown mice model may provide more insight into the TDP-43 pathological mechanism.

6.2.1.2 TDP-43 and C9ORF72

In patients with *C9orf72* expansion, both TDP-43 and p62 inclusions can be detected. The p62 inclusions core could contain DPRs surrounded by TDP-43. In addition, p62 overexpression antagonizes TDP-43 cytosolic aggregation, however reports suggest that TDP-43 may also tackle and trap p62, decreasing its autophagy functional component and reducing its capability to remove abnormal aggregates {Brady, 2011 #2384;Wang, 2013 #2385}. Rapamycin is a macrolide compound obtained from *Streptomyces hygroscopicus* which acts by selectively blocking the transcriptional activation of cytokines thereby inhibiting cytokine production. Studies in FTLD-U mice models with TDP-43 proteinopathies showed that rapamycin treatment effectively rescues the learning/memory impairment of these mice at 3 months of age and significantly slows down the age-dependent loss of their motor function. In addition, rapamycin decreased caspase-3 levels and neuronal loss in the forebrain of FTLD-U mice. Furthermore, it significantly decreased the number of cells with positive TDP-43 inclusions and the amount of full length TDP-43 and its cleavage products in the urea-soluble fraction of the cellular extract. The TDP-43 changes after rapamycin treatment is believed to be due to inhibition of rapamycin mammalian target (mTOR) which induces reduction in mTOR-regulated phospho-p70 S6 kinase (P-p70) and the p62 protein {Wang, 2013 #2385}. For future work, it would be interesting to look at the levels of hnRNP-E2 in FTLD-U mice brain considering its caspase-3 regulation activity and the effect of rapamycin on hnNRP-E2.

In patients with the *C9orf72* intronic expansion mutation, both the antisense and sense strands are transcribed from the expanded hexanucleotide (G4C2) locus and form nuclear RNA aggregates (RNA

foci) which may cause cellular death by sequestering functional RNA binding proteins {DeJesus-Hernandez, 2011 #831;Lee, 2013 #2387}. The expanded RNA also undergoes repeat associated non-ATG translation (RAN translation) which produces aggregation prone polypeptides that form inclusions in human FTD {Mori, 2013 #658}. Targeting the expanded (G4C2) transcripts is another therapeutic concept which has already proven successful in vitro {Donnelly, 2013 #2386}. In addition, antisense efficacy in motor neurons derived from C9orf72 carriers was demonstrated by another study {Sareen, 2013 #2388}. A promising research on C9orf72 transgenic mice showed decreased levels of mutant pathogenic mRNAs by the administration of antisense oligonucleotide drugs (AODs) therefore, decreasing RNA toxicity and disease symptoms {Lagier-Tourenne, 2013 #2404;Riboldi, 2014 #2405}. However, future studies are essential to clarify the mechanistic link of RNA foci and RAN proteins to neurodegeneration as well as to determine if such approach is likely to address the neurotoxicity in *C9orf72* cases.

In this study hnRNP-E2 was investigated in FTLD-TDP cases with the *C9orf72* expansion. Interestingly, hnRNP-E2 was not detected in any of the brain regions (frontal cortex, hippocampus and cerebellum) where TDP-43 and/or p62 pathology are detected. This finding increases the evidence for a different underlying mechanism of TDP-43 aggregation in different types of FTLD-TDP and specifically that TDP-43 may not be the driving force behind the neurodegeneration seen in C9orf72 expansion cases (a hypothesis backed up by recent publications investigating the role of DPRs in C9 ALS and FTLD {Gomez-Deza, 2015 #2248}{Davidson, 2014 #208}. The results also support the idea that therapeutic implications would need to be targeted rather than extrapolated to the FTD population at large. In the case of C9orf72 expansion, where a genetic test could be carried out, this would be viable but currently the only way to distinguish between the other subtypes is by clinical phenotype. The possibility that interacting proteins such as E2 might be detectable in CSF or blood would be an exciting move forward in subtype specific therapies.

6.2.2 Targeting TDP-43

The TDP-43 pathogenesis perspective of FTLD could be summarised in two main hypotheses, a toxic gain of function related to accumulation of cytosolic inclusions or a loss of function mechanism linked to depletion of endogenous nuclear TDP-43. Currently, TDP-43 proteinopathy and its endogenous function is not fully understood, thus the development of targeted therapeutics has not developed to expectations. Logical therapeutic suggestions would be restoration of TDP-43 nuclear function and decreasing the formation, or increasing the clearance, of TDP-43 aggregates. Loss of TDP-43 has significant implications on cellular integrity thus reduction of expression of TDP-43 is not a therapeutic option. Preventing cytoplasmic accumulation and retaining nuclear function may prove beneficial if their mechanisms are defined. Methylene blue (MB) and Dimebon (Latreperdie), which have proven successful in Phase II clinical trials for AD, have been shown to decrease TDP-43 aggregation in cellular studies. In SH-SY5Y cells, the number of TDP-43 aggregates was reduced by 50% and 45% following treatment with 0.05 μM MB or 5 μM Dimebon respectively. Meanwhile, the combined use of MB and Dimebon resulted in an 80 % reduction in the number of aggregates, which indicates that MB and Dimebon may be useful for the treatment of FTLD-U {Yamashita, 2009 #2389}. Another concept for lowering TDP-43 levels is through enhancing its clearance as it is demonstrated that TDP-43 inclusions are degraded by both autophagy and the ubiquitin-proteasome system. Disrupting the interaction of Heat Shock Protein 90 (Hsp90) with co-chaperone 37 (Cdc37) facilitated caspase-mediated TDP-43 nuclear retrotranslocation, leading to TDP-43 autophagic clearance, suggesting Cdc37/Hsp90 complex might hold promise as a potential therapeutic target {Jinwal, 2012 #2390}. Currently, our knowledge about TDP-43 biology is limited, which consequently limits the development of TDP-targeted therapies. Increased knowledge of basic TDP-43 functions and interactions should provide greater understanding of potential therapeutic target pathways. This project provided some insight into TDP-43 possible interaction with hnRNP-E2. However, further investigations using more sophisticated research tools such as animal models recapitulating TDP-43 pathology and patient specific induced pluripotent stem cells (iPSCs) should provide better understanding of FTLD-TDP pathology and hence a step forward toward FTLD-TDP therapy.

6.3 Conclusion

In conclusion, this project investigated several candidate TDP-43-binding proteins in the brain tissue of FTLD and ALS cases with confirmed TDP-43 pathology. Of the proteins investigated (RANBP1, Ubiquilin-2, hnRNP-M, hnRNP-C1/C2, hnRNP-Q and hnRNP-E2), Ubiquilin-2 and hnRNP-E2 showed striking and disease specific perinuclear and neuritic inclusions in the frontal cortex in FTLD-TDP pathological subtypes A and C. The role of hnRNP's in neurodegenerative conditions is an emerging area of research, with many hnRNPs linked to ALS and/or FTD through pathogenic mutations or their sequestration within the C9orf72 G4C2 expansion RNA foci, however, their disease specific mechanisms are poorly understood. This study is the first to show a direct association of an hnRNP with specific FTLD-TDP subtypes. The results increase the evidence that there are different pathways involved in TDP-43 aggregate formation and hence different underlying disease mechanisms occurring in the different pathological subtypes of FTLD. This could have implications for both further research directions for understanding of the mechanisms of neurodegeneration and the role of TDP-43 and for potential therapeutic interventions in these diseases.

References

AHMED, Z., BIGIO, E. H., BUDKA, H., DICKSON, D. W., FERRER, I., GHETTI, B., GIACCONE, G., HATANPAA, K. J., HOLTON, J. L., JOSEPHS, K. A., POWERS, J., SPINA, S., TAKAHASHI, H., WHITE, C. L., 3RD, REVESZ, T. & KOVACS, G. G. 2013. Globular glial tauopathies (GGT): consensus recommendations. *Acta Neuropathol,* 126**,** 537-44.

AHMED, Z., MACKENZIE, I. R., HUTTON, M. L. & DICKSON, D. W. 2007. Progranulin in frontotemporal lobar degeneration and neuroinflammation. *Journal of Neuroinflammation,* 4**,** 7.

AHMED, Z., SHENG, H., XU, Y. F., LIN, W. L., INNES, A. E., GASS, J., YU, X., WUERTZER, C. A., HOU, H., CHIBA, S., YAMANOUCHI, K., LEISSRING, M., PETRUCELLI, L., NISHIHARA, M., HUTTON, M. L., MCGOWAN, E., DICKSON, D. W. & LEWIS, J. 2010. Accelerated lipofuscinosis and ubiquitination in granulin knockout mice suggest a role for progranulin in successful aging. *Am J Pathol,* 177**,** 311-24.

AL-SARRAJ, S., KING, A., TROAKES, C., SMITH, B., MAEKAWA, S., BODI, I., ROGELJ, B., AL-CHALABI, A., HORTOBÁGYI, T. & SHAW, C. E. 2011. p62 positive, TDP-43 negative, neuronal cytoplasmic and intranuclear inclusions in the cerebellum and hippocampus define the pathology of C9orf72-linked FTLD and MND/ALS. *Acta Neuropathologica,* 122**,** 691-702.

ALAMI, N. H., SMITH, R. B., CARRASCO, M. A., WILLIAMS, L. A., WINBORN, C. S., HAN, S. S., KISKINIS, E., WINBORN, B., FREIBAUM, B. D., KANAGARAJ, A., CLARE, A. J., BADDERS, N. M., BILICAN, B., CHAUM, E., CHANDRAN, S., SHAW, C. E., EGGAN, K. C., MANIATIS, T. & TAYLOR, J. P. 2014. Axonal transport of TDP-43 mRNA granules is impaired by ALS-causing mutations. *Neuron,* 81**,** 536-43.

ALBERTS, B. 2002. Molecular biology of the cell. 4th ed. New York: Garland Science,.

ANDERSON, P. & KEDERSHA, N. 2008. Stress granules: the Tao of RNA triage. *Trends Biochem Sci,* 33**,** 141-50.

ARAI, T., HASEGAWA, M., AKIYAMA, H., IKEDA, K., NONAKA, T., MORI, H., MANN, D., TSUCHIYA, K., YOSHIDA, M., HASHIZUME, Y. & ODA, T. 2006. TDP-43 is a component of ubiquitin-positive tau-negative inclusions in frontotemporal lobar degeneration and amyotrophic lateral sclerosis. *Biochem Biophys Res Commun,* 351**,** 602-11.

ARMSTRONG, R. A., ELLIS, W., HAMILTON, R. L., MACKENZIE, I. R., HEDREEN, J., GEARING, M., MONTINE, T., VONSATTEL, J. P., HEAD, E., LIEBERMAN, A. P. & CAIRNS, N. J. 2010. Neuropathological heterogeneity in frontotemporal lobar degeneration with TDP-43 proteinopathy: a quantitative study of 94 cases using principal components analysis. *J Neural Transm,* 117**,** 227-39.

AYALA, V., GRANADO-SERRANO, A. B., CACABELOS, D., NAUDI, A., ILIEVA, E. V., BOADA, J., CARABALLO-MIRALLES, V., LLADO, J., FERRER, I., PAMPLONA, R. & PORTERO-OTIN, M. 2011a. Cell stress induces TDP-43 pathological changes associated with ERK1/2 dysfunction: implications in ALS. *Acta Neuropathol,* 122**,** 259-70.

AYALA, Y. M., DE CONTI, L., AVENDANO-VAZQUEZ, S. E., DHIR, A., ROMANO, M., D'AMBROGIO, A., TOLLERVEY, J., ULE, J., BARALLE, M., BURATTI, E. & BARALLE, F. E. 2011b. TDP-43 regulates its mRNA levels through a negative feedback loop. *EMBO J,* 30**,** 277-88.

AYALA, Y. M., PANTANO, S., D'AMBROGIO, A., BURATTI, E., BRINDISI, A., MARCHETTI, C., ROMANO, M. & BARALLE, F. E. 2005. Human, Drosophila, and C.elegans TDP43: nucleic acid binding properties and splicing regulatory function. *J Mol Biol,* 348**,** 575-88.

BAKER, M., MACKENZIE, I. R., PICKERING-BROWN, S. M., GASS, J., RADEMAKERS, R., LINDHOLM, C., SNOWDEN, J., ADAMSON, J., SADOVNICK, A. D., ROLLINSON, S., CANNON, A., DWOSH, E., NEARY, D., MELQUIST, S., RICHARDSON, A., DICKSON, D., BERGER, Z., ERIKSEN, J., ROBINSON, T., ZEHR, C., DICKEY, C. A., CROOK, R., MCGOWAN, E., MANN, D., BOEVE, B., FELDMAN, H. & HUTTON, M. 2006. Mutations in progranulin cause tau-negative frontotemporal dementia linked to chromosome 17. *Nature,* 442**,** 916-919.

BANG, J., SPINA, S. & MILLER, B. L. 2015. Frontotemporal dementia. *Lancet,* 386**,** 1672-82.

BARBER, R. D., HARMER, D. W., COLEMAN, R. A. & CLARK, B. J. 2005. GAPDH as a housekeeping gene: analysis of GAPDH mRNA expression in a panel of 72 human tissues. *Physiol Genomics,* 21**,** 389-95.

BARMADA, S. J., SKIBINSKI, G., KORB, E., RAO, E. J., WU, J. Y. & FINKBEINER, S. 2010. Cytoplasmic mislocalization of TDP-43 is toxic to neurons and enhanced by a mutation associated with familial amyotrophic lateral sclerosis. *J Neurosci,* 30**,** 639-49.
BEDARD, K. M., WALTER, B. L. & SEMLER, B. L. 2004. Multimerization of poly(rC) binding protein 2 is required for translation initiation mediated by a viral IRES. *RNA,* 10**,** 1266-76.
BEKENSTEIN, U. & SOREQ, H. 2013. Heterogeneous nuclear ribonucleoprotein A1 in health and neurodegenerative disease: from structural insights to post-transcriptional regulatory roles. *Mol Cell Neurosci,* 56**,** 436-46.
BENTMANN, E., HAASS, C. & DORMANN, D. 2013. Stress granules in neurodegeneration--lessons learnt from TAR DNA binding protein of 43 kDa and fused in sarcoma. *FEBS J,* 280**,** 4348-70.
BENTMANN, E., NEUMANN, M., TAHIROVIC, S., RODDE, R., DORMANN, D. & HAASS, C. 2012. Requirements for stress granule recruitment of fused in sarcoma (FUS) and TAR DNA-binding protein of 43 kDa (TDP-43). *J Biol Chem,* 287**,** 23079-94.
BISCHOFF, F. R., KREBBER, H., SMIRNOVA, E., DONG, W. & PONSTINGL, H. 1995. Co-activation of RanGTPase and inhibition of GTP dissociation by Ran-GTP binding protein RanBP1. *The EMBO Journal,* 14**,** 705-715.
BORRECA, A., GIRONI, K., AMADORO, G. & AMMASSARI-TEULE, M. 2016. Opposite Dysregulation of Fragile-X Mental Retardation Protein and Heteronuclear Ribonucleoprotein C Protein Associates with Enhanced APP Translation in Alzheimer Disease. *Mol Neurobiol,* 53**,** 3227-3234.
BORRONI, B., BONVICINI, C., ALBERICI, A., BURATTI, E., AGOSTI, C., ARCHETTI, S., PAPETTI, A., STUANI, C., DI LUCA, M., GENNARELLI, M. & PADOVANI, A. 2009. Mutation within TARDBP leads to frontotemporal dementia without motor neuron disease. *Hum Mutat,* 30**,** E974-83.
BRADY, O. A., MENG, P., ZHENG, Y., MAO, Y. & HU, F. 2011. Regulation of TDP-43 aggregation by phosphorylation and p62/SQSTM1. *J Neurochem,* 116**,** 248-59.
BRANDMEIR, N. J., GESER, F., KWONG, L. K., ZIMMERMAN, E., QIAN, J., LEE, V. M. & TROJANOWSKI, J. Q. 2008. Severe subcortical TDP-43 pathology in sporadic frontotemporal lobar degeneration with motor neuron disease. *Acta Neuropathol,* 115**,** 123-31.
BRAUN RJ, S. C., CARMONA-GUTIERREZ D, KHOURY CM, RING J, BÜTTNER S, MADEO F 2011. Neurotoxic 43-kDa TAR DNA-binding protein (TDP-43) triggers mitochondrion-dependent programmed cell death in yeast. *J Biological Chemistery,* 286**,** 19958-72.
BRELSTAFF, J., LASHLEY, T., HOLTON, J. L., LEES, A. J., ROSSOR, M. N., BANDOPADHYAY, R. & REVESZ, T. 2011. Transportin1: a marker of FTLD-FUS. *Acta Neuropathol,* 122**,** 591-600.
BRETTSCHNEIDER, J., ARAI, K., DEL TREDICI, K., TOLEDO, J. B., ROBINSON, J. L., LEE, E. B., KUWABARA, S., SHIBUYA, K., IRWIN, D. J., FANG, L., VAN DEERLIN, V. M., ELMAN, L., MCCLUSKEY, L., LUDOLPH, A. C., LEE, V. M., BRAAK, H. & TROJANOWSKI, J. Q. 2014. TDP-43 pathology and neuronal loss in amyotrophic lateral sclerosis spinal cord. *Acta Neuropathol,* 128**,** 423-37.
BRETTSCHNEIDER, J., VAN DEERLIN, V. M., ROBINSON, J. L., KWONG, L., LEE, E. B., ALI, Y. O., SAFREN, N., MONTEIRO, M. J., TOLEDO, J. B., ELMAN, L., MCCLUSKEY, L., IRWIN, D. J., GROSSMAN, M., MOLINA-PORCEL, L., LEE, V. M. & TROJANOWSKI, J. Q. 2012. Pattern of ubiquilin pathology in ALS and FTLD indicates presence of C9ORF72 hexanucleotide expansion. *Acta Neuropathol,* 123**,** 825-39.
BRODERICK, J., WANG, J. & ANDREADIS, A. 2004a. Heterogeneous nuclear ribonucleoprotein E2 binds to tau exon 10 and moderately activates its splicing. *Gene,* 331**,** 107-14.
BRODERICK, J., WANG, J. & ANDREADIS, A. 2004b. Heterogeneous nuclear ribonucleoprotein E2 binds to tau exon 10 and moderately activates its splicing. *Gene,* 331**,** 107-114.
BURATTI, E. & BARALLE, F. E. TDP-43: gumming up neurons through protein–protein and protein–RNA interactions. *Trends in Biochemical Sciences,* 37**,** 237-247.
BURATTI, E. & BARALLE, F. E. 2001. Characterization and functional implications of the RNA binding properties of nuclear factor TDP-43, a novel splicing regulator of CFTR exon 9. *J Biol Chem,* 276**,** 36337-43.
BURATTI, E. & BARALLE, F. E. 2012. TDP-43: gumming up neurons through protein-protein and protein-RNA interactions. *Trends Biochem Sci,* 37**,** 237-47.
BURATTI, E., DE CONTI, L., STUANI, C., ROMANO, M., BARALLE, M. & BARALLE, F. 2010. Nuclear factor TDP-43 can affect selected microRNA levels. *FEBS J,* 277**,** 2268-81.
BURATTI, E., DORK, T., ZUCCATO, E., PAGANI, F., ROMANO, M. & BARALLE, F. E. 2001. Nuclear factor TDP-43 and SR proteins promote in vitro and in vivo CFTR exon 9 skipping. *EMBO J,* 20**,** 1774-84.

BURATTI, E., ROMANO, M. & BARALLE, F. E. 2013. TDP-43 high throughput screening analyses in neurodegeneration: advantages and pitfalls. *Mol Cell Neurosci,* 56**,** 465-74.
BURD, D. 1994. Conserved structures and diversity of functions of RNA-binding proteins. . *Science* 265**,** 615–621.
BURRELL, J. R., HALLIDAY, G. M., KRIL, J. J., ITTNER, L. M., GOTZ, J., KIERNAN, M. C. & HODGES, J. R. 2016. The frontotemporal dementia-motor neuron disease continuum. *Lancet*.
BURRELL, J. R., KIERNAN, M. C., VUCIC, S. & HODGES, J. R. 2011. Motor neuron dysfunction in frontotemporal dementia. *Brain,* 134**,** 2582-94.
CAIRNS, N. J., NEUMANN, M., BIGIO, E. H., HOLM, I. E., TROOST, D., HATANPAA, K. J., FOONG, C., WHITE III, C. L., SCHNEIDER, J. A., KRETZSCHMAR, H. A., CARTER, D., TAYLOR-REINWALD, L., PAULSMEYER, K., STRIDER, J., GITCHO, M., GOATE, A. M., MORRIS, J. C., MISHRA, M., KWONG, L. K., STIEBER, A., XU, Y., FORMAN, M. S., TROJANOWSKI, J. Q., LEE, V. M. Y. & MACKENZIE, I. R. A. 2007. TDP-43 in Familial and Sporadic Frontotemporal Lobar Degeneration with Ubiquitin Inclusions. *The American Journal of Pathology,* 171**,** 227-240.
CALINI, D., CORRADO, L., DEL BO, R., GAGLIARDI, S., PENSATO, V., VERDE, F., CORTI, S., MAZZINI, L., MILANI, P., CASTELLOTTI, B., BERTOLIN, C., SORAR, G., CEREDA, C., COMI, G. P., D'ALFONSO, S., GELLERA, C., TICOZZI, N., LANDERS, J. E., RATTI, A. & SILANI, V. 2013. Analysis of hnRNPA1, A2/B1, and A3 genes in patients with amyotrophic lateral sclerosis. *Neurobiology of Aging,* 34**,** 2695.e11-2695.e12.
CALVIO, C., NEUBAUER, G., MANN, M. & LAMOND, A. I. 1995. Identification of hnRNP P2 as TLS/FUS using electrospray mass spectrometry. *Rna,* 1**,** 724-33.
CAPELL, A., LIEBSCHER, S., FELLERER, K., BROUWERS, N., WILLEM, M., LAMMICH, S., GIJSELINCK, I., BITTNER, T., CARLSON, A. M., SASSE, F., KUNZE, B., STEINMETZ, H., JANSEN, R., DORMANN, D., SLEEGERS, K., CRUTS, M., HERMS, J., VAN BROECKHOVEN, C. & HAASS, C. 2011. Rescue of progranulin deficiency associated with frontotemporal lobar degeneration by alkalizing reagents and inhibition of vacuolar ATPase. *J Neurosci,* 31**,** 1885-94.
CENIK, B., SEPHTON, C. F., DEWEY, C. M., XIAN, X., WEI, S., YU, K., NIU, W., COPPOLA, G., COUGHLIN, S. E., LEE, S. E., DRIES, D. R., ALMEIDA, S., GESCHWIND, D. H., GAO, F. B., MILLER, B. L., FARESE, R. V., JR., POSNER, B. A., YU, G. & HERZ, J. 2011. Suberoylanilide hydroxamic acid (vorinostat) up-regulates progranulin transcription: rational therapeutic approach to frontotemporal dementia. *J Biol Chem,* 286**,** 16101-8.
CHAUDHURY, A., CHANDER, P. & HOWE, P. H. 2010. Heterogeneous nuclear ribonucleoproteins (hnRNPs) in cellular processes: Focus on hnRNP E1's multifunctional regulatory roles. *RNA,* 16**,** 1449-62.
CHAUDHURY A, C. P., HOWE P. 2010. Heterogeneous nuclear ribonucleoproteins (hnRNPs) in cellular processes: Focus on hnRNP E1's multifunctional regulatory roles. *RNA Biol,* 16**,** 1449-1462.
CHEN-PLOTKIN, A. S., LEE, V. M. Y. & TROJANOWSKI, J. Q. 2010. TAR DNA-binding protein 43 in neurodegenerative disease. *Nat Rev Neurol,* 6**,** 211-20.
CHEN, H.-H., CHANG, J.-G., LU, R.-M., PENG, T.-Y. & TARN, W.-Y. 2008a. The RNA Binding Protein hnRNP Q Modulates the Utilization of Exon 7 in the Survival Motor Neuron 2 (SMN2) Gene. *Molecular and Cellular Biology,* 28**,** 6929-6938.
CHEN, H., HEWISON, M. & ADAMS, J. S. 2006. Functional characterization of heterogeneous nuclear ribonuclear protein C1/C2 in vitamin D resistance: a novel response element-binding protein. *J Biol Chem,* 281**,** 39114-20.
CHEN, Y., ZHOU, X., LIU, N., WANG, C., ZHANG, L., MO, W. & HU, G. 2008b. Arginine methylation of hnRNP K enhances p53 transcriptional activity. *FEBS Letters,* 582**,** 1761-1765.
CHO, S., MOON, H., LOH, T. J., OH, H. K., CHO, S., CHOY, H. E., SONG, W. K., CHUN, J. S., ZHENG, X. & SHEN, H. 2014. hnRNP M facilitates exon 7 inclusion of SMN2 pre-mRNA in spinal muscular atrophy by targeting an enhancer on exon 7. *Biochim Biophys Acta,* 1839**,** 306-15.
COLOMBRITA, C., ZENNARO, E., FALLINI, C., WEBER, M., SOMMACAL, A., BURATTI, E., SILANI, V. & RATTI, A. 2009. TDP-43 is recruited to stress granules in conditions of oxidative insult. *J Neurochem,* 111**,** 1051-61.
COOPER-KNOCK, J., WALSH, M. J., HIGGINBOTTOM, A., ROBIN HIGHLEY, J., DICKMAN, M. J., EDBAUER, D., INCE, P. G., WHARTON, S. B., WILSON, S. A., KIRBY, J., HAUTBERGUE,

G. M. & SHAW, P. J. 2014. Sequestration of multiple RNA recognition motif-containing proteins by C9orf72 repeat expansions. *Brain,* 137**,** 2040-51.
CRUTS, M., GIJSELINCK, I., VAN DER ZEE, J., ENGELBORGHS, S., WILS, H., PIRICI, D., RADEMAKERS, R., VANDENBERGHE, R., DERMAUT, B., MARTIN, J.-J., VAN DUIJN, C., PEETERS, K., SCIOT, R., SANTENS, P., DE POOTER, T., MATTHEIJSSENS, M., VAN DEN BROECK, M., CUIJT, I., VENNEKENS, K. L., DE DEYN, P. P., KUMAR-SINGH, S. & VAN BROECKHOVEN, C. 2006a. Null mutations in progranulin cause ubiquitin-positive frontotemporal dementia linked to chromosome 17q21. *Nature,* 442**,** 920-924.
CRUTS, M., GIJSELINCK, I., VAN DER ZEE, J., ENGELBORGHS, S., WILS, H., PIRICI, D., RADEMAKERS, R., VANDENBERGHE, R., DERMAUT, B., MARTIN, J. J., VAN DUIJN, C., PEETERS, K., SCIOT, R., SANTENS, P., DE POOTER, T., MATTHEIJSSENS, M., VAN DEN BROECK, M., CUIJT, I., VENNEKENS, K., DE DEYN, P. P., KUMAR-SINGH, S. & VAN BROECKHOVEN, C. 2006b. Null mutations in progranulin cause ubiquitin-positive frontotemporal dementia linked to chromosome 17q21. *Nature,* 442**,** 920-4.
D'ALTON, S. & LEWIS, J. 2014. Therapeutic and diagnostic challenges for frontotemporal dementia. *Frontiers in Aging Neuroscience,* 6.
D'ALTON, S. & LEWIS, J. 2014. Therapeutic and diagnostic challenges for frontotemporal dementia. *Frontiers in Aging Neuroscience,* 6.
DA CRUZ, S. & CLEVELAND, D. W. 2011. Understanding the role of TDP-43 and FUS/TLS in ALS and beyond. *Curr Opin Neurobiol,* 21**,** 904-19.
DATAR, K. V., DREYFUSS, G. & SWANSON, M. S. 1993. The human hnRNP M proteins: identification of a methionine/arginine-rich repeat motif in ribonucleoproteins. *Nucleic Acids Res,* 21**,** 439-46.
DAVIDSON, Y., KELLEY, T., MACKENZIE, I. R., PICKERING-BROWN, S., DU PLESSIS, D., NEARY, D., SNOWDEN, J. S. & MANN, D. M. 2007. Ubiquitinated pathological lesions in frontotemporal lobar degeneration contain the TAR DNA-binding protein, TDP-43. *Acta Neuropathol,* 113**,** 521-33.
DAVIDSON, Y., ROBINSON, A. C., LIU, X., WU, D., TROAKES, C., ROLLINSON, S., MASUDA-SUZUKAKE, M., SUZUKI, G., NONAKA, T., SHI, J., TIAN, J., HAMDALLA, H., EALING, J., RICHARDSON, A., JONES, M., PICKERING-BROWN, S., SNOWDEN, J. S., HASEGAWA, M. & MANN, D. M. 2016. Neurodegeneration in frontotemporal lobar degeneration and motor neurone disease associated with expansions in C9orf72 is linked to TDP-43 pathology and not associated with aggregated forms of dipeptide repeat proteins. *Neuropathol Appl Neurobiol,* 42**,** 242-54.
DAVIDSON, Y. S., BARKER, H., ROBINSON, A. C., THOMPSON, J. C., HARRIS, J., TROAKES, C., SMITH, B., AL-SARAJ, S., SHAW, C., ROLLINSON, S., MASUDA-SUZUKAKE, M., HASEGAWA, M., PICKERING-BROWN, S., SNOWDEN, J. S. & MANN, D. M. 2014. Brain distribution of dipeptide repeat proteins in frontotemporal lobar degeneration and motor neurone disease associated with expansions in C9ORF72. *Acta Neuropathol Commun,* 2**,** 70.
DAVIDSON, Y. S., FLOOD, L., ROBINSON, A. C., NIHEI, Y., MORI, K., ROLLINSON, S., RICHARDSON, A., BENSON, B. C., JONES, M., SNOWDEN, J. S., PICKERING-BROWN, S., HAASS, C., LASHLEY, T. & MANN, D. M. A. 2017. Heterogeneous ribonuclear protein A3 (hnRNP A3) is present in dipeptide repeat protein containing inclusions in Frontotemporal Lobar Degeneration and Motor Neurone disease associated with expansions in C9orf72 gene. *Acta Neuropathologica Communications,* 5**,** 31.
DE MATOS, L. L., TRUFELLI, D. C., DE MATOS, M. G. L. & DA SILVA PINHAL, M. A. 2010. Immunohistochemistry as an Important Tool in Biomarkers Detection and Clinical Practice. *Biomark Insights,* 5**,** 9-20.
DE MUYNCK, L. & VAN DAMME, P. 2011. Cellular effects of progranulin in health and disease. *J Mol Neurosci,* 45**,** 549-60.
DECHTAWEWAT, T., SONGPRAKHON, P., LIMJINDAPORN, T., PUTTIKHUNT, C., KASINRERK, W., SAITORNUANG, S., YENCHITSOMANUS, P.-T. & NOISAKRAN, S. 2015. Role of human heterogeneous nuclear ribonucleoprotein C1/C2 in dengue virus replication. *Virology Journal,* 12**,** 14.
DEJESUS-HERNANDEZ, M., MACKENZIE, I. R., BOEVE, B. F., BOXER, A. L., BAKER, M., RUTHERFORD, N. J., NICHOLSON, A. M., FINCH, N. A., FLYNN, H., ADAMSON, J., KOURI, N., WOJTAS, A., SENGDY, P., HSIUNG, G. Y., KARYDAS, A., SEELEY, W. W., JOSEPHS, K. A., COPPOLA, G., GESCHWIND, D. H., WSZOLEK, Z. K., FELDMAN, H., KNOPMAN, D. S., PETERSEN, R. C., MILLER, B. L., DICKSON, D. W., BOYLAN, K. B., GRAFF-RADFORD, N. R. & RADEMAKERS, R. 2011a. Expanded GGGGCC hexanucleotide

repeat in noncoding region of C9ORF72 causes chromosome 9p-linked FTD and ALS. *Neuron,* 72**,** 245-56.

DEJESUS-HERNANDEZ, M., MACKENZIE, I. R., BOEVE, B. F., BOXER, A. L., BAKER, M., RUTHERFORD, N. J., NICHOLSON, A. M., FINCH, N. C. A., GILMER, H. F., ADAMSON, J., KOURI, N., WOJTAS, A., SENGDY, P., HSIUNG, G. Y. R., KARYDAS, A., SEELEY, W. W., JOSEPHS, K. A., COPPOLA, G., GESCHWIND, D. H., WSZOLEK, Z. K., FELDMAN, H., KNOPMAN, D., PETERSEN, R., MILLER, B. L., DICKSON, D., BOYLAN, K., GRAFF-RADFORD, N. & RADEMAKERS, R. 2011b. Expanded GGGGCC hexanucleotide repeat in non-coding region of C9ORF72 causes chromosome 9p-linked frontotemporal dementia and amyotrophic lateral sclerosis. *Neuron,* 72**,** 245-56.

DENG, H. X., CHEN, W., HONG, S. T., BOYCOTT, K. M., GORRIE, G. H., SIDDIQUE, N., YANG, Y., FECTO, F., SHI, Y., ZHAI, H., JIANG, H., HIRANO, M., RAMPERSAUD, E., JANSEN, G. H., DONKERVOORT, S., BIGIO, E. H., BROOKS, B. R., AJROUD, K., SUFIT, R. L., HAINES, J. L., MUGNAINI, E., PERICAK-VANCE, M. A. & SIDDIQUE, T. 2011. Mutations in UBQLN2 cause dominant X-linked juvenile and adult-onset ALS and ALS/dementia. *Nature,* 477**,** 211-5.

DEWEY, C. M., CENIK, B., SEPHTON, C. F., DRIES, D. R., MAYER, P., 3RD, GOOD, S. K., JOHNSON, B. A., HERZ, J. & YU, G. 2011. TDP-43 is directed to stress granules by sorbitol, a novel physiological osmotic and oxidative stressor. *Mol Cell Biol,* 31**,** 1098-108.

DEWEY, C. M., CENIK, B., SEPHTON, C. F., JOHNSON, B. A., HERZ, J. & YU, G. 2012. TDP-43 aggregation in neurodegeneration: are stress granules the key? *Brain Res,* 1462**,** 16-25.

DIAPER, D. C., ADACHI, Y., SUTCLIFFE, B., HUMPHREY, D. M., ELLIOTT, C. J., STEPTO, A., LUDLOW, Z. N., VANDEN BROECK, L., CALLAERTS, P., DERMAUT, B., AL-CHALABI, A., SHAW, C. E., ROBINSON, I. M. & HIRTH, F. 2013. Loss and gain of Drosophila TDP-43 impair synaptic efficacy and motor control leading to age-related neurodegeneration by loss-of-function phenotypes. *Hum Mol Genet,* 22**,** 1539-57.

DICKSON, D. W., BERGERON, C., CHIN, S. S., DUYCKAERTS, C., HOROUPIAN, D., IKEDA, K., JELLINGER, K., LANTOS, P. L., LIPPA, C. F., MIRRA, S. S., TABATON, M., VONSATTEL, J. P., WAKABAYASHI, K. & LITVAN, I. 2002. Office of Rare Diseases neuropathologic criteria for corticobasal degeneration. *J Neuropathol Exp Neurol,* 61**,** 935-46.

DOMBERT, B., SIVADASAN, R., SIMON, C. M., JABLONKA, S. & SENDTNER, M. 2014. Presynaptic localization of Smn and hnRNP R in axon terminals of embryonic and postnatal mouse motoneurons. *PLoS One,* 9**,** e110846.

DONNELLY, C. J., ZHANG, P.-W., PHAM, J. T., HEUSLER, A. R., MISTRY, N. A., VIDENSKY, S., DALEY, E. L., POTH, E. M., HOOVER, B., FINES, D. M., MARAGAKIS, N., TIENARI, P. J., PETRUCELLI, L., TRAYNOR, B. J., WANG, J., RIGO, F., BENNETT, C. F., BLACKSHAW, S., SATTLER, R. & ROTHSTEIN, J. D. 2013. RNA Toxicity from the ALS/FTD C9ORF72 Expansion Is Mitigated by Antisense Intervention. *Neuron,* 80**,** 415-428.

DORMANN, D., MADL, T., VALORI, C. F., BENTMANN, E., TAHIROVIC, S., ABOU-AJRAM, C., KREMMER, E., ANSORGE, O., MACKENZIE, I. R., NEUMANN, M. & HAASS, C. 2012. Arginine methylation next to the PY-NLS modulates Transportin binding and nuclear import of FUS. *EMBO J,* 31**,** 4258-75.

DORMANN, D., RODDE, R., EDBAUER, D., BENTMANN, E., FISCHER, I., HRUSCHA, A., THAN, M. E., MACKENZIE, I. R., CAPELL, A., SCHMID, B., NEUMANN, M. & HAASS, C. 2010. ALS-associated fused in sarcoma (FUS) mutations disrupt Transportin-mediated nuclear import. *EMBO J,* 29**,** 2841-57.

DREYFUSS, G., KIM, V. N. & KATAOKA, N. 2002. Messenger-RNA-binding proteins and the messages they carry. *Nat Rev Mol Cell Biol,* 3**,** 195-205.

DREYFUSS, G., MATUNIS, M. J., PINOL-ROMA, S. & BURD, C. G. 1993. hnRNP proteins and the biogenesis of mRNA. *Annu. Rev. Biochem,* 62**,** 289–321.

DURAIYAN, J., GOVINDARAJAN, R., KALIYAPPAN, K. & PALANISAMY, M. 2012. Applications of immunohistochemistry. *Journal of Pharmacy & Bioallied Sciences,* 4**,** S307-S309.

EVANS, J. R., MITCHELL, S. A., SPRIGGS, K. A., OSTROWSKI, J., BOMSZTYK, K., OSTAREK, D. & WILLIS, A. E. 2003. Members of the poly (rC) binding protein family stimulate the activity of the c-myc internal ribosome entry segment in vitro and in vivo. *Oncogene,* 22**,** 8012-20.

EVERSOLE, A. & MAIZELS, N. 2000. In vitro properties of the conserved mammalian protein hnRNP D suggest a role in telomere maintenance. *Mol Cell Biol,* 20**,** 5425-32.

FAGERBERG, L., STADLER, C., SKOGS, M., HJELMARE, M., JONASSON, K., WIKING, M., ABERGH, A., UHLEN, M. & LUNDBERG, E. 2011. Mapping the subcellular protein distribution in three human cell lines. *J Proteome Res,* 10**,** 3766-77.

FECTO, F. & SIDDIQUE, T. 2011. Making connections: pathology and genetics link amyotrophic lateral sclerosis with frontotemporal lobe dementia. *J Mol Neurosci,* 45**,** 663-75.
FORMAN, M. S., MACKENZIE, I. R., CAIRNS, N. J., SWANSON, E., BOYER, P. J., DRACHMAN, D. A., JHAVERI, B. S., KARLAWISH, J. H., PESTRONK, A., SMITH, T. W., TU, P. H., WATTS, G. D., MARKESBERY, W. R., SMITH, C. D. & KIMONIS, V. E. 2006. Novel ubiquitin neuropathology in frontotemporal dementia with valosin-containing protein gene mutations. *J Neuropathol Exp Neurol,* 65**,** 571-81.
FREIBAUM, B. D., CHITTA, R. K., HIGH, A. A. & TAYLOR, J. P. 2010. Global analysis of TDP-43 interacting proteins reveals strong association with RNA splicing and translation machinery. *J Proteome Res,* 9**,** 1104-20.
FUJIMURA, K., KANO, F. & MURATA, M. 2008. Identification of PCBP2, a facilitator of IRES-mediated translation, as a novel constituent of stress granules and processing bodies. *RNA,* 14**,** 425-31.
FUJIMURA, K., KATAHIRA, J., KANO, F., YONEDA, Y. & MURATA, M. 2009. Selective localization of PCBP2 to cytoplasmic processing bodies. *Biochimica et Biophysica Acta (BBA) - Molecular Cell Research,* 1793**,** 878-887.
FUJITA, K., ITO, H., NAKANO, S., KINOSHITA, Y., WATE, R. & KUSAKA, H. 2008. Immunohistochemical identification of messenger RNA-related proteins in basophilic inclusions of adult-onset atypical motor neuron disease. *Acta Neuropathol,* 116**,** 439-45.
GAMI-PATEL, P., BANDOPADHYAY, R., BRELSTAFF, J., REVESZ, T. & LASHLEY, T. 2016. The presence of heterogeneous nuclear ribonucleoproteins in frontotemporal lobar degeneration with FUS-positive inclusions. *Neurobiology of Aging,* 46**,** 192-203.
GENDRON, T. F., RADEMAKERS, R. & PETRUCELLI, L. 2013. TARDBP mutation analysis in TDP-43 proteinopathies and deciphering the toxicity of mutant TDP-43. *J Alzheimers Dis,* 33 Suppl 1**,** S35-45.
GESER, F., MARTINEZ-LAGE, M., ROBINSON, J., URYU, K., NEUMANN, M., BRANDMEIR, N. J., XIE, S. X., KWONG, L. K., ELMAN, L., MCCLUSKEY, L., CLARK, C. M., MALUNDA, J., MILLER, B. L., ZIMMERMAN, E. A., QIAN, J., VAN DEERLIN, V., GROSSMAN, M., LEE, V. M. & TROJANOWSKI, J. Q. 2009. Clinical and pathological continuum of multisystem TDP-43 proteinopathies. *Arch Neurol,* 66**,** 180-9.
GHANEM, L. R., KROMER, A., SILVERMAN, I. M., CHATTERJI, P., TRAXLER, E., PENZO-MENDEZ, A., WEISS, M. J., STANGER, B. Z. & LIEBHABER, S. A. 2015. The Poly(C) Binding Protein Pcbp2 and Its Retrotransposed Derivative Pcbp1 Are Independently Essential to Mouse Development. *Mol Cell Biol,* 36**,** 304-19.
GHETTI, B., WSZOLEK, Z. K., BOEVE, B. F., SPINA, S. & GOEDERT, M. 2011. Frontotemporal Dementia and Parkinsonism Linked to Chromosome 17. *Neurodegeneration: The Molecular Pathology of Dementia and Movement Disorders.* Wiley-Blackwell.
GHOSH, D., SRIVASTAVA, G. P., XU, D., SCHULZ, L. C. & ROBERTS, R. M. 2008. A link between SIN1 (MAPKAP1) and poly(rC) binding protein 2 (PCBP2) in counteracting environmental stress. *Proc Natl Acad Sci U S A,* 105**,** 11673-8.
GIJSELINCK, I., VAN MOSSEVELDE, S., VAN DER ZEE, J., SIEBEN, A., PHILTJENS, S., HEEMAN, B., ENGELBORGHS, S., VANDENBULCKE, M., DE BAETS, G., BAUMER, V., CUIJT, I., VAN DEN BROECK, M., PEETERS, K., MATTHEIJSSENS, M., ROUSSEAU, F., VANDENBERGHE, R., DE JONGHE, P., CRAS, P., DE DEYN, P. P., MARTIN, J. J., CRUTS, M. & VAN BROECKHOVEN, C. 2015. Loss of TBK1 is a frequent cause of frontotemporal dementia in a Belgian cohort. *Neurology,* 85**,** 2116-25.
GOLDMAN, J. S., ADAMSON, J., KARYDAS, A., MILLER, B. L. & HUTTON, M. 2007. New genes, new dilemmas: FTLD genetics and its implications for families. *Am J Alzheimers Dis Other Demen,* 22**,** 507-15.
GOMEZ-DEZA, J., LEE, Y. B., TROAKES, C., NOLAN, M., AL-SARRAJ, S., GALLO, J. M. & SHAW, C. E. 2015. Dipeptide repeat protein inclusions are rare in the spinal cord and almost absent from motor neurons in C9ORF72 mutant amyotrophic lateral sclerosis and are unlikely to cause their degeneration. *Acta Neuropathol Commun,* 3**,** 38.
GORNO-TEMPINI, M. L., HILLIS, A. E., WEINTRAUB, S., KERTESZ, A., MENDEZ, M., CAPPA, S. F., OGAR, J. M., ROHRER, J. D., BLACK, S., BOEVE, B. F., MANES, F., DRONKERS, N. F., VANDENBERGHE, R., RASCOVSKY, K., PATTERSON, K., MILLER, B. L., KNOPMAN, D. S., HODGES, J. R., MESULAM, M. M. & GROSSMAN, M. 2011. Classification of primary progressive aphasia and its variants. *Neurology,* 76**,** 1006-14.

GROSSET, C., CHEN, C. Y., XU, N., SONENBERG, N., JACQUEMIN-SABLON, H. & SHYU, A. B. 2000. A mechanism for translationally coupled mRNA turnover: interaction between the poly(A) tail and a c-fos RNA coding determinant via a protein complex. *Cell,* 103**,** 29-40.
GUO, A., TAPIA, L., BAMJI, S. X., CYNADER, M. S. & JIA, W. 2010. Progranulin deficiency leads to enhanced cell vulnerability and TDP-43 translocation in primary neuronal cultures. *Brain Res,* 1366**,** 1-8.
GUSTIN, K. E. & SARNOW, P. 2002. Inhibition of nuclear import and alteration of nuclear pore complex composition by rhinovirus. *J Virol,* 76**,** 8787-96.
HAN, W., XIN, Z., ZHAO, Z., BAO, W., LIN, X., YIN, B., ZHAO, J., YUAN, J., QIANG, B. & PENG, X. 2013. RNA-binding protein PCBP2 modulates glioma growth by regulating FHL3. *J Clin Invest,* 123**,** 2103-18.
HANSON, K. A., KIM, S. H., WASSARMAN, D. A. & TIBBETTS, R. S. 2010. Ubiquilin modifies TDP-43 toxicity in a Drosophila model of amyotrophic lateral sclerosis (ALS). *J Biol Chem,* 285**,** 11068-72.
HASEGAWA, M., ARAI, T., NONAKA, T., KAMETANI, F., YOSHIDA, M., HASHIZUME, Y., BEACH, T. G., BURATTI, E., BARALLE, F., MORITA, M., NAKANO, I., ODA, T., TSUCHIYA, K. & AKIYAMA, H. 2008. Phosphorylated TDP-43 in frontotemporal lobar degeneration and amyotrophic lateral sclerosis. *Ann Neurol,* 64**,** 60-70.
HASEGAWA, M., NONAKA, T., TSUJI, H., TAMAOKA, A., YAMASHITA, M., KAMETANI, F., YOSHIDA, M., ARAI, T. & AKIYAMA, H. 2011. Molecular dissection of TDP-43 proteinopathies. *J Mol Neurosci,* 45**,** 480-5.
HATANPAA, K. J., BIGIO, E. H., CAIRNS, N. J., WOMACK, K. B., WEINTRAUB, S., MORRIS, J. C., FOONG, C., XIAO, G., HLADIK, C., MANTANONA, T. Y. & WHITE, C. L., 3RD 2008. TAR DNA-binding protein 43 immunohistochemistry reveals extensive neuritic pathology in FTLD-U: a midwest-southwest consortium for FTLD study. *J Neuropathol Exp Neurol,* 67**,** 271-9.
HEINER CR, H. K., CHEN S-M, GLASS JI, CHEN EY. 1998. Sequencing Multimegabase-Template DNA with BigDye Terminator Chemistry. *Genome Research.,* 8**,** 557-561.
HELMKEN, C., HOFMANN, Y., SCHOENEN, F., OPREA, G., RASCHKE, H., RUDNIK-SCHONEBORN, S., ZERRES, K. & WIRTH, B. 2003. Evidence for a modifying pathway in SMA discordant families: reduced SMN level decreases the amount of its interacting partners and Htra2-beta1. *Hum Genet,* 114**,** 11-21.
HERSHKO, A. & CIECHANOVER, A. 1998. The ubiquitin system. *Annu Rev Biochem,* 67**,** 425-79.
HODGES, J. R., DAVIES, R., XUEREB, J., KRIL, J. & HALLIDAY, G. 2003. Survival in frontotemporal dementia. *Neurology,* 61**,** 349-54.
HOEK, K. S., KIDD, G. J., CARSON, J. H. & SMITH, R. 1998. hnRNP A2 selectively binds the cytoplasmic transport sequence of myelin basic protein mRNA. *Biochemistry,* 37**,** 7021-9.
HOVHANNISYAN, R. H. & CARSTENS, R. P. 2007. Heterogeneous ribonucleoprotein m is a splicing regulatory protein that can enhance or silence splicing of alternatively spliced exons. *J Biol Chem,* 282**,** 36265-74.
HSIEH, S., CAGA, J., LESLIE, F. V., SHIBATA, M., DAVESON, N., FOXE, D., RAMSEY, E., LILLO, P., AHMED, R. M., DEVENNEY, E., BURRELL, J. R., HODGES, J. R., KIERNAN, M. C. & MIOSHI, E. 2016. Cognitive and Behavioral Symptoms in ALSFTD: Detection, Differentiation, and Progression. *J Geriatr Psychiatry Neurol,* 29**,** 3-10.
HSIUNG, G. Y., DEJESUS-HERNANDEZ, M., FELDMAN, H. H., SENGDY, P., BOUCHARD-KERR, P., DWOSH, E., BUTLER, R., LEUNG, B., FOK, A., RUTHERFORD, N. J., BAKER, M., RADEMAKERS, R. & MACKENZIE, I. R. 2012. Clinical and pathological features of familial frontotemporal dementia caused by C9ORF72 mutation on chromosome 9p. *Brain,* 135**,** 709-22.
HU, F., PADUKKAVIDANA, T., VAEGTER, C. B., BRADY, O. A., ZHENG, Y., MACKENZIE, I. R., FELDMAN, H. H., NYKJAER, A. & STRITTMATTER, S. M. 2010. Sortilin-mediated endocytosis determines levels of the frontotemporal dementia protein, progranulin. *Neuron,* 68**,** 654-67.
HUANG, S. N., MINASSIAN, H. & MORE, J. D. 1976. Application of immunofluorescent staining on paraffin sections improved by trypsin digestion. *Lab Invest,* 35**,** 383-90.
HUTTON, M., LENDON, C. L., RIZZU, P., BAKER, M., FROELICH, S., HOULDEN, H., PICKERING-BROWN, S., CHAKRAVERTY, S., ISAACS, A., GROVER, A., HACKETT, J., ADAMSON, J., LINCOLN, S., DICKSON, D., DAVIES, P., PETERSEN, R. C., STEVENS, M., DE GRAAFF, E., WAUTERS, E., VAN BAREN, J., HILLEBRAND, M., JOOSSE, M., KWON, J. M., NOWOTNY, P., CHE, L. K., NORTON, J., MORRIS, J. C., REED, L. A., TROJANOWSKI, J., BASUN, H., LANNFELT, L., NEYSTAT, M., FAHN, S., DARK, F., TANNENBERG, T., DODD,

P. R., HAYWARD, N., KWOK, J. B., SCHOFIELD, P. R., ANDREADIS, A., SNOWDEN, J., CRAUFURD, D., NEARY, D., OWEN, F., OOSTRA, B. A., HARDY, J., GOATE, A., VAN SWIETEN, J., MANN, D., LYNCH, T. & HEUTINK, P. 1998. Association of missense and 5'-splice-site mutations in tau with the inherited dementia FTDP-17. *Nature,* 393**,** 702-5.

IGAZ, L. M., KWONG, L. K., CHEN-PLOTKIN, A., WINTON, M. J., UNGER, T. L., XU, Y., NEUMANN, M., TROJANOWSKI, J. Q. & LEE, V. M. 2009. Expression of TDP-43 C-terminal Fragments in Vitro Recapitulates Pathological Features of TDP-43 Proteinopathies. *J Biol Chem,* 284**,** 8516-24.

ISHIHARA, K., ARAKI, S., IHORI, N., SHIOTA, J., KAWAMURA, M., YOSHIDA, M., HASHIZUME, Y. & NAKANO, I. 2005. Argyrophilic grain disease presenting with frontotemporal dementia: a neuropsychological and pathological study of an autopsied case with presenile onset. *Neuropathology,* 25**,** 165-70.

JANSSENS, J. & VAN BROECKHOVEN, C. 2013. Pathological mechanisms underlying TDP-43 driven neurodegeneration in FTLD-ALS spectrum disorders. *Hum Mol Genet,* 22**,** R77-87.

JINWAL, U. K., ABISAMBRA, J. F., ZHANG, J., DHARIA, S., O'LEARY, J. C., PATEL, T., BRASWELL, K., JANI, T., GESTWICKI, J. E. & DICKEY, C. A. 2012. Cdc37/Hsp90 protein complex disruption triggers an autophagic clearance cascade for TDP-43 protein. *J Biol Chem,* 287**,** 24814-20.

JOHNSON, B. S., MCCAFFERY, J. M., LINDQUIST, S. & GITLER, A. D. 2008. A yeast TDP-43 proteinopathy model: Exploring the molecular determinants of TDP-43 aggregation and cellular toxicity. *Proc Natl Acad Sci U S A,* 105**,** 6439-44.

JOHNSON, J. O., MANDRIOLI, J., BENATAR, M., ABRAMZON, Y., VAN DEERLIN, V. M., TROJANOWSKI, J. Q., GIBBS, J. R., BRUNETTI, M., GRONKA, S., WUU, J., DING, J., MCCLUSKEY, L., MARTINEZ-LAGE, M., FALCONE, D., HERNANDEZ, D. G., AREPALLI, S., CHONG, S., SCHYMICK, J. C., ROTHSTEIN, J., LANDI, F., WANG, Y.-D., CALVO, A., MORA, G., SABATELLI, M., MONSURRÒ, M. R., BATTISTINI, S., SALVI, F., SPATARO, R., SOLA, P., BORGHERO, G., GALASSI, G., SCHOLZ, S. W., TAYLOR, J. P., RESTAGNO, G., CHIÒ, A. & TRAYNOR, B. J. 2010. Exome Sequencing Reveals VCP Mutations as a Cause of Familial ALS. *Neuron,* 68**,** 857-864.

JOSEPHS, K. A., HODGES, J. R., SNOWDEN, J. S., MACKENZIE, I. R., NEUMANN, M., MANN, D. M. & DICKSON, D. W. 2011. Neuropathological background of phenotypical variability in frontotemporal dementia. *Acta Neuropathol,* 122**,** 137-53.

JOSEPHS, K. A., STROH, A., DUGGER, B. & DICKSON, D. W. 2009. Evaluation of subcortical pathology and clinical correlations in FTLD-U subtypes. *Acta Neuropathol,* 118**,** 349-58.

KABASHI, E., VALDMANIS, P. N., DION, P., SPIEGELMAN, D., MCCONKEY, B. J., VELDE, C. V., BOUCHARD, J.-P., LACOMBLEZ, L., POCHIGAEVA, K., SALACHAS, F., PRADAT, P.-F., CAMU, W., MEININGER, V., DUPRE, N. & ROULEAU, G. A. 2008. TARDBP mutations in individuals with sporadic and familial amyotrophic lateral sclerosis. *Nat Genet,* 40**,** 572-574.

KAFASLA, P., PATRINOU-GEORGOULA, M., LEWIS, J. D. & GUIALIS, A. 2002. Association of the 72/74-kDa proteins, members of the heterogeneous nuclear ribonucleoprotein M group, with the pre-mRNA at early stages of spliceosome assembly. *Biochem J,* 363**,** 793-9.

KAIVORINNE, A. L., MOILANEN, V., KERVINEN, M., RENTON, A. E., TRAYNOR, B. J., MAJAMAA, K. & REMES, A. M. 2014. Novel TARDBP sequence variant and C9ORF72 repeat expansion in a family with frontotemporal dementia. *Alzheimer Dis Assoc Disord,* 28**,** 190-3.

KANSAL, K., MAREDDY, M., SLOANE, K. L., MINC, A. A., RABINS, P. V., MCGREADY, J. B. & ONYIKE, C. U. 2016. Survival in Frontotemporal Dementia Phenotypes: A Meta-Analysis. *Dement Geriatr Cogn Disord,* 41**,** 109-22.

KASHIMA, T., RAO, N., DAVID, C. J. & MANLEY, J. L. 2007. hnRNP A1 functions with specificity in repression of SMN2 exon 7 splicing. *Hum Mol Genet,* 16**,** 3149-59.

KAWAHARA, Y. & MIEDA-SATO, A. 2012. TDP-43 promotes microRNA biogenesis as a component of the Drosha and Dicer complexes. *Proc Natl Acad Sci U S A,* 109**,** 3347-52.

KILEDJIAN, M., DAY, N. & TRIFILLIS, P. 1999. Purification and RNA Binding Properties of the Polycytidylate-Binding Proteins αCP1 and αCP2. *Methods,* 17**,** 84-91.

KIM, E. J., SIDHU, M., GAUS, S. E., HUANG, E. J., HOF, P. R., MILLER, B. L., DEARMOND, S. J. & SEELEY, W. W. 2012. Selective frontoinsular von Economo neuron and fork cell loss in early behavioral variant frontotemporal dementia. *Cereb Cortex,* 22**,** 251-9.

KIM, H. J., KIM, N. C., WANG, Y. D., SCARBOROUGH, E. A., MOORE, J., DIAZ, Z., MACLEA, K. S., FREIBAUM, B., LI, S., MOLLIEX, A., KANAGARAJ, A. P., CARTER, R., BOYLAN, K. B., WOJTAS, A. M., RADEMAKERS, R., PINKUS, J. L., GREENBERG, S. A., TROJANOWSKI, J. Q., TRAYNOR, B. J., SMITH, B. N., TOPP, S., GKAZI, A. S., MILLER, J., SHAW, C. E.,

KOTTLORS, M., KIRSCHNER, J., PESTRONK, A., LI, Y. R., FORD, A. F., GITLER, A. D., BENATAR, M., KING, O. D., KIMONIS, V. E., ROSS, E. D., WEIHL, C. C., SHORTER, J. & TAYLOR, J. P. 2013. Mutations in prion-like domains in hnRNPA2B1 and hnRNPA1 cause multisystem proteinopathy and ALS. *Nature,* 495**,** 467-73.

KIM, H. J., RAPHAEL, A. R., LADOW, E. S., MCGURK, L., WEBER, R. A., TROJANOWSKI, J. Q., LEE, V. M., FINKBEINER, S., GITLER, A. D. & BONINI, N. M. 2014. Therapeutic modulation of eIF2alpha phosphorylation rescues TDP-43 toxicity in amyotrophic lateral sclerosis disease models. *Nat Genet,* 46**,** 152-60.

KIM, J. H., PAEK, K. Y., CHOI, K., KIM, T. D., HAHM, B., KIM, K. T. & JANG, S. K. 2003. Heterogeneous nuclear ribonucleoprotein C modulates translation of c-myc mRNA in a cell cycle phase-dependent manner. *Mol Cell Biol,* 23**,** 708-20.

KIMONIS, V. E., MEHTA, S. G., FULCHIERO, E. C., THOMASOVA, D., PASQUALI, M., BOYCOTT, K., NEILAN, E. G., KARTASHOV, A., FORMAN, M. S., TUCKER, S., KIMONIS, K., MUMM, S., WHYTE, M. P., SMITH, C. D. & WATTS, G. D. 2008. Clinical studies in familial VCP myopathy associated with Paget disease of bone and frontotemporal dementia. *Am J Med Genet A,* 146A**,** 745-57.

KIPPS, C. M., HODGES, J. R. & HORNBERGER, M. 2010. Nonprogressive behavioural frontotemporal dementia: recent developments and clinical implications of the 'bvFTD phenocopy syndrome'. *Curr Opin Neurol,* 23**,** 628-32.

KOVACS, G. G., MURRELL, J. R., HORVATH, S., HARASZTI, L., MAJTENYI, K., MOLNAR, M. J., BUDKA, H., GHETTI, B. & SPINA, S. 2009. TARDBP variation associated with frontotemporal dementia, supranuclear gaze palsy, and chorea. *Mov Disord,* 24**,** 1843-7.

KOVACS, G. G., ROZEMULLER, A. J., VAN SWIETEN, J. C., GELPI, E., MAJTENYI, K., AL-SARRAJ, S., TROAKES, C., BODI, I., KING, A., HORTOBAGYI, T., ESIRI, M. M., ANSORGE, O., GIACCONE, G., FERRER, I., ARZBERGER, T., BOGDANOVIC, N., NILSSON, T., LEISSER, I., ALAFUZOFF, I., IRONSIDE, J. W., KRETZSCHMAR, H. & BUDKA, H. 2012. Neuropathology of the hippocampus in FTLD-Tau with Pick bodies: A study of the BrainNet Europe Consortium. *Neuropathol Appl Neurobiol*.

KOVACS, G. G., VAN DER ZEE, J., HORT, J., KRISTOFERITSCH, W., LEITHA, T., HÖFTBERGER, R., STRÖBEL, T., VAN BROECKHOVEN, C. & MATEJ, R. 2016. Clinicopathological description of two cases with SQSTM1 gene mutation associated with frontotemporal dementia. *Neuropathology,* 36**,** 27-38.

KOVAR, H. 2011. Dr. Jekyll and Mr. Hyde: The Two Faces of the FUS/EWS/TAF15 Protein Family. *Sarcoma,* 2011**,** 837474.

KWIATKOWSKI, T. J., JR., BOSCO, D. A., LECLERC, A. L., TAMRAZIAN, E., VANDERBURG, C. R., RUSS, C., DAVIS, A., GILCHRIST, J., KASARSKIS, E. J., MUNSAT, T., VALDMANIS, P., ROULEAU, G. A., HOSLER, B. A., CORTELLI, P., DE JONG, P. J., YOSHINAGA, Y., HAINES, J. L., PERICAK-VANCE, M. A., YAN, J., TICOZZI, N., SIDDIQUE, T., MCKENNA-YASEK, D., SAPP, P. C., HORVITZ, H. R., LANDERS, J. E. & BROWN, R. H., JR. 2009. Mutations in the FUS/TLS gene on chromosome 16 cause familial amyotrophic lateral sclerosis. *Science,* 323**,** 1205-8.

LAGIER-TOURENNE, C., BAUGHN, M., RIGO, F., SUN, S., LIU, P., LI, H. R., JIANG, J., WATT, A. T., CHUN, S., KATZ, M., QIU, J., SUN, Y., LING, S. C., ZHU, Q., POLYMENIDOU, M., DRENNER, K., ARTATES, J. W., MCALONIS-DOWNES, M., MARKMILLER, S., HUTT, K. R., PIZZO, D. P., CADY, J., HARMS, M. B., BALOH, R. H., VANDENBERG, S. R., YEO, G. W., FU, X. D., BENNETT, C. F., CLEVELAND, D. W. & RAVITS, J. 2013. Targeted degradation of sense and antisense C9orf72 RNA foci as therapy for ALS and frontotemporal degeneration. *Proc Natl Acad Sci U S A,* 110**,** E4530-9.

LAGIER-TOURENNE, C., POLYMENIDOU, M. & CLEVELAND, D. W. 2010. TDP-43 and FUS/TLS: emerging roles in RNA processing and neurodegeneration. *Hum Mol Genet,* 19**,** R46-64.

LAIRD, A. S., VAN HOECKE, A., DE MUYNCK, L., TIMMERS, M., VAN DEN BOSCH, L., VAN DAMME, P. & ROBBERECHT, W. 2010. Progranulin is neurotrophic in vivo and protects against a mutant TDP-43 induced axonopathy. *PLoS One,* 5**,** e13368.

LAMBERT, M. A., BICKEL, H., PRINCE, M., FRATIGLIONI, L., VON STRAUSS, E., FRYDECKA, D., KIEJNA, A., GEORGES, J. & REYNISH, E. L. 2014. Estimating the burden of early onset dementia; systematic review of disease prevalence. *European Journal of Neurology,* 21**,** 563-569.

LAW, W. J., CANN, K. L. & HICKS, G. G. 2006. TLS, EWS and TAF15: a model for transcriptional integration of gene expression. *Brief Funct Genomic Proteomic,* 5**,** 8-14.

LE BER, I., VAN BORTEL, I., NICOLAS, G., BOUYA-AHMED, K., CAMUZAT, A., WALLON, D., DE SEPTENVILLE, A., LATOUCHE, M., LATTANTE, S., KABASHI, E., JORNEA, L., HANNEQUIN, D. & BRICE, A. 2014. hnRNPA2B1 and hnRNPA1 mutations are rare in patients with "multisystem proteinopathy" and frontotemporal lobar degeneration phenotypes. *Neurobiol Aging,* 35**,** 934.e5-6.

LEE, G. & LEUGERS, C. J. 2012. Tau and Tauopathies. *Prog Mol Biol Transl Sci,* 107**,** 263-93.

LEE, Y.-B., CHEN, H.-J., PERES, JOÃO N., GOMEZ-DEZA, J., ATTIG, J., ŠTALEKAR, M., TROAKES, C., NISHIMURA, AGNES L., SCOTTER, EMMA L., VANCE, C., ADACHI, Y., SARDONE, V., MILLER, JACK W., SMITH, BRADLEY N., GALLO, J.-M., ULE, J., HIRTH, F., ROGELJ, B., HOUART, C. & SHAW, CHRISTOPHER E. 2013a. Hexanucleotide Repeats in ALS/FTD Form Length-Dependent RNA Foci, Sequester RNA Binding Proteins, and Are Neurotoxic. *Cell Reports,* 5**,** 1178-1186.

LEE, Y. B., CHEN, H. J., PERES, J. N., GOMEZ-DEZA, J., ATTIG, J., STALEKAR, M., TROAKES, C., NISHIMURA, A. L., SCOTTER, E. L., VANCE, C., ADACHI, Y., SARDONE, V., MILLER, J. W., SMITH, B. N., GALLO, J. M., ULE, J., HIRTH, F., ROGELJ, B., HOUART, C. & SHAW, C. E. 2013b. Hexanucleotide repeats in ALS/FTD form length-dependent RNA foci, sequester RNA binding proteins, and are neurotoxic. *Cell Rep,* 5**,** 1178-86.

LI, Y. Q., TAN, M. S., YU, J. T. & TAN, L. 2016. Frontotemporal Lobar Degeneration: Mechanisms and Therapeutic Strategies. *Mol Neurobiol,* 53**,** 6091-6105.

LING, S. C., POLYMENIDOU, M. & CLEVELAND, D. W. 2013. Converging mechanisms in ALS and FTD: disrupted RNA and protein homeostasis. *Neuron,* 79**,** 416-38.

LIU-YESUCEVITZ, L., BILGUTAY, A., ZHANG, Y. J., VANDERWEYDE, T., CITRO, A., MEHTA, T., ZAARUR, N., MCKEE, A., BOWSER, R., SHERMAN, M., PETRUCELLI, L. & WOLOZIN, B. 2010. Tar DNA binding protein-43 (TDP-43) associates with stress granules: analysis of cultured cells and pathological brain tissue. *PLoS One,* 5**,** e13250.

LLERES, D., DENEGRI, M., BIGGIOGERA, M., AJUH, P. & LAMOND, A. I. 2010. Direct interaction between hnRNP-M and CDC5L/PLRG1 proteins affects alternative splice site choice. *EMBO Rep,* 11**,** 445-51.

MACKENZIE, I. R. 2007a. The neuropathology and clinical phenotype of FTD with progranulin mutations. *Acta Neuropathol,* 114**,** 49-54.

MACKENZIE, I. R. 2007b. The neuropathology of FTD associated With ALS. *Alzheimer Dis Assoc Disord,* 21**,** S44-9.

MACKENZIE, I. R., ARZBERGER, T., KREMMER, E., TROOST, D., LORENZL, S., MORI, K., WENG, S. M., HAASS, C., KRETZSCHMAR, H. A., EDBAUER, D. & NEUMANN, M. 2013. Dipeptide repeat protein pathology in C9ORF72 mutation cases: clinico-pathological correlations. *Acta Neuropathol,* 126**,** 859-79.

MACKENZIE, I. R., BABORIE, A., PICKERING-BROWN, S., DU PLESSIS, D., JAROS, E., PERRY, R. H., NEARY, D., SNOWDEN, J. S. & MANN, D. M. 2006. Heterogeneity of ubiquitin pathology in frontotemporal lobar degeneration: classification and relation to clinical phenotype. *Acta Neuropathol,* 112**,** 539-49.

MACKENZIE, I. R., MUNOZ, D. G., KUSAKA, H., YOKOTA, O., ISHIHARA, K., ROEBER, S., KRETZSCHMAR, H. A., CAIRNS, N. J. & NEUMANN, M. 2011a. Distinct pathological subtypes of FTLD-FUS. *Acta Neuropathol,* 121**,** 207-18.

MACKENZIE, I. R. & NEUMANN, M. 2016. Molecular neuropathology of frontotemporal dementia: insights into disease mechanisms from postmortem studies. *J Neurochem*.

MACKENZIE, I. R., NEUMANN, M., BIGIO, E. H., CAIRNS, N. J., ALAFUZOFF, I., KRIL, J., KOVACS, G. G., GHETTI, B., HALLIDAY, G., HOLM, I. E., INCE, P. G., KAMPHORST, W., REVESZ, T., ROZEMULLER, A. J., KUMAR-SINGH, S., AKIYAMA, H., BABORIE, A., SPINA, S., DICKSON, D. W., TROJANOWSKI, J. Q. & MANN, D. M. 2009. Nomenclature for neuropathologic subtypes of frontotemporal lobar degeneration: consensus recommendations. *Acta Neuropathol,* 117**,** 15-8.

MACKENZIE, I. R., NEUMANN, M., BIGIO, E. H., CAIRNS, N. J., ALAFUZOFF, I., KRIL, J., KOVACS, G. G., GHETTI, B., HALLIDAY, G., HOLM, I. E., INCE, P. G., KAMPHORST, W., REVESZ, T., ROZEMULLER, A. J., KUMAR-SINGH, S., AKIYAMA, H., BABORIE, A., SPINA, S., DICKSON, D. W., TROJANOWSKI, J. Q. & MANN, D. M. 2010a. Nomenclature and nosology for neuropathologic subtypes of frontotemporal lobar degeneration: an update. *Acta Neuropathol,* 119**,** 1-4.

MACKENZIE, I. R. A., NEUMANN, M., BABORIE, A., SAMPATHU, D. M., PLESSIS, D. D., JAROS, E., PERRY, R. H., TROJANOWSKI, J. Q., MANN, D. M. A. & LEE, V. M. Y. 2011b. A harmonized classification system for FTLD-TDP pathology. *Acta Neuropathol,* 122**,** 111-3.

MACKENZIE, I. R. A., RADEMAKERS, R. & NEUMANN, M. 2010b. TDP-43 and FUS in amyotrophic lateral sclerosis and frontotemporal dementia. *The Lancet Neurology,* 9**,** 995-1007.
MAEKAWA, S., LEIGH, P. N., KING, A., JONES, E., STEELE, J. C., BODI, I., SHAW, C. E., HORTOBAGYI, T. & AL-SARRAJ, S. 2009. TDP-43 is consistently co-localized with ubiquitinated inclusions in sporadic and Guam amyotrophic lateral sclerosis but not in familial amyotrophic lateral sclerosis with and without SOD1 mutations. *Neuropathology,* 29**,** 672-83.
MAKEYEV, A. V., CHKHEIDZE, A. N. & LIEBHABER, S. A. 1999. A set of highly conserved RNA-binding proteins, alphaCP-1 and alphaCP-2, implicated in mRNA stabilization, are coexpressed from an intronless gene and its intron-containing paralog. *J Biol Chem,* 274**,** 24849-57.
MAKEYEV, A. V. & LIEBHABER, S. A. 2002. The poly(C)-binding proteins: a multiplicity of functions and a search for mechanisms. *RNA,* 8**,** 265-78.
MANN, D. M., ROLLINSON, S., ROBINSON, A., BENNION CALLISTER, J., THOMPSON, J. C., SNOWDEN, J. S., GENDRON, T., PETRUCELLI, L., MASUDA-SUZUKAKE, M., HASEGAWA, M., DAVIDSON, Y. & PICKERING-BROWN, S. 2013. Dipeptide repeat proteins are present in the p62 positive inclusions in patients with frontotemporal lobar degeneration and motor neurone disease associated with expansions in C9ORF72. *Acta Neuropathol Commun,* 1**,** 68.
MANN, M. 2006. Functional and quantitative proteomics using SILAC. *Nat Rev Mol Cell Biol,* 7**,** 952-8.
MAO, X., LIU, J., CHEN, C., ZHANG, W., QIAN, R., CHEN, X., LU, H., GE, J., ZHAO, C., ZHANG, D. & WANG, Y. 2016. PCBP2 Modulates Neural Apoptosis and Astrocyte Proliferation After Spinal Cord Injury. *Neurochem Res*.
MARKO, M., LEICHTER, M., PATRINOU-GEORGOULA, M. & GUIALIS, A. 2010. hnRNP M interacts with PSF and p54(nrb) and co-localizes within defined nuclear structures. *Exp Cell Res,* 316**,** 390-400.
MARKO, M., LEICHTER, M., PATRINOU-GEORGOULA, M. & GUIALIS, A. 2014. Selective interactions of hnRNP M isoforms with the TET proteins TAF15 and TLS/FUS. *Mol Biol Rep,* 41**,** 2687-95.
MARKOVTSOV, V., NIKOLIC, J. M., GOLDMAN, J. A., TURCK, C. W., CHOU, M. Y. & BLACK, D. L. 2000. Cooperative assembly of an hnRNP complex induced by a tissue-specific homolog of polypyrimidine tract binding protein. *Mol Cell Biol,* 20**,** 7463-79.
MARTIN, J. B. 1999a. Molecular basis of the neurodegenerative disorders. *N Engl J Med,* 340**,** 1970-80.
MARTIN, L. J. 1999b. Neuronal death in amyotrophic lateral sclerosis is apoptosis: possible contribution of a programmed cell death mechanism. *J Neuropathol Exp Neurol,* 58**,** 459-71.
MAYEDA, A. & KRAINER, A. R. 1992. Regulation of alternative pre-mRNA splicing by hnRNP A1 and splicing factor SF2. *Cell,* 68**,** 365-75.
MCAFEE, J. G., SOLTANINASSAB, S. R., LINDSAY, M. E. & LESTOURGEON, W. M. 1996. Proteins C1 and C2 of heterogeneous nuclear ribonucleoprotein complexes bind RNA in a highly cooperative fashion: support for their contiguous deposition on pre-mRNA during transcription. *Biochemistry,* 35**,** 1212-22.
MCDONALD, K. K., AULAS, A., DESTROISMAISONS, L., PICKLES, S., BELEAC, E., CAMU, W., ROULEAU, G. A. & VANDE VELDE, C. 2011. TAR DNA-binding protein 43 (TDP-43) regulates stress granule dynamics via differential regulation of G3BP and TIA-1. *Hum Mol Genet,* 20**,** 1400-10.
MCGURK, L., LEE, V. M., TROJANOWKSI, J. Q., VAN DEERLIN, V. M., LEE, E. B. & BONINI, N. M. 2014. Poly-A binding protein-1 localization to a subset of TDP-43 inclusions in amyotrophic lateral sclerosis occurs more frequently in patients harboring an expansion in C9orf72. *J Neuropathol Exp Neurol,* 73**,** 837-45.
MELCHIOR, F., PASCHAL, B., EVANS, J. & GERACE, L. 1993. Inhibition of nuclear protein import by nonhydrolyzable analogues of GTP and identification of the small GTPase Ran/TC4 as an essential transport factor. *J Cell Biol,* 123**,** 1649-59.
MERCADO, P. A., AYALA, Y. M., ROMANO, M., BURATTI, E. & BARALLE, F. E. 2005. Depletion of TDP 43 overrides the need for exonic and intronic splicing enhancers in the human apoA-II gene. *Nucleic Acids Res,* 33**,** 6000-10.
MESULAM, M. M. 2001. Primary progressive aphasia. *Ann Neurol,* 49**,** 425-32.
MEYEROWITZ, J., PARKER, S. J., VELLA, L. J., NG, D. C. H., PRICE, K. A., LIDDELL, J. R., CARAGOUNIS, A., LI, Q. X., MASTERS, C. L., NONAKA, T., HASEGAWA, M., BOGOYEVITCH, M. A., KANNINEN, K. M., CROUCH, P. J. & WHITE, A. R. 2011. C-Jun N-

terminal kinase controls TDP-43 accumulation in stress granules induced by oxidative stress. *Mol Neurodegener,* 6**,** 57.
MICHELOTTI, E. F., MICHELOTTI, G. A., ARONSOHN, A. I. & LEVENS, D. 1996. Heterogeneous nuclear ribonucleoprotein K is a transcription factor. *Mol Cell Biol,* 16**,** 2350-60.
MITSUYAMA, Y. & INOUE, T. 2009. Clinical entity of frontotemporal dementia with motor neuron disease. *Neuropathology,* 29**,** 649-54.
MIYOSHI, K. 2009. What is 'early onset dementia'? *Psychogeriatrics,* 9**,** 67-72.
MOHAGHEGHI, F., PRUDENCIO, M., STUANI, C., COOK, C., JANSEN-WEST, K., DICKSON, D. W., PETRUCELLI, L. & BURATTI, E. 2016. TDP-43 functions within a network of hnRNP proteins to inhibit the production of a truncated human SORT1 receptor. *Hum Mol Genet,* 25**,** 534-45.
MOISSE, K., MEPHAM, J., VOLKENING, K., WELCH, I., HILL, T. & STRONG, M. J. 2009. Cytosolic TDP-43 expression following axotomy is associated with caspase 3 activation in NFL-/- mice: support for a role for TDP-43 in the physiological response to neuronal injury. *Brain Res,* 1296**,** 176-86.
MONAHAN, Z., SHEWMAKER, F. & PANDEY, U. B. 2016. Stress granules at the intersection of autophagy and ALS. *Brain Res*.
MORI, K., ARZBERGER, T., GRASSER, F. A., GIJSELINCK, I., MAY, S., RENTZSCH, K., WENG, S. M., SCHLUDI, M. H., VAN DER ZEE, J., CRUTS, M., VAN BROECKHOVEN, C., KREMMER, E., KRETZSCHMAR, H. A., HAASS, C. & EDBAUER, D. 2013a. Bidirectional transcripts of the expanded C9orf72 hexanucleotide repeat are translated into aggregating dipeptide repeat proteins. *Acta Neuropathol,* 126**,** 881-93.
MORI, K., LAMMICH, S., MACKENZIE, I. R., FORNE, I., ZILOW, S., KRETZSCHMAR, H., EDBAUER, D., JANSSENS, J., KLEINBERGER, G., CRUTS, M., HERMS, J., NEUMANN, M., VAN BROECKHOVEN, C., ARZBERGER, T. & HAASS, C. 2013b. hnRNP A3 binds to GGGGCC repeats and is a constituent of p62-positive/TDP43-negative inclusions in the hippocampus of patients with C9orf72 mutations. *Acta Neuropathol,* 125**,** 413-23.
MORI, K., WENG, S. M., ARZBERGER, T., MAY, S., RENTZSCH, K., KREMMER, E., SCHMID, B., KRETZSCHMAR, H. A., CRUTS, M., VAN BROECKHOVEN, C., HAASS, C. & EDBAUER, D. 2013c. The C9orf72 GGGGCC repeat is translated into aggregating dipeptide-repeat proteins in FTLD/ALS. *Science,* 339**,** 1335-8.
MOURELATOS, Z., ABEL, L., YONG, J., KATAOKA, N. & DREYFUSS, G. 2001. SMN interacts with a novel family of hnRNP and spliceosomal proteins. *EMBO J,* 20**,** 5443-52.
MOURSY, A., ALLAIN, F. H. & CLERY, A. 2014. Characterization of the RNA recognition mode of hnRNP G extends its role in SMN2 splicing regulation. *Nucleic Acids Res,* 42**,** 6659-72.
MUNOZ, D. G., NEUMANN, M., KUSAKA, H., YOKOTA, O., ISHIHARA, K., TERADA, S., KURODA, S. & MACKENZIE, I. R. 2009. FUS pathology in basophilic inclusion body disease. *Acta Neuropathol,* 118**,** 617-27.
NAN, Y. N., ZHU, J. Y., TAN, Y., ZHANG, Q., JIA, W. & HUA, Q. 2014. Staurosporine induced apoptosis rapidly downregulates TDP- 43 in glioma cells. *Asian Pac J Cancer Prev,* 15**,** 3575-9.
NEARY, D., SNOWDEN, J. S., GUSTAFSON, L., PASSANT, U., STUSS, D., BLACK, S., FREEDMAN, M., KERTESZ, A., ROBERT, P. H., ALBERT, M., BOONE, K., MILLER, B. L., CUMMINGS, J. & BENSON, D. F. 1998. Frontotemporal lobar degeneration: a consensus on clinical diagnostic criteria. *Neurology,* 51**,** 1546-54.
NEUMANN, M., BENTMANN, E., DORMANN, D., JAWAID, A., DEJESUS-HERNANDEZ, M., ANSORGE, O., ROEBER, S., KRETZSCHMAR, H. A., MUNOZ, D. G., KUSAKA, H., YOKOTA, O., ANG, L. C., BILBAO, J., RADEMAKERS, R., HAASS, C. & MACKENZIE, I. R. 2011. FET proteins TAF15 and EWS are selective markers that distinguish FTLD with FUS pathology from amyotrophic lateral sclerosis with FUS mutations. *Brain,* 134**,** 2595-609.
NEUMANN, M., KWONG, L. K., LEE, E. B., KREMMER, E., FLATLEY, A., XU, Y., FORMAN, M. S., TROOST, D., KRETZSCHMAR, H. A., TROJANOWSKI, J. Q. & LEE, V. M. 2009a. Phosphorylation of S409/410 of TDP-43 is a consistent feature in all sporadic and familial forms of TDP-43 proteinopathies. *Acta Neuropathol,* 117**,** 137-49.
NEUMANN, M., KWONG, L. K., TRUAX, A. C., VANMASSENHOVE, B., KRETZSCHMAR, H. A., VAN DEERLIN, V. M., CLARK, C. M., GROSSMAN, M., MILLER, B. L., TROJANOWSKI, J. Q. & LEE, V. M. 2007a. TDP-43-positive white matter pathology in frontotemporal lobar degeneration with ubiquitin-positive inclusions. *J Neuropathol Exp Neurol,* 66**,** 177-83.
NEUMANN, M., MACKENZIE, I. R., CAIRNS, N. J., BOYER, P. J., MARKESBERY, W. R., SMITH, C. D., TAYLOR, J. P., KRETZSCHMAR, H. A., KIMONIS, V. E. & FORMAN, M. S. 2007b. TDP-

43 in the ubiquitin pathology of frontotemporal dementia with VCP gene mutations. *J Neuropathol Exp Neurol,* 66**,** 152-7.
NEUMANN, M., RADEMAKERS, R., ROEBER, S., BAKER, M., KRETZSCHMAR, H. A. & MACKENZIE, I. R. 2009b. A new subtype of frontotemporal lobar degeneration with FUS pathology. *Brain,* 132**,** 2922-31.
NEUMANN, M., ROEBER, S., KRETZSCHMAR, H. A., RADEMAKERS, R., BAKER, M. & MACKENZIE, I. R. 2009c. Abundant FUS-immunoreactive pathology in neuronal intermediate filament inclusion disease. *Acta Neuropathol,* 118**,** 605-16.
NEUMANN, M., SAMPATHU, D. M., KWONG, L. K., TRUAX, A. C., MICSENYI, M. C., CHOU, T. T., BRUCE, J., SCHUCK, T., GROSSMAN, M., CLARK, C. M., MCCLUSKEY, L. F., MILLER, B. L., MASLIAH, E., MACKENZIE, I. R., FELDMAN, H., FEIDEN, W., KRETZSCHMAR, H. A., TROJANOWSKI, J. Q. & LEE, V. M. 2006a. Ubiquitinated TDP-43 in frontotemporal lobar degeneration and amyotrophic lateral sclerosis. *Science,* 314**,** 130-3.
NEUMANN, M., SAMPATHU, D. M., KWONG, L. K., TRUAX, A. C., MICSENYI, M. C., CHOU, T. T., BRUCE, J., SCHUCK, T., GROSSMAN, M., CLARK, C. M., MCCLUSKEY, L. F., MILLER, B. L., MASLIAH, E., MACKENZIE, I. R., FELDMAN, H., FEIDEN, W., KRETZSCHMAR, H. A., TROJANOWSKI, J. Q. & LEE, V. M. Y. 2006b. Ubiquitinated TDP-43 in frontotemporal lobar degeneration and amyotrophic lateral sclerosis. *Science,* 314**,** 130-133.
NEUMANN, M., VALORI, C. F., ANSORGE, O., KRETZSCHMAR, H. A., MUNOZ, D. G., KUSAKA, H., YOKOTA, O., ISHIHARA, K., ANG, L. C., BILBAO, J. M. & MACKENZIE, I. R. 2012. Transportin 1 accumulates specifically with FET proteins but no other transportin cargos in FTLD-FUS and is absent in FUS inclusions in ALS with FUS mutations. *Acta Neuropathol,* 124**,** 705-16.
NIBLOCK, M. & GALLO, J. M. 2012. Tau alternative splicing in familial and sporadic tauopathies. *Biochem Soc Trans,* 40**,** 677-80.
NISHIMURA, A. L., SHUM, C., SCOTTER, E. L., ABDELGANY, A., SARDONE, V., WRIGHT, J., LEE, Y. B., CHEN, H. J., BILICAN, B., CARRASCO, M., MANIATIS, T., CHANDRAN, S., ROGELJ, B., GALLO, J. M. & SHAW, C. E. 2014. Allele-specific knockdown of ALS-associated mutant TDP-43 in neural stem cells derived from induced pluripotent stem cells. *PLoS One,* 9**,** e91269.
NONAKA, T., KAMETANI, F., ARAI, T., AKIYAMA, H. & HASEGAWA, M. 2009. Truncation and pathogenic mutations facilitate the formation of intracellular aggregates of TDP-43. *Hum Mol Genet,* 18**,** 3353-64.
ONG, S. E., BLAGOEV, B., KRATCHMAROVA, I., KRISTENSEN, D. B., STEEN, H., PANDEY, A. & MANN, M. 2002. Stable isotope labeling by amino acids in cell culture, SILAC, as a simple and accurate approach to expression proteomics. *Mol Cell Proteomics,* 1**,** 376-86.
ORPHANIDES, G. & REINBERG, D. 2000. RNA polymerase II elongation through chromatin. *Nature,* 407**,** 471-5.
OU, S. H., WU, F., HARRICH, D., GARCIA-MARTINEZ, L. F. & GAYNOR, R. B. 1995. Cloning and characterization of a novel cellular protein, TDP-43, that binds to human immunodeficiency virus type 1 TAR DNA sequence motifs. *J Virol,* 69**,** 3584-96.
PAHLICH, S., QUERO, L., ROSCHITZKI, B., LEEMANN-ZAKARYAN, R. P. & GEHRING, H. 2009. Analysis of Ewing sarcoma (EWS)-binding proteins: interaction with hnRNP M, U, and RNA-helicases p68/72 within protein-RNA complexes. *J Proteome Res,* 8**,** 4455-65.
PARK, E., IACCARINO, C., LEE, J., KWON, I., BAIK, S. M., KIM, M., SEONG, J. Y., SON, G. H., BORRELLI, E. & KIM, K. 2011. Regulatory roles of heterogeneous nuclear ribonucleoprotein M and Nova-1 protein in alternative splicing of dopamine D2 receptor pre-mRNA. *J Biol Chem,* 286**,** 25301-8.
PARK, Y. Y., KIM, S. B., HAN, H. D., SOHN, B. H., KIM, J. H., LIANG, J., LU, Y., RODRIGUEZ-AGUAYO, C., LOPEZ-BERESTEIN, G., MILLS, G. B., SOOD, A. K. & LEE, J. S. 2013. Tat-activating regulatory DNA-binding protein regulates glycolysis in hepatocellular carcinoma by regulating the platelet isoform of phosphofructokinase through microRNA 520. *Hepatology,* 58**,** 182-91.
PARONETT, E. M., MEECHAN, D. W., KARPINSKI, B. A., LAMANTIA, A.-S. & MAYNARD, T. M. 2015. Ranbp1, Deleted in DiGeorge/22q11.2 Deletion Syndrome, is a Microcephaly Gene That Selectively Disrupts Layer 2/3 Cortical Projection Neuron Generation. *Cerebral Cortex,* 25**,** 3977-3993.
PIGUET, O. 2013. Neurodegenerative disease: Frontotemporal dementia--time to target inflammation? *Nat Rev Neurol,* 9**,** 304-5.

PINOL-ROMA, S. & DREYFUSS, G. 1992. Shuttling of pre-mRNA binding proteins between nucleus and cytoplasm. *Nature,* 355**,** 730-2.
POLYMENIDOU, M., LAGIER-TOURENNE, C., HUTT, K. R., BENNETT, C. F., CLEVELAND, D. W. & YEO, G. W. 2012. Misregulated RNA processing in amyotrophic lateral sclerosis. *Brain Res,* 1462**,** 3-15.
RADEMAKERS, R., NEUMANN, M. & MACKENZIE, I. R. 2012. Advances in understanding the molecular basis of frontotemporal dementia. *Nat Rev Neurol,* 8**,** 423-34.
RAO, V. S., SRINIVAS, K., SUJINI, G. N. & KUMAR, G. N. S. 2014. Protein-Protein Interaction Detection: Methods and Analysis. *International Journal of Proteomics,* 2014**,** 12.
REBEIZ, J. J., KOLODNY, E. H. & RICHARDSON, E. P., JR. 1968. Corticodentatonigral degeneration with neuronal achromasia. *Arch Neurol,* 18**,** 20-33.
RECH, J. E., LESTOURGEON, W. M. & FLICKER, P. F. 1995. Ultrastructural morphology of the hnRNP C protein tetramer. *J Struct Biol,* 114**,** 77-83.
REN, M., VILLAMARIN, A., SHIH, A., COUTAVAS, E., MOORE, M. S., LOCURCIO, M., CLARKE, V., OPPENHEIM, J. D., D'EUSTACHIO, P. & RUSH, M. G. 1995. Separate domains of the Ran GTPase interact with different factors to regulate nuclear protein import and RNA processing. *Molecular and Cellular Biology,* 15**,** 2117-2124.
RENTON, ALAN E., MAJOUNIE, E., WAITE, A., SIMÓN-SÁNCHEZ, J., ROLLINSON, S., GIBBS, J. R., SCHYMICK, JENNIFER C., LAAKSOVIRTA, H., VAN SWIETEN, JOHN C., MYLLYKANGAS, L., KALIMO, H., PAETAU, A., ABRAMZON, Y., REMES, ANNE M., KAGANOVICH, A., SCHOLZ, SONJA W., DUCKWORTH, J., DING, J., HARMER, DANIEL W., HERNANDEZ, DENA G., JOHNSON, JANEL O., MOK, K., RYTEN, M., TRABZUNI, D., GUERREIRO, RITA J., ORRELL, RICHARD W., NEAL, J., MURRAY, A., PEARSON, J., JANSEN, IRIS E., SONDERVAN, D., SEELAAR, H., BLAKE, D., YOUNG, K., HALLIWELL, N., CALLISTER, JANIS B., TOULSON, G., RICHARDSON, A., GERHARD, A., SNOWDEN, J., MANN, D., NEARY, D., NALLS, MICHAEL A., PEURALINNA, T., JANSSON, L., ISOVIITA, V.-M., KAIVORINNE, A.-L., HÖLTTÄ-VUORI, M., IKONEN, E., SULKAVA, R., BENATAR, M., WUU, J., CHIÒ, A., RESTAGNO, G., BORGHERO, G., SABATELLI, M., HECKERMAN, D., ROGAEVA, E., ZINMAN, L., ROTHSTEIN, JEFFREY D., SENDTNER, M., DREPPER, C., EICHLER, EVAN E., ALKAN, C., ABDULLAEV, Z., PACK, SVETLANA D., DUTRA, A., PAK, E., HARDY, J., SINGLETON, A., WILLIAMS, NIGEL M., HEUTINK, P., PICKERING-BROWN, S., MORRIS, HUW R., TIENARI, PENTTI J. & TRAYNOR, BRYAN J. 2011. A Hexanucleotide Repeat Expansion in C9ORF72 Is the Cause of Chromosome 9p21-Linked ALS-FTD. *Neuron,* 72**,** 257-268.
RIBOLDI, G., ZANETTA, C., RANIERI, M., NIZZARDO, M., SIMONE, C., MAGRI, F., BRESOLIN, N., COMI, G. P. & CORTI, S. 2014. Antisense oligonucleotide therapy for the treatment of C9ORF72 ALS/FTD diseases. *Mol Neurobiol,* 50**,** 721-32.
ROBINSON, A. C., THOMPSON, J. C., WEEDON, L., ROLLINSON, S., PICKERING-BROWN, S., SNOWDEN, J. S., DAVIDSON, Y. S. & MANN, D. M. 2014. No interaction between tau and TDP-43 pathologies in either frontotemporal lobar degeneration or motor neurone disease. *Neuropathol Appl Neurobiol,* 40**,** 844-54.
ROEBER, S., MACKENZIE, I. R., KRETZSCHMAR, H. A. & NEUMANN, M. 2008. TDP-43-negative FTLD-U is a significant new clinico-pathological subtype of FTLD. *Acta Neuropathol,* 116**,** 147-57.
ROHRER, J. D., GESER, F., ZHOU, J., GENNATAS, E. D., SIDHU, M., TROJANOWSKI, J. Q., DEARMOND, S. J., MILLER, B. L. & SEELEY, W. W. 2010. TDP-43 subtypes are associated with distinct atrophy patterns in frontotemporal dementia. *Neurology,* 75**,** 2204-11.
ROHRER, J. D., NICHOLAS, J. M., CASH, D. M., VAN SWIETEN, J., DOPPER, E., JISKOOT, L., VAN MINKELEN, R., ROMBOUTS, S. A., CARDOSO, M. J., CLEGG, S., ESPAK, M., MEAD, S., THOMAS, D. L., DE VITA, E., MASELLIS, M., BLACK, S. E., FREEDMAN, M., KEREN, R., MACINTOSH, B. J., ROGAEVA, E., TANG-WAI, D., TARTAGLIA, M. C., LAFORCE, R., JR., TAGLIAVINI, F., TIRABOSCHI, P., REDAELLI, V., PRIONI, S., GRISOLI, M., BORRONI, B., PADOVANI, A., GALIMBERTI, D., SCARPINI, E., ARIGHI, A., FUMAGALLI, G., ROWE, J. B., COYLE-GILCHRIST, I., GRAFF, C., FALLSTROM, M., JELIC, V., STAHLBOM, A. K., ANDERSSON, C., THONBERG, H., LILIUS, L., FRISONI, G. B., PIEVANI, M., BOCCHETTA, M., BENUSSI, L., GHIDONI, R., FINGER, E., SORBI, S., NACMIAS, B., LOMBARDI, G., POLITO, C., WARREN, J. D., OURSELIN, S., FOX, N. C., ROSSOR, M. N. & BINETTI, G. 2015. Presymptomatic cognitive and neuroanatomical changes in genetic frontotemporal dementia in the Genetic Frontotemporal dementia Initiative (GENFI) study: a cross-sectional analysis. *Lancet Neurol,* 14**,** 253-62.

ROMANO, M., BURATTI, E., ROMANO, G., KLIMA, R., DEL BEL BELLUZ, L., STUANI, C., BARALLE, F. & FEIGUIN, F. 2014. Evolutionarily conserved heterogeneous nuclear ribonucleoprotein (hnRNP) A/B proteins functionally interact with human and Drosophila TAR DNA-binding protein 43 (TDP-43). *J Biol Chem,* 289**,** 7121-30.
ROSSOLL, W., JABLONKA, S., ANDREASSI, C., KRONING, A. K., KARLE, K., MONANI, U. R. & SENDTNER, M. 2003. Smn, the spinal muscular atrophy-determining gene product, modulates axon growth and localization of beta-actin mRNA in growth cones of motoneurons. *J Cell Biol,* 163**,** 801-12.
ROSSOLL, W., KRONING, A. K., OHNDORF, U. M., STEEGBORN, C., JABLONKA, S. & SENDTNER, M. 2002. Specific interaction of Smn, the spinal muscular atrophy determining gene product, with hnRNP-R and gry-rbp/hnRNP-Q: a role for Smn in RNA processing in motor axons? *Hum Mol Genet,* 11**,** 93-105.
ROYCHOUDHURY, P., PAUL, R. R., CHOWDHURY, R. & CHAUDHURI, K. 2007. HnRNP E2 is downregulated in human oral cancer cells and the overexpression of hnRNP E2 induces apoptosis. *Mol Carcinog,* 46**,** 198-207.
SAMPATHU, D. M., NEUMANN, M., KWONG, L. K., CHOU, T. T., MICSENYI, M., TRUAX, A., BRUCE, J., GROSSMAN, M., TROJANOWSKI, J. Q. & LEE, V. M. 2006. Pathological heterogeneity of frontotemporal lobar degeneration with ubiquitin-positive inclusions delineated by ubiquitin immunohistochemistry and novel monoclonal antibodies. *Am J Pathol,* 169**,** 1343-52.
SAREEN, D., O'ROURKE, J. G., MEERA, P., MUHAMMAD, A. K., GRANT, S., SIMPKINSON, M., BELL, S., CARMONA, S., ORNELAS, L., SAHABIAN, A., GENDRON, T., PETRUCELLI, L., BAUGHN, M., RAVITS, J., HARMS, M. B., RIGO, F., BENNETT, C. F., OTIS, T. S., SVENDSEN, C. N. & BALOH, R. H. 2013. Targeting RNA foci in iPSC-derived motor neurons from ALS patients with a C9ORF72 repeat expansion. *Sci Transl Med,* 5**,** 208ra149.
SCHLUDI, M. H., MAY, S., GRASSER, F. A., RENTZSCH, K., KREMMER, E., KUPPER, C., KLOPSTOCK, T., ARZBERGER, T. & EDBAUER, D. 2015. Erratum to: Distribution of dipeptide repeat proteins in cellular models and C9orf72 mutation cases suggests link to transcriptional silencing. *Acta Neuropathol,* 130**,** 557-8.
SCOTTER, E. L., CHEN, H. J. & SHAW, C. E. 2015. TDP-43 Proteinopathy and ALS: Insights into Disease Mechanisms and Therapeutic Targets. *Neurotherapeutics,* 12**,** 352-63.
SCOTTER, E. L., VANCE, C., NISHIMURA, A. L., LEE, Y.-B., CHEN, H.-J., URWIN, H., SARDONE, V., MITCHELL, J. C., ROGELJ, B., RUBINSZTEIN, D. C. & SHAW, C. E. 2014. Differential roles of the ubiquitin proteasome system and autophagy in the clearance of soluble and aggregated TDP-43 species. *Journal of Cell Science,* 127**,** 1263-1278.
SEAN, P., NGUYEN, J. H. C. & SEMLER, B. L. 2008. The linker domain of poly(rC) binding protein 2 is a major determinant in poliovirus cap-independent translation. *Virology,* 378**,** 243-253.
SEELEY, W. W., BAUER, A. M., MILLER, B. L., GORNO-TEMPINI, M. L., KRAMER, J. H., WEINER, M. & ROSEN, H. J. 2005. The natural history of temporal variant frontotemporal dementia. *Neurology,* 64**,** 1384-90.
SEELEY, W. W., CRAWFORD, R., RASCOVSKY, K., KRAMER, J. H., WEINER, M., MILLER, B. L. & GORNO-TEMPINI, M. L. 2008. Frontal paralimbic network atrophy in very mild behavioral variant frontotemporal dementia. *Arch Neurol,* 65**,** 249-55.
SEPHTON, C. F., CENIK, B., CENIK, B. K., HERZ, J. & YU, G. 2012. TDP-43 in central nervous system development and function: clues to TDP-43-associated neurodegeneration. *Biol Chem,* 393**,** 589-94.
SHA, S., HOU, C., VISKONTAS, I. V. & MILLER, B. L. 2006. Are frontotemporal lobar degeneration, progressive supranuclear palsy and corticobasal degeneration distinct diseases? *Nat Clin Pract Neurol,* 2**,** 658-65.
SHEN, W. C., LI, H. Y., CHEN, G. C., CHERN, Y. & TU, P. H. 2015. Mutations in the ubiquitin-binding domain of OPTN/optineurin interfere with autophagy-mediated degradation of misfolded proteins by a dominant-negative mechanism. *Autophagy,* 11**,** 685-700.
SHYU, A. B. & WILKINSON, M. F. 2000. The double lives of shuttling mRNA binding proteins. *Cell,* 102**,** 135-8.
SIEBEN, A., VAN LANGENHOVE, T., ENGELBORGHS, S., MARTIN, J.-J., BOON, P., CRAS, P., DE DEYN, P.-P., SANTENS, P., VAN BROECKHOVEN, C. & CRUTS, M. 2012a. The genetics and neuropathology of frontotemporal lobar degeneration. *Acta Neuropathologica,* 124**,** 353-372.

SIEBEN, A., VAN LANGENHOVE, T., ENGELBORGHS, S., MARTIN, J. J., BOON, P., CRAS, P., DE DEYN, P. P., SANTENS, P., VAN BROECKHOVEN, C. & CRUTS, M. 2012b. The genetics and neuropathology of frontotemporal lobar degeneration. *Acta Neuropathol,* 124**,** 353-72.
SKIBINSKI, G., PARKINSON, N. J., BROWN, J. M., CHAKRABARTI, L., LLOYD, S. L., HUMMERICH, H., NIELSEN, J. E., HODGES, J. R., SPILLANTINI, M. G., THUSGAARD, T., BRANDNER, S., BRUN, A., ROSSOR, M. N., GADE, A., JOHANNSEN, P., SORENSEN, S. A., GYDESEN, S., FISHER, E. M. C. & COLLINGE, J. 2005. Mutations in the endosomal ESCRTIII-complex subunit CHMP2B in frontotemporal dementia. *Nat Genet,* 37**,** 806-808.
SNOWDEN, J. S., HU, Q., ROLLINSON, S., HALLIWELL, N., ROBINSON, A., DAVIDSON, Y. S., MOMENI, P., BABORIE, A., GRIFFITHS, T. D., JAROS, E., PERRY, R. H., RICHARDSON, A., PICKERING-BROWN, S. M., NEARY, D. & MANN, D. M. 2011. The most common type of FTLD-FUS (aFTLD-U) is associated with a distinct clinical form of frontotemporal dementia but is not related to mutations in the FUS gene. *Acta Neuropathol,* 122**,** 99-110.
SOTO, C. 2003. Unfolding the role of protein misfolding in neurodegenerative diseases. *Nat Rev Neurosci,* 4**,** 49-60.
SREEDHARAN, J., BLAIR, I. P., TRIPATHI, V. B., HU, X., VANCE, C., ROGELJ, B., ACKERLEY, S., DURNALL, J. C., WILLIAMS, K. L., BURATTI, E., BARALLE, F., DE BELLEROCHE, J., MITCHELL, J. D., LEIGH, P. N., AL-CHALABI, A., MILLER, C. C., NICHOLSON, G. & SHAW, C. E. 2008. TDP-43 mutations in familial and sporadic amyotrophic lateral sclerosis. *Science,* 319**,** 1668-72.
STALEKAR, M., YIN, X., REBOLJ, K., DAROVIC, S., TROAKES, C., MAYR, M., SHAW, C. E. & ROGELJ, B. 2015. Proteomic analyses reveal that loss of TDP-43 affects RNA processing and intracellular transport. *Neuroscience,* 293**,** 157-70.
STRONG, M. J., VOLKENING, K., HAMMOND, R., YANG, W., STRONG, W., LEYSTRA-LANTZ, C. & SHOESMITH, C. 2007. TDP43 is a human low molecular weight neurofilament (hNFL) mRNA-binding protein. *Mol Cell Neurosci,* 35**,** 320-7.
SU, J. H., NICHOL, K. E., SITCH, T., SHEU, P., CHUBB, C., MILLER, B. L., TOMASELLI, K. J., KIM, R. C. & COTMAN, C. W. 2000. DNA damage and activated caspase-3 expression in neurons and astrocytes: evidence for apoptosis in frontotemporal dementia. *Exp Neurol,* 163**,** 9-19.
SUZUKI, N., KATO, S., KATO, M., WARITA, H., MIZUNO, H., KATO, M., SHIMAKURA, N., AKIYAMA, H., KOBAYASHI, Z., KONNO, H. & AOKI, M. 2012. FUS/TLS-immunoreactive neuronal and glial cell inclusions increase with disease duration in familial amyotrophic lateral sclerosis with an R521C FUS/TLS mutation. *J Neuropathol Exp Neurol,* 71**,** 779-88.
SYNOFZIK, M., BORN, C., ROMINGER, A., LUMMEL, N., SCHOLS, L., BISKUP, S., SCHULE, C., GRASSHOFF, U., KLOPSTOCK, T. & ADAMCZYK, C. 2014. Targeted high-throughput sequencing identifies a TARDBP mutation as a cause of early-onset FTD without motor neuron disease. *Neurobiol Aging,* 35**,** 1212.e1-5.
TAKEUCHI, R., TADA, M., SHIGA, A., TOYOSHIMA, Y., KONNO, T., SATO, T., NOZAKI, H., KATO, T., HORIE, M., SHIMIZU, H., TAKEBAYASHI, H., ONODERA, O., NISHIZAWA, M., KAKITA, A. & TAKAHASHI, H. 2016. Heterogeneity of cerebral TDP-43 pathology in sporadic amyotrophic lateral sclerosis: Evidence for clinico-pathologic subtypes. *Acta Neuropathol Commun,* 4**,** 61.
TAN, A. Y. & MANLEY, J. L. 2009. The TET family of proteins: functions and roles in disease. *J Mol Cell Biol,* 1**,** 82-92.
TAN, R. H., SHEPHERD, C. E., KRIL, J. J., MCCANN, H., MCGEACHIE, A., MCGINLEY, C., AFFLECK, A. & HALLIDAY, G. M. 2013. Classification of FTLD-TDP cases into pathological subtypes using antibodies against phosphorylated and non-phosphorylated TDP43. *Acta Neuropathol Commun,* 1**,** 33.
TANG, S.-L., GAO, Y.-L. & CHEN, X.-B. 2015. MicroRNA-214 targets PCBP2 to suppress the proliferation and growth of glioma cells. *International Journal of Clinical and Experimental Pathology,* 8**,** 12571-12576.
TAUTZ, D. & RENZ, M. 1983. An optimized freeze-squeeze method for the recovery of DNA fragments from agarose gels. *Anal Biochem,* 132**,** 14-9.
TEDESCHI, A., CICIARELLO, M., MANGIACASALE, R., ROSCIOLI, E., RENSEN, W. M. & LAVIA, P. 2007. RANBP1 localizes a subset of mitotic regulatory factors on spindle microtubules and regulates chromosome segregation in human cells. *Journal of Cell Science,* 120**,** 3748-3761.
TINGTING, P., CAIYUN, F., ZHIGANG, Y., PENGYUAN, Y. & ZHENGHONG, Y. 2006. Subproteomic analysis of the cellular proteins associated with the 3' untranslated region of the hepatitis C virus genome in human liver cells. *Biochem Biophys Res Commun,* 347**,** 683-91.

TOLLERVEY, J. R., CURK, T., ROGELJ, B., BRIESE, M., CEREDA, M., KAYIKCI, M., KONIG, J., HORTOBAGYI, T., NISHIMURA, A. L., ZUPUNSKI, V., PATANI, R., CHANDRAN, S., ROT, G., ZUPAN, B., SHAW, C. E. & ULE, J. 2011a. Characterizing the RNA targets and position-dependent splicing regulation by TDP-43. *Nat Neurosci,* 14**,** 452-8.

TOLLERVEY, J. R., CURK, T., ROGELJ, B., BRIESE, M., CEREDA, M., KAYIKCI, M., KONIG, J., HORTOBAGYI, T., NISHIMURA, A. L., ZUPUNSKI, V., PATANI, R., CHANDRAN, S., ROT, G., ZUPAN, B., SHAW, C. E. & ULE, J. 2011b. Characterizing the RNA targets and position-dependent splicing regulation by TDP-43. *Nat Neurosci,* 14**,** 452-458.

TOLNAY, M. & FRANK, S. 2007. Pathology and genetics of frontotemporal lobar degeneration: an update. *Clin Neuropathol,* 26**,** 143-56.

TOMONAGA, T. & LEVENS, D. 1995. Heterogeneous Nuclear Ribonucleoprotein-K Is a DNA-Binding Transactivator. *Journal of Biological Chemistry,* 270**,** 4875-4881.

TSAI, R. M. & BOXER, A. L. 2014. Treatment of Frontotemporal Dementia. *Current treatment options in neurology,* 16**,** 319-319.

TSUCHIYA, K., MITANI, K., ARAI, T., YAMADA, S., KOMIYA, T., ESAKI, Y., HAGA, C., YAMANOUCHI, H. & IKEDA, K. 2001. Argyrophilic grain disease mimicking temporal Pick's disease: a clinical, radiological, and pathological study of an autopsy case with a clinical course of 15 years. *Acta Neuropathol,* 102**,** 195-9.

TSUIJI, H., IGUCHI, Y., FURUYA, A., KATAOKA, A., HATSUTA, H., ATSUTA, N., TANAKA, F., HASHIZUME, Y., AKATSU, H., MURAYAMA, S., SOBUE, G. & YAMANAKA, K. 2013. Spliceosome integrity is defective in the motor neuron diseases ALS and SMA. *EMBO Mol Med,* 5**,** 221-34.

TSUJI, H., ARAI, T., KAMETANI, F., NONAKA, T., YAMASHITA, M., SUZUKAKE, M., HOSOKAWA, M., YOSHIDA, M., HATSUTA, H., TAKAO, M., SAITO, Y., MURAYAMA, S., AKIYAMA, H., HASEGAWA, M., MANN, D. M. & TAMAOKA, A. 2012. Molecular analysis and biochemical classification of TDP-43 proteinopathy. *Brain,* 135**,** 3380-91.

TYERS, M. & MANN, M. 2003. From genomics to proteomics. *Nature,* 422**,** 193-7.

UCHIDA, T., TAMAKI, Y., AYAKI, T., SHODAI, A., KAJI, S., MORIMURA, T., BANNO, Y., NISHITSUJI, K., SAKASHITA, N., MAKI, T., YAMASHITA, H., ITO, H., TAKAHASHI, R. & URUSHITANI, M. 2016. CUL2-mediated clearance of misfolded TDP-43 is paradoxically affected by VHL in oligodendrocytes in ALS. *Sci Rep,* 6**,** 19118.

URWIN, H., JOSEPHS, K. A., ROHRER, J. D., MACKENZIE, I. R., NEUMANN, M., AUTHIER, A., SEELAAR, H., VAN SWIETEN, J. C., BROWN, J. M., JOHANNSEN, P., NIELSEN, J. E., HOLM, I. E., DICKSON, D. W., RADEMAKERS, R., GRAFF-RADFORD, N. R., PARISI, J. E., PETERSEN, R. C., HATANPAA, K. J., WHITE, C. L., 3RD, WEINER, M. F., GESER, F., VAN DEERLIN, V. M., TROJANOWSKI, J. Q., MILLER, B. L., SEELEY, W. W., VAN DER ZEE, J., KUMAR-SINGH, S., ENGELBORGHS, S., DE DEYN, P. P., VAN BROECKHOVEN, C., BIGIO, E. H., DENG, H. X., HALLIDAY, G. M., KRIL, J. J., MUNOZ, D. G., MANN, D. M., PICKERING-BROWN, S. M., DOODEMAN, V., ADAMSON, G., GHAZI-NOORI, S., FISHER, E. M., HOLTON, J. L., REVESZ, T., ROSSOR, M. N., COLLINGE, J., MEAD, S. & ISAACS, A. M. 2010. FUS pathology defines the majority of tau- and TDP-43-negative frontotemporal lobar degeneration. *Acta Neuropathol,* 120**,** 33-41.

VALVERDE, R., EDWARDS, L. & REGAN, L. 2008. Structure and function of KH domains. *FEBS J,* 275**,** 2712-26.

VAN DEERLIN, V. M., LEVERENZ, J. B., BEKRIS, L. M., BIRD, T. D., YUAN, W., ELMAN, L. B., CLAY, D., WOOD, E. M., CHEN-PLOTKIN, A. S., MARTINEZ-LAGE, M., STEINBART, E., MCCLUSKEY, L., GROSSMAN, M., NEUMANN, M., WU, I. L., YANG, W. S., KALB, R., GALASKO, D. R., MONTINE, T. J., TROJANOWSKI, J. Q., LEE, V. M., SCHELLENBERG, G. D. & YU, C. E. 2008. TARDBP mutations in amyotrophic lateral sclerosis with TDP-43 neuropathology: a genetic and histopathological analysis. *Lancet Neurol,* 7**,** 409-16.

VANCE, C., ROGELJ, B., HORTOBAGYI, T., DE VOS, K. J., NISHIMURA, A. L., SREEDHARAN, J., HU, X., SMITH, B., RUDDY, D., WRIGHT, P., GANESALINGAM, J., WILLIAMS, K. L., TRIPATHI, V., AL-SARAJ, S., AL-CHALABI, A., LEIGH, P. N., BLAIR, I. P., NICHOLSON, G., DE BELLEROCHE, J., GALLO, J. M., MILLER, C. C. & SHAW, C. E. 2009. Mutations in FUS, an RNA Processing Protein, Cause Familial Amyotrophic Lateral Sclerosis Type 6. *Science,* 323**,** 1208-1211.

VENTER, J. C., ADAMS, M. D., MYERS, E. W., LI, P. W., MURAL, R. J., SUTTON, G. G., SMITH, H. O., YANDELL, M., EVANS, C. A., HOLT, R. A., GOCAYNE, J. D., AMANATIDES, P., BALLEW, R. M., HUSON, D. H., WORTMAN, J. R., ZHANG, Q., KODIRA, C. D., ZHENG, X. H., CHEN, L., SKUPSKI, M., SUBRAMANIAN, G., THOMAS, P. D., ZHANG, J., GABOR

MIKLOS, G. L., NELSON, C., BRODER, S., CLARK, A. G., NADEAU, J., MCKUSICK, V. A., ZINDER, N., LEVINE, A. J., ROBERTS, R. J., SIMON, M., SLAYMAN, C., HUNKAPILLER, M., BOLANOS, R., DELCHER, A., DEW, I., FASULO, D., FLANIGAN, M., FLOREA, L., HALPERN, A., HANNENHALLI, S., KRAVITZ, S., LEVY, S., MOBARRY, C., REINERT, K., REMINGTON, K., ABU-THREIDEH, J., BEASLEY, E., BIDDICK, K., BONAZZI, V., BRANDON, R., CARGILL, M., CHANDRAMOULISWARAN, I., CHARLAB, R., CHATURVEDI, K., DENG, Z., DI FRANCESCO, V., DUNN, P., EILBECK, K., EVANGELISTA, C., GABRIELIAN, A. E., GAN, W., GE, W., GONG, F., GU, Z., GUAN, P., HEIMAN, T. J., HIGGINS, M. E., JI, R. R., KE, Z., KETCHUM, K. A., LAI, Z., LEI, Y., LI, Z., LI, J., LIANG, Y., LIN, X., LU, F., MERKULOV, G. V., MILSHINA, N., MOORE, H. M., NAIK, A. K., NARAYAN, V. A., NEELAM, B., NUSSKERN, D., RUSCH, D. B., SALZBERG, S., SHAO, W., SHUE, B., SUN, J., WANG, Z., WANG, A., WANG, X., WANG, J., WEI, M., WIDES, R., XIAO, C., YAN, C., et al. 2001. The sequence of the human genome. *Science,* 291**,** 1304-51.

WAGGONER, S. A. & LIEBHABER, S. A. 2003. Identification of mRNAs associated with alphaCP2-containing RNP complexes. *Mol Cell Biol,* 23**,** 7055-67.

WAIBEL, S., NEUMANN, M., RABE, M., MEYER, T. & LUDOLPH, A. C. 2010. Novel missense and truncating mutations in FUS/TLS in familial ALS. *Neurology,* 75**,** 815-7.

WALTER, B. L., NGUYEN, J. H., EHRENFELD, E. & SEMLER, B. L. 1999. Differential utilization of poly(rC) binding protein 2 in translation directed by picornavirus IRES elements. *RNA,* 5**,** 1570-85.

WANG, I. F., TSAI, K. J. & SHEN, C. K. 2013. Autophagy activation ameliorates neuronal pathogenesis of FTLD-U mice: a new light for treatment of TARDBP/TDP-43 proteinopathies. *Autophagy,* 9**,** 239-40.

WANG, I. F., WU, L. S. & SHEN, C. K. J. 2008. TDP-43: an emerging new player in neurodegenerative diseases. *Trends in Molecular Medicine,* 14**,** 479-485.

WANG, Y., WANG, J., GAO, L., STAMM, S. & ANDREADIS, A. 2011a. An SRp75/hnRNPG complex interacting with hnRNPE2 regulates the 5' splice site of tau exon 10, whose misregulation causes frontotemporal dementia. *Gene,* 485**,** 130-8.

WANG, Y., WANG, J. N., GAO, L., STAMM, S. & ANDREADIS, A. 2011b. An SRp75/hnRNPG complex interacting with hnRNPE2 regulates the 5 ' splice site of tau exon 10, whose misregulation causes frontotemporal dementia. *Gene,* 485**,** 130-138.

WARRAICH, S. T., YANG, S., NICHOLSON, G. A. & BLAIR, I. P. 2010. TDP-43: A DNA and RNA binding protein with roles in neurodegenerative diseases. *International Journal of Biochemistry & Cell Biology,* 42**,** 1606-1609.

WEIGHARDT, F., BIAMONTI, G. & RIVA, S. 1996. The roles of heterogeneous nuclear ribonucleoproteins (hnRNP) in RNA metabolism. *Bioessays,* 18**,** 747-756.

WILLIAMS, K. L., WARRAICH, S. T., YANG, S., SOLSKI, J. A., FERNANDO, R., ROULEAU, G. A., NICHOLSON, G. A. & BLAIR, I. P. 2012. UBQLN2/ubiquilin 2 mutation and pathology in familial amyotrophic lateral sclerosis. *Neurobiology of Aging,* 33**,** 2527.e3-2527.e10.

WILS, H., KLEINBERGER, G., PERESON, S., JANSSENS, J., CAPELL, A., VAN DAM, D., CUIJT, I., JORIS, G., DE DEYN, P. P., HAASS, C., VAN BROECKHOVEN, C. & KUMAR-SINGH, S. 2012. Cellular ageing, increased mortality and FTLD-TDP-associated neuropathology in progranulin knockout mice. *J Pathol,* 228**,** 67-76.

WINTON, M. J., IGAZ, L. M., WONG, M. M., KWONG, L. K., TROJANOWSKI, J. Q. & LEE, V. M. Y. 2008. Disturbance of nuclear and cytoplasmic TAR DNA-binding protein (TDP-43) induces disease-like redistribution, sequestration, and aggregate formation. *Journal of Biological Chemistry,* 283**,** 13302-13309.

WOOLAWAY, K., ASAI, K., EMILI, A. & COCHRANE, A. 2007. HnRNP E1 and E2 have distinct roles in modulating HIV-1 gene expression. *Retrovirology,* 4.

WSZOLEK, Z. K., TSUBOI, Y., GHETTI, B., PICKERING-BROWN, S., BABA, Y. & CHESHIRE, W. P. 2006. Frontotemporal dementia and parkinsonism linked to chromosome 17 (FTDP-17). *Orphanet J Rare Dis,* 1**,** 30.

XU, Z. S. 2012. Does a loss of TDP-43 function cause neurodegeneration? *Mol Neurodegener,* 7**,** 27.

YAMASHITA, M., NONAKA, T., ARAI, T., KAMETANI, F., BUCHMAN, V. L., NINKINA, N., BACHURIN, S. O., AKIYAMA, H., GOEDERT, M. & HASEGAWA, M. 2009. Methylene blue and dimebon inhibit aggregation of TDP-43 in cellular models. *FEBS Lett,* 583**,** 2419-24.

YOU, F., SUN, H., ZHOU, X., SUN, W., LIANG, S., ZHAI, Z. & JIANG, Z. 2009. PCBP2 mediates degradation of the adaptor MAVS via the HECT ubiquitin ligase AIP4. *Nat Immunol,* 10**,** 1300-8.

YUO, C. Y., LIN, H. H., CHANG, Y. S., YANG, W. K. & CHANG, J. G. 2008. 5-(N-ethyl-N-isopropyl)-amiloride enhances SMN2 exon 7 inclusion and protein expression in spinal muscular atrophy cells. *Ann Neurol,* 63**,** 26-34.

ZELL, R., IHLE, Y., SEITZ, S., GUNDEL, U., WUTZLER, P. & GORLACH, M. 2008. Poly(rC)-binding protein 2 interacts with the oligo(rC) tract of coxsackievirus B3. *Biochem Biophys Res Commun,* 366**,** 917-21.

ZHANG, B., SEITZ, S., KUSOV, Y., ZELL, R. & GAUSS-MULLER, V. 2007a. RNA interaction and cleavage of poly(C)-binding protein 2 by hepatitis A virus protease. *Biochem Biophys Res Commun,* 364**,** 725-30.

ZHANG, Y. J., CAULFIELD, T., XU, Y. F., GENDRON, T. F., HUBBARD, J., STETLER, C., SASAGURI, H., WHITELAW, E. C., CAI, S., LEE, W. C. & PETRUCELLI, L. 2013. The dual functions of the extreme N-terminus of TDP-43 in regulating its biological activity and inclusion formation. *Hum Mol Genet,* 22**,** 3112-22.

ZHANG, Y. J., XU, Y. F., COOK, C., GENDRON, T. F., ROETTGES, P., LINK, C. D., LIN, W. L., TONG, J. M., CASTANEDES-CASEY, M., ASH, P., GASS, J., RANGACHARI, V., BURATTI, E., BARALLE, F., GOLDE, T. E., DICKSON, D. W. & PETRUCELLI, L. 2009. Aberrant cleavage of TDP-43 enhances aggregation and cellular toxicity. *Proceedings of the National Academy of Sciences of the United States of America,* 106**,** 7607-7612.

ZHANG, Y. J., XU, Y. F., DICKEY, C. A., BURATTI, E., BARALLE, F., BAILEY, R., PICKERING-BROWN, S., DICKSON, D. & PETRUCELLI, L. 2007b. Progranulin mediates caspase-dependent cleavage of TAR DNA binding protein-43. *J Neurosci,* 27**,** 10530-4.

ZHU, L., XU, M., YANG, M., YANG, Y., LI, Y., DENG, J., RUAN, L., LIU, J., DU, S., LIU, X., FENG, W., FUSHIMI, K., BIGIO, E. H., MESULAM, M., WANG, C. & WU, J. Y. 2014. An ALS-mutant TDP-43 neurotoxic peptide adopts an anti-parallel beta-structure and induces TDP-43 redistribution. *Hum Mol Genet,* 23**,** 6863-77.

ZHU, Y., SUN, Y., MAO, X. O., JIN, K. L. & GREENBERG, D. A. 2002. Expression of poly(C)-binding proteins is differentially regulated by hypoxia and ischemia in cortical neurons. *Neuroscience,* 110**,** 191-198.